



The
University
Of
Sheffield.

Access to Electronic Thesis

Author: Roger Singleton
Thesis title: Utilisation of Chip Thickness Models in Grinding
Qualification: PhD

This electronic thesis is protected by the Copyright, Designs and Patents Act 1988. No reproduction is permitted without consent of the author. It is also protected by the Creative Commons Licence allowing Attributions-Non-commercial-No derivatives.

This thesis was embargoed until June 2014.

If this electronic thesis has been edited by the author it will be indicated as such on the title page and in the text.

UTILISATION OF CHIP THICKNESS MODELS IN GRINDING



Submitted in partial fulfilment of the requirements for the
Degree of Doctor of Philosophy

by

Roger Ian Singleton

The University of Sheffield

Department of Mechanical Engineering

Advanced Manufacturing Research Centre with Boeing

March 2012

Supervisors: Prof. Keith Ridgway and Dr. M. Marshall

Abstract

Grinding is now a well established process utilised for both stock removal and finish applications. Although significant research is performed in this field, grinding still experiences problems with burn and high forces which can lead to poor quality components and damage to equipment. This generally occurs in grinding when the process deviates from its safe working conditions. In milling, chip thickness parameters are utilised to predict and maintain process outputs leading to improved control of the process. This thesis looks to further the knowledge of the relationship between chip thickness and the grinding process outputs to provide an increased predictive and maintenance modelling capability.

Machining trials were undertaken using different chip thickness parameters to understand how these affect the process outputs. The chip thickness parameters were maintained at different grinding wheel diameters for a constant productivity process to determine the impact of chip thickness at a constant material removal rate. Additional testing using a modified pin on disc test rig was performed to provide further information on process variables.

The different chip thickness parameters provide control of different process outputs in the grinding process. These relationships can be described using contact layer theory and heat flux partitioning. The contact layer is defined as the immediate layer beneath the contact arc at the wheel workpiece interface. The size of the layer governs the force experienced during the process. The rate of contact layer removal directly impacts the net power required from the system. It was also found that the specific grinding energy of a process is more dependent on the productivity of a grinding process rather than the value of chip thickness. Changes in chip thickness at constant material removal rate result in microscale changes in the rate of contact layer removal when compared to changes in process productivity. This is a significant piece of information in relation to specific grinding energy where conventional theory states it is primarily dependent on chip thickness.

Acknowledgements

I would first like to thank my supervisors Professor Keith Ridgway and Dr Matthew Marshall who have provided me with all the support required to put together this piece of work. In addition, the support from Dr Andy Bell and Dr Mark Massam, with their knowledge of grinding processes, has been invaluable both during my experimentation and write up. Also I must acknowledge the support of multiple staff within Rolls-Royce and Tyrolit for their input into this thesis.

The technical support of Ashley Godbehere, Paul Rigden and the workshop staff at the AMRC helped make the practical work of this thesis possible. I am also very grateful to Chris Ridgway for the assistance with all aspects of administration relating to this work.

Finally, to my friends and family who held me up through the rightful difficulties that a research degree like this presents. It is no surprise that you were there for me and I am constantly grateful for all the support you provide in everything I do. Thank you all.

Contents Page

1	Introduction	1
1.1	Background to the research	2
1.2	Project Scope	4
1.3	Thesis Outline	4
2	Literature Review	6
2.1	Introduction to Grinding	6
2.2	Creep Feed Grinding	10
2.2.1	History of Creep Feed Grinding	10
2.2.2	Fundamentals of Creep Feed Grinding	11
2.2.3	Developments of the Creep Feed Process	13
2.3	Wheel Wear in Grinding Applications	14
2.3.1	Wear Types in Grinding	14
2.3.2	Wear in Conventional Abrasive Creep Feed Grinding	16
2.4	Material Removal in Grinding	19
2.4.1	Chip Formation in Grinding	19
2.4.2	Forces in Grinding	21
2.4.3	Energy in Grinding	23
2.4.4	Effect of Parameters and Grain Shape on the Chip Formation Process	25
2.4.5	Tribology Techniques in Grinding Research	29
2.5	Grinding Energy and Surface Integrity	30
2.5.1	Specific Grinding Energy and Heat Flux	31
2.5.2	Energy Partition	34
2.5.3	Residual Stress and Metallurgical Damage	36
2.5.4	Temperature Measurement	37
2.6	Chip Thickness in Grinding	38
2.6.1	Grinding Chips	39
2.6.2	Undeformed Chip Thickness	41
2.6.3	Equivalent Chip Thickness	43
2.6.4	Chip Thickness Ratio	45
2.6.5	Effect of Chip Thickness on the Grinding Process	46
2.6.6	Summary of Grinding Chip Thickness Models	52
2.7	Summary and Hypothesis	53
3	Methodology	55
3.1	Experimental Equipment	55
3.1.1	Blohm Profimat 412	55
3.1.2	Makino A99	57
3.1.3	Aluminium Oxide Grinding Wheels	59
3.1.4	Conditioning the Grinding Wheel	60
3.1.5	Cutting Fluid	61
3.2	Experimental Development – How to evaluate the effect of chip thickness?	62
3.2.1	The Difficulties in Testing the Effect of Chip Thickness	62
3.2.2	Preliminary Setup and Method	64
3.2.3	Preliminary Grinding Test Results	68
3.2.4	Discussion and Experimental Improvements	71
3.3	Statistical Analysis	73

3.3.1	Statistical Techniques	74
3.3.2	Analysis of Results	77
3.4	Machining Trials – Assessment of Chip Thickness Models	80
3.4.1	Setup on Machine Tool	81
3.4.2	Test Piece Design and Manufacture	83
3.4.3	Parameters and Method	86
3.4.4	Data Collection	88
3.5	Modified Pin on Disc Testing – Assessment of Contact Area and Wheel Speed	98
3.5.1	Test Rig and Setup on Machine Tool	98
3.5.2	Test Piece Design and Wheel Conditioning	100
3.5.3	Parameters and Method	102
3.5.4	Data Collection	105
4	Assessment of Chip Thickness Models	108
4.1	The Effect of Chip Thickness on Specific Grinding Energy	109
4.2	Heat Flux and Workpiece Temperature	117
4.3	Surface Effects	125
4.4	The Effect of Vibration on Results	131
4.5	Statistical Analysis of Results and Critique of Testing Methodology	135
4.6	Summary	140
5	Effect of Wheel Speed and Contact Area on the Grinding Process	142
5.1	Effect of Wheel Speed	142
5.2	Effect of Contact Area	150
5.3	Validity of Test	159
5.4	Summary	163
6	Discussion	165
6.1	Relationship between Chip Thickness Models and Process Outputs	165
6.2	Effect of Chip Thickness and Productivity on Specific Grinding Energy	181
6.3	Relationship between Chip Thickness and Temperature	184
6.4	Utilisation of Chip Thickness in Grinding	191
6.5	Summary	194
7	Conclusions and Further Work	197
8	References	202
Appendix A	Cutting Fluid Data Sheets	
Appendix B	Table of Preliminary Experimental Parameters	
Appendix C	Table of Machining Trials Experimental Parameters	

Table of Figures

Figure 1.1.1	Interaction between inputs and outputs of grinding process after Chen et al [3].	2
Figure 1.1.2	Factors of conventional abrasive grinding process affecting the contact zone.	3
Figure 2.1.1	Image of grinding wheel surface showing variety of abrasive grain shape and distribution for standard Aluminium Oxide grinding wheel detailed by Helletsberger [4].	7
Figure 2.1.2	Image detailing the different types of grinding techniques currently utilised in manufacturing after Shaw [6]; (a) Surface Grinding, (b) Internal Grinding & (c) External Grinding.	8
Figure 2.1.3	Image detailing the different types of component manufactured using different either conventional or super abrasive grains from Andrew et al [8]; (a) Turbine Blade ground using conventional abrasives & (b) Carbide Milling Tools ground using super abrasives.	9
Figure 2.1.4	Figure 2.1.4 Process diagram highlighting the multiple inputs and outputs involved in abrasive machining applications by Marinescu et al [7].	10
Figure 2.2.2.1	Image showing the comparison in contact arc engagement by Shaw [6]; (a) Surface grinding application & (b) Creep Feed grinding.	11
Figure 2.3.1.1	Image detailing main wear mechanisms for abrasive grains during grinding by Malkin [5]; A – Grain Attrition, B – Grain Fracture and C – Bond Fracture.	15
Figure 2.3.1.2	Image detailing wear curve associated with volumetric loss of wheel for a cylindrical grinding setup after Malkin [5].	16
Figure 2.3.2.1	Image showing common methodology for measuring radial wear of a grinding wheel from Andrew et al [8].	17
Figure 2.3.2.2	Graph of specific grinding energy versus material removed highlighting the positive effect of applying CD conditions to the process after Pearce et al [8, 18].	18
Figure 2.4.1.1	Image of individual grain performing stages of material removal by Chen and Rowe [24].	20
Figure 2.4.1.2	Diagram of individual cutting edge showing large negative rake geometry after Komanduri [25].	21
Figure 2.4.2.1	Image of individual abrasive grain performing chip removal in grinding with details of force interactions by Helletsberger [4].	22
Figure 2.4.3.1	Image of individual abrasive grain performing chip removal in grinding with details of energy interactions by Helletsberger [4].	24
Figure 2.4.4.1	Image of different abrasive wear modes for single point scratch testing after Hokkirigawa and Kato [34]; (a) Ploughing, (b) Wedge Formation & (c) Cutting.	25

Figure 2.4.4.2	Image of showing wear map and associated wear modes related to degree of penetration D_p from Hokkirigawa and Kato [34].	27
Figure 2.4.4.3	Efficiency of the grinding process according to Helletsberger [4]; (a) Relationship of removed material thickness $h_{cu,eff}$ to grain penetration depth h_{ce} & (b) Table detailing impact of parameters on the efficiency of the grinding process.	28
Figure 2.4.5.1	Image of a pin on disc setup using a rotating grinding wheel and metal pin from Abbasi et al [45].	30
Figure 2.5.1.1	Graph of specific grinding energy versus chip thickness for grinding of steel alloys taken from Shaw [32].	32
Figure 2.5.1.2	Graph of e_c versus Q' for HEDG grinding of steel taken from Bell [48].	33
Figure 2.5.2.1	Diagram detailing the areas of heat partitioning in the grinding system by Mohamed et al [51].	34
Figure 2.5.4.1	Diagram of inclined thermocouple test piece with replaceable top hat test piece as used by Jin and Stephenson [65].	38
Figure 2.6.1.1	Image of simulated cutting paths of grinding grains showing variation in chip sizes for different grains [69].	40
Figure 2.6.1.2	Image of flowing style chip witnessed in grinding of Inconel 718 by Tso [70].	40
Figure 2.6.2.1	Diagram of theoretical individual grain cutting path.	41
Figure 2.6.3.1	Diagram illustrating the principle of equivalent chip thickness h_{eq} taken from Helletsberger [4].	44
Figure 2.6.4.1	Diagram illustrating MNIR principle taken from Bond [1].	45
Figure 2.6.5.1	Image of grinding charts relating process outputs to equivalent chip thickness by Snoeys and Peters [67].	47
Figure 2.6.5.2	Graph of specific grinding energy e_c versus equivalent chip thickness h_{eq} for varying grinding wheel speeds taken from Brinksmeier and Glwierzew [73].	48
Figure 3.1.1.1	Internal view of Blohm Profimat 412 grinding machine envelope including cutting fluid nozzle and dynamometer setup.	56
Figure 3.1.2.1	Makino A99 Machine Tool; (a) Image of Machine Exterior, (b) Internal machine envelope including Grinding Wheel, Dresser Roll and Pressure Cutting fluid Nozzle (PCN) Setup (c) Pressure Cutting fluid Nozzle axis setup and available movement.	58
Figure 3.1.3.1	Tyrolit Aluminium Oxide Grinding Wheels; (a) VIPER Specification, (b) STRATO Specification.	59
Figure 3.1.4.1	Side view of flat form diamond dresser roll used for dressing the Aluminium Oxide grinding wheels.	61
Figure 3.2.2.1	Experimental setup on Blohm machine tool detailing Inconel 718 material and steel sheet for tool wear measurement.	64

Figure 3.2.2.2	Image displaying experiment flow diagram describing the process for selecting parameters for each grinding cut performed in the preliminary tests.	67
Figure 3.2.2.3	Diagram illustrating the technique and definition of tool wear for the preliminary grinding testing.	68
Figure 3.2.3.1	Specific Grinding Energy versus Grinding Wheel Radius for constant chip thickness h_m for the different grinding cuts performed.	69
Figure 3.2.3.2	Vertical Force versus Grinding Wheel Radius for constant chip thickness h_m for the different grinding cuts performed.	69
Figure 3.2.3.3	Radial Wheel Wear versus Grinding Wheel Radius for constant chip thickness h_m for the different grinding cuts performed.	70
Figure 3.2.3.4	Surface Roughness versus Grinding Wheel Radius for constant chip thickness h_m for the different grinding cuts performed.	71
Figure 3.3.1.1	Box Plot diagram illustrating experimental block data variation used to aid the explanation of the ANOVA statistical technique.	75
Figure 3.4.1.1	Makino A99 grinding setup: (a) Grinding wheel, dresser roll and cutting fluid nozzle cut setup, (b) Work piece and pallet setup.	81
Figure 3.4.1.2	Image of cutting fluid nozzle utilised in machining trials.	82
Figure 3.4.1.3	Image of CAD sketch utilised to set the pressure cutting fluid nozzle (PCN) application angles.	83
Figure 3.4.2.1	Image of the inclined thermocouple testing rig design by Jin and Stephenson [65].	84
Figure 3.4.2.2	Diagram of angled test piece design showing thermocouple placement utilised in these experiments.	84
Figure 3.4.2.3	Image of the final test piece assembly; (a) View with test piece assembly placed on dynamometer, (b) End view detailing separate parts of assembly.	85
Figure 3.4.2.4	Individual components of test piece assembly; (a) Base Plate, (b) Thermo Plate, (c) Test Piece.	85
Figure 3.4.4.1	Force measurement equipment; (a) Kistler 9257A dynamometer with test piece assembly mounted, (b) Kistler 5017 Charge Amplifier utilised in force measurement.	89
Figure 3.4.4.2	Example of Force output profile; (a) Main experimental run, (b) Spark Out experimental run.	90
Figure 3.4.4.3	Image detailing the Tyrolit mobile power measurement equipment.	90
Figure 3.4.4.4	Example of power measurement output profile for the assessment of chip thickness models experiment.	91
Figure 3.4.4.5	Temperature measurement equipment; (a) Thermo plate test piece material with embedded thermocouples, (b) SquirrelView hardware box.	92

Figure 3.4.4.6	Example temperature measurement output profile for the assessment of chip thickness models experiment.	92
Figure 3.4.4.7	Vibration measurement equipment; (a) 352A21 accelerometer, (b) Embedded accelerometer in base plate, (c) Metalmax hardware.	93
Figure 3.4.4.8	Images of Radial Wear Procedure; (a) Grinding wheel overhang proving non cutting edges of grinding wheel radius used as reference in wear measurement, (b) Graphite wear coupon with wheel cut profile to measure radial wheel wear.	94
Figure 3.4.4.9	Setup of surface roughness measurement for metal test pieces; (a) Mitutoyo SJ-301 surface roughness measurement equipment, (b) Stylus on ground surface with measurement placements and directions detailed.	95
Figure 3.4.4.10	Graphite force measurement setup; (a) Graphite test piece in experimental setup, (b) Close up image of graphite test piece on dynamometer.	96
Figure 3.4.4.11	Graphite surface roughness measurement setup; (a) Mahr stylus profilometer, (b) Graphite test piece and stylus detailing measurement positions.	96
Figure 3.4.4.12	Cut-up sample for Surface Integrity testing; (a) Cut out section from main test piece material, (b) Close up view of cut out section showing testing surface.	97
Figure 3.5.1.1	Pin on disc setup on Makino A99 machine tool; (a) Setup overview and (b) Close up image highlighting Nickel Pin and Grinding wheel.	99
Figure 3.5.1.2	Pneumatic air regulator; (a) Setup overview and (b) Close up of digital pressure gauge.	99
Figure 3.5.2.1	Image of the diamond coated static dressing stick utilised in the modified pin on disc testing rig.	102
Figure 3.5.4.1	Image of pin actuator arm and load cell assembly detailing force measurement on test rig.	105
Figure 3.5.4.2	Additional images of pin on disc force measurement equipment; (a) Load cell during calibration on structural testing machine, (b) Digital read out equipment for force measurement.	106
Figure 3.5.4.3	Image of the Mitutoyo profilometer setup for measurement of nickel pin Ra value.	107
Figure 4.1	General graphical lay-out for presentation of results.	108
Figure 4.1.1	Smoothed Net Power output versus grinding wheel radius.	110
Figure 4.1.2	Vertical Force (F_v) and Horizontal Force (F_h) outputs measured from a Kistler Dynamometer versus grinding wheel radius.	112
Figure 4.1.3	Vertical and Horizontal Force per unit contact area versus grinding wheel radius.	113
Figure 4.1.4	Specific Grinding Energy versus wheel radius; ‘Force’ indicates values of e_c calculated from net horizontal force data and ‘Power’ indicates values of e_c calculated from net power data.	116

Figure 4.2.1	Calculated Heat Flux from Net Power data versus grinding wheel radius.	118
Figure 4.2.2	Thermocouple temperature values versus depth from ground surface to estimate ground surface temperature.	119
Figure 4.2.3	Graph of estimated ground Surface Temperature versus wheel radius.	120
Figure 4.2.4	Knoop Hardness versus depth beneath surface for test cuts R01 and R29 with h_{eq} maintained.	122
Figure 4.2.5	Knoop Hardness versus depth beneath surface for test cuts R01 and R31 with h_m maintained.	122
Figure 4.2.6	Knoop Hardness versus depth beneath surface for test cuts R01 and R36 with S maintained.	123
Figure 4.2.7	Deformation Depth of grain layer versus chip thickness maintenance parameter for test cuts R01 (baseline), R29 (h_{eq}), R31 (h_m) and R36 (S).	124
Figure 4.3.1	Measured surface roughness Ra versus wheel radius for cut surfaces on metal test pieces.	126
Figure 4.3.2	Measured surface roughness Ra versus wheel radius for cut surfaces on graphite test pieces.	127
Figure 4.3.3	Vertical and Horizontal Force versus grinding wheel radius for static graphite scratch tests.	128
Figure 4.3.4	Calculated Friction Coefficient versus grinding wheel radius for static graphite scratch tests.	129
Figure 4.3.5	Amount of wheel dressed during clearance move from workpiece versus grinding wheel radius.	130
Figure 4.3.6	Explanation of grit placement for constant spacing at varying grinding wheel diameters; (a) diagram of grit placement and distance values, (b) Table of results for different diameters.	131
Figure 4.4.1	Time domain amplitude signal data from embedded accelerometer; (a) Raw untreated signal with low frequency drift, (b) Signal treated with High Pass filter.	132
Figure 4.4.2	Variance value of treated amplitude data signal versus grinding wheel radius.	133
Figure 4.4.3	Skewness value of treated amplitude data signal versus grinding wheel radius.	134
Figure 4.4.4	Kurtosis value of treated amplitude data signal versus grinding wheel radius.	135
Figure 5.1.1	Graph detailing wear rate of Nickel Pin versus the grinding wheel speed for modified pin on disc trials.	143
Figure 5.1.2	Graph of face grinding chip thickness h_F [5] versus the grinding wheel speed for modified pin on disc trials.	145
Figure 5.1.3	Graph of grinding force ratio versus the grinding wheel speed for modified pin on disc trials.	146
Figure 5.1.4	Graph of net power versus the grinding wheel speed for modified pin on disc trials.	147
Figure 5.1.5	Graph of specific grinding energy versus the grinding wheel speed for modified pin on disc trials.	148

Figure 5.1.6	Surface topography of pin after testing; (a) Image of tested pin surface, and (b) Diagram detailing grain paths for different grinding setups.	149
Figure 5.1.7	Surface roughness of pin surface versus grinding wheel speed.	150
Figure 5.2.1	Experimental tooling after testing of 4mm diameter pin setup; (a) Grinding wheel with groove on surface and (b) Nickel pin with rounded end.	151
Figure 5.2.2	Figure 5.2.2 Graph of horizontal force versus time measured during testing; (a) For an 8mm diameter pin & (b) 12mm diameter pin showing stable cutting region.	152
Figure 5.2.3	Graph of wear rate versus pin diameter for modified pin on disc trials.	154
Figure 5.2.4	Graph of face grinding chip thickness h_F versus pin diameter for modified pin on disc trials.	155
Figure 5.2.5	Graph of force ratio versus pin diameter for modified pin on disc trials.	156
Figure 5.2.6	Graph of Net Power versus pin diameter for modified pin on disc trials.	157
Figure 5.2.7	Graph of specific grinding energy versus pin diameter for modified pin on disc trials.	158
Figure 5.2.8	Graph of Ra versus pin diameter for modified pin on disc trials.	159
Figure 5.3.1	Diagram showing contact area shapes between grinding wheel and workpiece; (a) Peripheral Creep Feed Grinding and (b) Modified Pin on Disc Test Setup.	160
Figure 5.3.2	Graph of specific grinding energy versus diameter dependent specific removal rate for modified pin on disc trials.	162
Figure 5.3.3	Graph of specific grinding energy versus effective radius dependent specific removal rate for modified pin on disc trials.	163
Figure 6.1.1	Diagram detailing geometric representation of chip thickness parameters; (a) S and h_m parameters, and (b) h_{eq} parameter.	166
Figure 6.1.2	Example graph detailing how the chip thickness parameters are plotted versus the wheel radius and the trends associated with maintaining the varying chip thickness models.	167
Figure 6.1.3	Comparative trends for chip thickness parameter and grinding process output; (a) S chip thickness parameter, and (b) Net Power output.	168
Figure 6.1.4	Contact Layer Theory; (a) Image highlighting contact layer zone & (b) Graph detailing the link between wheel speed and temperatures associated with the contact layer and ground surface by Tawakoli [43].	170
Figure 6.1.5	Graph of time to remove Contact Layer versus grinding wheel radius.	171

Figure 6.1.6	Comparative trends for chip thickness parameter and grinding process output; (a) h_{eq} chip thickness parameter, and (b) Force output.	173
Figure 6.1.7	Empirical grinding results showing relationship between Force and h_{eq} by Snoeys and Peters [67].	174
Figure 6.1.8	Force required to remove the contact layer volume versus grinding wheel radius.	176
Figure 6.1.9	Comparative trends for chip thickness parameter and grinding process output; (a) h_m chip thickness parameter, and (b) Force per Unit Area output.	178
Figure 6.2.1	Graph of e_c versus h for thesis data from both cutting trials and modified pin on disc experiment.	182
Figure 6.2.2	Graph of e_c versus Q' for thesis data from both cutting trials and modified pin on disc experiment.	183
Figure 6.3.1	Graph of Surface Temperature versus wheel radius for the different chip thickness models maintained in Chapter 4.	185
Figure 6.3.2	Variation in heat dissipation due to work piece velocity by Helletsberger [4].	186
Figure 6.3.3	Surface temperature versus wheel work piece contact length.	186
Figure 6.3.4	Measured surface temperature versus grinding wheel speed.	187
Figure 6.3.5	Cutting fluid convection coefficient for pure water versus wheel radius.	189
Figure 6.3.6	Predicted surface temperature versus wheel radius.	190

Table of Tables

Table 2.2.2.1	Table of comparison between pendulum and creep feed conditions after Shaw [6].	13
Table 2.6.5.1	Table detailing effect of changing chip thickness and productivity on process outputs for various literature sources.	51
Table 2.6.6.1	Table summarising the prominent chip thickness models utilised in the grinding process.	52
Table 3.1.1.1	Table detailing Blohm Profimat 412 machine specifications.	57
Table 3.1.2.1	Table detailing Makino A99 Machine Specifications.	58
Table 3.1.4.1	Table of dressing parameters for diamond roll on Aluminium Oxide wheel.	61
Table 3.2.1.1	Table of parameters used in the calculation of undeformed chip thickness and effects of changing the parameter values on the productivity Q' and undeformed chip thickness h_m .	63
Table 3.2.2.1	Table detailing the experimental run order for preliminary grinding tests.	66
Table 3.3.2.1	Table of results showing values for Pearson correlation coefficient between wheel radius and relevant process output and p-values for the different experiment variables.	78
Table 3.3.2.2	Table of results showing values for ANOVA F-statistic and p-values for process outputs for the different experiment variables.	79
Table 3.3.2.3	Table of results showing values required sample size per block for an experimental power of 0.95 based on output data from ANOVA analysis.	80
Table 3.4.2.1	Individual component details for test piece assembly.	86
Table 3.4.3.1	Grinding Parameters utilised in the assessment of chip thickness models experiment.	87
Table 3.4.3.2	Table showing predicted wheel speed changes for different wheel diameters at defined experimental blocks.	88
Table 3.5.2.1	Table of all Nickel Test Pin geometries utilised in the modified pin on disc testing rig.	101
Table 3.5.3.1	Table of parameters utilised in the modified pin on disc grinding test.	103
Table 3.5.3.2	Table of variables and run order utilised in the modified pin on disc grinding test.	104
Table 4.5.1	Table of results showing values for Pearson correlation coefficient between wheel radius and relevant process output and p-values for different chip thickness maintenance conditions.	137

Table 4.5.2	Table of results showing values for ANOVA F-statistic and p-values for process outputs under different chip thickness maintenance conditions.	139
Table B.1	Table of cuts performed for preliminary experiments including process parameters, chip thickness and outputs.	
Table C.1	Table of cuts performed for Chapter 4 machining trials including process parameters, chip thickness and outputs.	

Notation

a_{dp}	Post cut dressing amount	mm
a_e	Depth of cut for peripheral grinding applications	mm
A_{pin}	Surface area of nickel pin used in modified pin on disc trial	mm^2
A_w	Surface area of nickel pin used in modified pin on disc trial	mm^2
b	Grinding Wheel Width of Cut	mm
β_f	Cutting Fluid Constant	J^2/m^2K^2s
C	Number of cutting points per unit area	$1/mm^2$
d_e	Equivalent grinding wheel diameter	mm
d_{pin}	Diameter of nickel pin used in modified pin on disc trial	mm
d_s	Equivalent grinding wheel diameter	mm
d_w	Equivalent grinding wheel diameter	mm
D	Grinding wheel diameter	mm
DE	Deformation Energy	J
D_p	Degree of penetration	N/A
e_c	Specific Grinding Energy	J/mm^3
f	Shear Strength at contact interface	N/mm^2
f_{rd}	Dressing rate per wheel revolution	$\mu m/rev$
F	Force	N
F_A	Force per Unit Area	N/mm^2
$F_{fricBCh}$	Friction force between bond and chip for single grain	N
$F_{fricGCh}$	Friction force between grain and chip for single grain	N
F_{fricGW}	Friction force between grain and workpiece for single grain	N
F_h	Horizontal Force from creep feed grinding process	N
F''_h	Horizontal Force per unit area	N/mm^2

F_{hG}	Horizontal Force measured from Graphite scratch test	N
F_{nG}	Normal force on single grain	N
F_{nw}	Normal force on work piece from single grain	N
F_p	Normal force application on nickel pin	N
F_{stat}	F statistic utilised in ANOVA analysis	N/A
F_{tG}	Tangential force on single abrasive grain	N
F_{tw}	Tangential force on work piece from single grain	N
F_v	Vertical Force from creep feed grinding process	N
F''_v	Vertical Force per unit area	N/mm ²
F_{vG}	Vertical Force measured from Graphite scratch test	N
F_x	X-direction force from dynamometer	N
F_y	Y-direction force from dynamometer	N
F_z	Z-direction force from dynamometer	N
FR_{BCh}	Friction energy between bond and chip	J
FR_{GCh}	Friction energy between grain and chip	J
FR_{GW}	Friction energy between grain and workpiece	J
G	Grinding Ratio	N/A
h	Normalised grinding chip thickness	
h_a	Material Hardness	g/mm ²
h_c	Convection coefficient for grinding chip	W/m ² K
h_{ce}	Grain Penetration Depth	μm
h_{ch}	Chip Thickness for Abrasive Grain Illustration	μm
h_{cu}	Effective removed material thickness	μm
h_{eff}	Effective removed material thickness	μm
h_{el}	Elastic deformation depth from individual grain	μm
h_{ex}	Hex chip thickness parameter for milling applications	mm
h_{eq}	Equivalent chip thickness	μm
h_F	Face grinding chip thickness	μm
h_{fl}	Convection coefficient for cutting fluid	W/m ² K
h_m	Undeformed grinding chip thickness	μm

h_s	Convection coefficient for grinding wheel	W/m^2K
h_w	Convection coefficient for material workpiece	W/m^2K
HK	Knoop Hardness of material	g/mm^2
K	Number of Cutting Points around a grinding wheel periphery	N/A
Ku	Statistical Value of Kurtosis	N/A
l_c	Arc of contact between grinding wheel and workpiece	mm
l_k	Arc of contact between grinding wheel and workpiece	mm
L	Distance between grinding cutting edges	mm
p	Pearson correlation coefficient	N/A
P_f	Applied fluid pressure from coolant nozzle	bar
P_{Net}	Net power from the grinding process	kW
P_p	Applied pressure on nickel pin	N/mm^2
q	Ratio of grinding wheel speed to workpiece speed	N/A
q_{ch}	Heat flux transferred to the chip	W/m^2
q_{en}	Heat flux transferred to the environment	W/m^2
q_{fl}	Heat flux transferred to the cutting fluid	W/m^2
q_t	Total Heat flux from the grinding process	W/m^2
q_w	Heat flux transferred to the workpiece	W/m^2
Q'	Material removal rate per mm of grinding wheel width	$mm^3/s/mm$
Q'_d	Material removal rate per mm of nickel pin diameter	$mm^3/s/mm$
Q'_{er}	Material removal rate per mm of nickel pin effective radius	$mm^3/s/mm$
Q'_w	Material removal rate per mm of grinding wheel width	$mm^3/s/mm$
r	Ratio of chip width to chip thickness	N/A
r_{esr}	Effective square radius of nickel pin	mm
r_G	Radius of individual grain	mm
r_s	Grinding Wheel Radius	mm

Ra	Average Surface Profile Roughness	μm
S	Feed per grinding cutting edge	μm
SH	Shearing energy associated with grain chip formation	J
Sk	Statistical value of skewness	N/A
t	Time/Undeformed grinding chip thickness as defined by Shaw [6]	s/μm
t _{res}	Residence time of abrasive grain in contact arc	s
T	Temperature	°C
T _b	Boiling Temperature of cutting fluid	°C
T _c	Measured Surface Temperature	°C
T _{ch}	Temperature of grinding chip	°C
T _{max}	Measured Surface Temperature	°C
u	Specific Grinding Energy	J/mm ³
v _f	Face grinding feed rate	mm/min
v _w	Grinding workpiece feed rate	mm/min
V _a	Statistical value of Variance	N/A
V _c	Grinding Wheel Speed	m/s
V _s	Grinding Wheel Speed	m/s
ΔV	Wear rate of nickel pin / Productivity of face grinding process	mm ³ /s
ΔV _s	Change in grinding wheel volume	mm ³
ΔV _w	Change in work piece volume	mm ³
μ	Grinding force ratio	N/A
z	Depth below ground surface	μm
Z'	Material removal rate per mm of grinding wheel width	mm ³ /s/mm

AlOx	Aluminium Oxide
AMRC	Advanced Manufacturing Research Centre
ANOVA	Analysis of Variance
CAD	Computer Aided Design

CBN	Cubic Boron Nitride
CD	Continuous Dressing
CFG	Creep Feed Grinding
CTR	Chip Thickness Ratio
fpt	Feed per Tooth
HEDG	High Efficiency Deep Grinding
MNIR	Maximum Normal Infeed Rate
PCN	Pressure Coolant Nozzle
PVD	Physical Vapour Deposition
SGE	Specific Grinding Energy
RR	Rolls-Royce PLC
VIPER	Vitreous Performance Extreme Removal

Chapter 1 - Introduction

Grinding is a chip forming metal removal process traditionally used either to produce a suitably smooth surface or to machine materials that were too hard for other conventional chip machining methods. However, technology developments over the last 50 years have developed grinding into a process also capable of producing very high material removal rates. Although a well-established stock removal technique, problems associated with surface damage through grinding burn still exist for operations within production environments. This occurs due to excessive heat being transferred to the workpiece surface as a result of abusive grinding conditions. Production engineers desire methods and parameters that will provide improved consistency and control for grinding processes such that the onset of abusive grinding conditions can be prevented and ultimately predicted. Large organisations, like Rolls-Royce, continue to invest in developing techniques to achieve this [1]. This is essential in grinding as deviation from safe working parameters can lead to a rapid breakdown in the process resulting in damage to components and machinery. This research aims to address the issues of improving the prediction and control capabilities that can be applied to grinding processes.

Support for the research has been provided by Roll-Royce PLC and the grinding wheel manufacturer Tyrolit. Both have an interest in grinding research. Rolls-Royce are the second largest supplier of gas turbine engines internationally with around 40% of their internal manufacturing processes associated with either rough or finish grinding operations. Tyrolit are the largest supplier of conventional abrasive tooling to the UK Aerospace market and manufacture the aluminium oxide grinding wheels utilised by RR in their Vitreous Performance Extreme Removal (VIPER) grinding operations. Both maintain a strong relationship with the Advanced Manufacturing Research Centre (AMRC) and provided tooling and expertise in relation to this research work.

1.1 Background to the Research

With all chip machining processes, the outputs from the system during manufacture are generated from the interaction between the cutting edge and workpiece material. In grinding, this interaction is performed by abrasive grains resulting in a large amount of small chips. For milling, undeformed chip thickness is utilised to predict and maintain process outputs [2]. An increased knowledge of how chip thickness affects the process outputs in grinding can lead to improved predictive and maintenance capability.

Chip thickness in grinding applications varies in comparison to milling processes. The outputs of the grinding process are a result of the summation of multiple single abrasive grain/workpiece interactions. The size of each individual chip is dependent on the wheel topography and the kinematics of the grinding process as shown in Figure 1.1.1. If the grinding chip geometry/thickness can be controlled, then a level of control of the process outputs may be established. Grinding has the added complexity that the cutting edges are not defined. The abrasive grains that form the cutting edges in grinding are random in shape and distribution within the wheel. This adds complexity when developing modelling techniques for application in a grinding process.

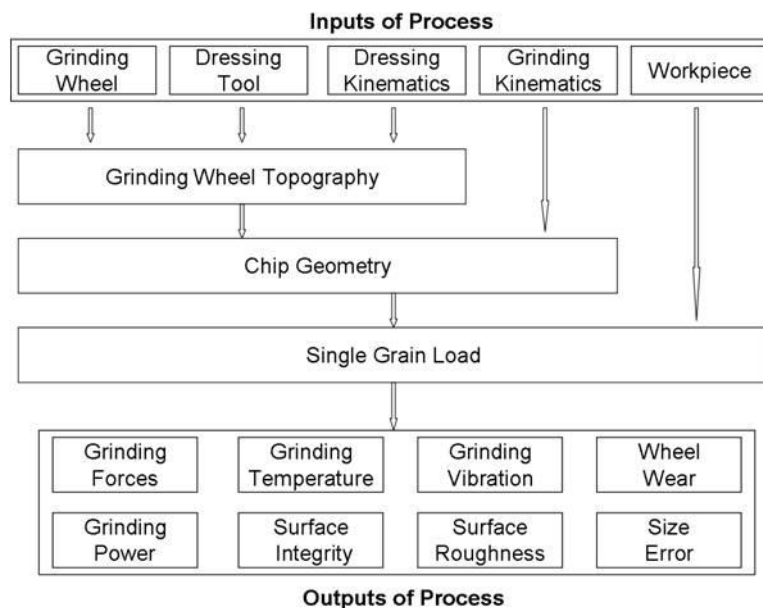


Figure 1.1.1 Interaction between inputs and outputs of grinding process after Chen et al [3].

The chip thickness in grinding is dependent on a number of factors that affect how the abrasive grain interacts with the workpiece material in the cut zone as shown in Figure 1.1.1. In addition, conventional grinding processes also have the added complexity of changing wheel diameter due to the re-conditioning required to keep the abrasive grains sharp. This results in a change in the contact zone geometry and kinematics of the abrasive grains as the wheel reduces in diameter during production operations. This and a number of other factors that can lead to changes in chip thickness within the contact zone are detailed in Figure 1.1.2.

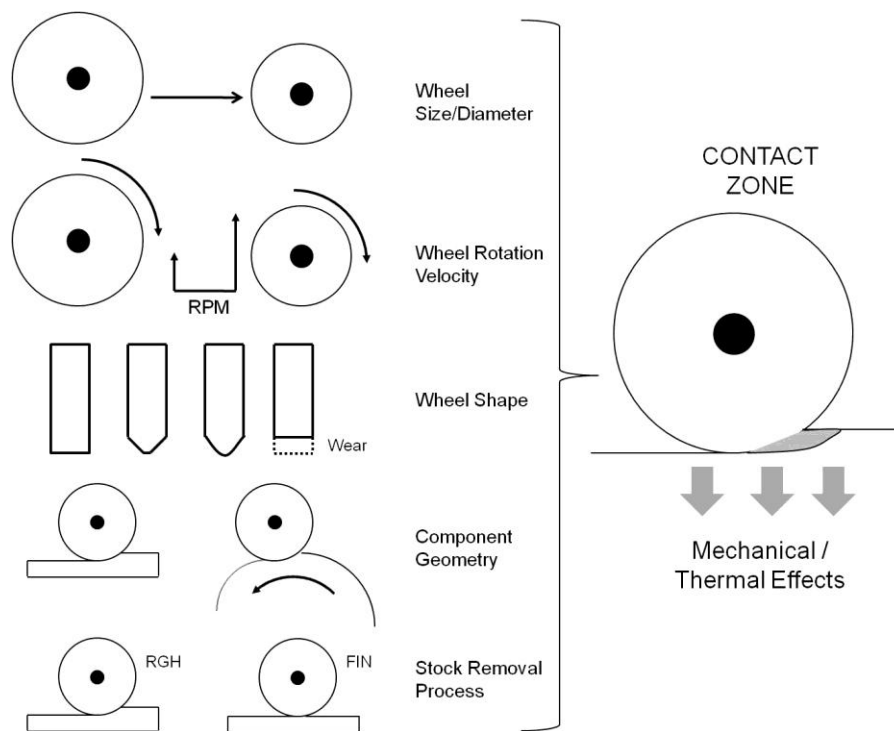


Figure 1.1.2 Factors of conventional abrasive grinding process affecting the contact zone.

The large number of factors shown in Figure 1.1.2 provides a wide range of methods and variables that could be used to investigate the effect of chip thickness on the process outputs in grinding. In addition, it highlights the difficulties of maintaining consistency within the contact zone when grinding. There is therefore a need for further investigation into the relationship between chip thickness and the outputs of the grinding process in order to provide

improved control. This knowledge can be used as a platform for predictive modelling for a range of grinding processes.

1.2 Project Scope

Considering the desire for improved control of the grinding process, the aim of the research is:

- To further our knowledge of the relationship between chip thickness models and outputs of the grinding process.

The primary objectives include:

- Provide experimental output data showing how the grinding process changes with chip thickness.
- Identify key parameters and their effect on the grinding process in isolation of chip thickness.
- Provide examples on how chip thickness can be used in grinding to provide improved prediction and control of the process.

The application of Creep Feed Grinding was chosen as the process for the research. This is due to the authors experience in this application and the relevance to Rolls-Royce and Tyrolit. In addition, there are large changes in grinding wheel diameter for conventional abrasive creep feed processes, which has the potential to result in variation of both the chip thickness and process outputs. This makes it a suitable application for further investigation.

1.3 Thesis Outline

This thesis presents the work performed to achieve the aim set out in section 1.2. It begins with a review of the literature covering material relevant to the grinding process. This covers an introduction to grinding with specific focus on the creep feed application and the complexities of using conventional abrasives. It continues with an overview of grinding tribology and how material is removed by an individual abrasive grain. The concept of specific grinding energy, the heat generated from the process and the potential impact on surface integrity is

considered. Finally, a number of chip thickness models and their application in the grinding process is discussed.

Several sets of experiments were performed in order to collect the data required to assess the relationship between chip thickness and the process outputs. This is presented in Chapter 3, the Experimental Methodology, which outlines the grinding trials performed utilising different chip thickness models at a number of grinding wheel diameters. A subsequent experiment utilising a modified pin on disc setup is detailed in order to isolate the effects of contact area and grinding wheel speed. This section also includes details of pre-trial work and statistical techniques all used to increase the likelihood of detecting trend behaviour during the main experimental trials.

Chapters 4 and 5 detail the results of the trials presented in the experimental methodology. The effect on process outputs of chip thickness is displayed in Chapter 4 with an inclusion of post experiment analysis of surface effects. Chapter 5 presents the results from the modified pin on disc test. The results show the effect of varying grinding wheel speed and contact area on the grinding process.

The Discussion is presented in Chapter 6 drawing together the data from Chapters 4 and 5. Relationships between the chip thickness models and process outputs are developed, and examples of where the use of chip thickness can provide improved control within grinding are presented. Chapter 7 draws conclusions on the research and presents recommendations for future work.

Chapter 2 - Literature Review

The review of the literature explores the grinding process and its relationship to chip thickness. The creep feed grinding process and its application using conventional abrasives is detailed. The material removal process by individual grains is outlined including what effect changing process variables has on this mechanism. Specific grinding energy and its effect on the surface integrity are considered before the introduction of the prominent chip thickness models currently developed for grinding. Finally, the review highlights the effect of varying chip thickness on the outputs of the grinding process.

2.1 Introduction to Grinding

Grinding is one of the most complex manufacturing processes with respect to material removal. Although classed as a chip machining process, it differs significantly from the more traditional processes of milling, drilling and turning as the material is removed by undefined cutting edges. With grinding, the material removal occurs with a very large number of these undefined cutting edges, whose shape, orientation and distribution are random due to the manufacturing process of the grinding wheel [4]. Magnified images detailing examples of typical grinding wheel topography are shown in Figure 2.1.1. The cutting edges are the protruding geometry of hard abrasive grains which are immersed in a bond structure forming a grinding wheel. It is the random nature of these grains and their interactions with the work material that make the process so complex and difficult to model.



Figure 2.1.1 Image of grinding wheel surface showing variety of abrasive grain shape and distribution for standard Aluminium Oxide grinding wheel detailed by Helletsberger [4].

Grinding is an essential process for the majority of industrial components manufactured today. Malkin [5] states that society today would be impossible without grinding. It is required to sharpen cutting tools, to produce bearings used in most mechanical devices and is also essential for computer based and optical components. The primary purposes of grinding are either in creating a desired surface finish or cutting material that is too hard for conventional machining. Bearings, mirrors and silicon applications for the information technology industry provide examples where a very smooth surface finish is required. The grinding of hardened gears and cutting tools highlight hard material components which are difficult to machine. Grinding has also developed from a finishing process into an effective stock removal process. The application of creep feed grinding and its derivatives provide comparable material removal rates to milling and turning making it an integral part of new high productivity manufacturing solutions.

The applications listed above highlight the wide scope of the grinding process which can be applied in many forms within industry. The operations are generally defined by the geometry of the component to be machined. The more common applications are surface and cylindrical grinding which cover geometry associated with flat, straight cutting and components with curvature. Shaw [6] states the 3 most important processes employed in grinding are surface, internal

and external. The common grinding applications can be seen in Figure 2.1.2. One or more of these 3 types are utilised in most grinding applications.

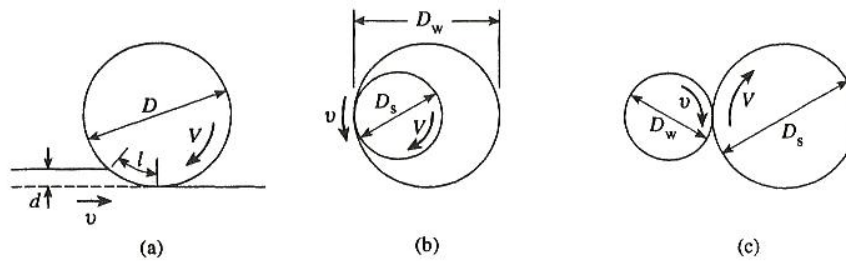


Figure 2.1.2 Image detailing the different types of grinding techniques currently utilised in manufacturing after Shaw [6]; (a) Surface Grinding, (b) Internal Grinding & (c) External Grinding.

The operations detailed in Figure 2.1.2 can be utilised with various tooling and parameter setups. The main factor that governs the appropriate selection is the material being ground which characterizes the make-up of the grinding tooling. Marinescu et al [7] stated that the hardness of the abrasive grain must be harder than the workpiece at the temperature of the interaction. The standard tooling in grinding is a wheel composed of abrasive grains and a bond structure to retain them. The abrasive grits are classed as either conventional abrasives or superabrasives depending on their hardness value. An example of a common application for each abrasive type is detailed in Figure 2.1.3. The main conventional abrasives utilised are Aluminium Oxide or Silicon Carbide. The selection of abrasive type is dependent on the hardness and chemical properties of the ground material. These are held within either resinoid or vitrified bonding systems. Superabrasives include Diamond and Cubic Boron Nitride (CBN). These are utilised mainly with resinoid and metallic bonds, although some vitrified applications do exist. Typically these are utilised in the manufacture of very hard brittle materials.

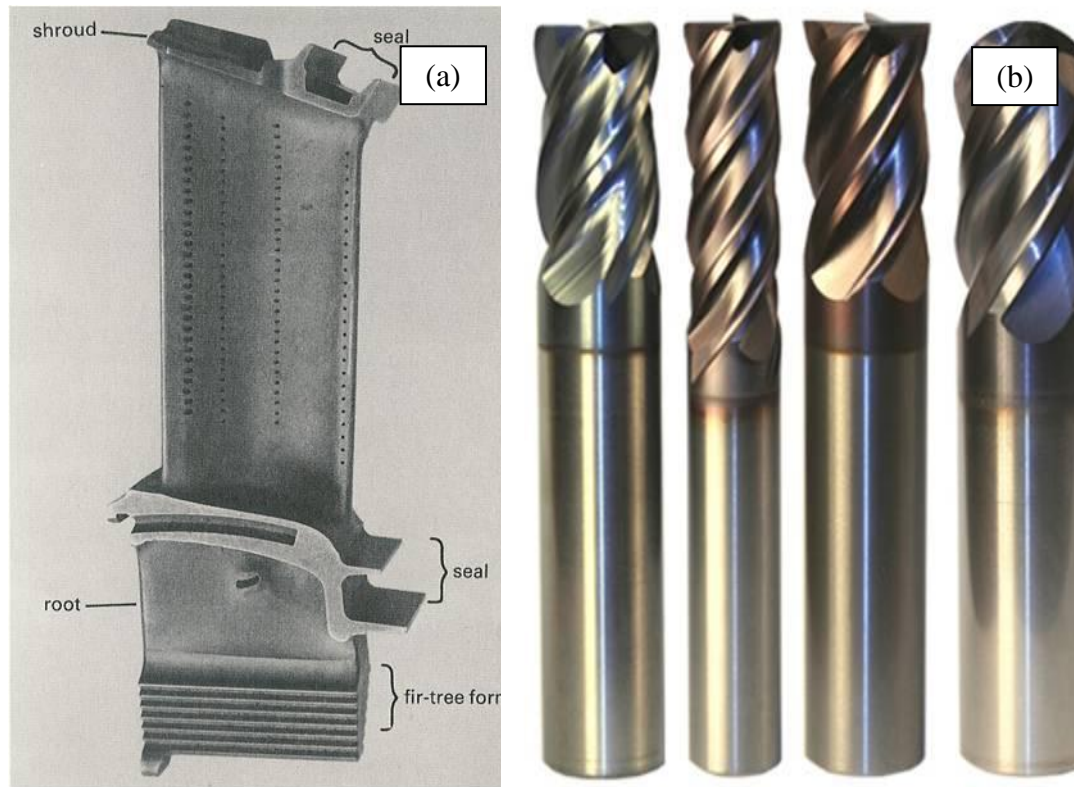


Figure 2.1.3 Image detailing the different types of component manufactured using different either conventional or super abrasive grains from Andrew et al [8]; (a) Turbine Blade ground using conventional abrasives & (b) Carbide Milling Tools ground using superabrasives.

Section 2.1 outlines just how many different parameters and setups there are in the grinding process. The complexity is further highlighted in Figure 2.1.4 which shows the additional considerations involved when planning a process. Considering only the kinematics in isolation involves the inclusion of wheel topography, depth of cut, workpiece feed rate, wheel speed and the relevant geometries of the grinding wheel and component.

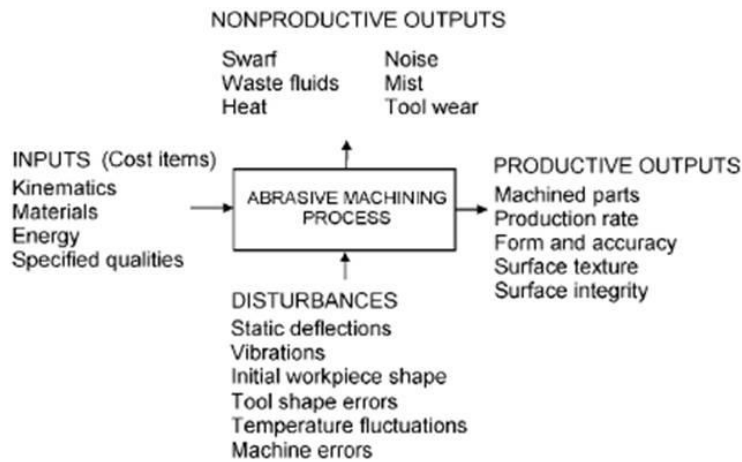


Figure 2.1.4 Process diagram highlighting the multiple inputs and outputs involved in abrasive machining applications by Marinescu et al [7].

The grinding process is very complex as a result of the undefined cutting edges and with so many different types of grinding with varying requirements it is important to be specific when approaching research in this area. This research has focussed specifically on the area of Creep Feed Grinding (CFG) using conventional abrasives due its extensive use in Aerospace applications and the challenges associated with large changes in wheel diameter during the process.

2.2 Creep Feed Grinding

As stated above, creep feed grinding (CFG) was selected as the application for this research. As such it is important to understand the unique characteristics of this application which are detailed in this section.

2.2.1 History of Creep Feed Grinding

The traditional and most well known function of grinding processes has been in the role of finishing, creating a surface with desired roughness properties. Creep Feed Grinding essentially is a stock removal process and moved grinding into direct competition with milling and broaching. Although characterised by a slow feed rate, the material removal rate is significantly larger than traditional surface grinding [9]. It was invented in the late 1950's by Edmund and Gerhard Lang when incorrect cutting parameters were accidentally applied in a cutting trial. This resulted in a low (creep) feed rate cutting pass being performed with a large

depth of cut. Remarkably little grinding burn was witnessed leading to increased research into this new application. After further investigation, CFG entered large scale production in the late 1960's and early 1970's.

Creep Feed Grinding has been significantly utilised in manufacturing operations within the UK aerospace sector [8]. The major applications have included the manufacture of turbine blades, vanes and seal components requiring deep slot forms. These contain complex features such as fir tree roots, which can be machined by CFG at a much reduced cost in comparison to milling. The common materials are nickel based super alloys which are difficult to machine. In addition, CFG is ideal for the manufacture of steel components especially in their hardened condition. Common steel components include gears, labyrinth seals and complex automotive applications. It can be seen that CFG is utilised where there are hard to machine materials or complex geometries. These tend to occur on components that have key design functions and are sensitive to damage during manufacture. This makes it very important to understand the effects of the creep feed grinding process on the component material.

2.2.2 Fundamentals of Creep Feed Grinding

The creep feed process is very different to that of conventional surface grinding. This is due to the altered contact conditions between the wheel and workpiece which has a significant impact on the mechanics of the process. The large depth of cut significantly increases the arc of contact at the cut zone as shown by the comparison between creep feed and surface grinding shown in Figure 2.2.2.1.

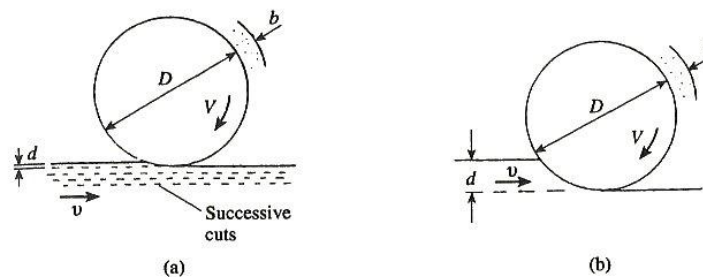


Figure 2.2.2.1 Image showing the comparison in contact arc engagement by Shaw [6]; (a) Surface grinding application & (b) Creep Feed grinding.

The difference in depth of cut combined with the variation in workpiece feed rate has a significant impact on the kinematics of the process in the contact arc. This is best shown as a comparison between the 2 processes as presented by Shaw [6] in Table 2.2.2.1. The comparison is made using the same wheel specification, wheel speed and material removal rate. The equations utilised to make the kinematic calculations are obtained from the same source. The important differences between the processes include:

- The arc of contact is approximately 10 times larger in CFG
- The chip thickness is reduced in CFG
- The overall force per mm of wheel width is 3 times larger in CFG
- The force per grit is lower in CFG

The most significant variation is the increase in contact length and subsequent time an abrasive grain is in contact with the workpiece material for creep feed conditions. The increased contact provides more rubbing between the grain and workpiece leading to higher temperatures generated at the cut zone. The increase in temperature for increased contact length was shown by Wager and Gu [10] although not for a creep feed application. According to Werner [11], an increased contact zone results in; increased total grinding force, reduced average force per grit, increased temperature in the wheel-work contact zone and reduced temperatures in the generated work surface. The increase in total grinding force is due to an increased number of grits in contact with the workpiece at any time.

Variable	Surface Grinding	Creep Feed Grinding
Depth of Cut (mm)	0.0051	5.1
Feed Rate (mm/min)	18600	186
Active grits per area (cm ⁻²)	186	93
Arc of contact (mm)	1.14	11.4
Mean Undeformed Chip Thickness (µm)	1.08	0.40
Specific Energy (MPa)	55.2	165
Tangential Force per Width (N/mm)	0.28	0.841
Radial Force per Width (N/mm)	0.56	1.681
Tangential Force per Grit (N)	1.33	0.80
Radial Force per Grit (N)	2.66	1.60

Table 2.2.2.1 Table of comparison between pendulum and creep feed conditions after Shaw [6].

The combination of these effects can lead to problems within creep feed applications especially with regards to surface integrity in ground components. The large forces require high stiffness machines and high energy requirements which can lead to significant build up of heat in the contact zone. The role of cutting fluid is very important in creep feed grinding as the majority of the heat is partitioned into this during the cutting process [12]. Optimised fluid delivery setups are therefore essential to avoid workpiece burn. Although creep feed grinding is an effective method of material removal, the increased depth of cut and slow feed rate require careful application to avoid workpiece damage during the process.

2.2.3 Developments of the Creep Feed Process

Due to its capability as a stock removal process, many developments have been made to improve the productivity of the creep feed process. A specific

application using high pressure cutting fluid was patented by Rolls-Royce [13] to create the VIPER grinding process. The high pressure cutting fluid acts as both a cleaning and cooling function on the grinding wheel leading to a significant increase in productivity. This technique is utilised heavily in their blade manufacturing facilities.

Another significant development of the creep feed process came from the application of CBN at very high wheel and workpiece speeds in the High Efficiency Deep Grinding (HEDG) process [14]. The high workpiece speeds produce different grinding conditions in comparison to surface or creep feed processes. The increased temperature in the contact zone makes the material softer and easier to remove, and the high temperatures generated are removed quickly with the grinding chips to avoid workpiece damage. The HEDG process is a significant development from creep feed grinding and is one of the highest productivity grinding processes currently available to production.

2.3 Wheel Wear in Grinding Applications

Wear in the grinding process has an impact on the shape of the cutting edges which can lead to variation in the contact zone kinematics. The rate of wear is dependent on the wheel type utilised for a particular manufacturing operation. With conventional Aluminium Oxide abrasives, which are considered in this thesis, the rate of wear is high and its effects can be witnessed after only a short cutting period. As this effect could have influence on the cutting mechanism, the subject of grinding wheel wear is introduced in this section.

2.3.1 Wear Types in Grinding

Wear in the grinding process is a well studied phenomenon. The reason for this is highlighted by Chen et al [3] who state that wear on the grinding wheel has a direct effect on workpiece quality and efficiency. In a production environment, the reduction in wheel radius is a measure of the wheel wear during grinding. This value is important in production as it can affect a components dimensional tolerance and depending on the type of wear, can adversely affect the surface

integrity. Typically, this radial reduction is the result of 3 types of wear mechanism. Malkin [5] defines these as attrition, grain fracture and bond fracture as shown in Figure 2.3.1.1. These vary in their severity and impact on the radial loss of the wheel form. In addition, they can all impact the chip formation for an individual abrasive grain subsequently affecting the mechanics of the material removal process.

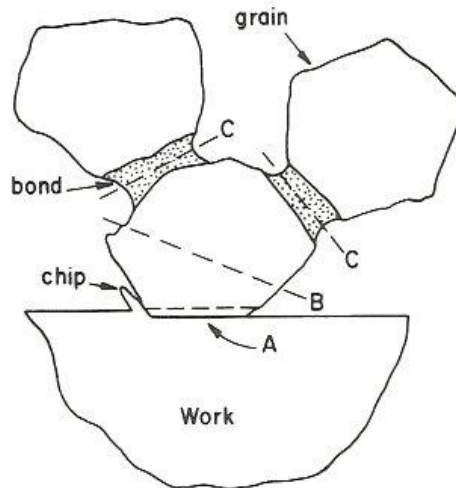


Figure 2.3.1.1 Image detailing main wear mechanisms for abrasive grains during grinding by Malkin [5]; A – Grain Attrition, B – Grain Fracture and C – Bond Fracture.

Although the wear associated with a conventional abrasive grinding wheel occurs at a much higher rate in comparison to high-speed steel and carbide milling or turning processes, the stages of tool wear development are similar. Figure 2.3.1.2 shows typical wear behaviour with high initial wear, a steady state region in the middle and an accelerated region at the end. The final stage would indicate a break-down of wheel form in the grinding process and a dressing operation would be required. If the wheel is not re-dressed this can lead to wheel collapse which is explored by Badger [15]. This is a point where the power and force build up due to excessive attrition of the grains and the wheel undergoes significant grain and bond fracture. This can lead to a dramatic loss of wheel radius but has the effect of refreshing the wheel surface and reducing the force and power.

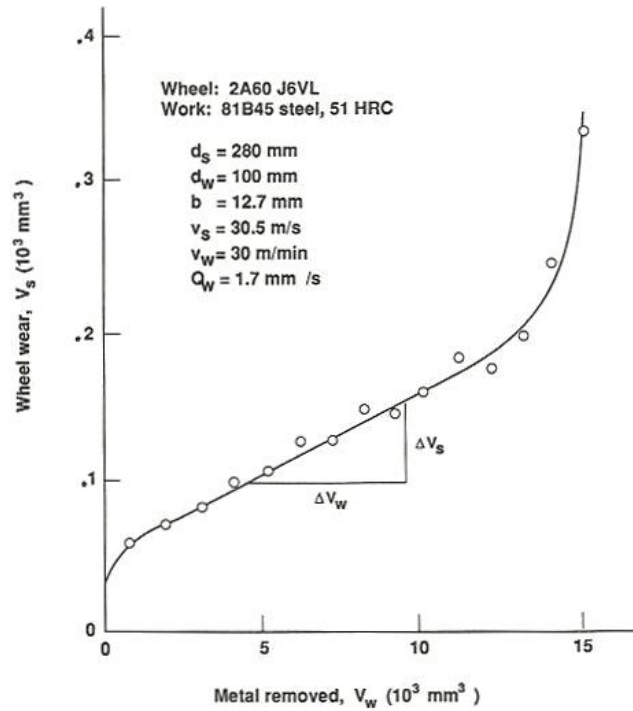


Figure 2.3.1.2 Image detailing wear curve associated with volumetric loss of wheel for a cylindrical grinding setup after Malkin [5].

The gradient of the trend line shown in the steady state region in Figure 2.3.1.2 represents the volume of wheel lost against the volume of material removed. This gradient is the G-ratio parameter and is utilised as an assessment of the grinding wheel performance in resisting wear. It is characterised by equation (2.3.1):

$$G = \frac{\Delta V_W}{\Delta V_S} \quad (2.3.1)$$

Where ΔV_W = Volume of workpiece material removed (mm^3)

ΔV_S = Volume of wheel lost due to wear (mm^3)

A high G-ratio indicates a good ability to resist wheel wear. The value of G-ratio is dependent on a number of variables within the manufacturing process including tooling specification, parameters and workpiece material.

2.3.2 Wear in Conventional Abrasive Creep Feed Grinding

The wear in creep feed grinding using conventional abrasives can vary in comparison to surface grinding or processes using super abrasives as a result of

the varying contact conditions. Andrew et al [8] states that wear in CFG is commonly measured either in terms of radial or profile wear. The radial wear is measured by a loss in wheel radius generally by machining a shim in a workpiece. The discrepancy between the actual and desired wheel radius is then recorded. This measurement technique is detailed in Figure 2.3.2.1. It is an appropriate method as significant amounts of wheel can be removed as a result of wear when using conventional abrasives in creep feed applications.

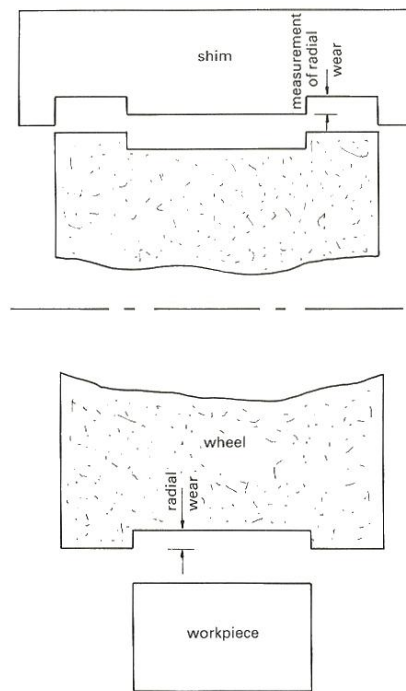


Figure 2.3.2.1 Image showing common methodology for measuring radial wear of a grinding wheel from Andrew et al [8].

The long arc of contact in the creep feed process results in the grit being in contact with the workpiece for a long period of time in comparison to surface grinding. This leads to a large amount of rubbing which tends to generate wear flats, through attrition wear, on the cutting grains. Work performed by Ye and Pearce [16] shows that an increased contact time for the grain results in an increase in radial wheel wear. In addition, the increased rubbing can lead to an increase in the amount of wear flat area on the abrasive grains. This leads to higher forces and an increased chance of burn as shown by LaChance et al [17]. This highlights just how important it is to constantly re-dress the grinding wheel within CFG.

The benefit of dressing was highlighted by Pearce et al [18] as cited in Andrew et al [8] when the specific grinding energy of a worn wheel was significantly reduced by applying a dressing operation mid cycle as shown in Figure 2.3.2.2. To take maximum advantage of this effect, the application of continuous dressing (CD) in cycle was introduced to the process of CFG. Sekine et al [19] and Inasaki [20] showed the effect of applying continuous dressing resulting in the dramatic stabilisation and reduction in force, power and energy. Work by Osterle and Li [21] also confirms that the application of CD has the same positive effect of reducing specific grinding energy and surface temperature in the grinding of Nickel-based superalloys. However, the trade off with continuous dressing is that the consumption of the wheel is increased dramatically and there is a continuous change in wheel diameter.

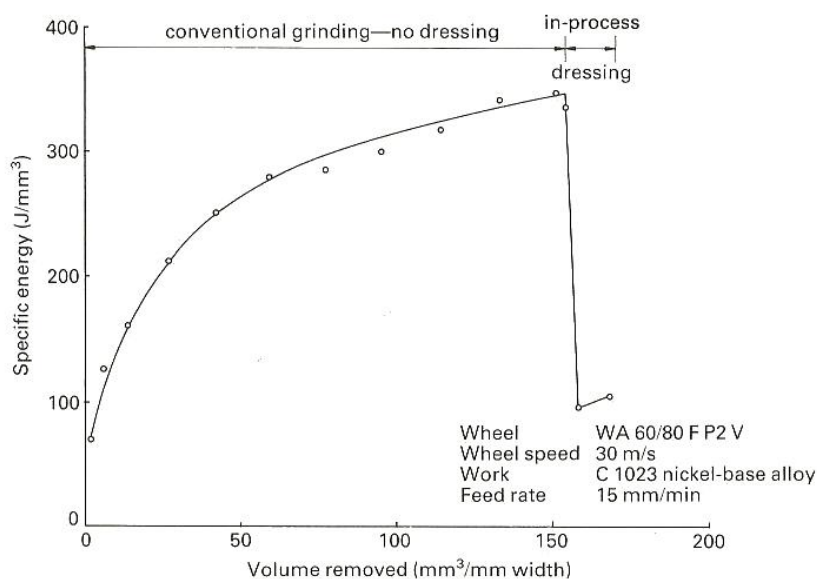


Figure 2.3.2.2 Graph of specific grinding energy versus material removed highlighting the positive effect of applying CD conditions to the process after Pearce et al [8, 18].

Due to the effects of wear, the majority of creep feed grinding operations with conventional abrasives either utilise CD or have a significant number of dressing cycles within the production operation. This results in a large amount of wheel consumption and large changes in wheel diameter over the operational life of a grinding tool. The diameters can range from 500mm down to 250mm in certain production setups. This change in wheel diameter can have significant impact on

the production process in terms of the contact zone kinematics, chip thickness and subsequent effects on the process outputs of force, power, wear and vibration. However, little research has been performed to understand the effect of changing wheel geometry for constant productivity conditions. Tonshoff et al [22] looked at the impact of replacing a large diameter corundum wheel with a small diameter CBN wheel to reduce tooling cost within a process. It was found that the change in wheel diameter had a significant impact on the amount of wear and force experienced by the component material. However, the wheels had a different grain type which makes the comparison between large and small diameter wheels difficult to quantify. Wakuda et al [23] has limited data for different wheel diameters showing that force reduces at lower wheel diameters. Overall, there is little information about how the process changes for a single grinding wheel over its operational life. With the problems associated with workpiece burn that can be caused from a small change in grinding conditions, this is an area of research that requires further investigation.

2.4 Material Removal in Grinding

Prior to exploring the relevant grinding chip thickness models, it is important to consider how individual abrasive grains interact with the workpiece material resulting in material removal. The summation of these individual interactions determines the outputs of the grinding process. This section focuses on how material is removed by individual grains. This includes the consideration of the forces and energy generated during this process and how this interaction can change with the application of different process parameters. In addition, this section looks at additional testing techniques that can be used to support cutting trials in grinding research.

2.4.1 Chip Formation in Grinding

Material removal in grinding occurs as a result of multiple cuts produced from a number of individual grain workpiece interactions. When an individual grain interacts with the workpiece surface there are several mechanisms that occur during the process of material removal and are described by Chen and Rowe

[24]. When a grain engages in up cut grinding, it initially slides along the workpiece surface of the material due to the elastic deflection of the system. When the elastic limit is reached, ploughing occurs as a result of plastic deformation. As the grain penetrates deeper into the material, the tearing stress of the material is passed and metal is removed by chip formation. The process is outlined in Figure 2.4.1.1.

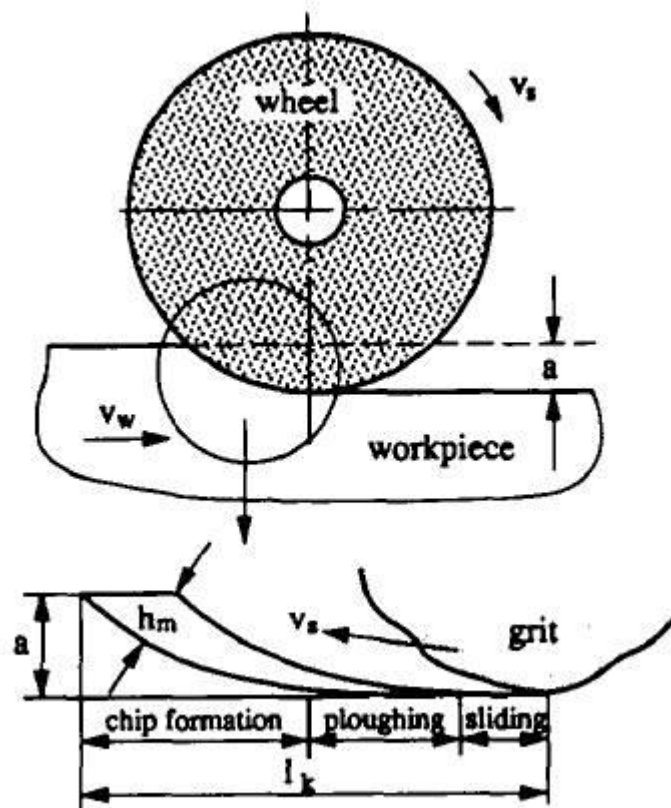


Figure 2.4.1.1 Image of individual grain performing stages of material removal by Chen and Rowe [24].

Each individual grain contact is unique due to the stochastic nature of abrasive grains in grinding wheels and its method of material removal is dependent on a number of factors. These include the shape of the cutting grain, its placement on the wheel and the penetration of the grain into the material. Work performed by Komanduri [25] and Matsuo et al [26] explore the effect of various shapes of cutting tools in machining applications. The results show a significant increase in friction force with large negative rake angles on the cutting edge. This is why the forces and temperatures produced in grinding are high as the majority of abrasive

grains present a large negative rake angle during the chip formation process. The negative rake angle of a cutting edge is detailed in Figure 2.4.1.2.

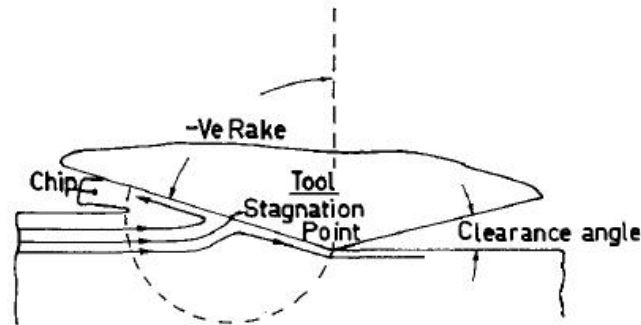


Figure 2.4.1.2 Diagram of individual cutting edge showing large negative rake geometry after Komanduri [25].

In addition to the shape of individual grains, their distribution within the grinding wheel can have an influence on the cutting mechanism. This is because the alignment and seating of an abrasive grain in the bond structure can alter the effective rake angle and how deep it penetrates the material. Hecker et al [27] used detailed microscopy images to examine the grinding wheel surface. One of the images recorded a 0.16mm^2 surface area which identified 4 individual grains with varying cutting edges and protrusion distances from the wheel bond. Butler et al [28] showed that with so many different shapes and distributions not all the cutting edges are involved in material removal. This shows how complex it is to accurately model the grinding kinematics and chip thickness geometry for individual abrasive grains in the contact zone.

2.4.2 Forces in Grinding

When the chip formation mechanism described in section 2.4.1 takes place, there are a number of mechanical and thermal effects that occur as a result of the interaction. With the abrasive grain both deforming and removing the workpiece material, force is generated and energy changes take place. The summation of these individual interactions results in the mechanical and thermal outputs from the grinding process.

The forces generated in grinding are the result of the entire abrasive grain/workpiece interaction. Durgumahanti [29] considers the force to be separated into 2 parts; the cutting deformation force and frictional force. The cutting deformation force is further divided between ploughing and chip formation forces. Considering the tribology of the process, the frictional force is developed when shearing the asperity contacts between the grain and workpiece. The deformation force is generated from the atoms moving within the material structure and in the chip formation force required to provide the shearing of the material in the shear plane [30]. All the forces generated in the process occur at various stages during the grain/workpiece interaction detailed in section 2.4.1, and are resolved and measured in the tangential or normal direction as detailed in Figure 2.4.2.1. In creep feed grinding, the normal force is referred to as the vertical force and the tangential force is described as the horizontal force. It is known that the normal force has significant impact upon the workpiece integrity due to its relation to friction and heat generation whereas the tangential force mainly affects the grinding power requirements as it is associated with the chip formation mechanism [2].

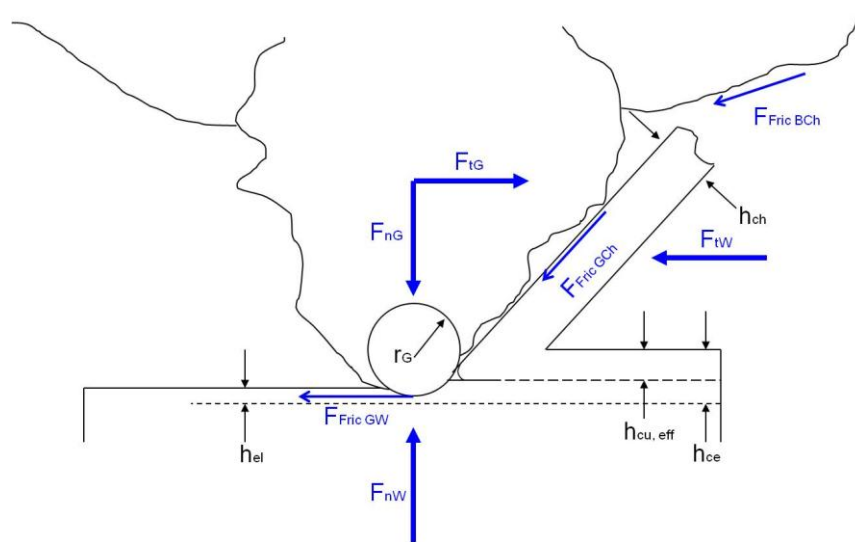


Figure 2.4.2.1 Image of individual abrasive grain performing chip removal in grinding with details of force interactions by Helletsberger [4].

The magnitude of the normal and tangential forces change during the chip formation process [4]. When undergoing deformation, the effect of normal force is much more prominent as a result of large frictional forces. As soon as the

material exceeds its yield stress and begins to peel away, the tangential forces increase significantly. At this point in time the grinding power consumption is high. Chang and Wang [31] proposed that the tangential grinding force was dependent on chip size and an increase would result in a higher force output based upon a single grain contact. The experiments showed that an increase in depth of cut directly increased the force due to the increase in chip thickness. Durgumahanti [29] confirmed the same response by increasing the workpiece feed rate. An increase in grinding wheel speed for otherwise constant parameters has the effect of reducing the chip size and thickness.

2.4.3 Energy in Grinding

When an abrasive grain moves through the workpiece material, work is performed and forces are generated. Energy is the ability to perform work and it is exchanged during the grain/workpiece interaction. In both grinding and cutting, almost all the energy is dissipated as heat [32] due to the large amount of material deformation at all stages of the process. This section considers the energy transfer for a single abrasive grain interaction. The concept of specific grinding energy (SGE) and its impact as a process output is considered in section 2.5.

Conservation of energy is a useful concept utilised in research of the grinding process. All energy changes, which are experienced primarily as heat, are absorbed by some part of the grinding system. Changes in energy are generally perceived to be the result of sliding, ploughing and chip formation [5], similar to the grinding force. Guo and Malkin [12] produced an in depth paper providing a thermal analysis of the grinding process reviewing a large proportion of the development work for heat generation. They identify that the heat energy generated at the individual grit level has a negative impact on the workpiece material at a macro level. This is dependent on the amount of heat generated and where it flows within the grinding system. Work performed by Jin and Stephenson [33] has focused on the methodology of calculating heat partitioning within the grinding system. It is identified that there are many sources of heat

generation and potential sinks for the energy within the process. These are detailed for an individual grain in Figure 2.4.3.1.

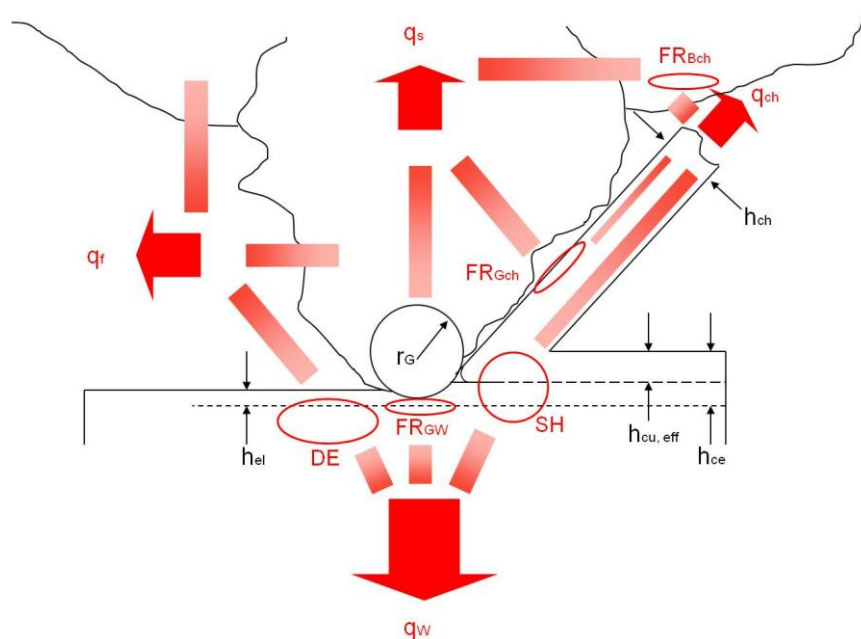


Figure 2.4.3.1 Image of individual abrasive grain performing chip removal in grinding with details of energy interactions by Helletsberger [4].

The heat is developed by friction between the grain, workpiece, chip and bond in multiple areas of the contact. In addition, the effects of deformation and shearing provide a significant amount of heat generation. The heat generated can flow into the workpiece material, the grinding wheel, the chip or the general environment which is primarily the cutting fluid. It is preferable for the grinding chip, wheel or cutting fluid to absorb the majority of the heat formed to prevent workpiece burn and damage.

The energy and force outputs detailed in Sections 2.4.2 and 2.4.3 have been considered for an individual grain. The information presented is intended to show the development of the force and energy for a single abrasive grain on a micro scale. This knowledge provides useful context when understanding changes in measured process outputs from a machine tool experiment.

2.4.4 Effect of Parameters and Grain Shape on the Chip Formation Process

The chip formation process for an individual grinding grain is influenced by many variables. This section describes the effect of process parameters and grain shape on the chip formation mechanism. This is considered for an individual grain/workpiece contact and focuses primarily on work containing single grit experiments.

The process of grinding can be represented as an example of 2 body abrasive wear. It is made up of numerous instances of a hard grinding grain sliding across a workpiece resulting in a loss of material. The study of abrasive wear concentrates largely on 3 types of wear modes most commonly observed [34]. These include ploughing, wedge formation and cutting as shown in Figure 2.4.4.1. Other work has classified different modes or variations on those listed above [35], but the extremes of the wear behaviour are classified by ploughing and cutting of the antagonist material.

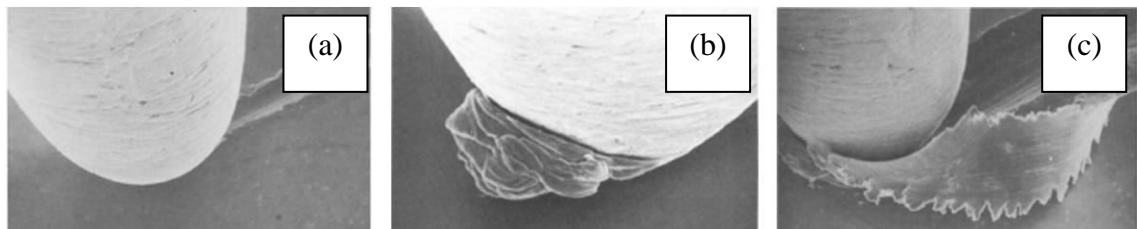


Figure 2.4.4.1 Image of different abrasive wear modes for single point scratch testing after Hokkirigawa and Kato [34]; (a) Ploughing, (b) Wedge Formation & (c) Cutting.

Research exploring the different modes of wear and the reasons for their occurrence are primarily identified through the use of scratch tests. There are many types of scratch tests which vary in their application. Wang and Subhash [36] discuss the varying forms of tests from the basic sliding test to the rotating/pendulum setup. It is stated that the rotating test duplicates most realistically the interaction between a grinding grit medium and a workpiece. The varying depth of the cutting tip into the work material replicates the effects of changing micro hardness and attack angle between the grit and the workpiece. Using scratch testing methods, the modes of wear can be identified and

distinguished. A useful parameter in the classification of these modes is discussed by Kato [37] as the degree of penetration (D_p) of a single point scratch pin into the workpiece material. How the pin penetrates into the material determines what wear mode develops. The higher the value of D_p the more cutting as opposed to ploughing is performed by the pin and vice versa. The equation for D_p is detailed in equation (2.4.1):

$$D_p = \frac{h_a}{a} \quad (2.4.1)$$

Where h_a = Depth of penetration

a = radius of the single point scratch pin

Hokkirigawa and Kato [34] perform a number of scratch experiments using different materials and tooling geometries. The rig consisted of a Scanning Electron Microscope (SEM) to provide optical outputs of the wear modes and strain gauges to monitor force. The higher the D_p value the more cutting is observed as shown in Figure 2.4.4.2. The further an abrasive tip penetrates into a workpiece material, the more cutting occur as a result of the interaction. The work uses a rotating test piece with the abrasive pin applied like a lathe tool. A more accurate representation of a single grit contact is shown by Vingsbo and Hogmark [38] in their development of a pendulum grooving test. A carbide pin in the shape of a pyramid was used to represent an abrasive grain. The grinding energy rapidly decreased with an increase in material removal which is equivalent to a larger value of D_p corresponding with increased cutting in the contact zone.

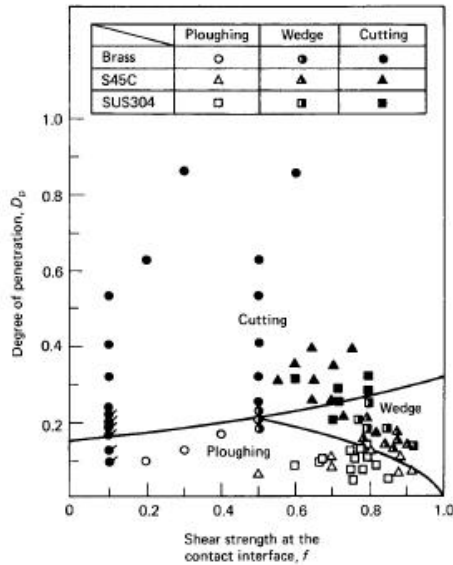


Figure 2.4.4.2 Image of showing wear map and associated wear modes related to degree of penetration D_p from Hokkirigawa and Kato [34].

The penetration depth is analogous to a grinding parameter presented by Helletsberger [4]. The parameter is defined as a ratio of removed material thickness $h_{cu,eff}$ to grain penetration depth h_{ce} as detailed in Figure 2.4.4.3(a). The parameters $h_{cu,eff}$ and h_{ce} are detailed graphically in Figure 2.4.2.1. This relationship and the chip formation depth influence whether material is removed or deformed in the contact zone. A high amount of material removal compared to material deformation is classed as a high efficiency grinding process. The criterion is summarised in Figure 2.4.4.3(b). This shows that an efficient grinding process is also promoted when; the friction between the wheel and workpiece is high, the grain cutting edge radius r_G and wheel diameter D_{eq} is small, the cutting edge entry angle η is steep, the wheel speed V_s/V_c is high or the more brittle the workpiece material.

$$(a) \frac{h_{cu,eff}}{h_{ce}} = \text{function} \left(\frac{h_{cu}}{r_G}, \text{penetration angle } \eta, \text{friction, } v_C, \text{flow behaviour of the material} \right)$$

Efficiency of the grinding process		Chip formation depth T_μ	$\frac{h_{cu,eff}}{h_{ce}}$	Friction grain-material	r_G D_{eq}	η	v_C S	Workpiece
is	High	Small	High	High	Small	Steep	High	Brittle
	Low	High	Low	Low	Large	Flat	Low	Tougher / more ductile

Figure 2.4.4.3 Efficiency of the grinding process according to Helletsberger [4]; (a) Relationship of removed material thickness $h_{cu,eff}$ to grain penetration depth h_{ce} & (b) Table detailing impact of parameters on the efficiency of the grinding process.

The grain shape can impact the efficiency of the grinding process as discussed in section 2.4.1. Barge et al [39] performed some single cutting edge analysis using a milling insert with a large negative rake angle in a pendulum scratch test setup. The scratch test was performed using a number of different cut depths and cutting tool speeds. It is a useful paper as it identifies different wear mechanisms associated with individual grains under varying conditions. A further example is presented by Steffens and König [40] who show analytically that friction and ploughing are reduced with high grain penetration. In addition, the ratio of normal to tangential force for an individual cutting edge is reduced with higher values of chip thickness indicating reduced rubbing and ploughing. Nguyen and Butler [41] also consider the effect of rake angle on whether a grain would cut or plough. The numerical simulation provides useful results in predicting the surface topography of a workpiece surface but the work does not detail how this relates to the mechanics of the process. Fang [42] details a study considering the effect of rake angle on chip machining. Using negative rake tools, it was found that as the rake angle becomes less negative, the cutting force increased and the thrust/normal force on the tool decreased. The sharper the grain interface, the increased amount of cutting is promoted in the tool/workpiece interaction. This is an important reason why the grinding wheels are constantly reconditioned through dressing processes to maintain sharp cutting edges which reduces the heat effects from the grinding process.

In addition to the grain shape, the grinding wheel/cutting tool speed has a significant influence on the mechanics of the process. The wheel speed directly affects heat generation in the cut zone which is generated due to the internal and external friction arising from elastic and plastic deformations, as well as the shearing and cutting action. Tawakoli shows how the contact zone temperature increases with wheel speed [43]. This would make it easier to cut the material reducing the forces experienced and is confirmed by Barge et al [39]. This is reinforced by Cai et al [44] using both single grit and heavy grinding experiments. It is proposed that increased heat in the contact zone causes softening of the material making it easier to machine.

The summation of the individual abrasive grain interactions determines the mechanical and thermal heat effects experienced during a grinding process. The material removal mechanism generates the forces and energy from the grinding process. This can be affected by the shape and distribution of the abrasive grains and the process parameters applied. This is important to consider when investigating the relationship between chip thickness and the process outputs, as other factors can be responsible for changes in the grinding outputs besides chip thickness.

2.4.5 Tribology Techniques in Grinding Research

The study of the material removal process for an individual cutting edge considers the interaction between the abrasive grain and the workpiece. Tribology is the science of interacting surfaces and is closely linked with grinding. As a result, it is useful to understand what additional tools and techniques from tribology research can be utilised to complement grinding research. The application of single grit scratch testing has been outlined above but other techniques have been utilised in the field of grinding research.

A useful method is the pin on disc test utilised by Abbasi et al [45] as shown in Figure 2.4.5.1. A standard pin on disc trial utilises a rotating metal disc with a hardened pin applied at a known force. Pin on disc tests investigate friction behaviour between the pin and the metallic surface. In addition, the wear

behaviour of the contact is investigated. Figure 2.4.5.1 shows the modified pin on disc test using a grinding wheel as the rotating media with metal shaped pins applied under known loads. The horizontal forces can be measured for a known applied vertical force allowing calculation of the friction coefficient/force ratio in grinding. This particular test setup is utilised to test the wear behaviour between different metal alloys. Klocke et al [46] used a pin on disc tribology test to investigate the grinding process. The results detail the change in friction coefficient and wear behaviour at different applied loads on the grinding contact.



Figure 2.4.5.1 Image of a pin on disc setup using a rotating grinding wheel and metal pin from Abbasi et al [45].

The tribology of the grinding contact is important but is difficult to investigate in isolation of the complicated chip formation process. The pin on disc test has been shown in the literature to provide an alternative test to investigate grinding parameters in constant load, flat contact conditions without the complexity of peripheral grinding kinematics.

2.5 Grinding Energy and Surface Integrity

Creep feed grinding exhibits high force and energy requirements in comparison to other chip machining processes. As almost all of the energy generated in a grinding process turns to heat, which can lead to potential workpiece burn, this can have a significant impact on the surface integrity of a component. The following section outlines specific grinding energy (SGE), its relationship to

surface integrity and methods of temperature measurement used to evaluate heat partition to the workpiece.

2.5.1 Specific Grinding Energy and Heat Flux

Specific grinding energy (SGE) is the amount of energy required to remove a specific volume of material. The heat flux is the flow of heat energy through a specific area in a set period of time. Specific energy in grinding is large compared to other machining processes [6] due to the large amount of rubbing and deformation combined with material removal. The specific grinding energy e_c can be calculated using the net power from the grinding spindle or the horizontal grinding force measured from the process as detailed in equations (2.5.1) and (2.5.2) respectively. Equation (2.5.2) which uses horizontal force in its calculation is presented for surface grinding applications but its applicability to creep feed grinding is not known. The heat flux q_t is shown in equation (2.5.3).

$$e_c = \frac{P_{Net}}{v_w \cdot b \cdot a_e} \quad (2.5.1)$$

$$e_c = \frac{F_h \cdot V_s}{v_w \cdot b \cdot a_e} \quad (2.5.2)$$

$$q_t = \frac{P_{Net}}{l_c \cdot b} \quad (2.5.3)$$

Chip thickness is related to the specific grinding energy both in standard machining and in grinding. The relationship presented by Shaw [6] is defined in equation (2.5.4). In metal cutting, n is approximated around 0.2 with a value between 0.8 and 1.0 for grinding.

$$u \approx \frac{1}{t^n} \quad (2.5.4)$$

Where $u = e_c$ Specific Grinding Energy (J/mm^3)

$t =$ Grinding Chip Thickness (mm)

$n =$ Constant

This relationship is highlighted by Shaw [32] when plotting specific grinding energy versus maximum chip thickness as shown in Figure 2.5.1.1. However, the larger values of chip thickness correspond with an increase in productivity. Therefore the reduction in specific grinding energy could be due to either a change in chip thickness or productivity. A number of examples follow this trend for Steel material. Wenfeng et al [47] witnesses the same power law relationship when grinding a Nickel based superalloy.

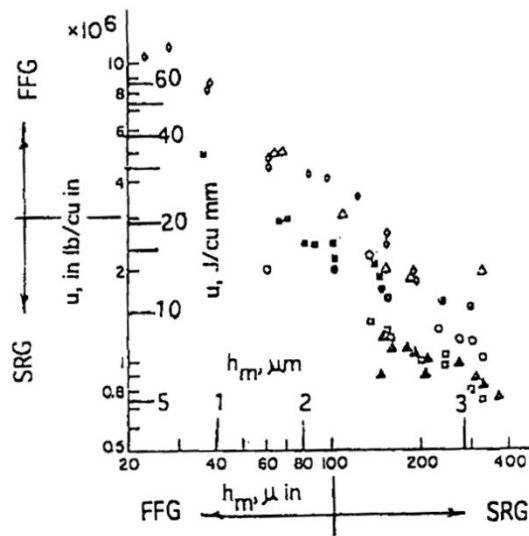


Figure 2.5.1.1 Graph of specific grinding energy versus chip thickness for grinding of steel alloys taken from Shaw [32].

The specific grinding energy is also related to productivity within the grinding literature. Bell [48] and Stephenson and Jin [49] suggest the use of the power law relationship detailed in equation (2.5.5).

$$e_c = \frac{A}{Q_w^n} \quad (2.5.5)$$

Where $Q'_w = \text{Material removal rate} / \text{Productivity}$
 $A, n = \text{Constants}$

It is shown through experimentation that e_c reduces towards a minimum constant value with an increase in productivity as shown in Figure 2.5.1.2 conforming to the power law relationship detailed in equation (2.5.5). This is considered for creep feed grinding moving into HEDG conditions at the higher grinding wheel speeds.

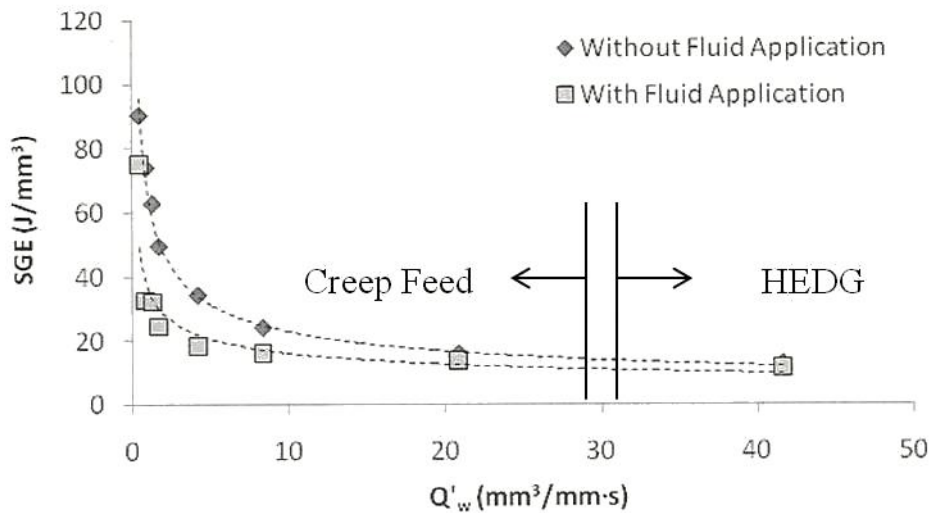


Figure 2.5.1.2 Graph of e_c versus Q' for HEDG grinding of steel taken from Bell [48].

Specific grinding energy is an important parameter as it provides an indication of the heat generated in the contact zone. It is also a useful method of comparison between different grinding processes describing how efficient a particular setup is at removing material. It is stated that SGE is dependent on both chip thickness and productivity. However, the examples found in the literature do not test the variation of SGE with chip thickness in isolation of productivity. Therefore it is unclear which parameter has the greater effect on the specific grinding energy. This gap in the literature will be investigated in this thesis.

2.5.2 Energy Partition

The energy generated during a grinding process is primarily converted to heat. The heat is partitioned to 4 areas within the grinding system. Jin et al [50] considered the 4 main attributes of the system where the heat flux generated during the cutting process can be partitioned. These include the workpiece, grinding wheel, cutting fluid and chips as shown in Figure 2.5.2.1.

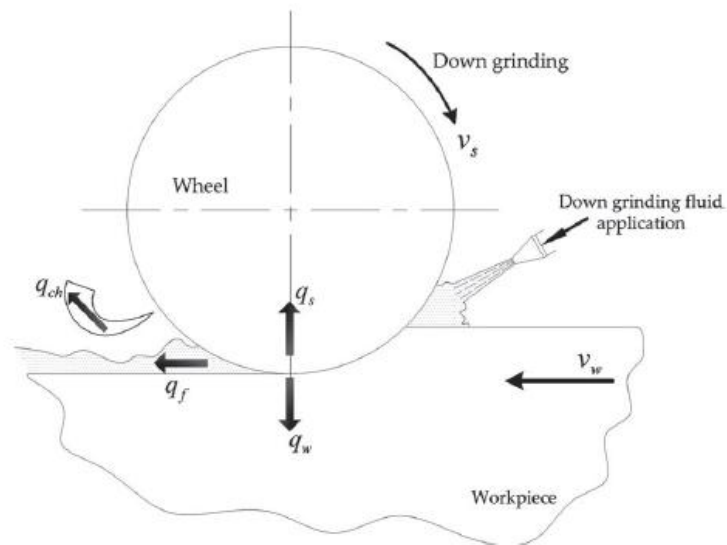


Figure 2.5.2.1 Diagram detailing the areas of heat partitioning in the grinding system by Mohamed et al [51].

Each of the partitions has a heat transfer coefficient which is dependent on a number of material and operational parameters. The total heat flux is detailed in equation (2.5.6) with each heat partition calculation shown in equations (2.5.7 – 2.5.10). According to the equations presented, the amount of heat partitioned is dependent on the heat transfer coefficient and the temperature produced in the cut zone. The amount of heat partitioned to the grinding chips is dependent on the chip temperature. These temperatures are dependent on the material being ground and the cutting conditions applied.

$$q_t = q_w + q_s + q_f + q_{ch} \quad (2.5.6)$$

$$q_w = h_w \cdot T_{max} \quad (2.5.7)$$

$$q_s = h_s \cdot T_{max} \quad (2.5.8)$$

$$q_f = h_f \cdot T_{max} \quad T_{max} \leq T_b \quad (2.5.9)$$

$$q_{ch} = h_{ch} \cdot T_{ch} \quad (2.5.10)$$

Where q_w = heat flux to workpiece material (W/mm²)

q_s = heat flux to grinding wheel (W/mm²)

q_{ch} = heat flux to grinding chips (W/mm²)

q_f = heat flux to cutting fluid (W/mm²)

Where h_w = convection coefficient for material workpiece (W/m²K)

h_s = convection coefficient for grinding wheel (W/m²K)

h_{ch} = convection coefficient for grinding chip (W/m²K)

h_f = convection coefficient for cutting fluid (W/m²K)

Although the energy produced in grinding is large, only the amount partitioned to the workpiece is detrimental [12]. Malkin and Guo [52] wrote a detailed paper providing a thermal analysis of the grinding process. The heat partition to the workpiece material is approximately 90% for conventional surface grinding processes. Conversely, although the specific grinding energy in CFG processes is high compared to surface grinding, there is little evidence of corresponding thermal damage on the workpiece surface. This is due to the cooling effect of fluid at the grinding zone in creep feed grinding applications resulting in a large amount of heat being partitioned to the cutting fluid. As a result for creep feed grinding, the paper quotes very low workpiece energy partitions from 1.3% to 5.4% for carbon steel, with even lower values predicted for Nickel based alloys. However, the cooling effect from the cutting fluid can become ineffective at certain temperatures due to the film boiling effect. This is where the fluid begins to boil and creates an insulated micro layer of air between the contact zone and cutting fluid inhibiting the flow of heat away from the cut zone. This can lead to large amounts of heat partition to the workpiece material resulting in component burn.

The application of cutting fluid is critical to controlling the amount of heat that enters the workpiece in creep feed grinding. Pu et al [53] displays the huge increase in workpiece temperature from around 120°C to over 900°C when the cutting fluid application is insufficient to the contact zone. Webster et al [54] and [55] highlights the significant influence the cutting fluid application in CFG has on the surface quality of ground material through experiments varying the amount of fluid applied to the cut zone. Increased fluid supply provides improved surface integrity of the workpiece material.

2.5.3 Residual Stress and Metallurgical Damage

Large values of specific grinding energy result in high values of heat flux and temperature within the cut zone. Large amounts of heat can lead to metallurgical damage and can produce negative residual stress conditions within ground components [56]. It can also change the microstructure and surface hardness of the workpiece material to an undesired state. The majority of grinding processes result in compressive residual stress in the surface due to the large forces generated. However, this section considers the effect of abusive conditions, that when not controlled, can lead to the damage explained above.

Chen and Rowe [57] state that low tensile residual stress is very important in ground components. If high tensile residual stresses remain, the service life of a component may be reduced through the mechanisms of fatigue or corrosion. Huang and Ren [58] showed that surface roughness and residual stress had a significant influence on fatigue life behaviour. Reduced tensile residual stress from machined coupon experiments correlated with increased fatigue life of the component. Tensile stress is generated through heating and cooling at the surface. The rise in workpiece temperature in grinding depends on how much heat enters the workpiece material [57]. This is related to the amount of energy generated during the process. It is generally thought that reduced values of e_c would lead to improved residual stress conditions as seen by Zhang et al [59]. However, Fathallah et al [60] showed that tensile residual stress reduced with increasing e_c . This highlights the importance of energy partitioning. The residual stress in a component is dependent on the amount of heat flux passing into the

material not necessarily the overall amount of energy generated during the process. Maintaining consistent values of specific grinding energy and ratios of heat partitioning is important in preventing component damage. This is highlighted by Stephenson et al [61] when investigating burn threshold diagrams, where small increases in SGE can initiate burn in the workpiece surface.

2.5.4 Temperature Measurement

The strong relationship between heat partitioned to the workpiece and the effect on surface integrity highlights the importance of being able to measure the surface temperature during a grinding process. Knowledge of the surface temperature provides the means of understanding if a process is detrimental to a component irrespective of energy consumption. However, the measurement techniques are complicated in most material removal operations caused by lack of access to the cutting zone and in a number of cases the addition of cutting fluids. This section details the prominent techniques used in the measurement of surface temperature in grinding operations.

Temperature measurement has been researched extensively in numerous engineering scenarios. Recent review papers by Komanduri and Hou [62] and Davies et al [63] provide information in significant detail on the numerous techniques available. These include thermocouples, infra-red techniques, thermal paints, metallography and materials of known melting temperatures. The selection of the appropriate technique is application specific and dependent on factors including temperature range, signal properties, size, cost and ease of use.

The thermocouple technique of measuring temperature has been utilised since the 1920's [63]. It is a junction between 2 different metals that produces a voltage due to a temperature difference. The simplicity and low cost of the technique means it has been utilised significantly in various grinding applications. Focusing on creep feed applications, Kim et al [64] used a single k-type thermocouple placed at the end of a single hole to measure temperature beneath the ground surface. This same technique was repeated by Guo and Malkin [12] advancing further the work on heat flux and energy. Multiple cuts were taken above the

thermocouple with each getting nearer to the sensor. This gave temperature distributions at varying depths under the ground surface with the pass 0.25mm above considered as the surface temperature. Having the temperature at varying depths is important in trying to obtain a value for the surface temperature. Knowing this, Jin and Stephenson [65] created an angle test piece, see Figure 2.5.4.1, using multiple thermocouples to obtain the temperatures at different depths for an individual grinding pass. This method is more efficient with respect to cuts required and provides more accurate data on the temperature distribution.

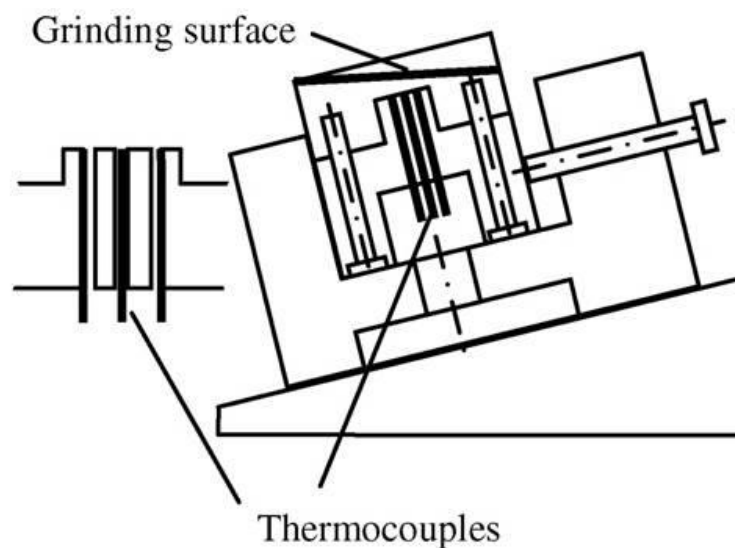


Figure 2.5.4.1 Diagram of inclined thermocouple test piece with replaceable top hat test piece as used by Jin and Stephenson [65].

The thermocouple technique is the preferred option for this thesis due to cost and the large amounts of cutting fluid that inhibit techniques like infra-red imaging. Other suitable techniques include metallography and materials of known melting temperature. The most effective use of these techniques in grinding is with Physical Vapour Deposition of pure metals as used by Kato and Fuji [66]. The work shows good results but the manufacture of multiple test pieces using this technique is not economic.

2.6 Chip Thickness in Grinding

The grinding chip is the individual piece of material produced through the grain interaction with the workpiece in the contact zone. It is during this process that

the mechanical and thermal outputs of the process are generated. The thickness of the grinding chip is determined from tooling geometry and applied process parameters. It is widely understood that the chip thickness has a significant impact on the magnitude of the mechanical and thermal outputs of the process. Maintenance of grinding chip thickness has been identified as a potential method for achieving greater control of the outputs from the grinding process. This section explores the prominent models associated with chip thickness in grinding and investigates the impact of chip thickness on the grinding process outputs.

Numerous chip thickness models have been developed for grinding. The majority of them are detailed in the review papers by Snoeys et al [67] and Tonshoff et al [68]. Both reviews detail the models developed for basic kinematic equations and maximum undeformed chip thickness. These are the 2 principle approaches taken towards describing chip thickness in grinding. The maximum undeformed chip thickness considers a single cutting edge in forming a comma shaped chip whereas the other parameters consider the ratio of material being removed to the grinding wheel speed. The derivations for each method of chip thickness estimation are detailed in this section.

2.6.1 Grinding Chips

Material is removed in grinding through multiple small chips. This results in many different types of grinding chips being produced within the contact zone at any one time. Konig et al [69] states that to understand the outputs of the grinding process a knowledge of the kinematics is required reaffirming the premise of this thesis. This includes the grain distribution in the wheel and the kinematic factors of the contact conditions. It details simulation work that shows the various cut paths and chip thicknesses performed by the different grinding grains as detailed in Figure 2.6.1.1. It also details that the process parameters have a key interaction on whether grains perform material removal or merely rub the workpiece surface. Although a useful piece of work, it highlights the fact that there are many sizes of chip which makes the process of chip thickness calculation in grinding very time consuming.

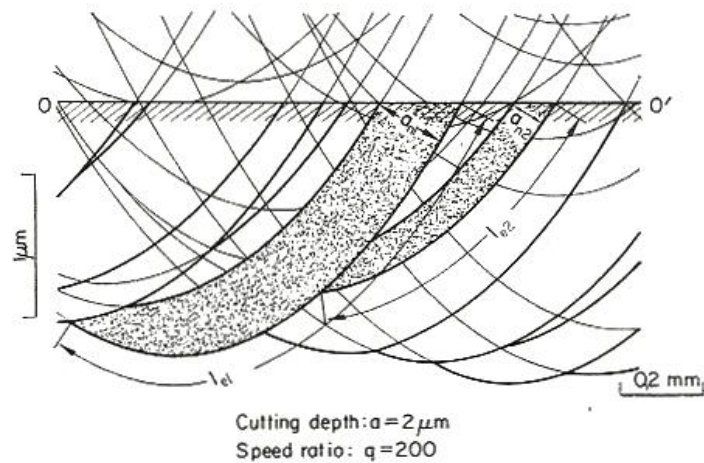


Figure 2.6.1.1 Image of simulated cutting paths of grinding grains showing variation in chip sizes for different grains [69].

Due to the huge variation in chip thicknesses over the numerous different abrasive grains present in the contact zone, many different types of chip can be formed during the cutting process. Tso [70] performed research into chip types produced in grinding. Many different types of chip were identified including knife, slice, ripping, shearing and flowing; each type is detailed visually in the paper. The optimum type in relation to process performance was a flowing style chip as seen in Figure 2.6.1.2. Interestingly, the type of chip produced altered the measured force from the process highlighting the relevance of the theory presented in section 2.4. The chip type was dependent on the material, wheel type and process inputs although only the variation in wheel type and cutting fluid application was presented in the results.

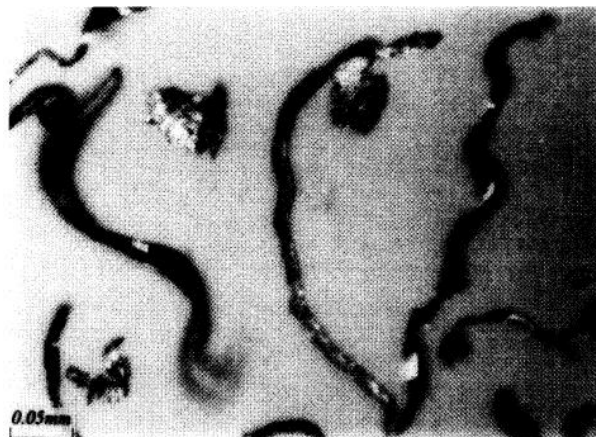


Figure 2.6.1.2 Image of flowing style chip witnessed in grinding of Inconel 718 by Tso [70].

This section highlights that the chips produced in grinding vary considerably and it can be hard to estimate the geometry. In addition, there are difficult to measure physically. This is due to the stochastic nature of the abrasive grains in the wheel structure. The principal chip thickness models in the literature make assumptions to the grain distribution in the wheel structure to create models estimating chip thickness. It would be very difficult to consider each grain individually and create a viable model for application. The models presented in the following sections represent the principal equations used in grinding.

2.6.2 Undeformed Chip Thickness

Early chip thickness models in grinding were developed from comparing the process to milling and assuming the cutting points are equally spaced around the wheel periphery. Many examples of original attempts to model the undeformed chip thickness are detailed in the paper by Snoeys et al [67]. The following derivation is taken from Malkin [5] with the idealised grain cutting path detailed in Figure 2.6.2.1. The setup shown details a down grinding setup with both the wheel and table velocities acting in the same direction.

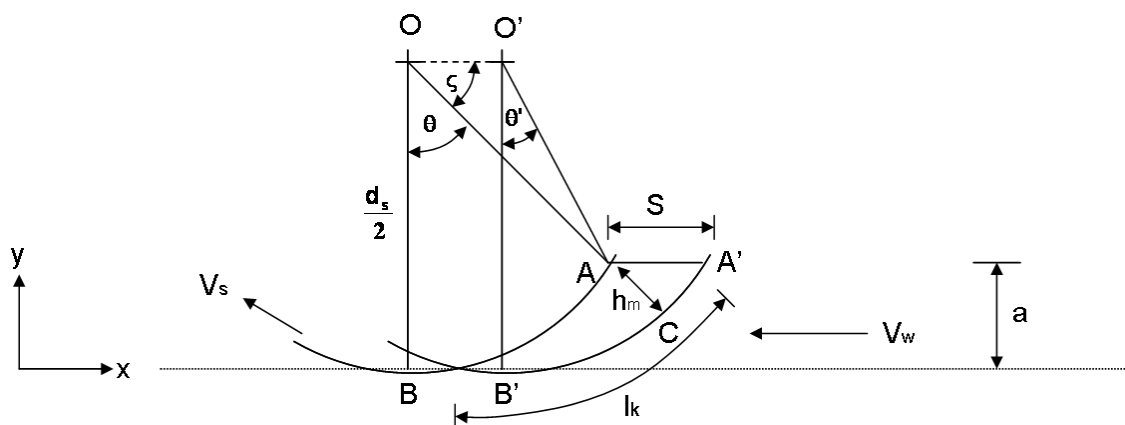


Figure 2.6.2.1 Diagram of theoretical individual grain cutting path.

The first significant parameter to consider is the Feed per Cutting Point, S . This is estimated by calculating the time it takes for a single cutting edge/abrasive grain to pass through its cutting arc of contact between B' and A' . This assumes a grain is in cut for the entirety of the arc length. The distance travelled in the

feed direction, S , is calculated with equation (2.6.1). This parameter is analogous to the feed per tooth parameter utilised in milling [71].

$$S = v_w \cdot t_{res} \quad (2.6.1)$$

Where $t_{res} = \frac{l_k}{v_s}$ = residence time of abrasive grain in contact arc (s)

The maximum undeformed chip thickness, h_m , is defined as the maximum depth of cut that an individual abrasive grain experiences during cutting. The physical size is dependent on a number of factors including grain shape and distribution, but the theoretical distance detailed in figure 2.6.2.1 is used for this derivation. The cutting path is approximated by circular arcs moving a linear distance as a result of the table feed.

The value of h_m is calculated from resolving the distance:

$$h_m = O'C - O'A = \frac{d_s}{2} - O'A \quad (2.6.2)$$

Through trigonometry and substituting for the S parameter detailed in (2.6.1):

$$h_m = 2 \cdot S \cdot \frac{a_e}{d_s}^{\frac{1}{2}} = 2 \cdot S \cdot \frac{a_e}{d_e}^{\frac{1}{2}} = 2 \cdot L \cdot \frac{v_w}{v_s} \cdot \frac{a_e}{d_s}^{\frac{1}{2}} \quad (2.6.3)$$

Where L = distance between cutting edges (mm)

The value of L is calculated from grinding wheel information based on the number of cutting points per unit area. The number of cutting points around any line of the wheel periphery K can be calculated:

$$K = C \pi \cdot d_e \cdot b_c = \frac{\pi \cdot d_s}{L} \quad (2.6.4)$$

Where C = number of cutting points per unit area of wheel ($1/\text{mm}^2$)

b_c = chip width (mm)

Resolving to find L and calculating the chip width b_c in relation to the maximum chip thickness, the value of h_m is defined as:

$$h_m = \frac{4}{C \cdot r} \frac{v_w}{V_s} \frac{a}{d_s}^{\frac{1}{2}} \quad (2.6.5)$$

Where r = ratio of chip width to thickness

The values of C and r are calculated using information related to wheel specification and grinding parameters. Work performed by Gopal and Rao [72] incorporates a stiffness ratio between the wheel and workpiece to further improve the accuracy of chip thickness in predicting surface roughness. The equation defined in (2.6.5) is the form that will be evaluated for providing improved control of the process in this research.

2.6.3 Equivalent Chip Thickness

Equivalent chip thickness h_{eq} , was introduced by the CIRP grinding committee as a basic parameter that includes the dominant grinding parameters of material removal rate and grinding wheel speed as described by Snoeys et al [67]. It is based on the principle of continuity between the material removed from the workpiece and the conversion to a representative amount of grinding chips. This is the key principle of the h_{eq} model and is detailed in Figure 2.6.3.1.

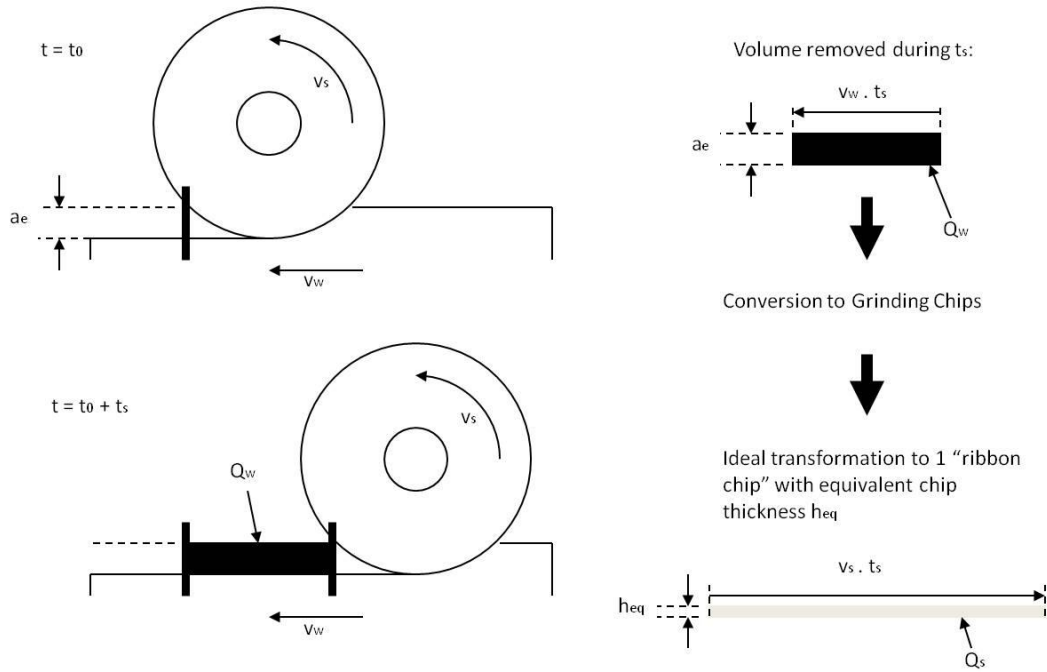


Figure 2.6.3.1 Diagram illustrating the principle of equivalent chip thickness h_{eq} taken from Helletsberger [4].

The derivation of the formula follows the procedure detailed in the figure above. The volume of material Q_w removed during a discrete time period is detailed in (2.6.6):

$$Q_w = a_e \cdot v_w \cdot t_c \cdot b = Q_s \quad (2.6.6)$$

The equation assumes an ideal transformation of all workpiece material cut during the process into one idealised ribbon shape chip which is defined by the grinding wheel parameters.

$$Q_s = Q_{eq} = h_{eq} \cdot V_s \cdot t_s \cdot b \quad (2.6.7)$$

Through this assumption the definition of the equivalent chip thickness is described by (2.6.8)

$$h_{eq} = \frac{a_e \cdot v_w}{v_s} = \frac{a_e}{q} = \frac{Q'_w}{V_s} \quad (2.6.8)$$

As the amount of material being removed increases, an increase in V_s is required to maintain the value of h_{eq} . This is analogous to rolling processes in material fabrication where higher roller speeds are required to cope with a greater reduction in material size through the roller assembly.

2.6.4 Chip Thickness Ratio

The chip thickness ratio (CTR) is an industry driven parameter that is introduced by Bond [1] as an internal Rolls-Royce method of process control when grinding aerospace parts. It states that grain life and component burn are governed by the arc of contact and the chip thickness it experiences. Maintenance of these parameters should provide control over the mechanical and thermal characteristics of the process. CTR works by considering the Maximum Normal Infeed Rate (MNIR) which was introduced by Andrew et al [8] and detailed in Figure 2.6.4.1.

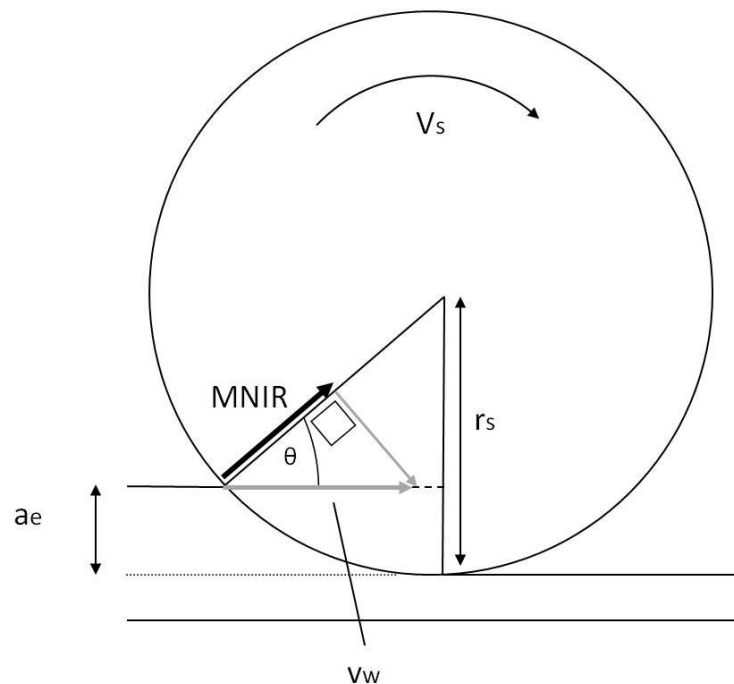


Figure 2.6.4.1 Diagram illustrating MNIR principle taken from Bond [1].

The value of CTR utilises the relationship between MNIR and the grinding wheel speed. MNIR is a measure of how much the grinding wheel plunges into the workpiece material and can be calculated from equation (2.6.9).

$$MNIR = v_w \cdot \cos \theta \quad (2.6.9)$$

The value of θ is calculated through geometry:

$$\theta = \sin^{-1} \frac{r_s - a_e}{r_s} \quad (2.6.10)$$

The value for CTR is the ratio of MNIR to grinding wheel speed as detailed in (2.6.11).

$$CTR = \frac{MNIR}{v_s} \quad (2.6.11)$$

Typically, application of this means the wheel velocity must increase as the wheel reduces in diameter to maintain CTR, which is analogous to h_m . This would also be the case for an increase in productivity.

2.6.5 Effect of Chip Thickness on the Grinding Process

There are many methods and models associated with chip thickness in grinding as detailed above. In order to use chip thickness as a potential method for improved control in a grinding system, it is important to understand the effects of varying this parameter on the outputs of the process. Snoeys et al [67] introduced the equivalent chip thickness h_{eq} parameter and also presented a grinding chart showing the impact of h_{eq} on the process outputs. An example of the grinding charts is detailed in Figure 2.6.5.1. It shows an increase in force with an increase in h_{eq} . In addition, there is an increase in the surface roughness and a decrease in the G ratio of the process as h_{eq} is increased.

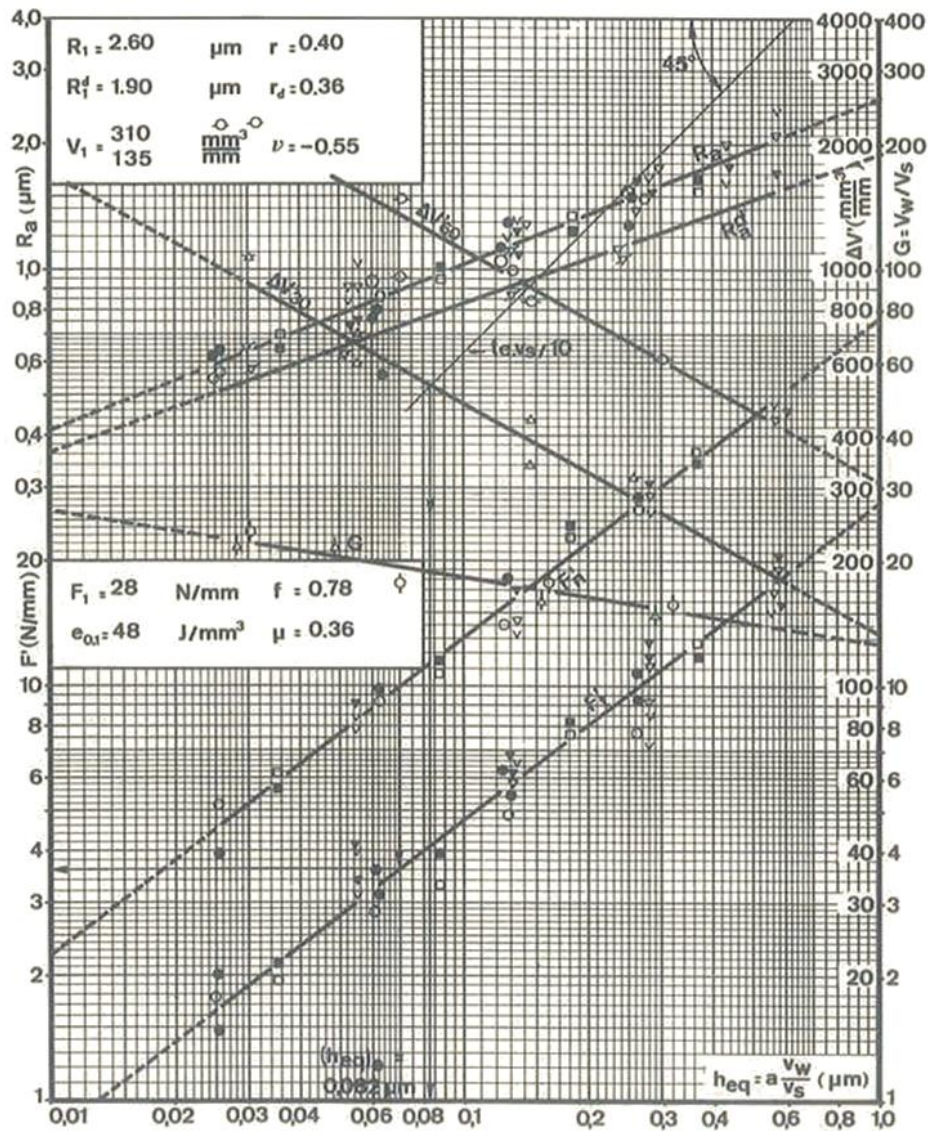


Figure 2.6.5.1 Image of grinding charts relating process outputs to equivalent chip thickness by Snoeys and Peters [67].

Brinksmeier and Glwierzew [73] also test the h_{eq} value whilst investigating chip formation for a face grinding application. They obtained specific grinding energy data at different wheel speeds for a constant value of equivalent chip thickness. The same procedure is then repeated at a number of different h_{eq} values as shown in Figure 2.6.5.2. The workpiece feed rate is adjusted to maintain h_{eq} at the different grinding wheel speeds. The results showed that for a constant value of h_{eq} an increase in wheel speed produced a lower value of specific grinding energy. However, the productivity increases with the grinding wheel speed even at a constant value of h_{eq} . The specific grinding energy follows the same behaviour as detailed in section 2.5. In addition, the specific grinding energy also

decreased with an increase in the value of h_{eq} . It was concluded that both the chip thickness and wheel speed have an impact on the chip formation mechanism with an increase in both promoting increased cutting conditions in the contact zone. Although useful, the data was obtained on Steel material and at low grinding speeds which is not equivalent to the grinding processes investigated in this thesis.

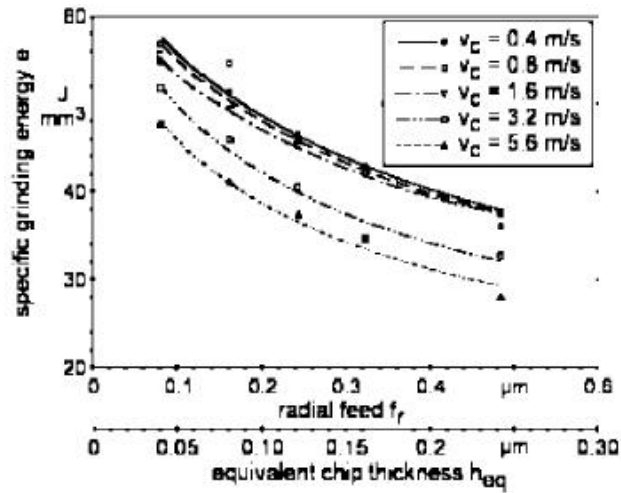


Figure 2.6.5.2 Graph of specific grinding energy e_c versus equivalent chip thickness h_{eq} for varying grinding wheel speeds taken from Brinksmeier and Glwierzew [73].

Chip thickness is closely linked to productivity in grinding as the calculation for each shares the main grinding parameters of workpiece feed rate and depth of cut. To investigate the impact of chip thickness on process outputs it is important to find examples in the literature where either the chip thickness or productivity is changed in isolation of the other. Brinksmeier and Glwierzew [73] witnessed the trend of reduced specific grinding energy for increased chip thickness h_{cu} at constant velocity when performing a single grit experiment in the same paper as above. Again this struggles with the same issue that productivity changed as well as chip thickness. Tang et al [74] isolates the effect of chip thickness for a constant productivity cut. A reduction in grinding forces is noticed when increasing wheel speed for constant productivity. Aurich et al [75] provides useful results when investigating grinding using defined pattern tools. The experimentation is performed at a constant value of productivity at different depths of cut. The workpiece feed rate is decreased accordingly to maintain the productivity value. The average chip thickness reduced as the depth of cut

increased due to an increased number of abrasive grains in contact for identical material removal rate. Results are presented for different wheel types and cutting fluid applications. Interestingly, for dry grinding the spindle power and forces remained almost constant at the different depths of cut showing that constant productivity appeared to keep the process outputs at similar values. The reduction in chip thickness did not appear to affect this. The power and force increased when cutting fluid was used but this is related to increased mechanical requirements from drawing fluid through the contact zone.

Fathallah et al [60] perform surface grinding experiments at different wheel speeds whilst maintaining a maximum grain depth of cut. This is equivalent to a maximum undeformed chip thickness value. The results show that an increase in wheel speed for constant chip thickness resulted in more tensile residual stress. This indicates that the contact zone temperature increases at higher wheel speeds although a change in the cutting fluid conditions is identified as the cause. Again this work does not isolate chip thickness from productivity. The affect of wheel speed on specific grinding energy was considered by Heinzl and Bleil [76] when looking at using the size effect in grinding for work hardening in metal surfaces. Face grinding experiments show that specific grinding energy increases significantly at lower wheel speeds for constant chip thickness. This is a result of increased ploughing at the lower wheel speeds. Interestingly, this results in better residual stress effects on the surface which is indicative of increased plastic deformation as opposed to surface heating resulting in softening effects. Again productivity changes with the application of different wheel speeds.

Looking at the effect of chip thickness for creep feed applications, Huang [77] showed that the specific force increases with maximum chip thickness combined with a reduction in specific grinding energy. However, this is for machining of ceramic material. Other examples of an increase in productivity reducing specific grinding energy are shown by Sekine et al [19] and Maeda et al [78]. These both consider Inconel material. Shang et al [79] confirmed the trend of a reduction in force with chip thickness for constant productivity in a creep feed application.

The majority of the literature investigates parameters in isolation such as wheel speed, productivity or chip thickness. Obviously other aspects of the cut zone are changing at the same time and it is hard to track these variations. This is notable in the literature above where it is difficult to assess if maintaining chip thickness does maintain process outputs. Table 2.6.5.1 summarises the input parameters and the effect on process outputs from the literature above to clarify the interrelationships witnessed. The literature clearly shows that the specific grinding energy is closely related to productivity and that the chip thickness has a significant impact on the force output from the process.

Work Reference	Application Type	Inputs	Effect on Output
Brinksmeier and Glwierzew [73]	Face Grinding	$h_{eq} - \text{Constant}$ $Q' - \uparrow$	$e_c - \downarrow$
	Single Grit Testing	$h_{cu} - \text{Constant}$ $Q' - \uparrow$	$e_c - \downarrow$
Tang et al [74]	Surface Grinding	$h_m - \downarrow$ $Q' - \text{Constant}$	$F - \downarrow$
Aurich et al [75]	Dry Surface Grinding	$h_m - \downarrow$ $Q' - \text{Constant}$	$P - \text{Constant}$ $F - \text{Constant}$
Fathallah et al [60]	Surface Grinding	$h_m - \text{Constant}$ $Q' - \uparrow$	Increase in tensile residual stress
Heinzel and Bleil [76]	Face Grinding	$h_m - \text{Constant}$ $Q' - \uparrow$	$e_c - \downarrow$
Sekine et al [19]	Creep Feed Grinding	$h_m - \uparrow$	$e_c - \downarrow$
Maeda et al [78]		$Q' - \uparrow$	$F - \uparrow$
Shang et al [79]	Creep Feed Grinding	$h_m - \downarrow$ $Q' - \text{Constant}$	$F - \downarrow$

Table 2.6.5.1 Table detailing effect of changing chip thickness and productivity on process outputs for various literature sources.

A number of tests are performed looking at changing wheel speed, depth of cut or workpiece feed rate. The values of chip thickness and productivity change when these parameters are varied. There is no test that specifically looks at the maintenance of productivity and chip thickness for different geometry wheels in order to assess if process outputs can be better controlled. This highlights the opportunity to explore this research idea further within this thesis.

2.6.6 Summary of Grinding Chip Thickness Models

There are a number of methodologies for estimating chip thickness in grinding as detailed in this section. Table 2.6.6.1 provides a summary of the main models in the literature for future reference in this thesis.

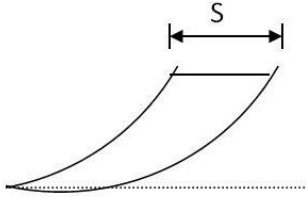
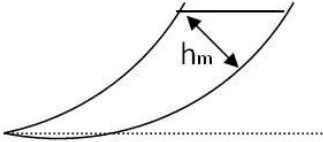
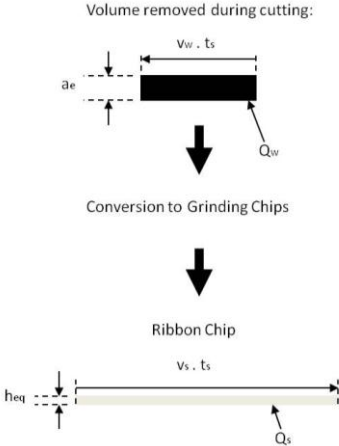
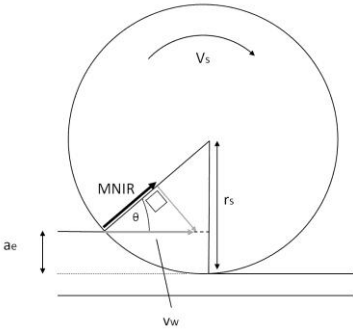
Name	Notation	Chip Thickness Geometry	Equation
Feed per Cutting Point	S		$S = v_w \cdot t_{res}$
Undeformed Chip Thickness	h_m		$h_m = \frac{4}{C \cdot r} \frac{v_w}{V_s} \frac{a_e}{d_e}^{\frac{1}{2}}$
Equivalent Chip Thickness	h_{eq}	<p>Volume removed during cutting:</p>  <p>Conversion to Grinding Chips</p> <p>Ribbon Chip</p>	$h_{eq} = \frac{a_e \cdot v_w}{V_s} = \frac{Q'_w}{V_s}$
Chip Thickness Ratio	CTR		$CTR = \frac{MNIR}{V_s}$

Table 2.6.6.1 Table summarising the prominent chip thickness models utilised in the grinding process.

2.7 Summary and Hypothesis

The literature review has generated a number of questions to investigate with respect to the relationship between chip thickness and the outputs of the grinding process. The review begins with an introduction to grinding with specific reference to the Creep Feed application. The challenges presented in creep feed grinding are due to the large forces and temperatures generated as a result of the large contact area between the wheel and workpiece as described by Werner [11]. Wear associated with the use of conventional abrasive tooling results in significant changes in wheel geometry through the loss of radial form and dressing. Limited work has been performed investigating the effect of this change in wheel geometry on the grinding outputs.

An introduction to the chip formation process of an individual abrasive grain is presented when considering the tribology of the grinding process. The outputs from the grinding process are the summation of individual grain interactions and the review presents the effects of penetration depth [34] and wheel speed [39, 44] on the chip formation mechanism. Testing is performed using single grit interactions and shows the increased cutting action of a grain at higher penetration depths and grinding wheel speeds.

Specific grinding energy and the subsequent heat flux is introduced including the partition heat sinks present in the grinding system. Work by Shaw [32] and Jin & Stephenson [33] identify that the majority of heat in the creep feed grinding process is transferred to the cutting fluid. The amount of energy and where it transfers can have significant impact on the surface integrity of ground components as shown by Huang and Ren [58]. Control of the specific grinding energy is very important in grinding applications combined with an understanding of the workpiece surface temperatures to avoid damage to a component. An inclined thermocouple method for temperature measurement developed by Jin and Stephenson [65] is presented as a useful technique for use in cutting trials.

The review is concluded with an introduction of the prominent chip thickness models including equivalent chip thickness h_{eq} [67] and undeformed chip thickness h_m as presented by Malkin [5]. An evaluation of the effect of chip thickness on the grinding process is investigated for both h_{eq} by Brinksmeier and Glwierzew [73] and h_m by Tang et al [74]. Changes in the specific grinding energy and force are noticed with changing chip thickness but these are combined with changes in productivity. This leaves a gap in the knowledge with respect to isolating the effect of chip thickness from productivity and using this to improve control of the process outputs for changing wheel geometry.

The thesis therefore considers the following questions with respect to the literature review:

- Does changing wheel diameter have a significant impact on the grinding process outputs for a constant productivity application
- What impact does chip thickness have on the grinding process in isolation of productivity especially in relation to specific grinding energy that can be detrimental to the surface integrity of ground components
- Are the common chip thickness models useful in providing improved control over the process outputs for a creep feed grinding application

Chapter 3 - Methodology

This chapter introduces the equipment, experimental methodology and data collection techniques utilised to obtain data used to answer the research questions presented in Chapter 2 of this thesis. The section also includes details of preliminary work and statistical analysis which assisted in refining the main research work performed.

3.1 Experimental Equipment

Section 3.1 introduces the equipment utilised in the research. This encompasses the machine tools and associated tooling used in the grinding trials. The 2 machines used include a Blohm Profimat 412 located at the Tyrolit R&D centre in Schwaz, Austria, and a Makino A99 located at the Advanced Manufacturing Research Centre (AMRC) in Rotherham, UK. The Blohm machine tool was utilised during a 3 month sabbatical to the Tyrolit R&D centre which constituted the preliminary work, detailed in section 3.2, performed for this thesis. The Makino A99 was included in the research as it uses smaller grinding wheel sizes that provided better conditions for the main experiments. The reasoning for this is explained further in section 3.2. As a result, the Makino A99 was utilised in the experiments that produced the results detailed in Chapters 4 and 5. Both platforms are capable of providing Creep Feed grinding conditions.

The grinding wheels and associated conditioning materials were provided by the abrasive wheel manufacturer, Tyrolit. Aluminium Oxide grinding wheels were selected due to their suitability for grinding Inconel 718 material. In addition, Aluminium Oxide applications typically deal with large changes in wheel diameters during grinding operations. How the outputs of the grinding process vary as a result of the change in wheel diameter is a key question in this research.

3.1.1 Blohm Profimat 412

The Blohm Profimat 412 is a 3-axis grinding machine capable of performing both surface and creep feed operations. Figure 3.1.1.1 shows the machining area

inside the machine tool. Creep Feed grinding uses a 2-nozzle cutting fluid setup; a cutting fluid nozzle for applying flood conditions to the contact zone and a jet cleaning nozzle providing a scrubbing action on the wheel. The cutting fluid nozzle applied 120 l/min of cutting fluid at 10 bar with the cleaning nozzle providing 30 l/min at a pressure of 17 bar. In addition, the figure details the continuous dress (CD) diamond dresser roll and workpiece attached to the force dynamometer.

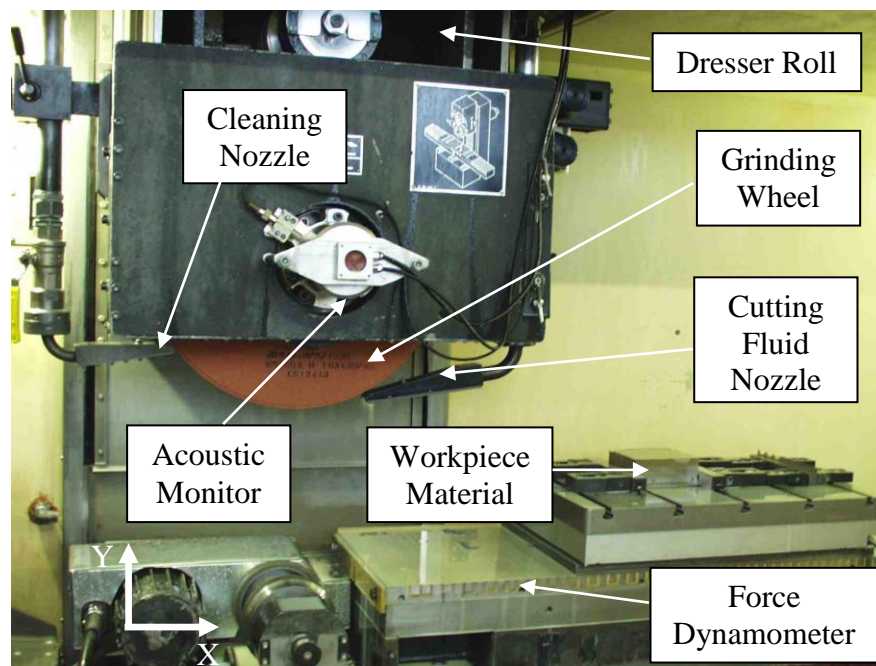


Figure 3.1.1.1 Internal view of Blohm Profimat 412 grinding machine envelope including cutting fluid nozzle and dynamometer setup.

The machine manufacturer's specification is detailed in Table 3.1.1.1.

Parameter	Specification
X-Axis Travel	1320mm
Y-Axis Travel	535mm
Z-Axis Travel	250mm
X-Axis Feed Rate	20 – 25000mm/min
Y-Axis Feed Rate	1 – 2000mm/min
Z-Axis Feed Rate	1 – 4000mm/min
Spindle Speed Range	30 – 3000rpm
Spindle Power	92kW
Grinding Wheel Diameter Range	350mm – 500mm

Table 3.1.1.1 Table detailing Blohm Profimat 412 machine specifications.

The machine was retrofitted with a spindle load sensor providing a reading of the spindle power to an oscilloscope at the side of the machine tool. In addition, an acoustic emission sensor was fitted to establish when contact occurs between the dressing roll and the grinding wheel. This output is also displayed on the oscilloscope. The machine tool utilises water based synthetic cutting fluid from a 1000 litre tank. The specification of which is detailed in section 3.1.5.

3.1.2 Makino A99

The Makino A99 is a converted 5-axis milling platform that has been built to include continuous dress VIPER grinding capability. VIPER grinding is defined by a Rolls-Royce patent and relates to a grinding process undertaken with a high pressure, high flow rate cutting fluid nozzle setup. Figure 3.1.2.1 shows the machine tool and the typical grinding setup including CD diamond dresser roll and programmable Pressure Cutting fluid Nozzle (PCN). The machine is capable of providing cutting fluid up to a flow rate of 150 l/min at 100 bar. A flow rate of 120 l/min at a pressure of 15 bar was applied in this experimentation to represent creep feed grinding conditions.

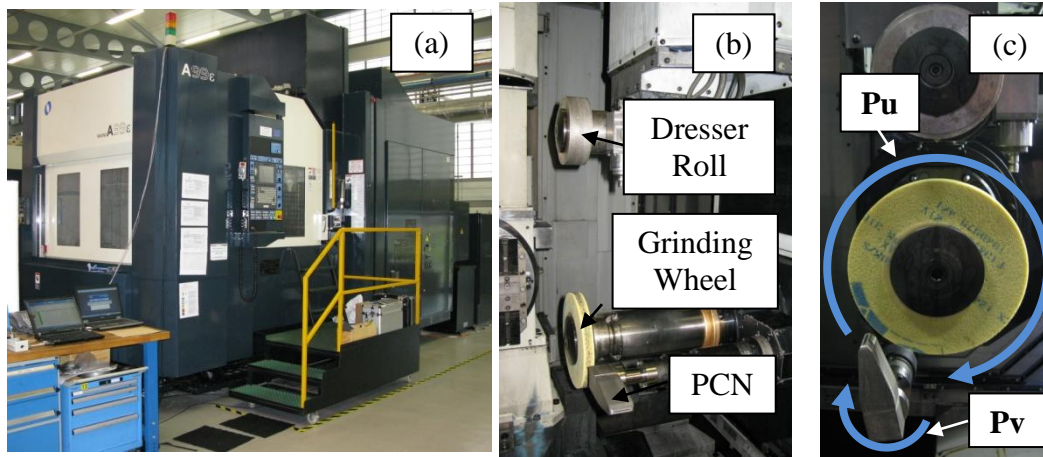


Figure 3.1.2.1 Makino A99 Machine Tool; (a) Image of Machine Exterior, (b) Internal machine envelope including Grinding Wheel, Dresser Roll and Pressure Cutting fluid Nozzle (PCN) Setup (c) Pressure Cutting fluid Nozzle axis setup and available movement.

The specification of the machine tool is detailed in Table 3.1.2.1.

Parameter	Specification
X-Axis Travel	1250mm
Y-Axis Travel	1100mm
Z-Axis Travel	1250mm
A-Axis Travel	0deg – 360deg (continuous rotation)
B-Axis Travel	-90deg – 180deg
U-Axis Travel	350mm
Pallet Size	320mm x 320mm
Rapid Feed Rate	50000mm/min
Cutting Feed Rate	1 – 50000mm/min
Jog Feed Rate	1 – 8000mm/min
Spindle Speed Range	20 – 10000rpm
Spindle Power	45kW
Grinding Wheel Diameter Range	150mm – 300mm

Table 3.1.2.1 Table detailing Makino A99 Machine Specifications.

Customized features on the Makino A99 include the programmable Pressure Cutting fluid Nozzle (PCN) unit which allows accurate placement of the cutting

fluid nozzle with respect to the grinding wheel. This system can move independently around 2 axes, Pu and Pv, which are detailed in Figure 3.1.2.1(c). This allows flexible and repeatable placement of the cutting fluid nozzle in relation to the cut zone which is important in providing consistent input conditions to the grinding process. Another customized element is the CD capability of the machine tool. This machine also uses water based cutting fluids which are provided from a 4000 litre tank. The large tank size allows the provision of cutting fluid at high flow rates.

3.1.3 Aluminium Oxide Grinding Wheels

This work utilises Tyrolit Aluminium Oxide grinding wheels for the research performed. The 2 types of wheel used in the thesis are the XA60-E13-VPR (VIPER) and F13A70-66-21V (STRATO) specifications shown in Figures 3.1.3.1(a) and 3.1.3.1(b) respectively.

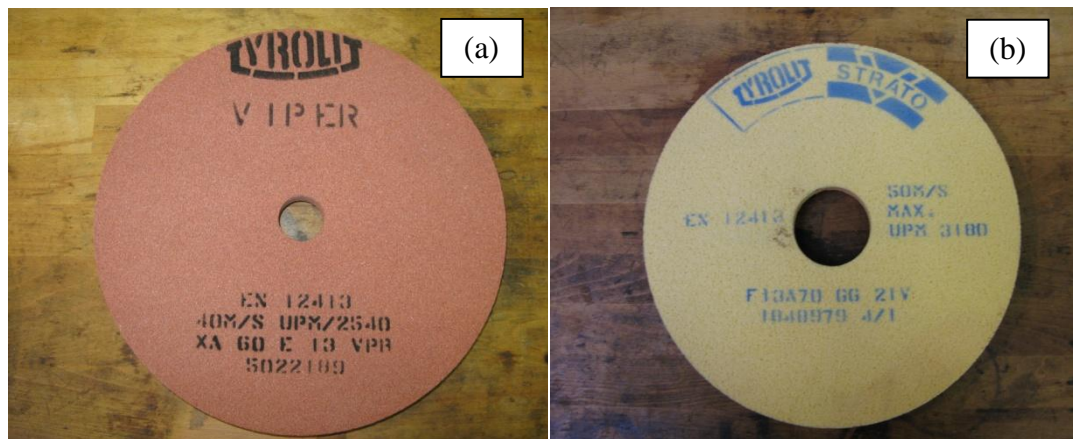


Figure 3.1.3.1 Tyrolit Aluminium Oxide Grinding Wheels; (a) VIPER Specification, (b) STRATO Specification.

These types of grinding wheels were utilised because of the link to aerospace applications where they are used extensively. In addition, this thesis is based around understanding chip thickness in relation to improving the control of process outputs, and these types of grinding wheels have high friability resulting in the requirement for frequent dressing cycles. This results in large changes in wheel diameter which is desired for the experiments included in this thesis.

Aluminium Oxide is a conventional abrasive grain type. The high friability makes it suitable for tough materials where wheel clogging can occur. The ability for the grain to fracture easily allows fresh cutting grains to be exposed more readily. Both the VIPER and STRATO wheels utilised are similar in composition. The specifications include a vitrified bond structure with a 60 abrasive grit size. Even though the STRATO specification states a 70 grit size on the product code, Tyrolit have confirmed that it is actually a 60 grit wheel and product codes can vary according to manufacturer. Although the 2 wheel types are similar, the VIPER specification grinding wheel has a slightly increased bond strength allowing for greater porosity in the wheel structure which allows improved fluid application to the contact zone to maximise the effect of the patented VIPER process. This could lead to variation in the magnitude of response outputs between the different experiment setups when using different tooling. However, each experiment is performed using a single wheel allowing trend behaviour to be established whilst minimising the effect of changing wheel topography and performance.

The VIPER specification grinding wheel was utilised in the preliminary grinding experiments performed at the Tyrolit R&D facility detailed in section 3.2. The STRATO specification was utilised in the experiments performed on the Makino A99; the methodology for these experiments are detailed in sections 3.4 and 3.5. The reason for the difference in tooling setups was due to availability of the wheels at the respective locations. In addition, the VIPER specification grinding wheel provided reduced radial wheel wear for the non CD experiments detailed in section 3.2. The CD experiments performed on the Makino A99 displayed more stable cutting conditions using the STRATO specification.

3.1.4 Conditioning the Grinding Wheel

As mentioned in section 3.1.3, Aluminium Oxide grinding wheels require regular reconditioning. This is performed through dressing with a diamond dresser roll as shown in Figure 3.1.4.1. Both the Blohm and Makino machine tools utilised the same dresser roll specification. Each of the dresser tools utilised were considered to be in good operating condition under visual observation.



Figure 3.1.4.1 Side view of flat form diamond dresser roll used for dressing the Aluminium Oxide grinding wheels.

The dresser roll incorporates a layer of diamond electroplated in a nickel bond around a steel core. The roll is rotated and fed onto the grinding wheel at set parameters. The dressing parameters utilised in these experiments are detailed in Table 3.1.4.1.

Parameter	Value
Dress Ratio	0.8
Dress Direction	Same direction / Synchronous
Dress Infeed Rate	0.1 $\mu\text{m}/\text{rev}$

Table 3.1.4.1 Table of dressing parameters for diamond roll on Aluminium Oxide wheel.

The parameters were selected to provide wheel topography suitable for creep feed grinding [80]. The dressing parameters and tooling were constant for both machine tools. Both the Blohm Profimat 412 and Makino A99 have the capability to grind using either non-CD or CD processes.

3.1.5 Cutting Fluid

Both of the machine tools utilised fully synthetic cutting fluids. Processes utilising conventional AlOx wheels typically use water based fully synthetic fluids to maximise the effect of cooling in the contact zone.

The Blohm profimat utilised Rhenus R-Flex cutting fluid at an applied concentration of 4%. The Makino A99 utilised a Houghton product HOCUT 768. This again was a synthetic emulsion applied in the machine at 5% concentration. The data sheets for both cutting fluids are available in appendix A of this thesis.

3.2 Experimental Development – How to evaluate the effect of chip thickness?

Section 3.2 investigates the best method to evaluate the effect of chip thickness on the grinding process. This includes experimental work and presentation of results which were obtained at Tyrolit's R&D centre in Schwaz, Austria. These results have been included in the methodology as they provide important lessons learnt for the experiment presented in Chapter 4.

3.2.1 The Difficulties in Testing the Effect of Chip Thickness

This thesis focuses on furthering the knowledge of the relationship between chip thickness and the outputs of the grinding process. This is considered for constant productivity for the reasons identified in Chapter 2. The majority of investigation into the effect of chip thickness on process outputs has been combined with changes in productivity. It is unknown if changes in the process outputs are due to variation in productivity or chip thickness.

Utilising a constant productivity process makes it more challenging to provide an experiment with a range of chip thickness values. Equation (3.2.1) details the undeformed chip thickness as presented by Malkin [5] and defined in Section 2.6. The equation contains multiple terms that affect the kinematics of the contact zone. These apply to 3 broad categories including the wheel topography, the speed ratio between wheel and workpiece and distances that affect the size of the contact arc including depth of cut and grinding wheel diameter.

$$h_m = \underbrace{\frac{4}{C \cdot r}}_{\text{Wheel Topography}} \underbrace{\frac{v_w}{V_s}}_{\text{Speed Ratio}} \underbrace{\frac{a_e}{d_s}}_{\text{Contact Arc}}^{\frac{1}{2}}^{\frac{1}{2}} \quad (3.2.1)$$

Changes in any of these terms affect the value of calculated undeformed chip thickness. The effects of changing each parameter detailed in equation (3.2.1) are shown in relation to the productivity Q' and the chip thickness value h_m in Table 3.2.1.1. Green colouring indicates an increase in the value of Q' or h_m, yellow represents an unchanged value and red shows a decreasing value.

Parameter	Effect on Productivity Q'		Effect on Chip Thickness h _m	
	If Increased	If Decreased	If Increased	If Decreased
C	N/A	N/A	Smaller	Larger
r	N/A	N/A	Smaller	Larger
V _w	Higher	Lower	Larger	Smaller
V _s	N/A	N/A	Smaller	Larger
a _e	Higher	Lower	Larger	Smaller
d _s	N/A	N/A	Smaller	Larger

Table 3.2.1.1 Table of parameters used in the calculation of undeformed chip thickness and effects of changing the parameter values on the productivity Q' and undeformed chip thickness h_m.

For a constant productivity process, the only parameters that can be utilised to provide a change in chip thickness include those associated with the wheel topography, the grinding wheel speed and wheel diameter. It is understood that productivity can also be maintained by changing the table feed and depth of cut at the same time but this results in a variation in the total amount of material removed. This would have an additional impact on the process outputs and makes it more difficult to isolate the pure effect of varying chip thickness.

As 1 grinding wheel will be used for each experiment, an assumption was made that C and r remain constant with a change in grinding wheel diameter. Measurement of the wheel topography at all the varying wheel diameters would be difficult to perform and very time consuming. This would not be viable for the experiments planned and the use of the same grinding wheel at different wheel diameters reduces the impact of changing wheel topography. This leaves only 2 parameters available to alter the value of h_m in a constant productivity process, the grinding wheel diameter and the wheel speed.

3.2.2 Preliminary Setup and Method

With consideration to Section 3.2.1, a preliminary experiment was planned in order to assess the method of testing using changing grinding wheel diameter to create different chip thickness conditions for a constant productivity process. The work was performed on the Blohm machine tool detailed in section 3.1.1 using the VIPER tooling and dressing parameters outlined in sections 3.1.3 and 3.1.4 respectively. Blocks of Inconel 718 material, 130mm in length and 90mm width, were utilised for the testing and mounted on the dynamometer detailed in Figure 3.2.2.1.

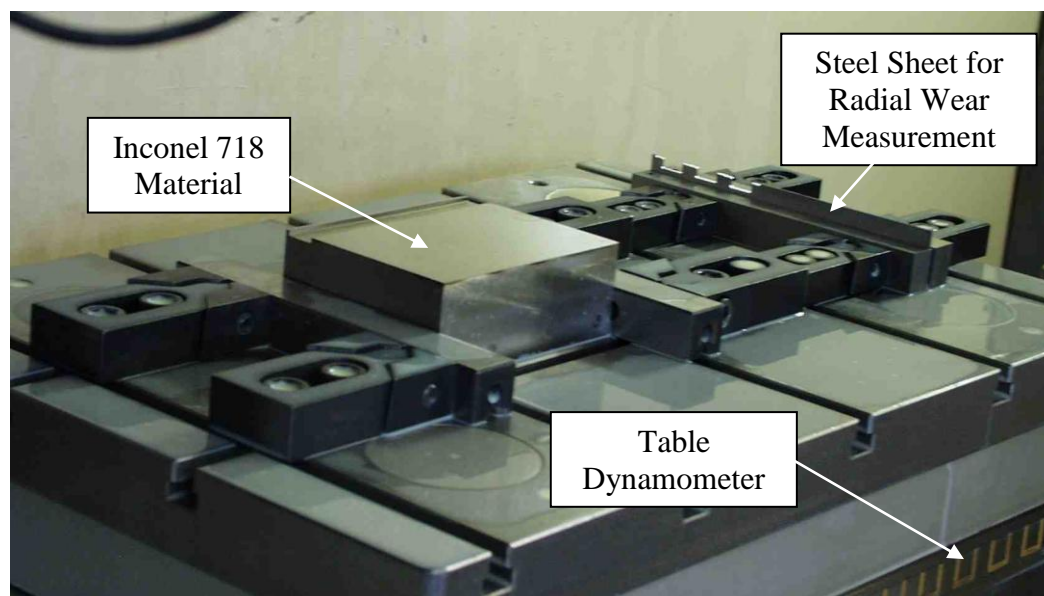


Figure 3.2.2.1 Experimental setup on Blohm machine tool detailing Inconel 718 material and steel sheet for tool wear measurement.

Using the 2 available parameters to vary chip thickness with constant material removal, the experiment was designed to use the grinding wheel at varying diameters. This has additional benefit as it represents the operational life of a grinding wheel in a production environment. The experiment outline and run order is detailed in Table 3.2.2.1. This shows the wheel being tested at various wheel diameters which are defined as experimental blocks. For any defined grinding wheel diameter, the wheel speed is altered in order to provide a constant value of undeformed chip thickness h_m . The values of C and r which represent the wheel topography are estimated and maintained for the experiment. The number of cutting points per unit area C , was estimated at 0.93 from data provided by Helletsberger [4] for the wheel specification provided. It is understood that this value may vary between wheel specifications and different areas of the grinding wheel, however the accurate assessment of wheel topography is very time consuming and complicated. An assumption is made to use a consistent value of C for all calculations in this thesis with the potential variation in wheel surface topography minimised through the use of a single wheel for each experiment performed. The ratio of chip width to thickness r , was defined as 1. This assumes an equilateral triangle chip cross section, as shown in Malkin [5], although it is understood that this will vary between abrasive grains and as a result of wear on the grinding wheel.

The experiment is defined in order to examine whether the process outputs are maintained over the life of the wheel by applying constant values of chip thickness. This hypothesis is tested for 3 experiment variables which include; up or down cutting, CD or Non-CD wheel conditioning and high or low productivity arranged in each block using a factorial design. The same cut types defined by the experimental variables are performed in each experimental block. The only variation in the cut parameters is the change in grinding wheel speed to maintain the value of chip thickness h_m . Block 1 represents the wheel diameter at its maximum limit (500mm), Block 2 describes the middle diameter size range (425mm) and Block 3 represents the wheel at its minimum operational diameter (350mm). The cuts within an experimental block are performed at grinding wheel diameters as close to the ranges specified in Table 3.2.2.1 as possible. The high and low productivity cuts maintain different values of h_m for the various

experimental blocks. A full table of cuts performed is detailed in Appendix B. The grinding wheel is dressed on the machine tool to the desired diameters. The wheel surface is refreshed through a short dress cycle before each cut is performed within an experimental Block. The setup and order was chosen so that an individual grinding is used for all the cuts performed to minimise the effect of different wheel topography.

Run Order	Variables			Parameters		
Blocks	Grinding Direction	Dressing Type	Q' (mm ³ /s/mm)	Feed Rate (mm/min)	Depth of Cut (mm)	Wheel Speed (m/s)
1 (500mm wheel diameter range)	Up	Non-CD	35	1050	2	36
	Up	CD	35	1050	2	
	Up	Non-CD	60	1200	3	
	Down	Non-CD	35	1050	2	
2 (425mm wheel diameter range)	Up	Non-CD	35	1050	2	Variable Use Chip Thickness Calculation to maintain h_m
	Up	CD	35	1050	2	
	Up	Non-CD	60	1200	3	
	Down	Non-CD	35	1050	2	
3 (350mm wheel diameter range)	Up	Non-CD	35	1050	2	Variable Use Chip Thickness Calculation to maintain h_m
	Up	CD	35	1050	2	
	Up	Non-CD	60	1200	3	
	Down	Non-CD	35	1050	2	

Table 3.2.2.1 Table detailing the experimental run order for preliminary grinding tests.

Figure 3.2.2.2 details a flow diagram of the experimental method. The grinding process represents each cut performed. The inputs remain constant for each cut include the grinding wheel, its pre-dressing conditioning and the process parameters governing material removal rate. The value of the current grinding wheel diameter is entered into the chip thickness equation and the wheel speed V_s is calculated to maintain the value of h_m for the first cuts performed in Block 1. Other factors that may affect the process outputs are monitored or controlled to improve the reliability of the experiment.

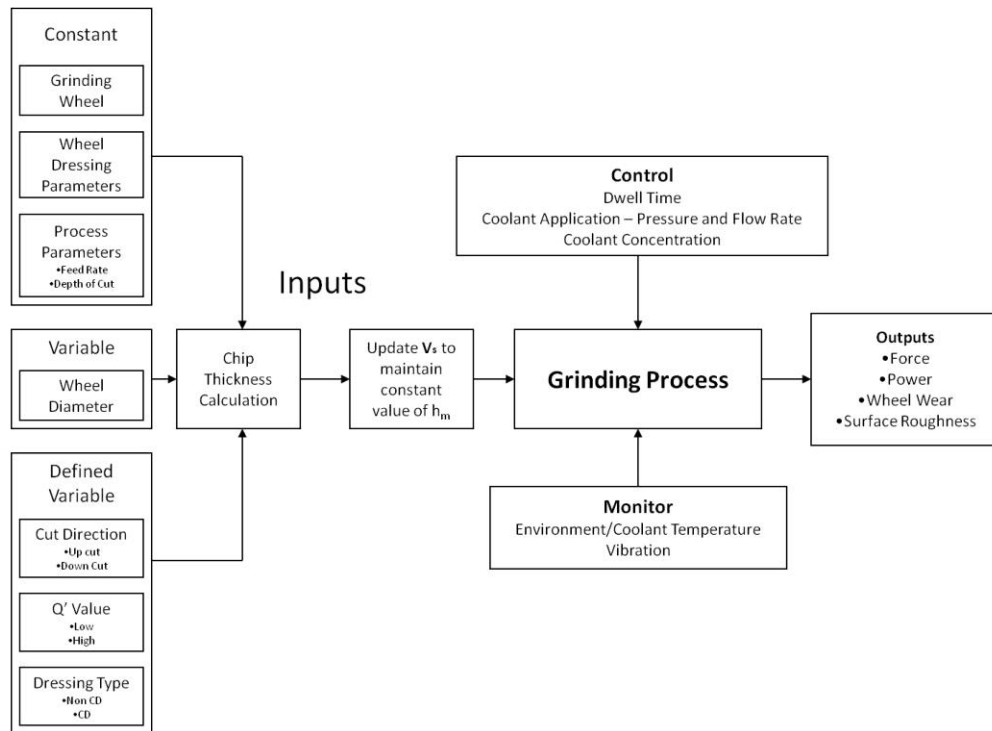


Figure 3.2.2.2 Image displaying experiment flow diagram describing the process for selecting parameters for each grinding cut performed in the preliminary tests.

The cutting fluid nozzle was set to a known position of 2mm above the cut surface and the fluid flow applied at an angle of 10° to the machine x-axis. This was adjusted with a change in grinding wheel diameter to ensure consistency for all the cuts performed. In addition, the cutting fluid concentration was monitored daily and modified if required to ensure consistency in the experiment.

The outputs from the grinding process provide the data to establish if maintaining a constant value of h_m . A Kistler dynamometer and oscilloscope is utilised to collect the feed and normal force data. Both the average and maximum outputs are recorded. The power reading in kW is taken directly from the machine tool spindle using a hall effect monitor and recorded in the oscilloscope.

The wheel wear is defined as any loss of grinding wheel radius during a grinding cut, not as a result of the dressing procedure. It is measured against a referenced wheel profile as shown in Figure 3.2.2.3. A freshly dressed tool provides a reference cut in a steel sheet of 3mm thickness. Another cut is performed in the steel sheet after each grinding cut and before the wheel is re-dressed, to establish

the difference in tool radius as a result of the grinding process. The surface roughness is measured using a profilometer at multiple points along the cut length for each grinding cut performed.

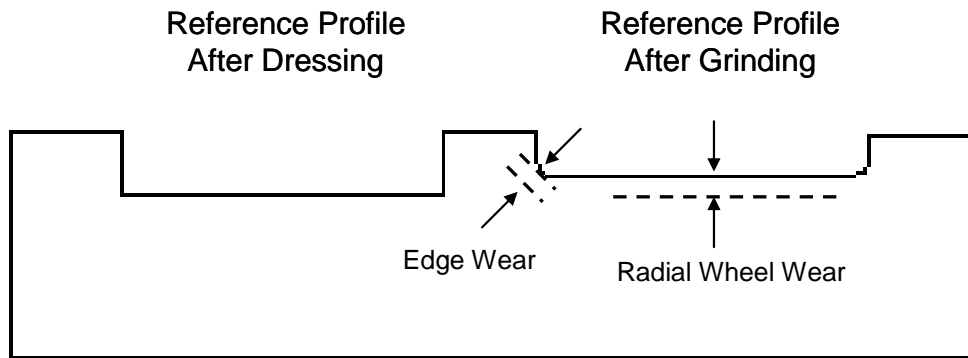


Figure 3.2.2.3 Diagram illustrating the technique and definition of tool wear for the preliminary grinding testing.

3.2.3 Preliminary Grinding Test Results

Figures 3.2.3.1 to 3.2.3.4 detail the results from the preliminary grinding tests. All the graphs display wheel radius on the abscissa. The values on the abscissa are reversed to show the change in process outputs from a large to a small diameter grinding wheel. The graphs presented all utilise identical labelling for the legend. The cut direction is denoted by Up or Down. The high value of productivity is labelled Q'60, the low value by Q'35 and continuous dress cuts are labelled CD.

Figure 3.2.3.1 details the specific grinding energy e_c calculated from equation (2.5.1) utilising the spindle power outputs from the experiment. The "Up Q'35" cut displays a flat trend line with the other Non-CD cuts showing slight increases in power at reduced wheel diameters. The down cut produces a lower value of e_c for the same productivity and appears to have less variation in the results. The value of e_c when using CD increases as the wheel reduces in diameter. A significant reduction in the specific grinding energy is apparent when the productivity of the process is increased.

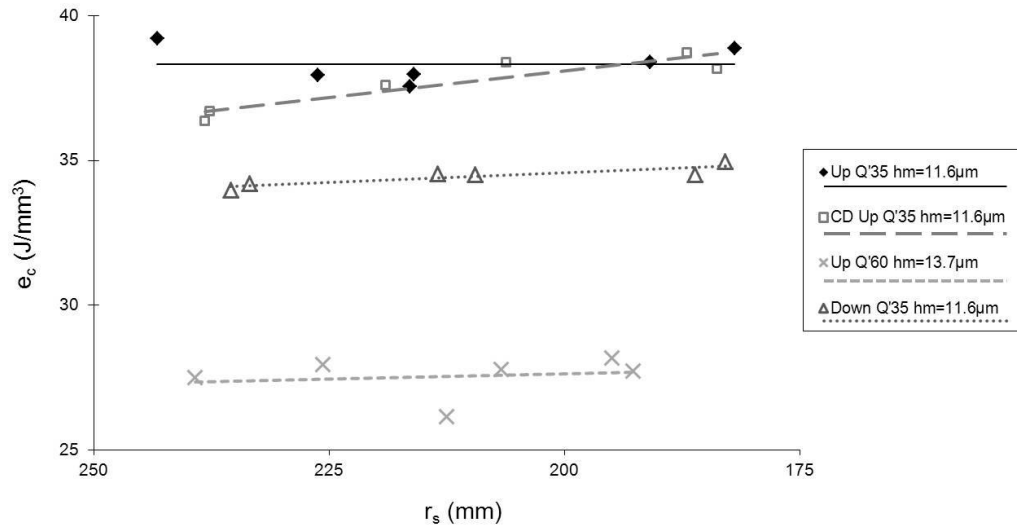


Figure 3.2.3.1 Specific Grinding Energy versus Grinding Wheel Radius for constant chip thickness h_m for the different grinding cuts performed.

The vertical force results are presented in Figure 3.2.3.2. All the results reduce in value as the wheel reduces in size. The high productivity cuts provide higher vertical forces in comparison to the low productivity results. Both the application of CD and down cutting direction provides lower vertical forces.

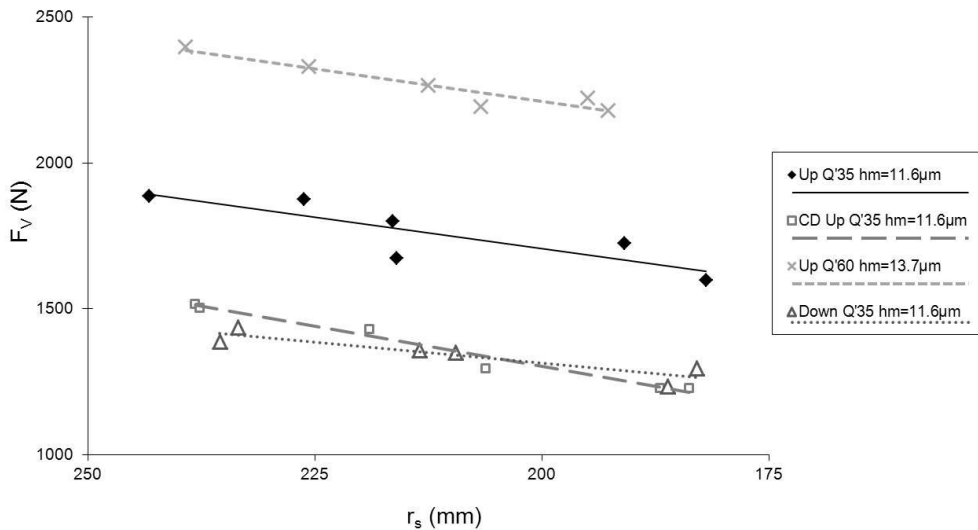


Figure 3.2.3.2 Vertical Force versus Grinding Wheel Radius for constant chip thickness h_m for the different grinding cuts performed.

Radial wheel wear is shown in Figure 3.2.3.3, with all non CD cuts showing an increase at the low values of wheel radius. Higher productivity and the

application of down cutting all increased the wheel wear. The application of CD resulted in negligible measured wear.

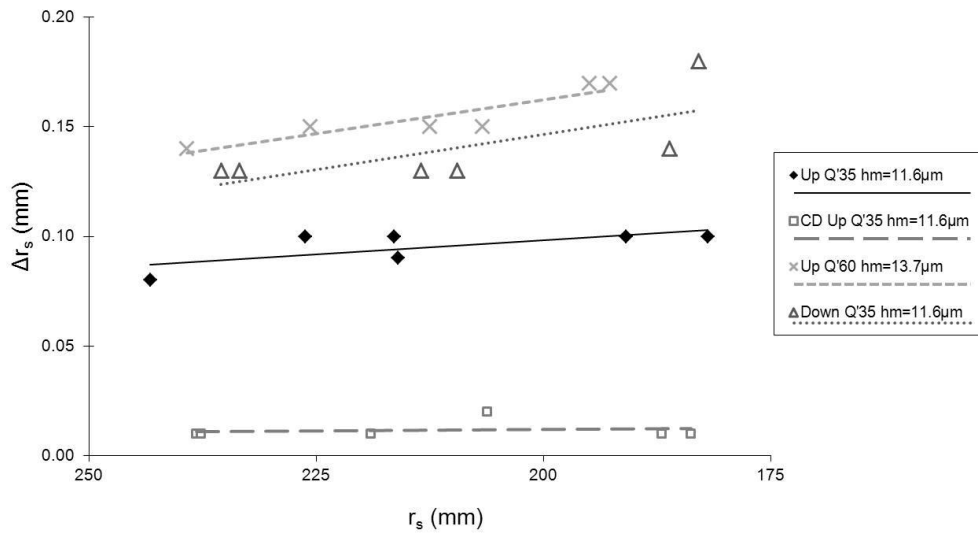


Figure 3.2.3.3 Radial Wheel Wear versus Grinding Wheel Radius for constant chip thickness h_m for the different grinding cuts performed.

Figure 3.2.3.4 provides results for the surface roughness measurements of the finished ground surfaces. This was lowest when CD was applied. The majority of the Non-CD cuts show a small increase in Ra at the lower values of wheel radius. The higher values of Ra were witnessed where the measured wheel wear was also high.

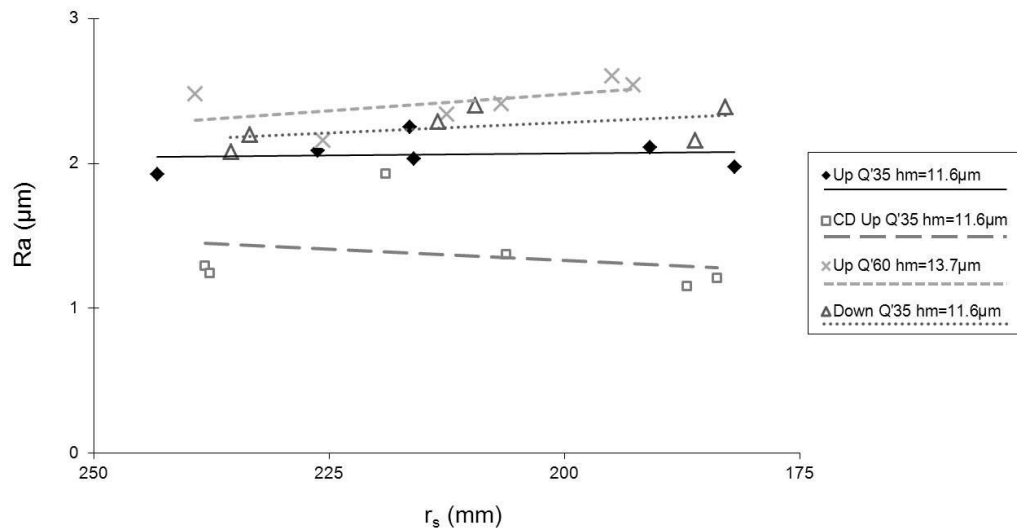


Figure 3.2.3.4 Surface Roughness versus Grinding Wheel Radius for constant chip thickness h_m for the different grinding cuts performed.

All the cut types performed produced some variation in the process outputs. The reasons for this are explored in section 3.2.4.

3.2.4 Discussion and Experimental Improvements

The specific grinding energy results highlight that the application of the different experimental variables has a significant effect on the process outputs. The increase in e_c over the life of the grinding wheel is largest when CD is applied. This is likely to be linked with the effects of wear from the Non-CD cuts. The radial wheel wear increases at the smaller wheel diameters for the Non-CD cuts which has the effect of reduced power usage whilst grinding. Separating the effect of wheel wear on the process outputs in future testing, by using CD for all the cuts performed, would be beneficial. The change in the value of specific grinding energy from the large diameter to small diameter grinding wheel is minimal for the results presented. It is indicative that either the maintenance of chip thickness has a beneficial effect on maintaining the specific grinding energy or the range of the experiment may not be large enough. The values of V_s used to maintain h_m ranged between 35 to 41 m/s when reducing the diameter from 500mm to 350mm in this experiment. To provide improved conditions in order to validate the impact of using chip thickness models to maintain process

outputs, a larger range of wheel diameters should be tested with the application of continuous dressing.

All the setups showed a decrease in the vertical force F_v as the wheel reduced in diameter. As the chip thickness remains constant, the variation must be due to another variable. The effect could be due to the variation in contact area or a change in material hardness. The change in material properties may be a result of increased temperature in the cut zone at higher grinding wheel speeds for the small grinding wheel diameter cuts. Temperature measurement should be included in the main experimental trials to understand this effect.

This work focuses on grinding as a stock removal process therefore knowledge of the specific grinding energy and force outputs are of high importance to avoid potential workpiece and machine damage. However, knowledge of the surface roughness provides additional information on the grinding process. The high radial wear measured for the Non-CD cuts indicates they are experiencing some degree of grain/bond fracture wear mechanism. This is reinforced by the high value of R_a for non CD cuts in comparison to the CD data. CD should be used in the main experiments to understand the effect of maintaining chip thickness on the process outputs in isolation of wheel wear.

A further observation from the experiment was the variation in dynamic performance of the grinding system at various wheel diameters. Although not directly measured, there were notable differences in the sound of the system and the subsequent dynamic component of the force output. This has the potential to add error into the experiment. The measurement of vibration to understand how it varies at different wheel diameters must be considered for future testing. It was also observed that down cutting provided more stable conditions. The concept of up and down cutting is similar to the definition used in milling. The down cut direction also produced less scatter in the results for specific grinding energy and the vertical force in comparison to the equivalent up cut grinding cuts performed. This is due to the mechanics of the down grinding process where the forces are lower and more directed into the structure of the machine resulting in more stable conditions.

This preliminary work has shown that there are changes in the grinding process outputs even when chip thickness is maintained. However, the test does not contain enough potential variation in chip thickness or isolate the effects of wheel wear on the process outputs to be conclusive. For this setup, the chip thickness value would change by a maximum of 10% if the wheel speed was not updated. As such, the following suggestions are made in order to improve future experimentation:

- Increase the range of grinding wheel diameters utilised in the testing to provide a greater potential variance in chip thickness value for a constant productivity process. This will also result in larger ranges of grinding wheel speeds applied in order to maintain a constant value of undeformed chip thickness.
- Measure net power from the machine spindle by using spark out passes. This would be used in the calculation of e_c according to equation (2.5.1).
- Inclusion of workpiece surface temperature measurement to aid in the explanation of output variation.
- Application of CD for all testing to isolate the effect of wheel wear.
- Monitor vibration to understand how it varies with different wheel diameters and grinding wheel speeds.
- Down cutting is preferable with respect to process stability and reducing the scatter witnessed in process outputs.

3.3 Statistical Analysis

The preliminary testing in section 3.2 investigates what effect maintaining chip thickness has on the process outputs. It is testing the ability of the chip thickness model to maintain process outputs for changing grinding wheel diameter. Observations of the results can be made to generate qualitative conclusions about the grinding behaviour, but quantitative analysis can provide a more definitive assessment of whether changes witnessed in the process outputs are due to the effect of changing wheel diameter or another source of variation within the grinding process.

Quantitative methods utilise statistical techniques to assess whether relationships exist between experimental variables and identify the source of variation in the outputs of an experiment. The techniques used in this section to assess the results presented in section 3.2 include; an assessment of linearity between the process outputs and the grinding wheel diameter to establish if a relationship exists between the 2 variables, analysis to identify whether variation in the process outputs is due to the changing wheel diameter or the inherent random nature of the grinding process, and finally a calculation of the number of grinding trials required in order to establish statistical significance if the current data set is insufficient to provide an answer. The techniques are described below and applied to the data in section 3.2 to provide further information on the experiment. The same statistical techniques are utilised in further results chapters.

3.3.1 Statistical Techniques

This section outlines the statistical techniques utilised for the data assessment. They are common methods of data analysis and were performed using Minitab 15 software.

Correlation

Correlation tests produce an output known as the Pearson correlation coefficient r . This coefficient determines whether 2 variables are linearly related. The linearity of the test is the key output. A value of ± 1 describes a perfect positive or negative linear relationship respectively. It is important to note that correlation only determines if there is a trend but does not imply causality. The value of 0 represents no linear relationship; however another type of relationship could exist between the variables. In this analysis, the correlation test is the first test to be applied for this data as the majority of results have had a linear trend line applied to them. The result will be indicative of how well the trend describes the behaviour.

The 2 primary values included in this test are the Pearson coefficient r and the p -value which determines the appropriateness of rejecting the null hypothesis. For this test, the null hypothesis is that there is no correlation between the 2 variables. Both values will be included in the results.

Analysis of Variance (ANOVA) – Hypothesis Testing

Analysis of Variance (ANOVA) is a useful technique for testing whether the process outputs vary between different experimental blocks. Figure 3.3.1.1 aids the explanation. The box plot detailed shows process output data for 3 blocks used in a hypothetical experiment. Each of the data boxes has an average for the results contained within the block and a spread of data used to calculate that average value. The ANOVA analysis identifies whether variation between block average values is due to the spread of the data or a difference between the experimental block outputs. The ANOVA analysis also establishes the statistical significance of this result using hypothesis testing. In relation to this work it determines whether the grinding process outputs are different as a result of changing wheel diameter, represented by different blocks, or due to another source of variation within the experiment.

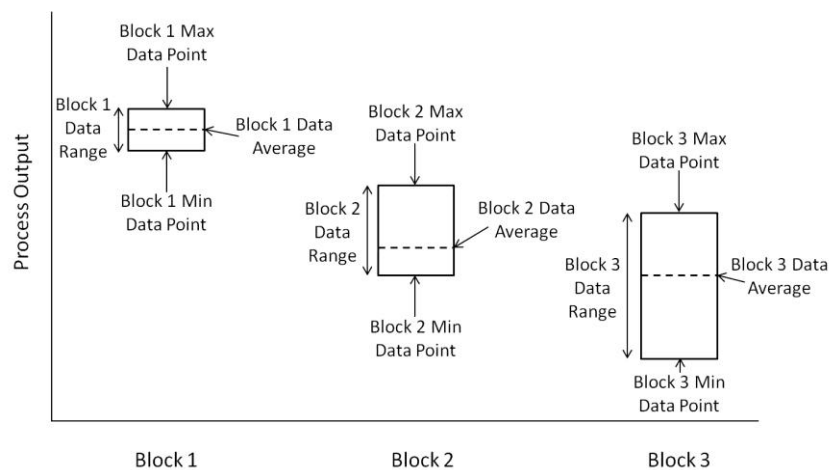


Figure 3.3.1.1 Box Plot diagram illustrating experimental block data variation used to aid the explanation of the ANOVA statistical technique.

The ANOVA method of testing looks at the variation between experimental Block averages as a ratio against the internal Block variation. This technique determines the difference between the Block mean values and tests the

significance of that result. The analysis presents 2 parameters as an output. The first is the F statistic which is a ratio between mean square values of the Blocks and the mean square of the error. A high value of F indicates that the variation is more attributed to the change in conditions between the experimental blocks as opposed to the spread of results within the block. The p-value again determines the appropriateness of rejecting the null hypothesis. Both values will be included in the results presented.

Power and Sample Size

The technique of power and sample size calculations allows a user to establish the required size an experiment should be to enable statistical judgment and how likely an effect will be detected for a particular experiment. This section will establish if the experimentation performed was sufficient in sample size to identify variation between experimental blocks as a result of a change in the grinding wheel diameter.

Power is the likelihood that an effect or difference will be found when one truly exists. This results in correctly rejecting the null hypothesis. When utilised for ANOVA, this means it is the likelihood that the statistically different means between experimental blocks will be found. Typical values of power are between 0.8 and 0.99 with the lower value generally considered as a minimum. A common value used in analysis is 0.95 and has been utilised in the results presented in this section.

The sample size technique is used to plan the correct number of experimental repeats to be performed during a testing procedure in order to establish a defined power of an experiment. By using a defined power value and having an understanding of the expected variation between the average values of different experimental blocks, an adequate sample size can be calculated. This is a useful technique to use when process output data is available providing an indication of the variation that can be expected. The results presented in section 3.2 can be used to calculate sample size for this analysis.

3.3.2 Analysis of Results

The results are presented in table format for each of the statistical tests performed. Within each table, the different process outputs analysed are detailed in the first column. These are presented against each type of experimental setup, which is detailed along the first row. The colour in the tables defines the appropriateness of rejecting the null hypothesis. Green indicates a correct rejection can be made as the p-value is <0.05 , yellow indicates a borderline rejection where $0.05 < p < 0.10$, and red indicates no statistical significance for rejecting the null hypothesis where $0.10 < p$.

The results of the correlation analysis between the process outputs and the grinding wheel radius are detailed in Table 3.3.2.1. The results show that a strong linear trend exists between F_V and the grinding wheel radius for all the experiment conditions. There are less statistically significant trends when considering the specific grinding energy indicating there is more scatter in the results presented. The application of continuous dressing and the use of down cutting provides reduced scatter. As a result, stronger statistical trends are identified for e_c using these experiment variables. There is some statistically significant correlation calculated between the radius of the grinding wheel and the profile wear but this is only significant for the Up Q'60 conditions. The effect of higher productivity for the Up Q'60 conditions provides an increased amount of radial wear measured at the small wheel diameters. As a clear increase in radial wear amount is evident from the results, a strong linear trend is calculated from the data. There is no statistically significant correlation for R_a versus the grinding wheel radius.

	Up Q'35	CD Up Q'35	Up Q'60	Down Q'35
e_c	$r = -0.004$ $p = 0.994$	-0.916 0.010	-0.175 0.740	-0.875 0.022
F_v	0.850 0.032	0.986 0.000	-0.948 0.004	0.914 0.011
Δr_s	-0.688 0.131	N/A	-0.905 0.013	-0.715 0.111
Ra	-0.116 0.826	0.253 0.628	-0.521 0.289	-0.485 0.330

Table 3.3.2.1 Table of results showing values for Pearson correlation coefficient between wheel radius and relevant process output and p-values for the different experiment variables.

The results from the ANOVA analysis are presented in Table 3.3.2.2. The only significant result showing variation between experimental blocks for the process output e_c , is when continuous dressing is utilised. The Non-CD cuts have flat linear trends for the reasons explained in section 3.2, which results in the ANOVA analysis not identifying any significant variation between the experimental blocks. The results for F_v show statistical significance between experimental blocks for the majority of the experimental variables tested. The change in F_v with wheel radius is witnessed in Figure 3.2.3.2. The results from the wear and Ra outputs show that scatter within the experimental blocks accounts for the majority of variation between results. Controlling the wear through the application of continuous dressing would provide improved conditions in order to assess the relationship between chip thickness and the process outputs.

	Up Q'35	CD Up Q'35	Up Q'60	Down Q'35
e_c	$F_{Stat} = 1.39$ $p = 0.374$	11.42 0.040	1.04 0.455	4.91 0.113
F_v	4.59 0.122	12.92 0.034	7.96 0.063	10.72 0.043
Δr_s	0.60 0.604	N/A	21.00 0.017	2.25 0.253
Ra	0.65 0.585	2.30 0.248	1.94 0.288	1.64 0.331

Table 3.3.2.2 Table of results showing values for ANOVA F-statistic and p-values for process outputs for the different experiment variables.

The Power and Sample Size analysis is important to assess if the experiment has the required amount of tests to statistically detect variation in the grinding process outputs. The results shown in Table 3.3.2.3 show the required sample size to provide a successful ANOVA analysis at an experimental power of 0.95. The analysis uses the variation between experimental blocks calculated from the ANOVA analysis above. Table 3.3.2.3 shows that the sample size required is low for the force values and much higher for some of the specific grinding energy and surface roughness outputs. A minimum sample size of 3 is recommended even for data that had clear variation between experimental blocks. Sample sizes of 27 runs per block were recommended for some of the profile wear and surface roughness process outputs in order to provide statistically significant results. The scatter in these results is large therefore requiring a large amount of repeats to statistically detect variation between the experimental blocks. The use of CD should be applied to minimise the scatter in the results.

	Up Q'35	CD Up Q'35	Up Q'60	Down Q'35
e_c	16	3	18	5
F_v	5	3	4	3
Δr_s	27	N/A	3	11
Ra	27	9	11	11

Table 3.3.2.3 Table of results showing values required sample size per block for an experimental power of 0.95 based on output data from ANOVA analysis.

The statistical analysis of the results shows that the force outputs change with wheel radius. A change in specific grinding energy is only witnessed under CD conditions when chip thickness is maintained. This is because higher radial wear changes the power requirements at the small grinding wheel diameters. In order to fully assess the relationship between chip thickness and process outputs, this variable effect of wear must be removed from the testing. The analysis presented in this section re-affirms the recommendations made in section 3.2 by implementing continuous dressing, the down cutting direction and the use of a larger grinding wheel diameter range. This would provide improved output data to provide better analysis of the relationship between chip thickness and the process outputs. A minimum sample size of 3 is recommended per experimental block.

3.4 Machining Trials – Assessment of Chip Thickness Models

The preliminary testing in section 3.2 showed that certain trends in the grinding behaviour were evident but improvements to the experiment were necessary. An experiment was proposed incorporating the recommendations highlighted from the preliminary testing. A decision was made to move from the Blohm machine to the Makino A99 platform. This was chosen both due to machine availability and increased flexibility of the platform. The grinding wheel diameter range on the Makino allowed for a greater range of chip thickness values to be tested for a constant productivity process. The experiment is similar in setup to that detailed in section 3.2. An increased number of the chip thickness models defined in section 2.6 were included in the testing to understand which provided the most improved control of the process outputs. These included the undeformed chip

thickness h_m , the equivalent chip thickness h_{eq} and the feed per cutting edge model S . This section outlines the setup and methodology utilised for the machining trials performed on the Makino A99.

3.4.1 Setup on Machine Tool

The setup on the machine tool was prepared in order to replicate creep feed grinding conditions. The system is capable of performing Up/Down grinding by adjusting the nozzle placement and movement of the machine tool. CD Down grinding was selected for these trials to eliminate the effects of wear and to provide improved dynamic stability. The grinding tooling and cutting fluid nozzle setup is detailed in Figure 3.4.1.1.

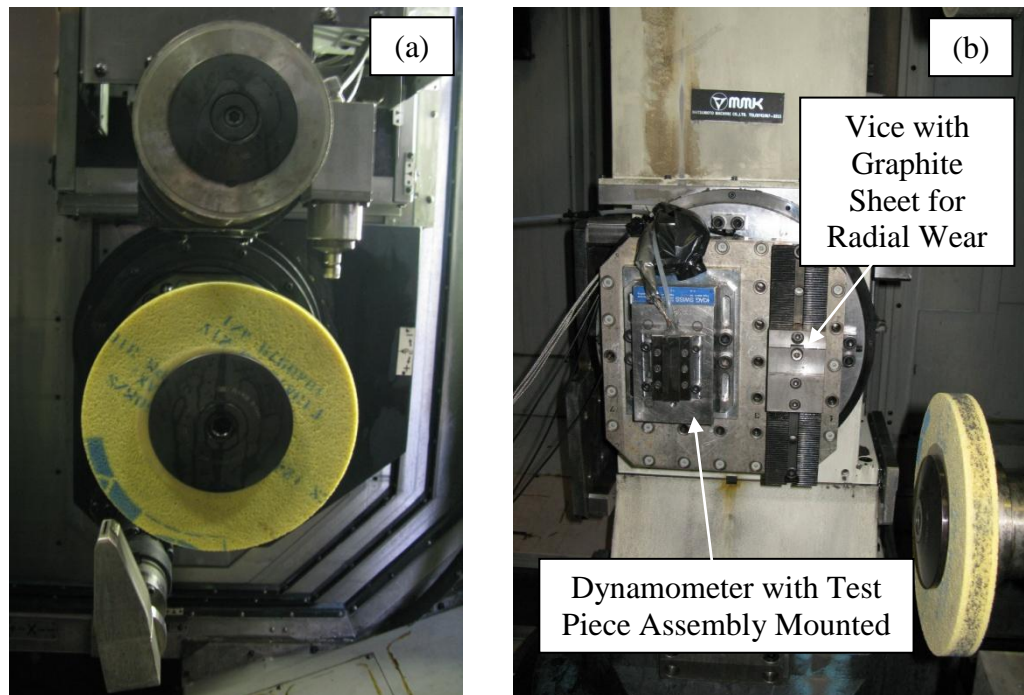


Figure 3.4.1.1 Makino A99 grinding setup: (a) Grinding wheel, dresser roll and cutting fluid nozzle cut setup, (b) Work piece and pallet setup.

Figure 3.4.1.1(a) shows the CD capability of the machine tool. In addition, it shows the grinding wheel and the cutting fluid nozzle utilised in the testing. The nozzle was manufactured to provide a straight laminar flow of cutting fluid which represents creep feed grinding conditions. A close up of the nozzle is shown in Figure 3.4.1.2. Figure 3.4.1.1(b) shows the workpiece setup with the test piece assembly mounted on a dynamometer. A machining vice is located

adjacent to the dynamometer. This is utilised to hold graphite sheets which are used as part of the measurement for radial wheel wear which is detailed in section 3.4.4.



Figure 3.4.1.2 Image of cutting fluid nozzle utilised in machining trials.

With a changing wheel diameter, the position of the cutting fluid application is also affected. Providing consistent application of cutting fluid is vital in order to maintain control within the experiment. To ensure the cutting fluid was applied to the same point of the cut zone at each wheel diameter, a sketch program was created in CAD to provide the correct application angles for the PCN. The fluid was consistently aimed at a distance of 10mm from the cut surface and an approach angle of 10 degrees, as seen in Figure 3.4.1.3, for the varying grinding wheel diameters. Considering the fluid positioning capability of the Makino A99, it is understood that the application detailed above will result in some variation in the nozzle orifice distance from the cut zone as the wheel changes in diameter. However, the use of the approach detailed in the figure is designed to apply the optimised consistency of fluid application for the changing wheel geometry in a creep feed setup.

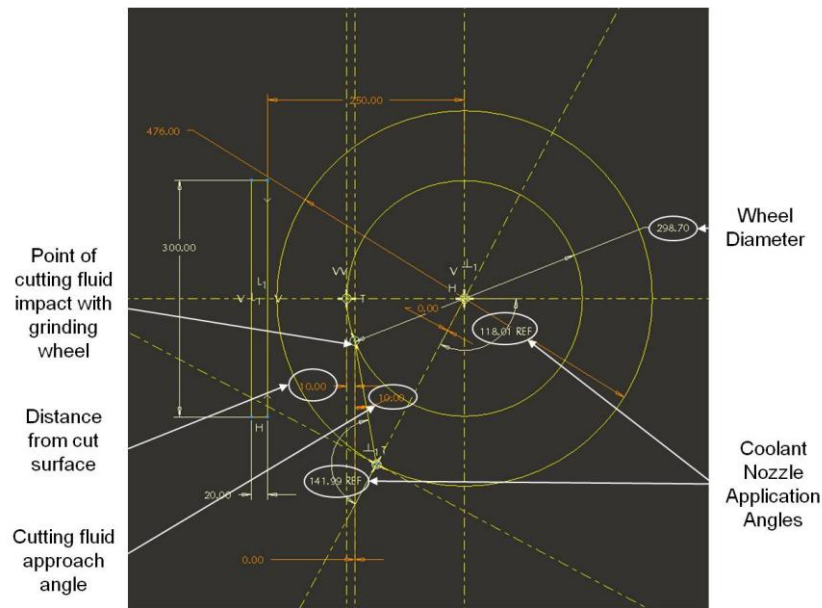


Figure 3.4.1.3 Image of CAD sketch utilised to set the pressure cutting fluid nozzle (PCN) application angles.

3.4.2 Test Piece Design and Manufacture

The material for the experimentation was selected as Inconel 718 to replicate the preliminary testing. The requirement to include temperature measurement resulted in a more complex test piece design in comparison to the material block utilised in section 3.2. The in-process measurements, defined as any data capture that occurs during cutting, include force, power, temperature and vibration. Force and power are non-invasive on the test piece but the temperature and vibration require the application of physical sensors embedded within the material.

The temperature measurement had the most significant impact on the design of the test piece. Multiple cuts were required at different grinding wheel diameters so a method of measuring temperature at a consistent depth below the cut surface for multiple experiments was required. Thermocouples were decided upon as the best option with respect to cost and performance. Work by Jin and Stephenson [65] using an inclined thermocouple testing rig was selected as the appropriate method as it provided temperature measurements at multiple distances below the ground surface with an easy method of changing test pieces. Their rig design is shown in Figure 3.4.2.1.

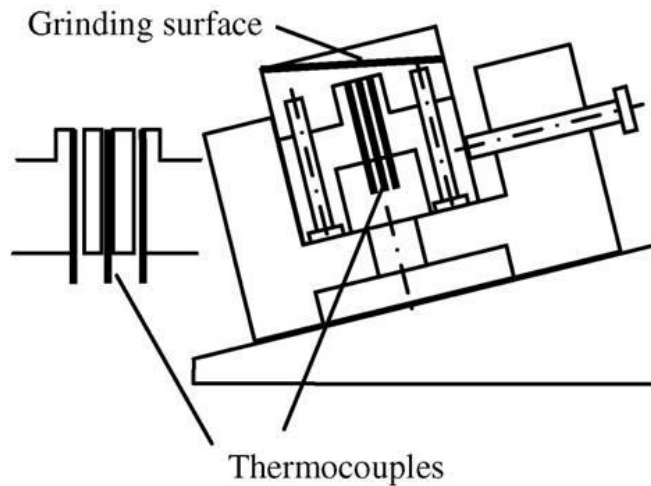


Figure 3.4.2.1 Image of the inclined thermocouple testing rig design by Jin and Stephenson [65].

Placing the test piece on an angle allows simultaneous temperature measurements at various depths beneath the surface. This requires “top hat” style test pieces to be manufactured that can be easily placed on top of a plate containing embedded thermocouples. The design utilised in this experiment does not change significantly from that presented in Figure 3.4.2.1 but instead uses an inclined thermo plate at the bottom of the assembly rather than an inclined vice and the number of thermocouples has been increased to 5 to provide additional temperature data. The design utilised can be seen in Figure 3.4.2.2.

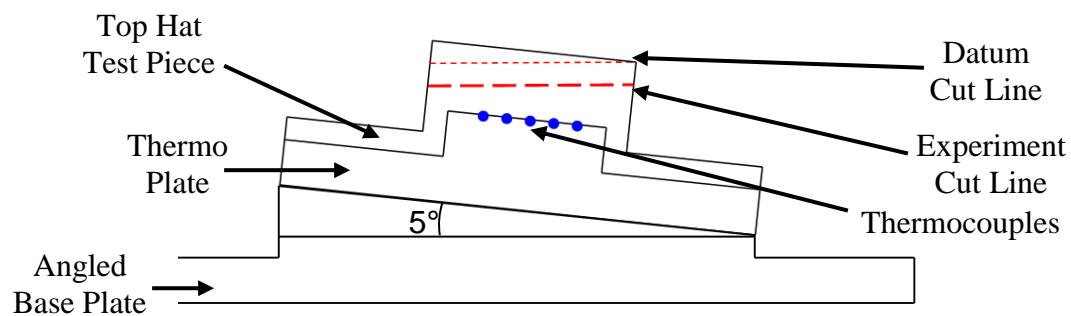


Figure 3.4.2.2 Diagram of angled test piece design showing thermocouple placement utilised in these experiments.

The thermocouples are placed at a 5° angle which provides the different depths of temperature measurement beneath the ground surface. Each individual top hat test piece is loaded and a datum pass performed to flatten the top of the test piece material. The experimental cut is then performed. This procedure ensures the

distance between each thermocouple and the ground surface is constantly maintained for the same amount of material removal. The design was decided upon as the best method for performing multiple test cuts and incorporating temperature measurement. The test pieces and additional work holding were manufactured from solid using stock material. Figure 3.4.2.3 shows the actual test piece assembly utilised in the experiments.

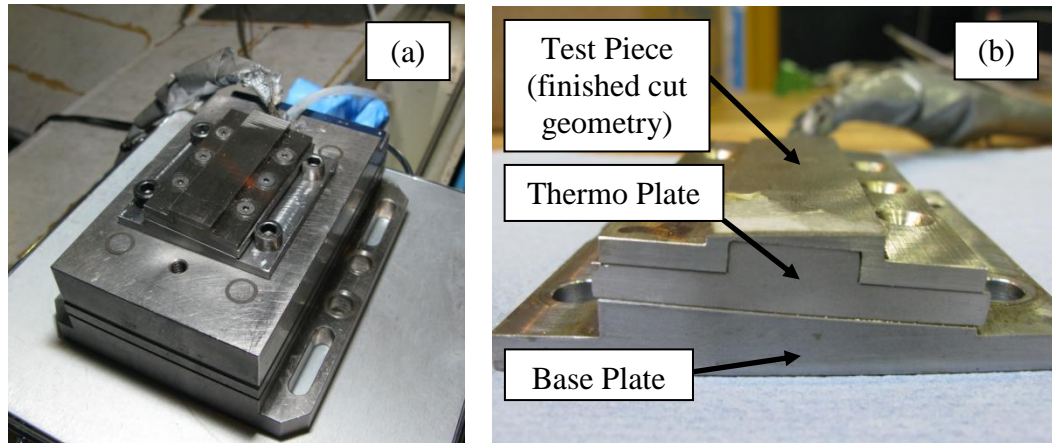


Figure 3.4.2.3 Image of the final test piece assembly; (a) View with test piece assembly placed on dynamometer, (b) End view detailing separate parts of assembly.

The test piece assembly is made up of 3 separate components; the workpiece, the thermo plate and the base plate. Each individual component is detailed in Figure 3.4.2.4.

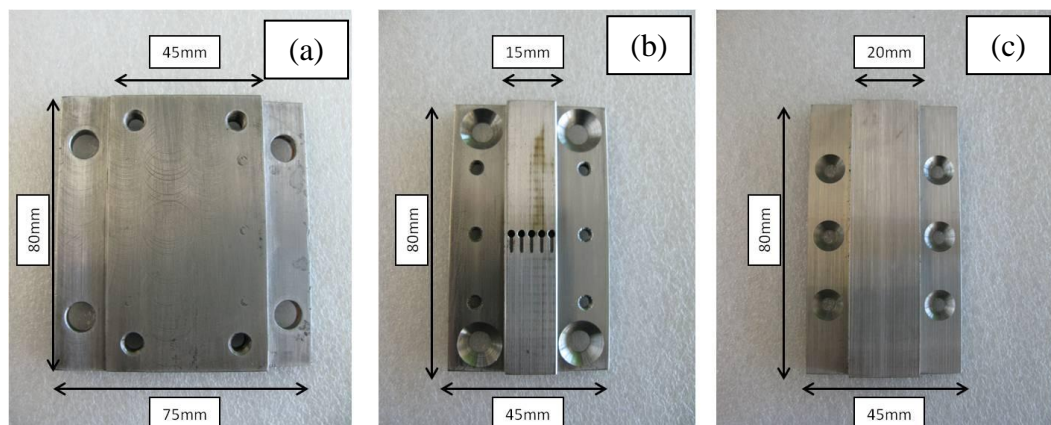


Figure 3.4.2.4 Individual components of test piece assembly; (a) Base Plate, (b) Thermo Plate, (c) Test Piece.

The setup requires 3 individual components to allow placement of an accelerometer and thermocouples for the vibration and temperature measurement. A slot for embedding an accelerometer was made in the angled base plate structure to allow vibration measurement during cut. The exact setup of the vibration measurement is detailed in section 3.4.4. The details of each individual component used in the test piece assembly are detailed in Table 3.4.2.1.

Component	Material	Manufacture	Function
Base Plate (1 off)	Tool Steel	Milled from Steel Block	To house embedded accelerometer To provide 5 degree angle for thermo plate and test piece To fixture thermo plate
Thermo Plate (1 off)	Inconel 718	Milled, drilled, ground and EDM'd from Inconel Bar Stock	To house embedded thermocouples Fixture test piece
Test Piece (50 off)	Inconel 718	Ground and drilled from Inconel Bar Stock	To provide cutting material for grinding process

Table 3.4.2.1 Individual component details for test piece assembly.

3.4.3 Parameters and Method

The experiment was designed to assess the effect of maintaining chip thickness on the process outputs for a constant productivity process. The decision was made to follow the same experimental outline as detailed in section 3.2. The range of wheel diameters used on the Makino provided an increased variation in

chip thickness over the operational life of the grinding wheel. In addition, more chip thickness models were included to assess their ability to maintain process outputs if they are kept at a constant value. Again, productivity was kept constant for all the chip thickness models. As a result the majority of the cutting parameters remain constant with only wheel speed varying with a change in grinding wheel diameter. The dressing parameters and cutting fluid location are detailed in sections 3.1.4 and 3.4.1 respectively. The parameters are detailed in Table 3.4.3.1.

Parameter	Symbol	Value
Grinding Direction	N/A	Down
Fluid Pressure	P_f	15 bar
Fluid Flow Rate	V_f	120 l/min
Continuous Dress	N/A	Yes
Work Piece Feed Rate	v_w	500 mm/min
Depth of Cut	a_e	1 mm
Width of Cut	b	20 mm
Material Removal Rate	Q'	8.33 mm ³ /mm/s

Table 3.4.3.1 Grinding Parameters utilised in the assessment of chip thickness models experiment.

The parameters were selected to provide creep feed grinding conditions. The depth of cut was kept to 1mm in order to maximise the number of work piece components that could be manufactured from the bar stock material. CD was applied to eliminate wear as a variable from the system. The wheel was divided into 4 approximate diameter ranges each representing an experimental block. The wheel speed was adjusted for each chip thickness equation to maintain the value established at the first cut. The experimental procedure is outlined in Table 3.4.3.2.

Experimental Block	Wheel Diameter D_s (mm)	V_s (m/s) Maintaining S Calculated from equation (2.6.1)	V_s (m/s) Maintaining h_{eq} Calculated from equation (2.6.8)	V_s (m/s) Maintaining h_m Calculated from equation (2.6.5)
1	300	35.0	35.0	35.0
2	250	32.0	35.0	38.3
3	200	28.6	35.0	42.8
4	160	25.6	35.0	47.9

Table 3.4.3.2 Table showing predicted wheel speed changes for different wheel diameters at defined experimental blocks.

The wheel speed is identical for all chip models at the largest wheel diameter, block 1. A test cut with 2 repeats is performed for each chip thickness model within each experimental block. For blocks 2, 3 and 4, the wheel speed is adjusted as shown in Table 3.4.3.2 depending on which chip thickness model is maintained. The value of wheel speed in the table shown is calculated for the diameter listed. As CD cutting is utilised there is a small range of cutting diameters within each experimental block. The wheel speed is calculated individually for each cut to an accuracy of 2 decimal places in order to improve the accuracy of the experiment.

3.4.4 Data Collection

This section details the data collection requirements for the experiment. This is separated into both in-process data, obtained during cutting, and post-process data which is collected after the experimental run.

In-Process Data

The in-process data collection includes the Force, Power, Temperature and Vibration. The force data was collected using a Kistler 9257A 3-axis dynamometer. This was connected to the data collection laptop via a charge

amplifier and recorded using dynoware software. The force measurement setup is detailed in Figure 3.4.4.1.

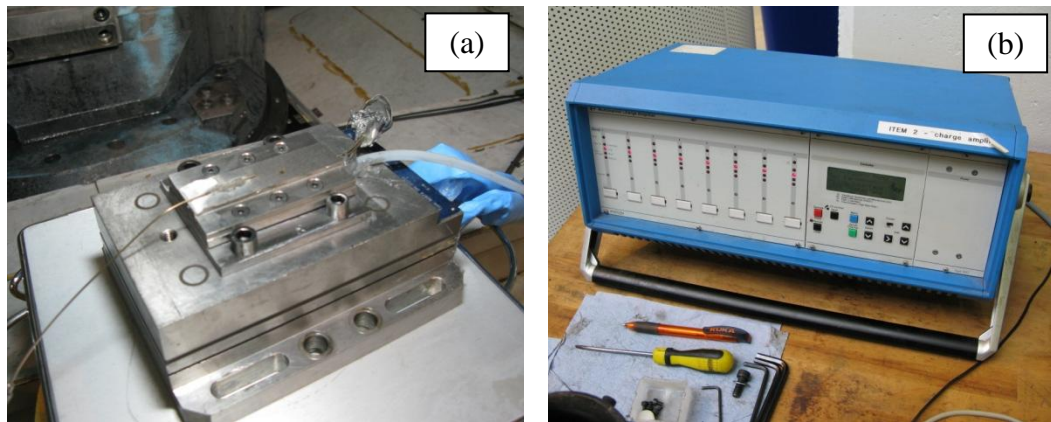


Figure 3.4.4.1 Force measurement equipment; (a) Kistler 9257A dynamometer with test piece assembly mounted, (b) Kistler 5017 Charge Amplifier utilised in force measurement.

Specific grinding energy is a key parameter and relies upon calculating either the net power or net grinding force. The net results are those that are experienced purely from cutting the material and negate the effect of wheel rotation and cutting fluid application. To achieve this, the total force and sparkout force were measured for each experimental run. The spark out force is defined as all force data that does not directly contribute to material removal. The method for obtaining the net force data was:

1. Perform Datum cut experimental pass.
2. Set cut depth to 0mm and re-perform Datum cut. Record Sparkout Force data.
3. Set cut depth to 1mm and perform Main Experimental cut. Record Total Force data.

This creates 2 force profiles which are detailed in Figure 3.4.4.2. F_y provides the force in the horizontal direction detailed by the red line with F_z representing the vertical force measurement denoted by the purple line. The force output profiles displayed the following behaviour:

1. Fast Ramp up to full cut engagement.
2. Stable cutting region. Max force in this region represents the maximum total force.

3. Spike in F_y from cutting fluid flow impacting the side of the dynamometer when leaving cut.
4. The offset witnessed in the sparkout force data between F_y and F_z highlights how the cutting fluid impacts different parts of the dynamometer at different times of the cut. The sparkout force value is the maximum measured from the stable data region.

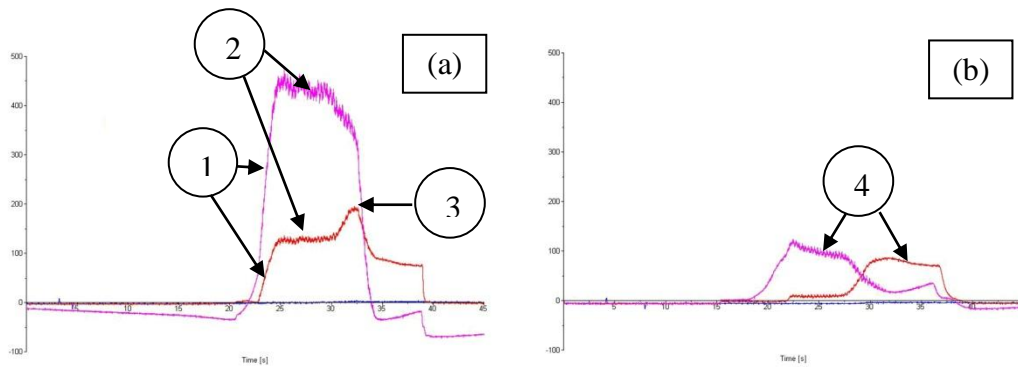


Figure 3.4.4.2 Example of Force output profile; (a) Main experimental run, (b) Spark Out experimental run.

The spindle power was measured using a Hall Effect monitor provided by Tyrolit. The power signal was monitored using Leitsungmessung software provided by Tyrolit on the measurement laptop. The equipment is shown in Figure 3.4.4.3.



Figure 3.4.4.3 Image detailing the Tyrolit mobile power measurement equipment.

The net power is again the important value to be used in further analysis so both the total and sparkout power are required. These were obtained using the same methodology as for the force measurement. A typical power output profile is detailed in Figure 3.4.4.4 showing the following information:

1. Ramp up into cut.
2. Steady state Total and Sparkout power profiles when fully engaged. The maximum value for each from this region is utilised in the calculation of net power.

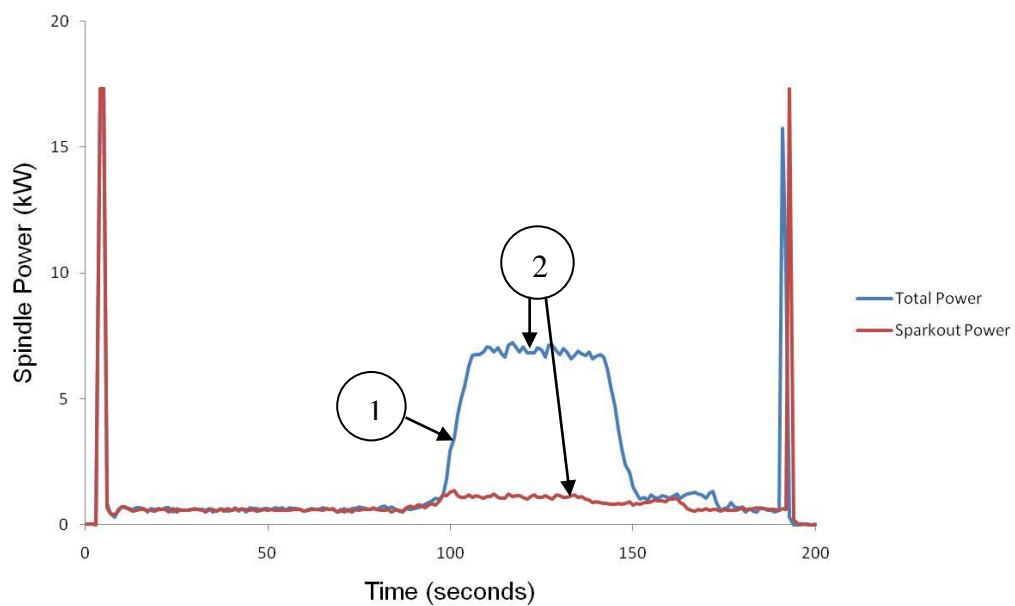


Figure 3.4.4.4 Example of power measurement output profile for the assessment of chip thickness models experiment.

Temperature was recorded using 5 standard 1mm diameter k-type thermocouples embedded and compressed between the thermo plate and test piece components. The thermocouple data was measured and recorded using SquireView software connected by USB to the measurement laptop. The equipment and hardware is detailed in Figure 3.4.4.5.

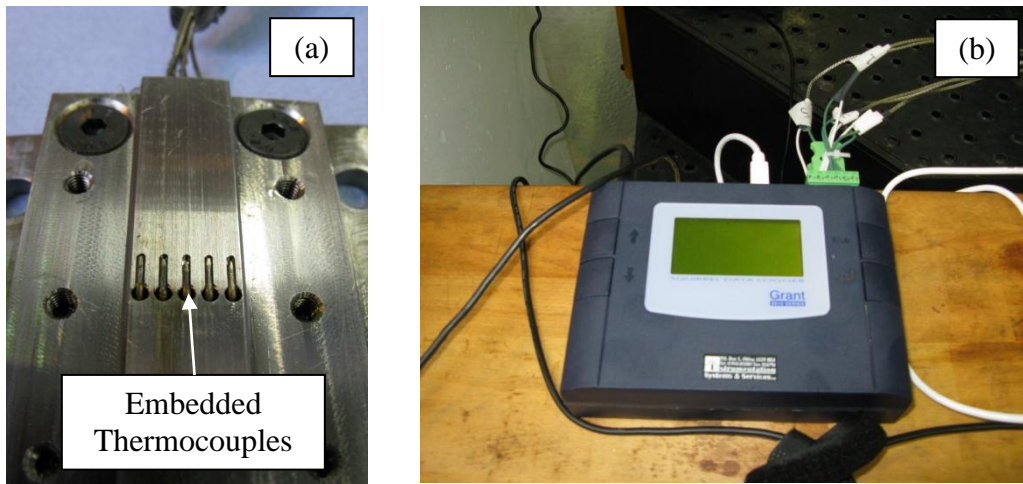


Figure 3.4.4.5 Temperature measurement equipment; (a) Thermo plate test piece material with embedded thermocouples, (b) SquirrelView hardware box.

An example of an individual experimental run temperature output is detailed in Figure 3.4.4.6. All 5 thermocouple outputs are detailed. The maximum temperature on the profile indicates the point at which the wheel is directly cutting above a thermocouple.

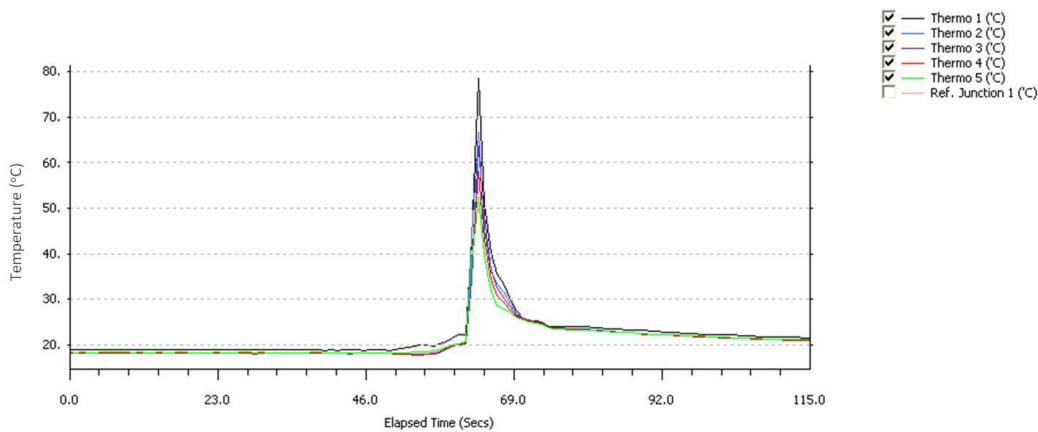


Figure 3.4.4.6 Example temperature measurement output profile for the assessment of chip thickness models experiment.

The data from the 5 thermocouples is individually recorded from the data output. These data points are combined in a graphical method to estimate the ground surface temperature during each cut performed. The method for this is detailed in the results section in Chapter 4.

The vibration in the system was measured using a PCB accelerometer, specification 352A21. This is a teardrop style accelerometer with a sensitivity of 10mV/g. This was estimated to be an appropriate sensitivity for this particular application. This is based on preliminary testing performed to establish the magnitude of vibration produced from the process. The accelerometer was glued to the angles base plate in a pre-machined slot. Gluing provides improved contact conditions between the 2 surfaces in order to allow more accurate vibration measurement. The accelerometer output was measured using the TXF Metalmax vibration monitoring software system via the measurement laptop. The setup is detailed in Figure 3.4.4.7.

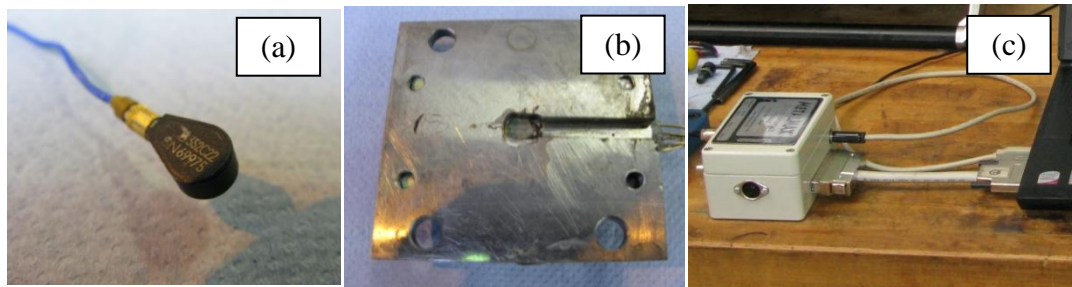


Figure 3.4.4.7 Vibration measurement equipment; (a) 352A21 accelerometer, (b) Embedded accelerometer in base plate, (c) Metalmax hardware.

Post-Process Data

The post-process measurements include radial wheel wear measurement and analysis of the ground surface. This section outlines the methods for each of these measurements performed.

Radial wear measurement for this experiment was defined as a checking procedure due to the application of continuous dressing. Measurements were performed to assess the loss of radial form beyond that programmed for the CD process. It was expected that the CD process would provide sufficient in-process dressing conditions to maintain wheel form and prevent uncontrolled wheel wear. The radial wear measurement was performed utilising a graphite test specimen. After the grinding wheel had performed the main experimental cut, the wheel would perform an additional cut through a graphite test specimen leaving

an imprint of the radial profile. The non cutting areas of the grinding wheel shown in Figure 3.4.4.8 (a) provide a reference surface to determine if any radial wear has occurred. The imprint left in the graphite coupon was examined under an optical microscope to establish if any uncontrolled wheel wear had taken place. An example of the microscope image is shown in Figure 3.4.4.8 (b). This particular image shows no sign of additional uncontrolled wear.

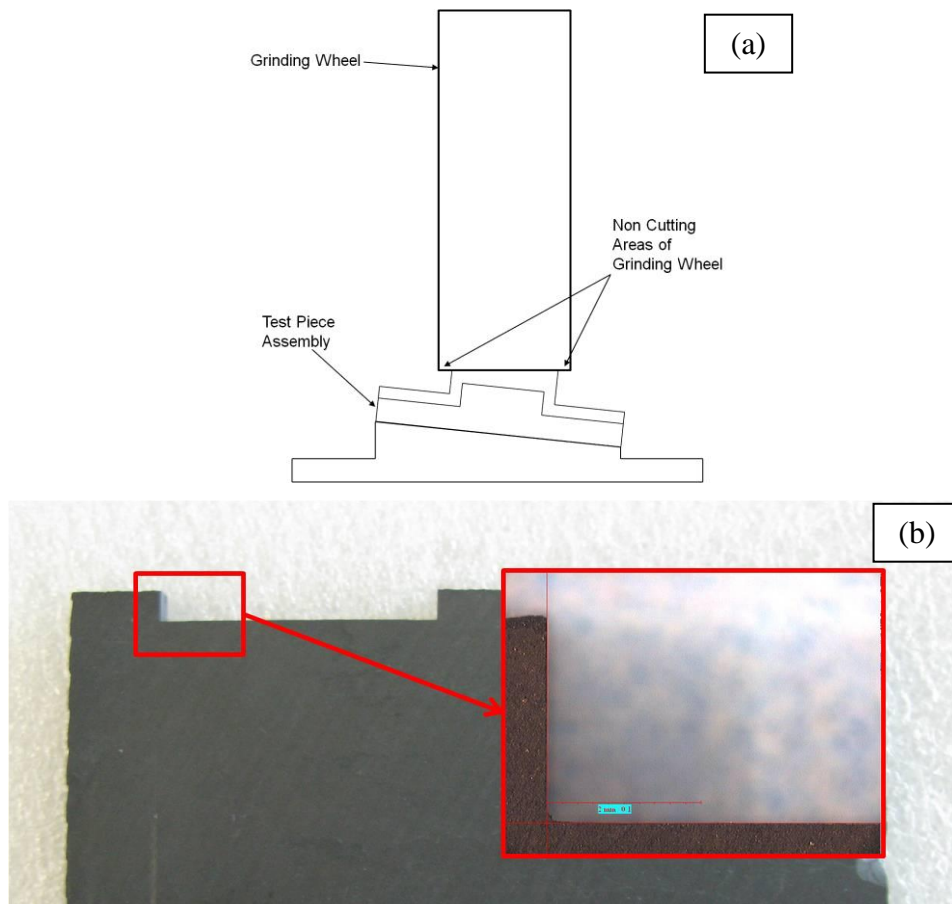


Figure 3.4.4.8 Images of Radial Wear Procedure; (a) Grinding wheel overhang proving non cutting edges of grinding wheel radius used as reference in wear measurement, (b) Graphite wear coupon with wheel cut profile to measure radial wheel wear.

The surface roughness of the ground metal surfaces was also investigated as a post process measurement. The measurements were performed using a Mitutoyo SJ-301 mobile profilometer as shown in Figure 3.4.4.9 (a). The measurements were taken at 3 points along the grinding direction with the stylus measuring across the cut direction. This is detailed in Figure 3.4.4.9 (b). Measurement line 1

was taken approximately 15mm from the start of the test piece, measurement 2 in the middle of the test piece and measurement 3 taken approximately 15mm away from the end of the test piece edge. These were moved slightly if the surface had any significant imperfections at these points. The average Ra value taken from the 3 measurements was utilised in the results.

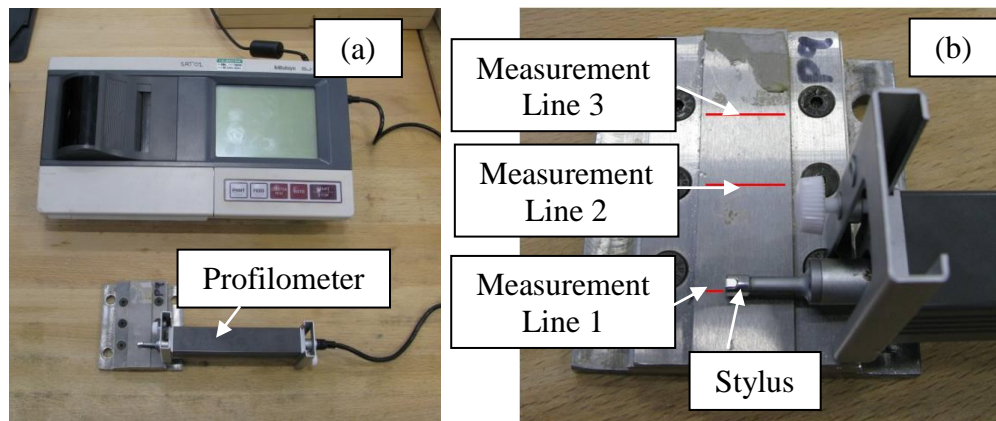


Figure 3.4.4.9 Setup of surface roughness measurement for metal test pieces; (a) Mitutoyo SJ-301 surface roughness measurement equipment, (b) Stylus on ground surface with measurement placements and directions detailed.

A scratch test using the stationary grinding wheel was performed on a graphite test piece to obtain information about the wheel surface topography. The custom test piece, shown in Figure 3.4.4.10, was designed to attach easily to the dynamometer after a test cut was performed. A static scratch test with the grinding wheel held stationary was performed at 0.25mm depth of cut along 1 of the graphite test piece surfaces. The force output was also recorded during the scratch test in order to assess if the contact conditions changed between the wheel and graphite depending on the experimental cut performed.

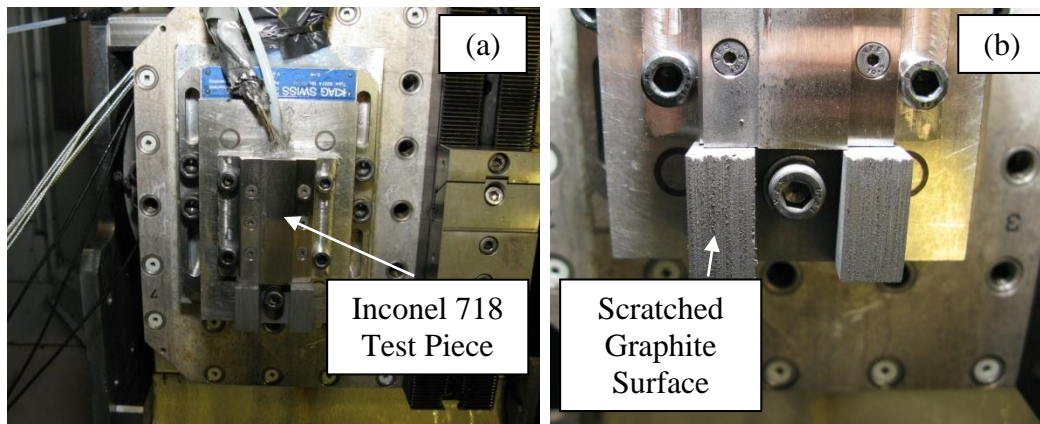


Figure 3.4.4.10 Graphite force measurement setup; (a) Graphite test piece in experimental setup, (b) Close up image of graphite test piece on dynamometer.

Upon completion of the scratch test, the graphite test piece would be removed from the machine tool and taken to the laboratory for a surface roughness measurement of the scratch surface. The test was developed to leave an imprint of the wheel topography on its surface that can be measured by a stylus on a profilometer. For the graphite, the Mahr profilometer was used as the stylus pressure could be more tightly controlled to prevent break away of the graphite surface. The equipment is shown in Figure 3.4.4.11 (a). Again 3 measurement positions were taken as detailed in Figure 3.4.4.11 (b). Gauge blocks were utilised to provide repeatable positioning for each setup. Similar to the Ra measurements on the metallic surfaces, the average of the 3 measurements was utilised as the output for analysis in the results.

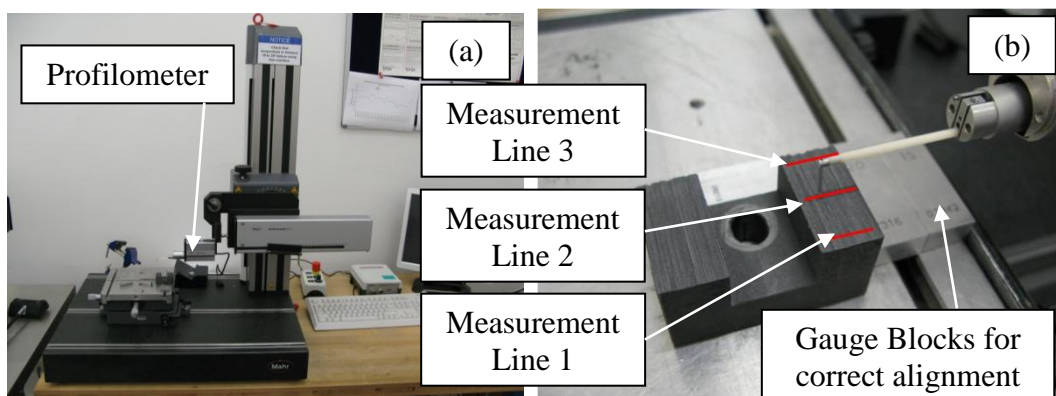


Figure 3.4.4.11 Graphite surface roughness measurement setup; (a) Mahr stylus profilometer, (b) Graphite test piece and stylus detailing measurement positions.

The additional post process measurements considered the surface integrity of the ground material. This required cut-up samples of the ground material to test for subsurface hardness and deformation. Figure 3.4.4.12 (a) displays an example of a removed sample taken from the main test material. The surface used in the surface integrity measurements is shown facing forward in Figure 3.4.4.12 (b). This surface was selected due to it being in the middle of the cut width and is aligned in the grinding feed direction. Multiple measurements were taken for both hardness and deformation along the surface length. Due to the time intensive nature of the testing, only 4 cut-up sections were taken. These included cuts R01 (baseline), R29 (h_{eq}), R31 (h_m) and R36 (S) which represented the baseline cutting conditions, and an example for each of the chip thickness models maintained from block 4. A table of the experimental runs is detailed in Appendix C for clarification. The Knoop Hardness was taken at selected depth intervals up to 250 μ m from the cut surface; at 4 different points along the cut direction. Microscope images detailing the grain deformation were taken along the surface using the Leica microscope. The grain deformation depth was measured from these images at 10 points along the cut surface. An average value for both the Hardness and Grain Deformation results was calculated from all the data points measured. The average value was utilised in the results chapter for this experiment.

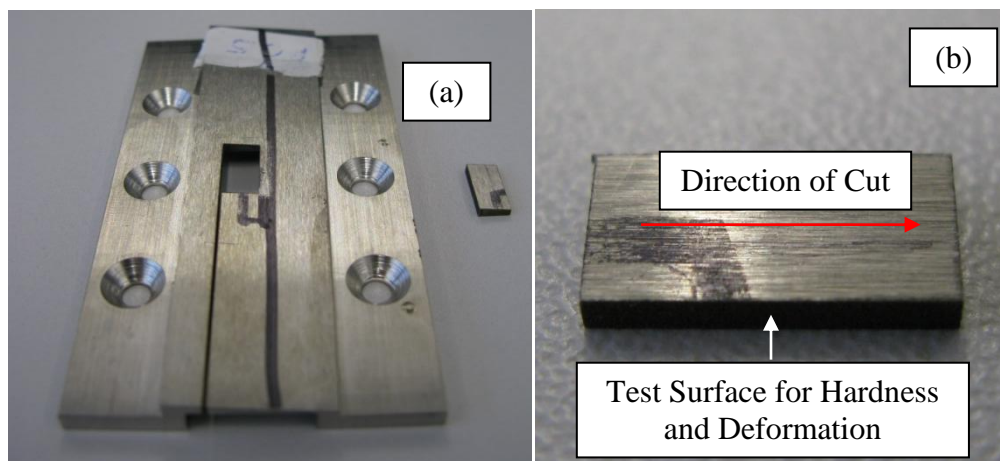


Figure 3.4.4.12 Cut-up sample for Surface Integrity testing; (a) Cut out section from main test piece material, (b) Close up view of cut out section showing testing surface.

3.5 Modified Pin on Disc Testing – Assessment of Contact Area and Wheel Speed

The results produced from the experiments detailed in Section 3.4 required a variation in testing methodology to investigate certain process variables under simplified conditions. Although different chip thickness models were maintained in the cutting trials detailed above, variations in the contact area and grinding wheel speed were still present. This modified pin on disc experiment aims to investigate the effects of those 2 parameters on the grinding contact conditions. A flat contact Nickel Pin is fed into a rotating grinding wheel. These flat conditions remove the more complex kinematic conditions associated with peripheral grinding allowing a pure assessment of the contact conditions at the surface. Pins of varying diameters, and hence contact areas, were tested at a variety of grinding wheel speeds.

3.5.1 Test Rig and Setup on Machine Tool

This experiment uses a tribological pin on disc testing rig primarily developed for investigating metal on metal contacts. A typical application of this rig would utilise a hardened steel pin on a softer metallic tube on a centre lathe setup. The rig is utilised to assess the friction coefficient at a number of different process inputs. The idea to utilise this rig in the grinding environment was due to the work outlined in Chapter 2 of this thesis. The grinding wheel becomes the rotating media and a metal pin is pushed against the surface under a known pressure. The decision to rotate the grinding wheel rather than a piece of nickel material was due to the difficulties in getting high surface speeds on a lathe platform. Applying a nickel pin to a rotating grinding wheel takes advantage of the natural machine setup. The horizontal force is measured as an output and the force ratio, which is analogous to the friction coefficient for grinding, can be calculated for the known applied vertical force. Figure 3.5.1.1 details the friction rig setup inside the Makino A99 machine tool. In addition to the rig, a dressing stick and cutting fluid nozzle are detailed in Figure 3.5.1.1 (b). The cutting fluid nozzle was set to apply a high flow and low pressure fluid application to the contact zone. The dressing stick was an addition to the testing rig to provide

continuous dressing during experimentation to replicate the conditions of the machine trials. Its manufacture and application are detailed in section 3.5.2.

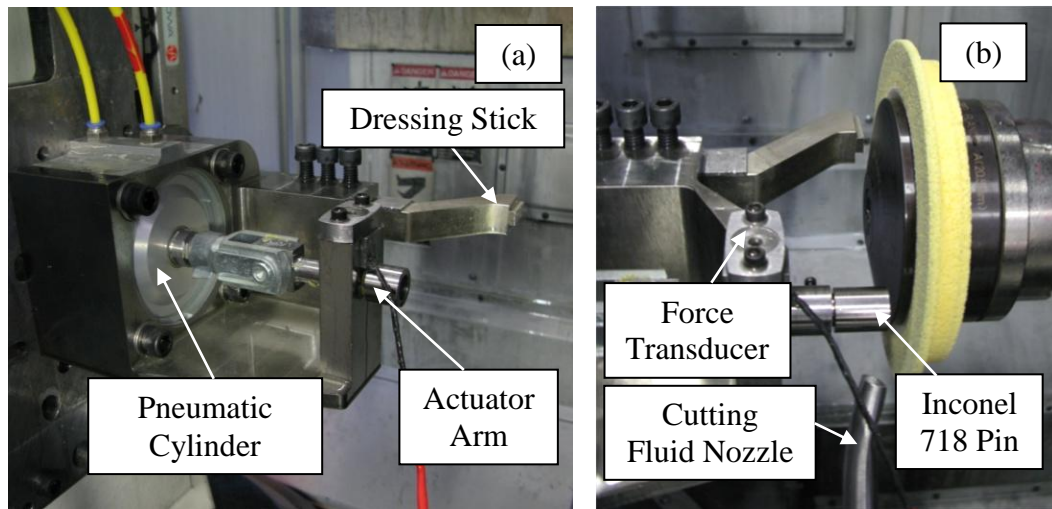


Figure 3.5.1.1 Pin on disc setup on Makino A99 machine tool; (a) Setup overview and (b) Close up image highlighting Nickel Pin and Grinding wheel.

The vertical force is applied by a pneumatic cylinder that drives the pin actuator. The pneumatic cylinder can operate between 0-10 bar pressure range that is controlled through an air pressure regulator connected to the main airline in the factory. This allowed for the vertical force on the pin to be varied for different pin diameters and is detailed in Figure 3.5.1.2.

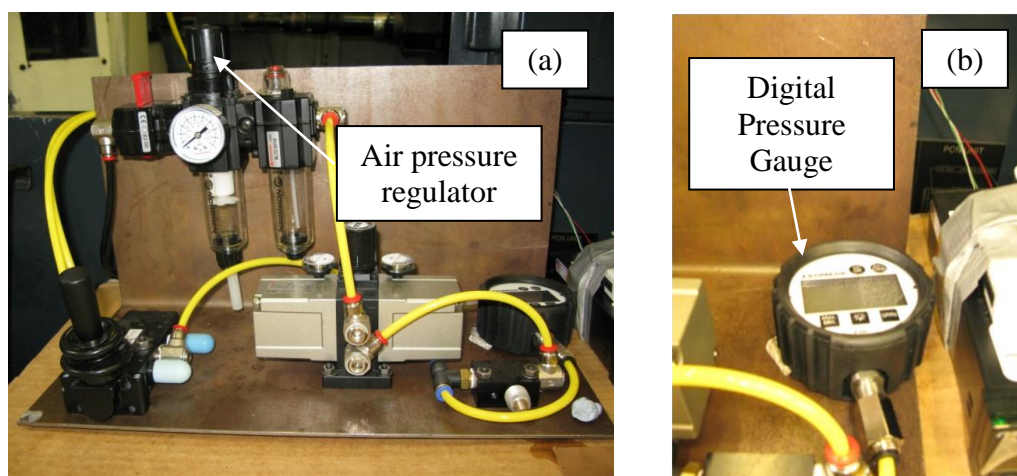


Figure 3.5.1.2 Pneumatic air regulator; (a) Setup overview and (b) Close up of digital pressure gauge.

3.5.2 Test Piece Design and Wheel Conditioning

The test piece is defined as the nickel pin for this experiment. For consistency between the machining trials and the pin on disc test, the same grade of Inconel 718 was utilised for all the test pieces. This section details the manufacture of these pins, the dimensions utilised and details of the dressing stick utilised to replicate continuous dress conditions.

A number of different pin diameters were used in the experiment to replicate the variation in contact area experienced in the machining trials. The rig holder assembly only retains pins of 14mm diameter; therefore the pins were manufactured with a stepped diameter as shown in Table 3.5.2.1. The retention diameter of 14mm was maintained for all the pin types and the diameter of engagement, representing contact area with the grinding wheel, was machined to various sizes. The pins were manufactured from a 2m length of 20mm diameter Inconel 718 Bar. The manufacturing method included sawing the individual pins to length and then turning to the geometry detailed below on a centre lathe. The number of pins required for each of the diameter types were determined by the testing regime which is detailed in section 3.5.3. The reason for the large number of 12mm diameter pins was that these were utilised at different grinding wheel speeds where the contact area was kept constant.

Diameter of Engagement (mm)	Number of Pins Required	Pin Geometry
4	3	
8	3	
12	18	
16	3	
20	3	

Table 3.5.2.1 Table of all Nickel Test Pin geometries utilised in the modified pin on disc testing rig.

The inclusion of the dressing stick was to provide continuous dressing in order to replicate the cutting conditions detailed in section 3.4. The dressing stick had a diamond coated section that was fed at a defined feed rate onto to the front edge of the grinding wheel providing a continuous dressing action. The pin on disc test rig was originally designed to hold a lathe turning tool to machine the material

surface that was in contact with the pin. This has the benefit of constantly refreshing the surface which is desirable for tribological testing. The dressing stick was thus designed to fit into the centre lathe mounting position and present the flat diamond coated section to dress the grinding wheel. The dressing stick is shown in Figure 3.5.2.1. The diamond was plated onto the metal surface and retained using a Nickel bond.

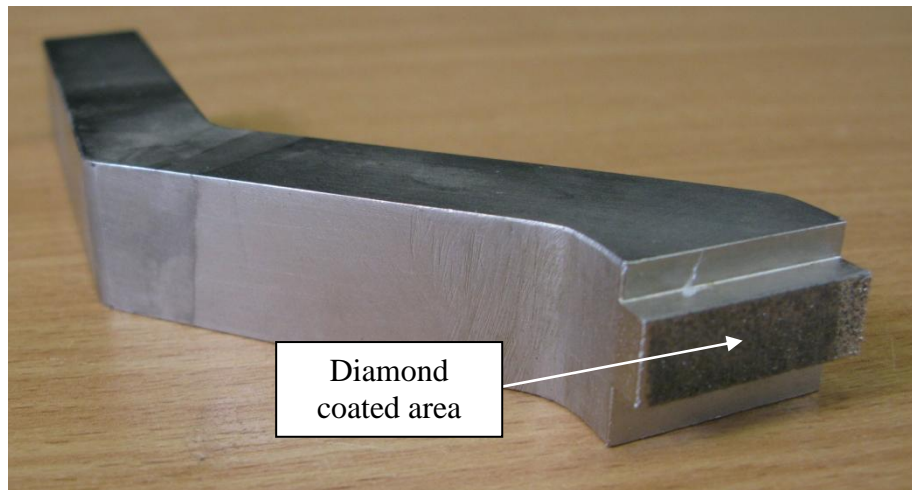


Figure 3.5.2.1 Image of the diamond coated static dressing stick utilised in the modified pin on disc testing rig.

The nickel pins and the dressing stick were all customised parts designed to convert the rig from a standard pin on disc test to provide a flat contact test for a grinding application. The materials and designs were chosen to best replicate the conditions provided from the machining trials in section 3.4.

3.5.3 Parameters and Method

The purpose of this experiment is to isolate the effect on process outputs of changing contact area and grinding wheel speed. Wheel speed is investigated as this is the parameter that has been altered in the machining trials to maintain chip thickness for constant productivity. The contact area is included to understand the impact of changing grinding wheel diameter on the outputs from the process. The parameters utilised for this testing are detailed in Table 3.5.3.1 and differ to the cutting trials in section 3.4 due to the change in experimental setup. The primary differences are that the grinding process is now a vertical feed, flat

contact which provides different kinematic conditions to peripheral grinding. The chip formation is not dependent on cut direction as opposed to up or down cutting. In addition, it is now a constant force process as opposed to constant productivity. The amount of material and the rate of its removal will be affected by the conditions in the contact zone. The applied pressure on the nickel pin was selected at 15 bar which equates to 1.5 N/mm^2 . This value represents the average vertical force per unit of contact area measured from the cutting trials in section 3.4. For consistency between experiments, the force applied to the pin by the pneumatic cylinder is referred to as the vertical force. The applied vertical force to the pin was adjusted accordingly to apply a consistent pin pressure with the different contact areas. Continuous dressing parameters were again chosen to represent the conditions in section 3.4. Flood cutting fluid application was applied to quench the contact area. This was provided from the nozzle assembly shown in Figure 3.5.1.1 (b).

Parameter	Symbol	Value
Fluid Pressure	P_f	5 bar
Fluid Flow Rate	V_f	50 l/min
Continuous Dress	N/A	Yes
Dress Rate	f_{rd}	1 $\mu\text{m}/\text{rev}$
Applied Pin Pressure	P_p	15 bar / 1.5 N/mm^2
Vertical Force Application d = 4mm 8mm 12mm 16mm 20mm	F_p	19 N 75 N 170N 302 N 471N
Time in Cut	t_p	Approx 10 s

Table 3.5.3.1 Table of parameters utilised in the modified pin on disc grinding test.

To isolate the variables independently the experiments were divided into 2 discrete tests detailed in Table 3.5.3.2. Each test maintains 1 of the variables then

ramps the other through a range of values. The grinding wheel utilised in the both the machining trials and pin on disc experiments has a maximum surface speed rating of 50m/s. As a result the grinding wheel speed range was defined between 10 – 50 m/s to assess the full potential range of application. The grinding pin diameters were selected to represent the contact areas between the wheel and workpiece in the cutting trials. The maximum pin diameter that could be utilised was 20mm as a result of the grinding wheel geometry and dressing stick setup on the machine tool. The diameter of the test pins were varied in 4mm intervals up to the maximum value of 20mm. Both experiment variables provide a significant range of application that represents the changes witnessed in the machining trials in section 3.4.

Test	Contact Diameter d_{pin} (mm)	Grinding Wheel Speed V_s (m/s)
Contact Area Assessment	4	30
	8	
	12	
	16	
	20	
Wheel Speed Assessment	12	10
		20
		30
		40
		50

Table 3.5.3.2 Table of variables and run order utilised in the modified pin on disc grinding test.

Each of the test setups included 2 additional repeats to improve the quality of the experiment. The pin diameter was changed through the use of different grinding pins with the grinding wheel speed altered through the machine tool control. Wheel speed was calculated at the central point of the pin contact area. The application of cutting fluid and continuous dressing remained constant for all the test cuts performed.

3.5.4 Data Collection

Similar to the methodology in section 3.4, the data collection for this experiment consisted of both in-process and post-process techniques. This section details the methods utilised beginning with the in-process data.

In-Process Data

The in-process data measurements were limited to mechanical outputs for this experiment. One of the most important outputs for this experiment is the force ratio between the horizontal and vertical force components as this provides useful information on the contact conditions between the wheel and workpiece. As the rig is designed to apply and maintain a set vertical force on the pin, the only measured value is that of the horizontal or cutting force component. This is measured from a single direction compressive load cell as shown in Figure 3.5.4.1. The grinding wheel is rotated to provide the cut direction shown in the figure. When the pin makes contact through the application of vertical force, a moment is created around the arm pivot forcing the actuator arm upwards into the load cell assembly. The resistance provided by the load cell assembly is measured as the horizontal force output.

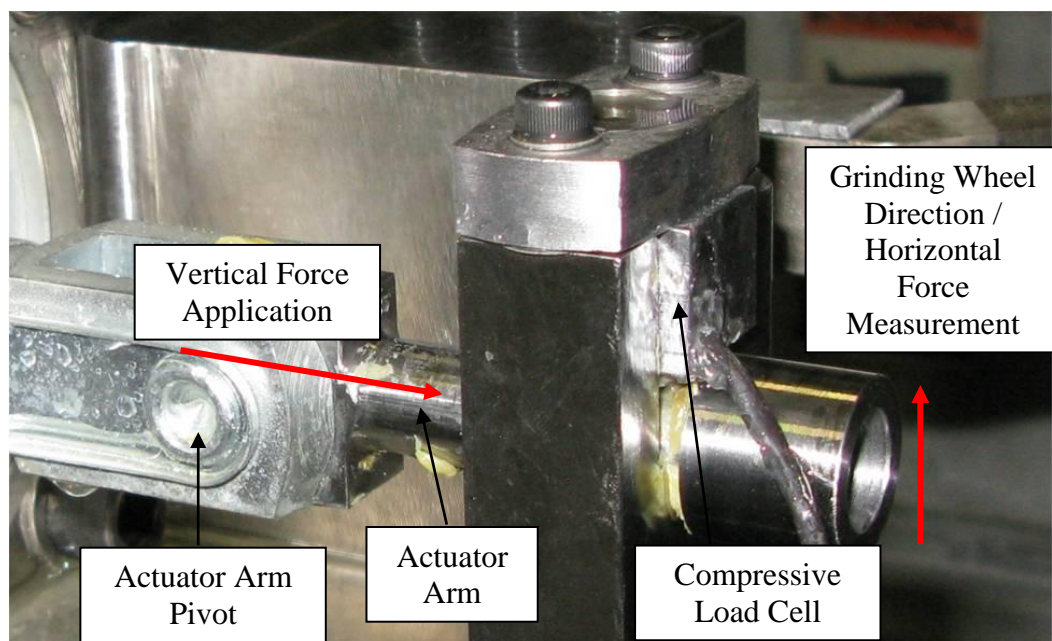


Figure 3.5.4.1 Image of pin actuator arm and load cell assembly detailing force measurement on test rig.

The load cell was calibrated using a compression structural testing machine detailed in Figure 3.5.4.2 (a). The reading from the applied load was calibrated against the digital read out display in Figure 3.5.4.2 (b). This also provided a force reading during experimentation. The sampled force data was logged using labview software for further analysis.

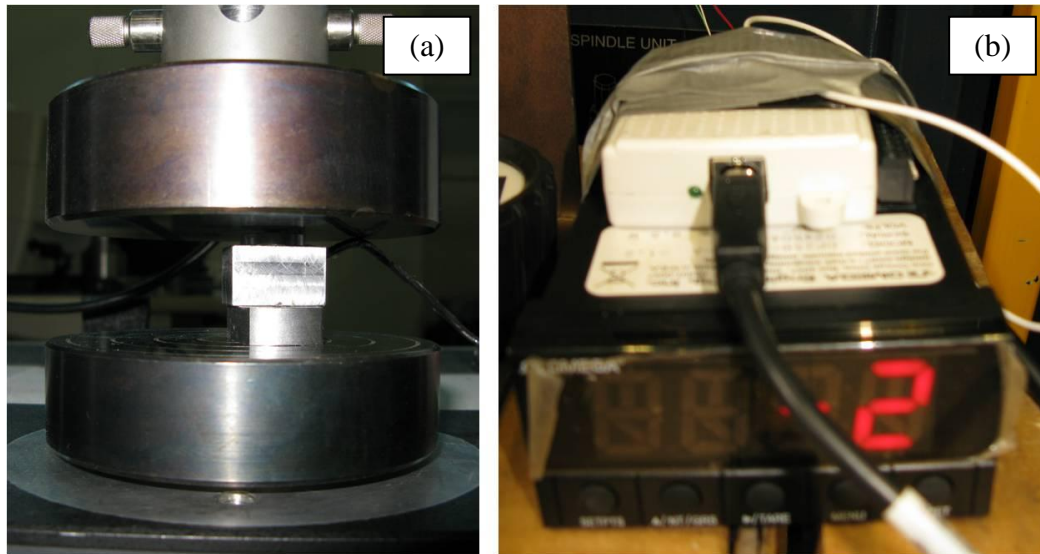


Figure 3.5.4.2 Additional images of pin on disc force measurement equipment; (a) Load cell during calibration on structural testing machine, (b) Digital read out equipment for force measurement.

Power monitoring was also included as an output for this experiment. The same equipment was utilised for this experiment as in the machining trials in section 3.4. Again the Net Power was calculated from Spark-Out Power measurements taken with the spindle rotating and the cutting fluid system activated with no load applied.

Post-Process Data

The post-process data collection for this experiment was significantly less than for the machining trials. It includes a measurement of the nickel pin wear and the surface roughness of the machined test pin surface. The pin wear was assessed as a volumetric loss of material. To measure this, the pin was weighed on scales with a 0.01g resolution both before and after a test was performed. The weight

difference was used in conjunction with the relevant pin geometry to calculate the rate of volumetric pin wear. The surface roughness of the pin surface was measured using the profilometer detailed in Figure 3.4.4.9. A single measurement line down the middle of the pin surface was used with the stylus oriented to measure across the grain direction of travel. The average of 3 repeat measurements was calculated and utilised as the output in the results section. The experimental setup for the nickel pin surface roughness measurement is detailed in Figure 3.5.4.3.

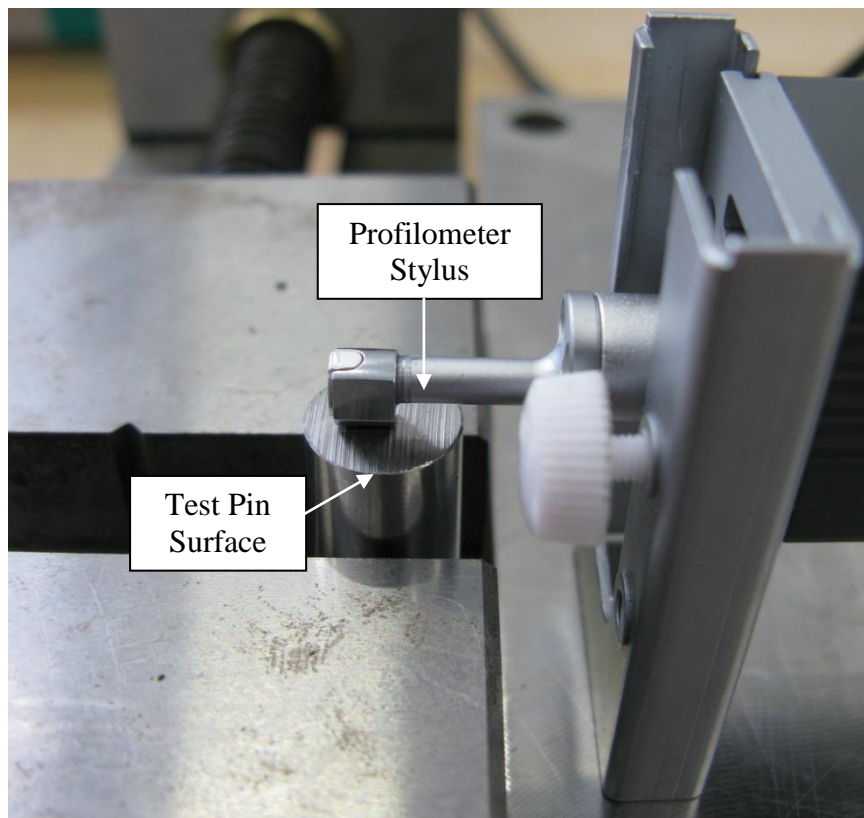


Figure 3.5.4.3 Image of the Mitutoyo profilometer setup for measurement of nickel pin Ra value.

Chapter 4 - Assessment of Chip Thickness Models

This chapter details the results of the experiments defined in section 3.4. The results assess the effect of maintaining different chip thickness models on the grinding process outputs.

As the experiment uses changing wheel diameter to alter the chip thickness for constant productivity, the grinding wheel becomes gradually smaller as the testing progresses. Considering this, results are presented with the grinding wheel radius r_s values plotted in reverse order on the abscissa for the majority of the graphs detailing a process output. Figure 4.1 shows an example of the graphical setup where specific process outputs e.g. force, power, etc would be plotted on the ordinate against the grinding wheel radius on the abscissa.

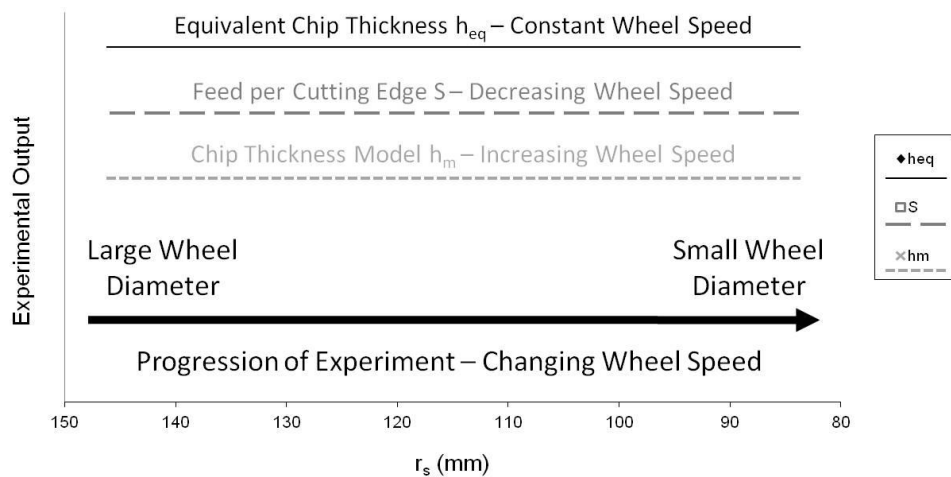


Figure 4.1 General graphical lay-out for presentation of results.

The value of chip thickness is maintained by adjusting the wheel speed as the wheel diameter changes. The change in wheel speed is dictated by the relevant chip thickness model used. These are presented again in equations (4.1), (4.2) and (4.3) for reference:

$$h_{eq} = \frac{a_e \cdot v_w}{V_s} \quad [67] \quad (4.1)$$

$$S = v_w \cdot t_{res} \quad [5] \quad (4.2)$$

$$h_m = \frac{4}{C \cdot r} \frac{v_w}{V_s} \frac{a_e}{d_e}^{\frac{1}{2}} \quad [5] \quad (4.3)$$

A reduction in grinding wheel diameter produces the following changes in wheel speed in order to maintain the chip thickness value at constant productivity; h_{eq} wheel speed remains constant, S wheel speed reduces and for h_m wheel speed increases. Figure 4.1 also shows the relevant labelling utilised for the varying data sets. These remain consistent for the majority of the results presented. Each chip thickness model data set indicates that the defined chip model size is maintained at varying wheel diameters. The results have been presented in this way to show the progression of the grinding process outputs, whilst maintaining the different chip thickness models, as the wheel reduces in diameter.

Furthermore, results for the radial wheel wear have not been included in this chapter. This is due to the testing being performed under continuous dress conditions. Checks for additional radial wear of the wheel beyond the programmed dressing infeed amount were performed. None of the cut setups performed experienced radial wheel wear in excess of the programmed CD amount.

4.1 The Effect of Chip Thickness on Specific Grinding Energy

The aim of maintaining chip thickness is to attempt to improve control of the grinding process outputs. Shaw [6] suggests that the specific grinding energy in grinding is related to the chip thickness as detailed in equation (4.1.1).

$$u \sim \frac{1}{t^n} \quad (4.1.1)$$

Where u = Specific Grinding Energy

t = Grinding Chip Thickness

n = integer defined by process, between 0.8 and 1.0 for grinding

This equation suggests that specific grinding energy remains constant with the application of a constant chip thickness. This section examines the specific grinding energy of the grinding process as the wheel reduces in diameter and chip thickness is maintained.

Figure 4.1.1 details the net power calculated for the different chip thickness model data sets. All the power results utilise the maximum power value taken from smoothed spindle power data. The net power was calculated from the maximum value taken from both the cutting and spark out data. A linear trend provides the best description of how net power decreased along with the grinding wheel radius. The largest decrease was witnessed whilst maintaining the h_m model. The net power experienced a 0.7kW drop in power requirements over the life of the wheel. The S model and h_{eq} models also showed a reduction in net power of 0.1kW and 0.4kW respectively.

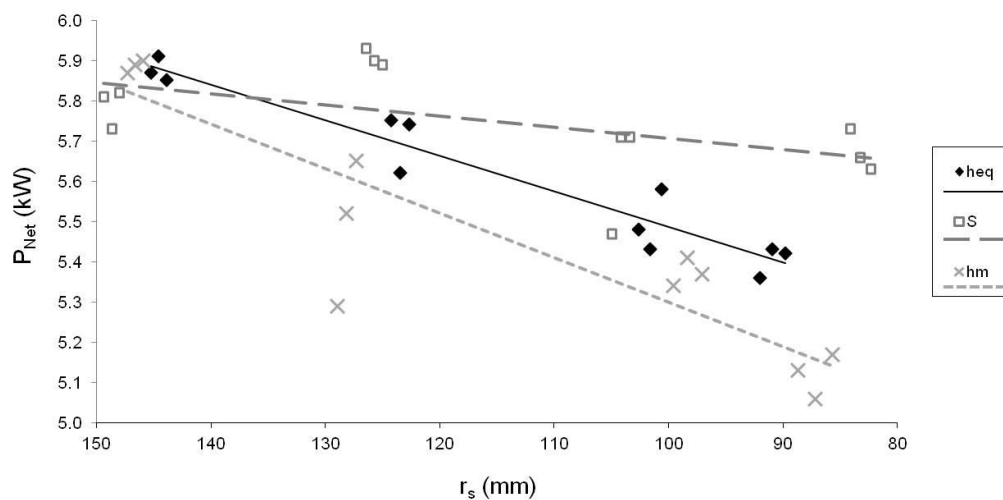


Figure 4.1.1 Smoothed Net Power output versus grinding wheel radius.

The force output is important both as an alternate method of calculating specific grinding energy but also as a mechanical output that can affect the production

process with respect to fixture and spindle deflection. Figure 4.1.2 shows the result for the maximum net force output measured during experimentation. Both the vertical and horizontal components are included in the same graph. These labels for the force components are preferable in creep feed grinding due to the large depth of cut changing the resolved direction of the calculated normal force component. The scatter in all the force results are much reduced providing clear linear trends for all the chip thickness models. The vertical force shows significant variation in the force outputs between the chip thickness models at the small wheel diameters; with a difference of more than 200N between the S and h_m models. The pattern of behaviour between the chip thickness models is similar to Figure 4.1.1; the h_m model providing the lowest output value and the S model the highest output value at the small grinding wheel diameters. However, unlike the results for P_{Net} , the S model shows an increase in force as the grinding wheel reduces in diameter. When the grinding wheel speed is maintained in the h_{eq} model, there is a small drop in the force output with reducing wheel diameter. The pattern for the horizontal force results is similar to the vertical force although less variation in the force values is present between the chip thickness model data sets.

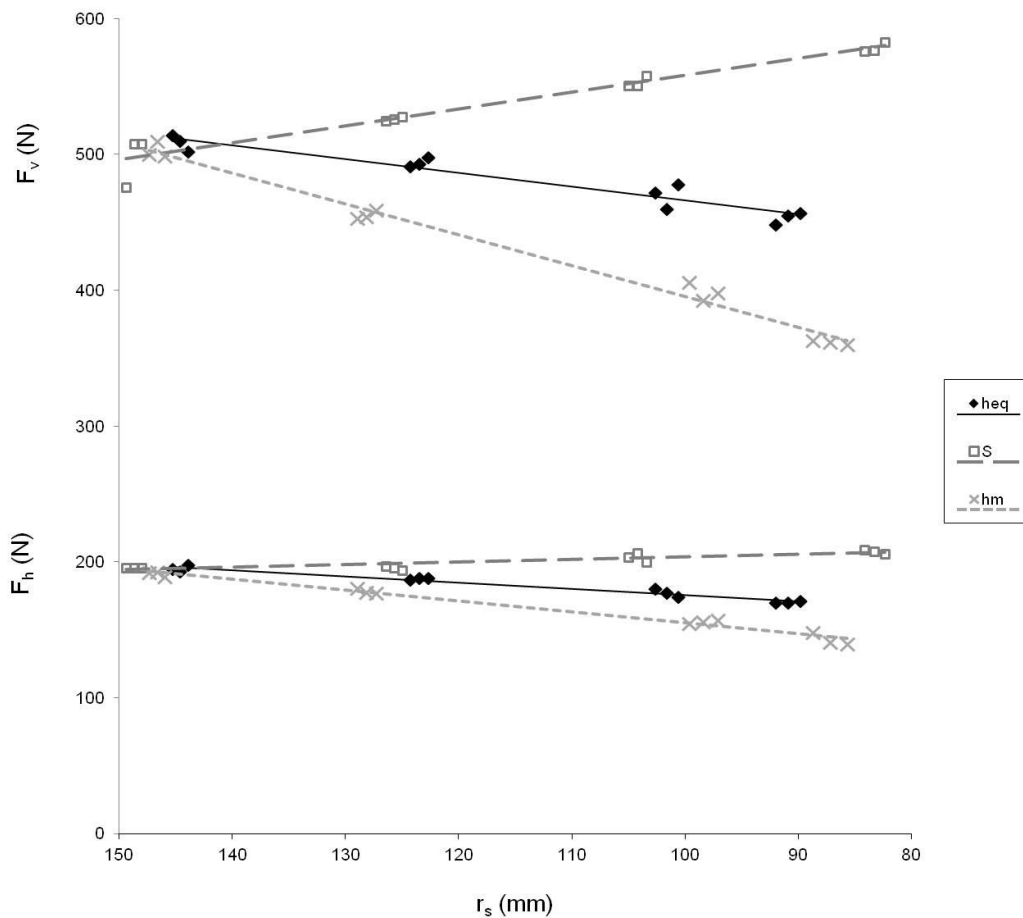


Figure 4.1.2 Vertical Force (F_v) and Horizontal Force (F_h) outputs measured from a Kistler Dynamometer versus grinding wheel radius.

The change in force output detailed in Figure 4.1.2 can be attributed to the reduction in contact area as the wheel diameter reduced. Figure 4.1.3 plots the force per unit contact area against grinding wheel radius to assess this effect. The results show that the force per unit area remains consistent with changing wheel radius for the h_m model for both the horizontal and vertical force components. The h_{eq} model shows a slight increase with the S model displaying a larger increase. The overall force output is produced from the summation of the individual forces experienced by each abrasive grain. The data presented in Figure 4.1.3 provides a representative value of the force experienced by an individual grain. This is due to the estimation of the number of grits per unit area on the wheel surface, detailed in section 3.2, giving a value of approximately $0.93/\text{mm}^2$. The results show that the h_m model provides consistent force per unit

of contact area. This agrees well with the analytical development of h_m which is estimated by maintaining a maximum chip thickness for an individual ideal cutting grain.

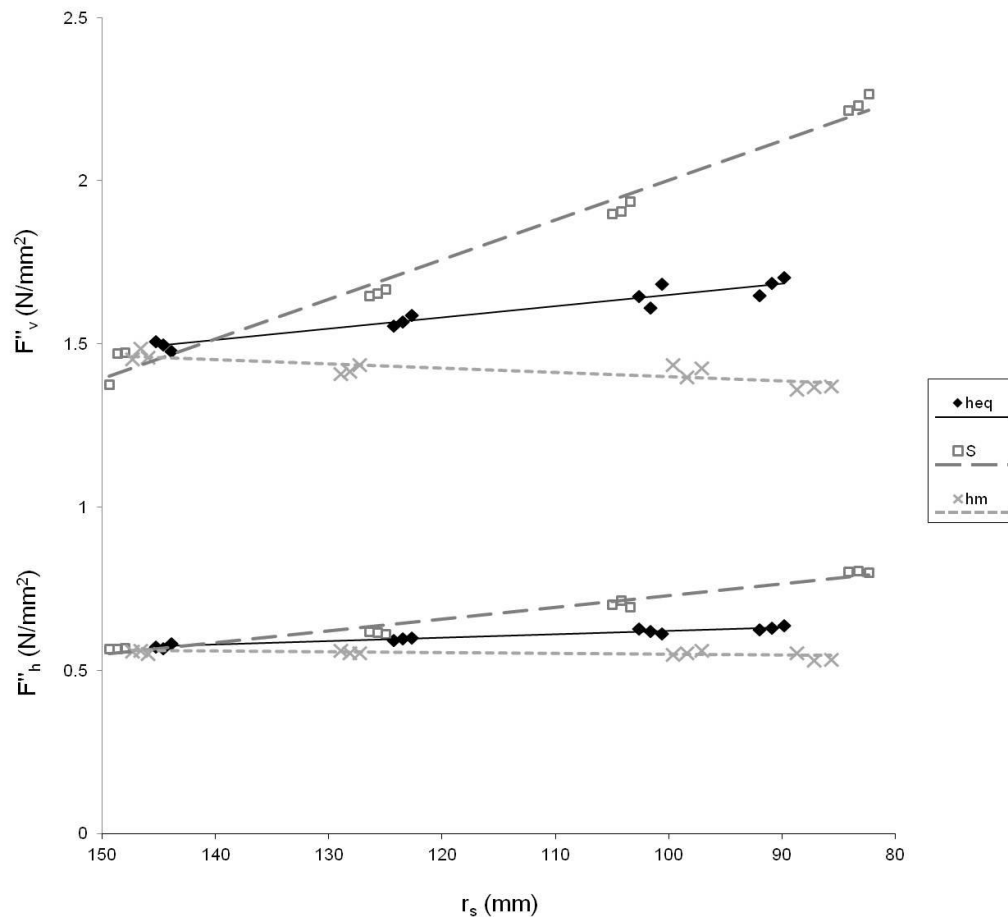


Figure 4.1.3 Vertical and Horizontal Force per unit contact area versus grinding wheel radius.

The specific grinding energy (SGE), Figure 4.1.4, was calculated utilising both the net horizontal force and net power data detailed above. The value of e_c is higher using the net force data as shown in Figure 4.1.4(a) in comparison to the net power data detailed in Figure 4.1.4(b). Furthermore, the behavioural trends of the chip thickness model data sets are different depending on whether the force or power is used to calculate the specific grinding energy. The reason for the increase in e_c when calculated using the horizontal force data is due to the larger net force results in comparison to net power. An explanation for this could be the spark out methodology utilised in this experiment not providing a true

representation of spark out force. Due to constraints on the test piece geometry, a spark out pass was performed by running the grinding wheel over the cut surface at zero depth of cut. The spark out force measured may be increased if the grinding wheel had been stopped during cut with a full contact arc engaged due to increased push off in the contact zone from the coolant [81]. A full arc of contact engagement during the spark out pass would have resulted in larger values of spark out force thereby reducing the overall Net Force. This would have led to the values between net power and net force to be more comparable.

Considering the results from the net horizontal force data in Figure 4.1.4(a); h_m showed a small decrease of approximately 1 J/mm^3 with wheel radius, h_{eq} decreased by 5 J/mm^3 and the S model showed a decrease of 7 J/mm^3 . This is very different to the results presented for the net power data set. The difference in trend behaviour between the force and power data sets in Figure 4.1.4 can be explained by the calculation for e_c from the net horizontal force data. The calculation detailed in Shaw [6] and presented in section 2.5 is dependent on the value of F_h and V_s . It is shown again in equation (4.1.2) for reference. The bottom line of the equation remains constant in this experiment as the grinding process is performed at constant productivity.

$$e_c = \frac{F_h \cdot V_s}{v_w \cdot b \cdot a_e} \quad (4.1.2)$$

Where F_h = Net Horizontal Force

V_s = Grinding Wheel Speed

Equation (4.1.2) was designed for surface grinding applications and the effect of wheel speed seems to dominate the calculation of e_c for this experiment using creep feed conditions. In consideration of this, the S model in Figure 4.1.4(a) shows a significant reduction in SGE with decreasing wheel radius. As the results in Figure 4.1.2 highlight a net horizontal force increase for the S model, the reduction in wheel speed, associated with the maintenance of S, presents itself as the dominant factor in the calculation. This indicates that the value of V_s has more influence on the results for e_c which do not correlate with the net power

data. It is suggested that equation (4.1.2) may not be suitable for the calculation of e_c in this experiment. For the reasons presented, only net power results will be utilised in the calculation and analysis of specific grinding energy for the remainder of this thesis.

Figure 4.1.4(b) details the e_c results provided by the net power data. These show different trend behaviours to the values calculated from the net horizontal force data. Here the h_m model displays the largest reduction in e_c with decreasing wheel radius. This provides interesting discussion in relation to equation (4.1.1) as the h_m model is largely considered to be a good estimation of grinding chip thickness. With chip thickness maintained, there is still a change in the specific grinding energy of the process. Evidently, there are other factors that affect the energy requirements of the process aside from pure kinematic calculation. Considering the other chip thickness model data sets, the S model shows little variation with wheel radius as all the results are within a range of 1 J/mm^3 and the h_{eq} model showing a reduction of approximately 2 J/mm^3 over the diameter range of the grinding wheel. The trends of e_c calculated from the net power data, mirror the results in Figure 4.1.1 as the productivity remains constant during the experiment.

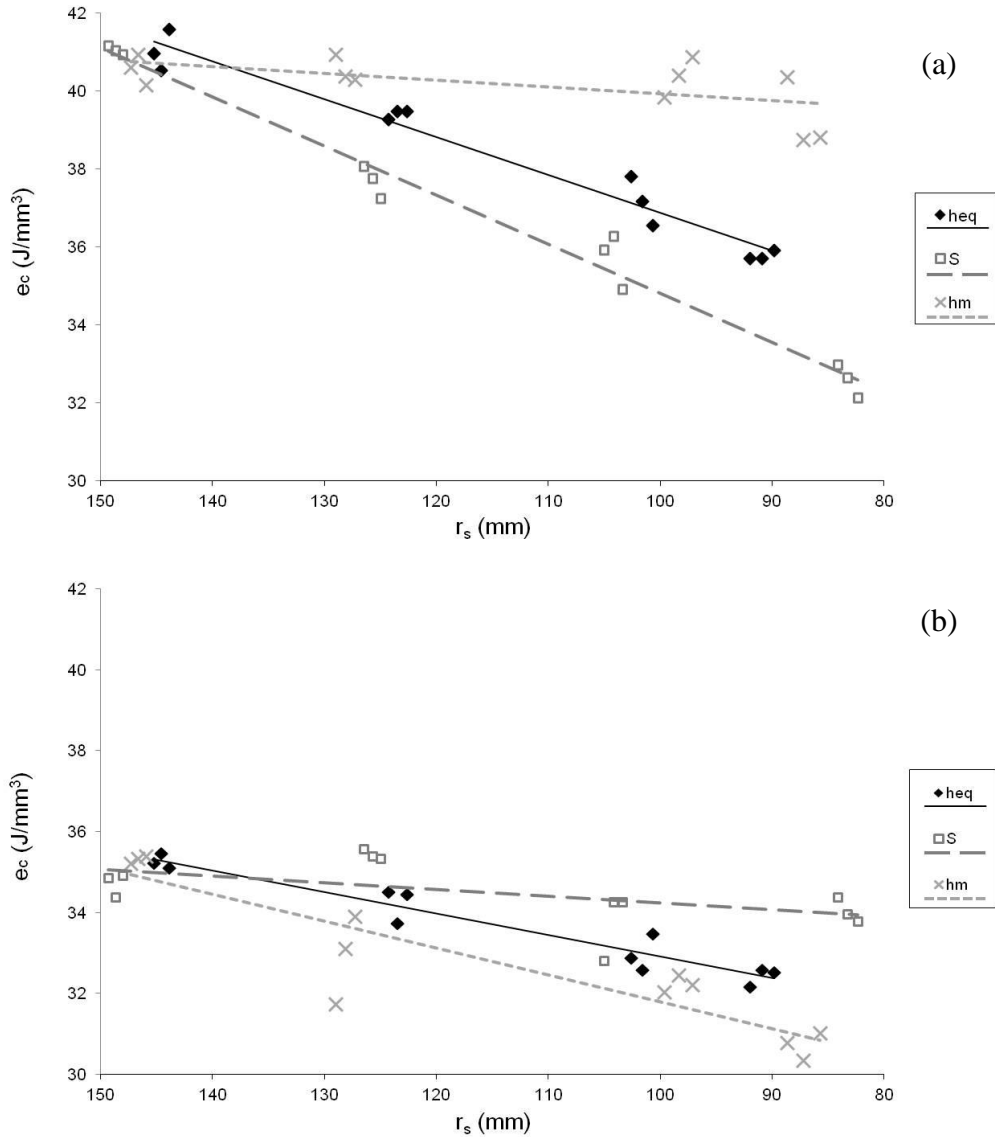


Figure 4.1.4 Specific Grinding Energy versus wheel radius; (a) e_c calculated from net horizontal force data and (b) e_c calculated from net power data.

The specific grinding energy output varies over the diameter range of the wheel even with the application of models to maintain chip thickness. The variation is smallest for the S chip thickness parameter. It is proposed that the effect of changing contact area and grinding wheel speed has an impact on the energy required by the process. The reasons for this are explored further in Chapters 5 and 6.

4.2 Heat Flux and Workpiece Temperature

The specific grinding energy considered in section 4.1 can have a significant impact on the temperatures experienced by the workpiece in grinding as the majority of the energy is converted into heat during the process. As referenced in section 2.5, this can have significant effects on the surface integrity and subsequently the fatigue life of components [58]. This section investigates the calculated heat flux from the process and temperature outputs whilst maintaining the various chip thickness models.

The heat flux into the contact zone was calculated by dividing the net power by the contact area between the wheel and workpiece. The results are detailed in Figure 4.2.1. The general trend is different to the SGE energy results as the heat flux increased with a reduction in grinding wheel radius for all the chip thickness models. This is due to the contact area reducing at a faster rate in comparison to the net power. The S model showed the largest increase, the h_{eq} model providing the second largest increase with the h_m model displaying the smallest change over the progression of the experiment. This increase in value for all the chip models indicates that a temperature rise would be expected in the surface of the workpiece when considering the effect of heat flux in isolation. Empirical work on creep feed grinding of a Nickel-Base alloy [8], showed that the power flux, equivalent to heat flux, resulting in workpiece burn was between 10 – 20 W/mm² depending on grinding wheel speed. These values are similar to the values measured from this experiment and a rise of over 4 W/mm² is shown from the S model data. This highlights the importance of the ability to maintain heat flux in order to avoid workpiece burn. It should be noted that no energy partitioning has been considered for the results in Figure 4.2.1 which could significantly affect the amount of heat flux entering the workpiece. This is considered in greater detail in Chapter 6.

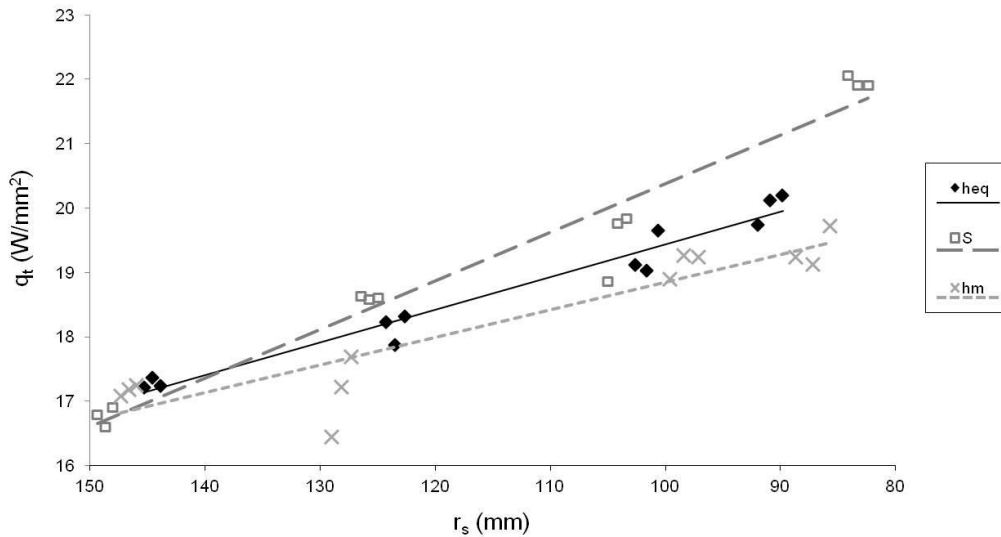


Figure 4.2.1 Calculated Heat Flux from Net Power data versus grinding wheel radius.

Temperature measurements were taken from embedded thermocouples in the workpiece assembly to provide data on the thermal effects of the process. The embedded thermocouples were placed at varying depths below the cut surface in order to provide a temperature distribution. An example of the different thermocouple outputs for a single experimental cut is shown in Figure 4.2.2. Using the principle outlined by Kato and Fuji [66], a logarithmic scale was placed on the ordinate and a linear trend line applied to the data set to estimate the ground surface temperature T_c . An example from an individual cut is presented in Figure 4.2.2 providing an approximate value for T_c of 101°C. It is these temperatures that are utilised in the results for this section.

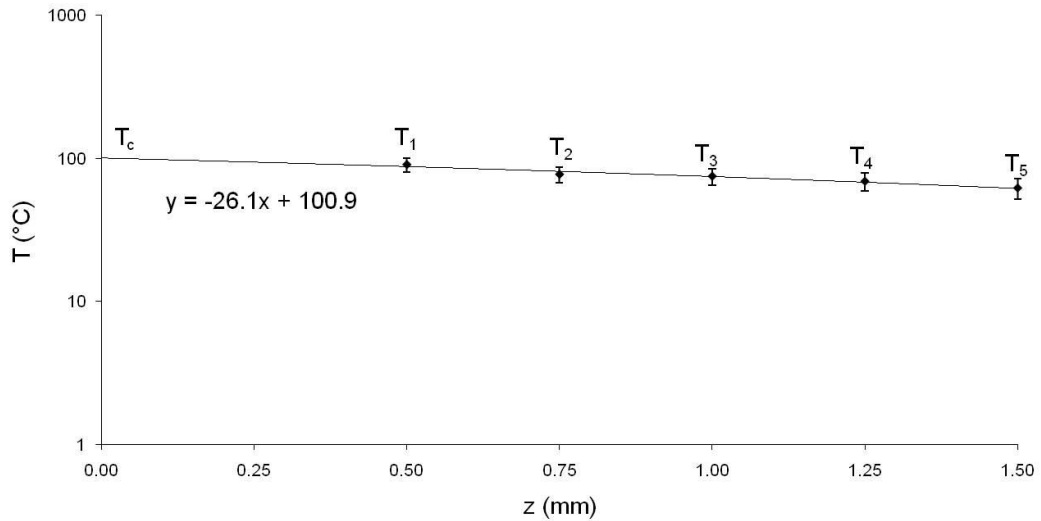


Figure 4.2.2 Thermocouple temperature values versus depth from ground surface to estimate ground surface temperature.

Figure 4.2.3 details the estimated workpiece surface temperature for all the experiments performed, calculated from the embedded thermocouple data. Linear trend lines have been applied to the individual data sets for each chip thickness model. The h_m data set shows a general reduction in temperature, h_{eq} remaining constant with the S model data showing a gradual increase as the wheel diameter reduces. It is noted that a significant amount of scatter is present in these results and the trend lines applied used to describe the variation in surface temperature with wheel radius are a best fit. The trends for the surface temperature do not match to the calculated increase in heat flux for all the chip thickness models utilised as shown in Figure 4.2.1. Even the maintenance of h_m results in an increase in heat flux which does not correlate to the decrease witnessed in surface temperature. Although the temperature results do not match the heat flux, the order between the chip thickness models correlates with the temperature results with the maintenance of S producing the least desired workpiece conditions followed by h_{eq} and h_m respectively. This discrepancy between the heat flux and surface temperature trends are explored further in Chapter 6.

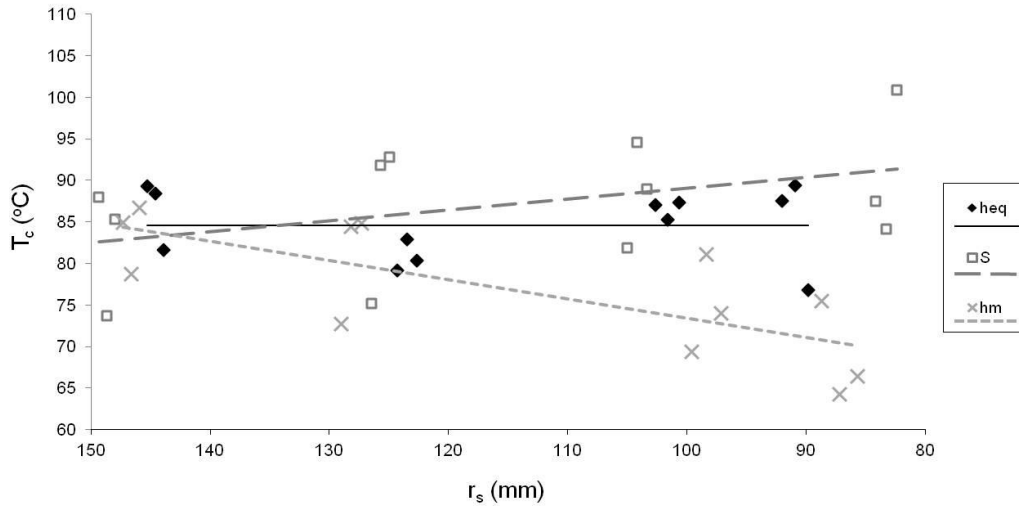


Figure 4.2.3 Graph of estimated ground Surface Temperature versus wheel radius.

As shown in Figure 4.2.3, the variation in surface temperature over the life of a wheel can be up to 35°C for the same productivity cut at the small wheel diameters by maintaining different forms of chip thickness model. Considering the burn out temperature for water is around 150°C [8], where the creep feed process can become very unstable, this kind of variation could be significant. However, the results also show that the inherent scatter variation of the h_{eq} chip thickness model data is up to 15°C. This highlights how difficult it is to maintain a constant output of temperature in a grinding process under identical input parameters. The temperature results presented are indicative of the grinding behaviour and are combined with the other output data to understand the effect of maintaining chip thickness on the process outputs. The statistical significance of the trends in the data sets is assessed in section 4.5.

An obvious discrepancy exists between the increasing heat flux for all chip thickness models at reduced wheel diameters and the surface temperature data. The major difference between the models is the change in grinding wheel speed which can have an impact on the thermal characteristics of the grinding process. Theoretical topics explaining this behaviour include contact layer theory and convection coefficients, which are investigated in Chapter 6.

To further investigate the in-process measurements of heat flux and temperature, some laboratory based surface integrity analysis was performed. A small number of samples from the data set were selected due to time intensive nature of the laboratory work. The samples were selected to represent the initial conditions of the experiment, with the grinding wheel at its largest diameter, and the extremities of maintaining the chip thickness models at the smallest wheel diameter. The baseline cut R01 represents the starting conditions with results R29, R31 and R36 representing the smallest wheel diameters whilst maintaining h_{eq} , h_m and S respectively. The run order of the experiments is shown in appendix C and details which results are represented by R01, R29, R31 and R36.

Figures 4.2.4 to 4.2.6 shows the Knoop hardness at varying depths below the machined surface for the R01, R29, R31 and R36 cuts detailed above. The flat horizontal black line shows the bulk hardness for the material averaged over the test piece range. The bulk hardness of the material was approximately $220 \text{ g/mm}^2 \pm 30 \text{ g/mm}^2$. This value is quite low for Inconel 718 as the material has been annealed. The choice to use annealed material was to provide consistent material properties across the test pieces which were manufactured from bar stock. The opposing argument for this selection is that the effects of thermal softening are difficult to detect through surface integrity analysis. The tests were included to identify any significant changes in behaviour to provide confidence in the results from the experiments.

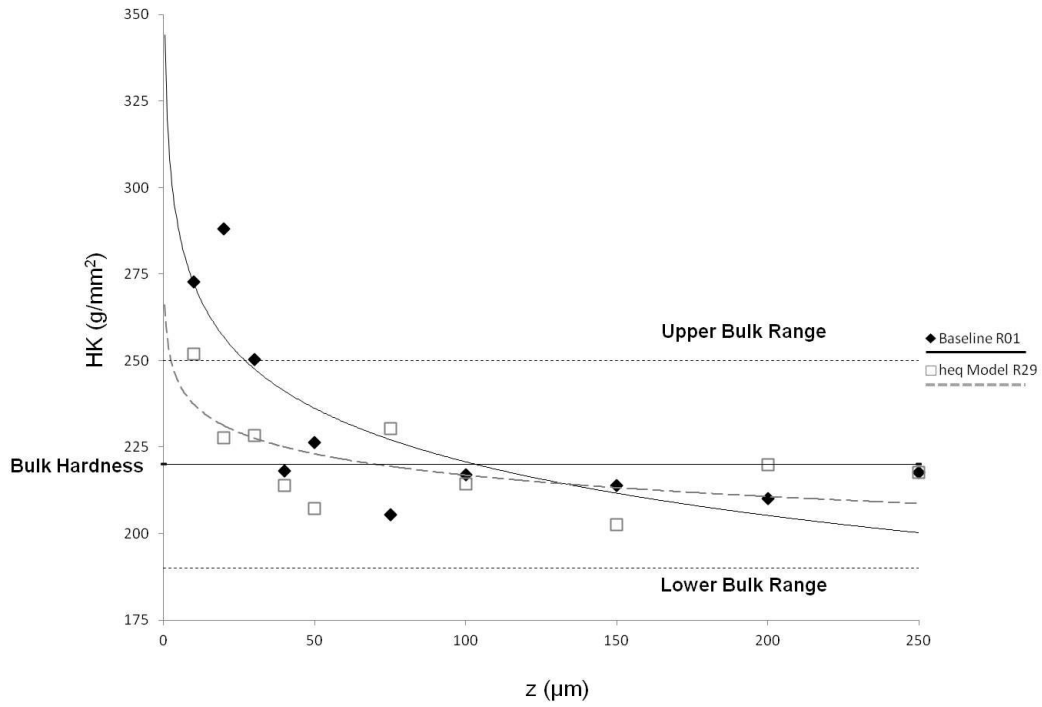


Figure 4.2.4 Knoop Hardness versus depth beneath surface for test cuts R01 and R29 with h_{eq} maintained.

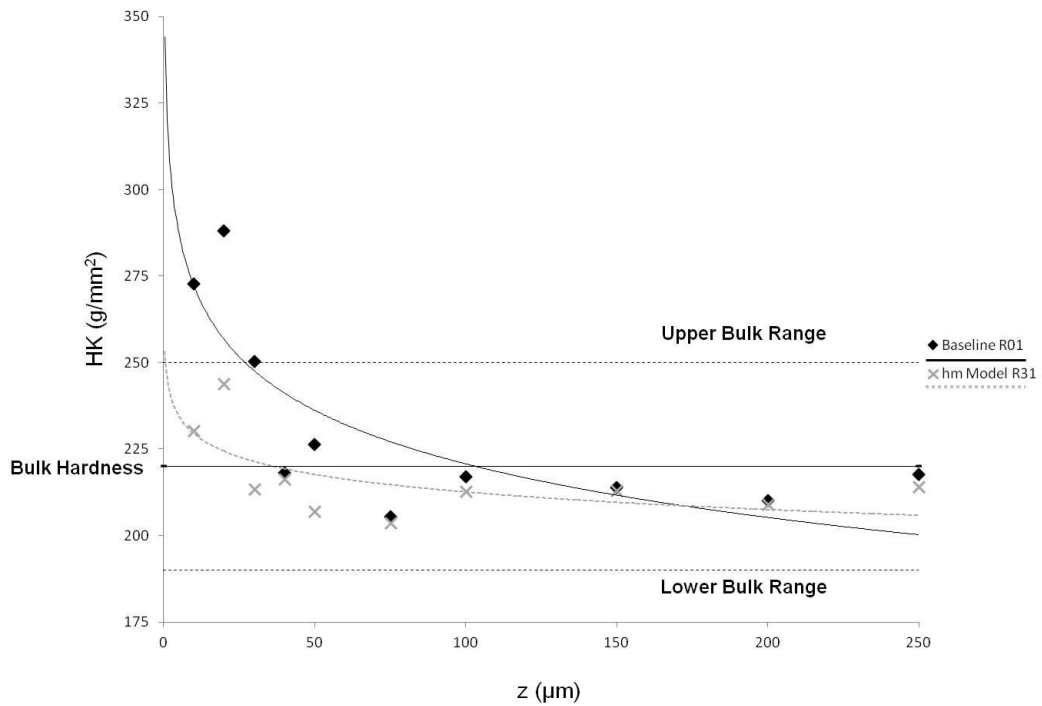


Figure 4.2.5 Knoop Hardness versus depth beneath surface for test cuts R01 and R31 with h_m maintained.

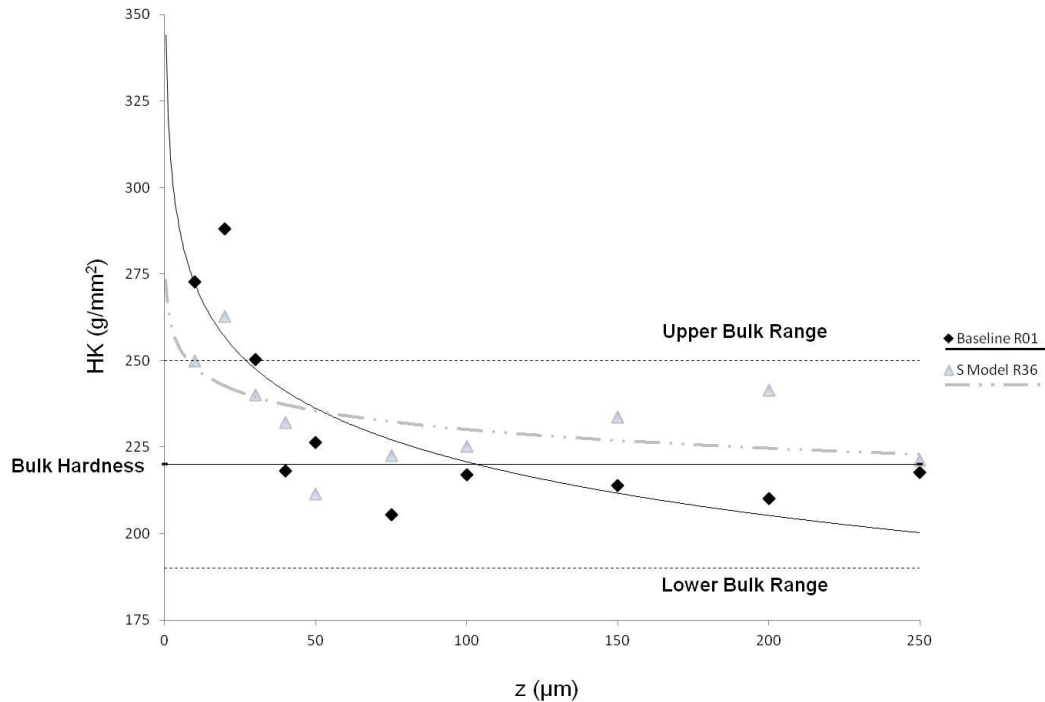


Figure 4.2.6 Knoop Hardness versus depth beneath surface for test cuts R01 and R36 with *S* maintained.

The majority of machining processes experience work hardening at the cut surface before returning to bulk hardness at a greater depth. Changes in the surface hardness can indicate variation in thermal or mechanical effects. The results in the figures have been plotted using a logarithmic data fit, similar to other hardness profile analysis, although scatter in the data does result in some deviation from the plotted trend lines. The baseline result R01 has the highest hardness at the surface but also returns to the lowest bulk hardness at a greater depth. There is little difference between the surface hardness values for R29, R31 and R36. The order of hardness from high to low, both at the surface and when returned to bulk, is R36 S, R29 h_{eq} and R31 h_m chip thickness models. The hardness testing does not show any significant surface effects due to the application of different chip thickness models.

Additional analysis performed looked at grain deformation depth beneath the workpiece finished surfaces. Multiple measurements were taken along the cut up section and the average is presented in Figure 4.2.7. The variation from the average is indicated by error bars. A larger deformation depth indicates more

mechanical working at the machined surface. The baseline R01 test piece and R36 display similar results which correlate with the higher force outputs for these cuts as detailed in Figure 4.1.2. The h_m and h_{eq} chip thickness models incur a reduced depth of deformation. This can occur through a softening of the material at raised temperatures or through a reduction in force applied to the surface. The temperature range experienced in this experiment is not large enough to cause significant softening so the difference in deformation depth is primarily due to mechanical effects. This is supported by the force results in section 4.1 reinforcing that the cuts where the S chip thickness model is maintained experience the highest forces at the small wheel diameter of all the chip thickness models tested.

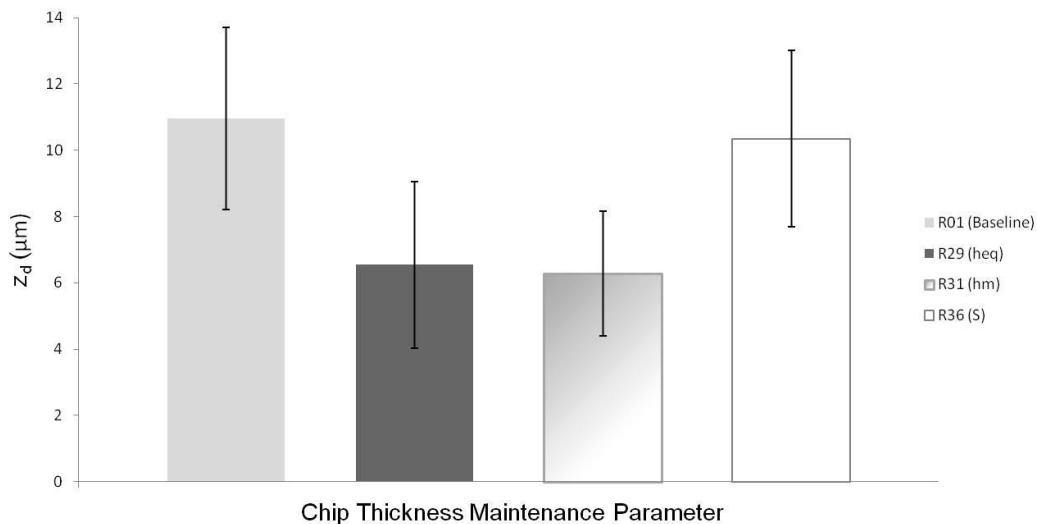


Figure 4.2.7 Deformation Depth of grain layer versus chip thickness maintenance parameter for test cuts R01 (baseline), R29 (h_{eq}), R31 (h_m) and R36 (S).

The results detailed in Figures 4.2.4 to 4.2.7 were performed to provide a post-process analysis of the experiments in order to validate any changes witnessed by the in-process measurements. No significant changes were identified from the surface integrity analysis. Inconel 718 would require much larger temperature variation during experimentation for considerably longer periods of time in order to identify significant hardness and deformation changes due to temperature effects. The application of the annealing process to the material was useful in order to normalise the base stock providing consistency over the multiple test

pieces, but left the material in an already softened state. The post-process analysis provides confidence to the force results by linking larger values of force to increased deformation depth below the ground surface.

Considering the in-process measurements detailed in section 4.2, the maintenance of different chip thickness models appears to have an impact on the surface temperatures measured during the grinding process. However, these changes are not identified in the surface integrity analysis as the temperature variations are not large enough to result in a change of material hardness. The explanation for the change in measured temperatures during the experiment is explored later in the thesis.

4.3 Surface Effects

Surface quality is a primary reason why grinding processes are implemented in a manufacturing process. The focus on the surface is essential for finishing operations although the effects from a roughing operation can have significant impact on the type and number of finishing cuts required. Although consideration of the surface quality are primarily for finishing operations rather than the roughing process reported here, the surface outputs can provide useful information with respect to the grinding behaviour. In addition, measurement of the surface quality is another useful output to investigate whether the maintenance of chip thickness can improve the control of the grinding process outputs.

Surface roughness measurements for each of the cuts performed are detailed in Figure 4.3.1. R_a was utilised as the output measurement as it is the most commonly used surface roughness parameter in the aerospace sector. The results presented show little variation in the value of R_a between the chip thickness models. There is little variation in the results as the process was performed under constant continuous dress (CD) conditions. The use of CD will have the most influence, in comparison to the application of varying chip thickness models, on the surface topography of the wheel and subsequently the machined surface roughness. The small trends that are visible in Figure 4.3.1 show a small increase

in Ra with a reduction in wheel radius which is most noticeable for the S model data set. However, the majority of the surfaces measured are within 0.2 Ra of each other showing a consistent surface roughness output for the process.

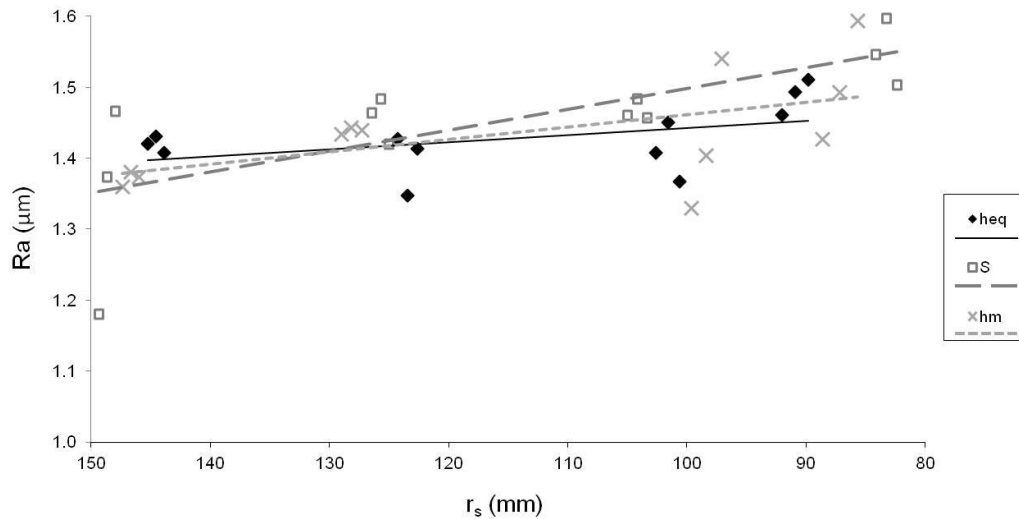


Figure 4.3.1 Measured surface roughness Ra versus wheel radius for cut surfaces on metal test pieces.

In addition to the metallic test pieces, the surface of the wheel was characterised using a graphite block scratch test detailed in section 3.5. Originally, this test was to be utilised for a non-CD process where different chip thicknesses would have impact on the wheel structure and topography. With the application of CD to provide a constant wear assessment of the process outputs, the graphite test is a useful measure of experimental consistency and to detect any major deviations in the CD conditions. It is an innovative way of establishing static wheel topography and providing additional information about the grinding process. In addition, it is a useful measurement to support the surface roughness measurements taken from the metallic test pieces.

Figure 4.3.2 shows the Ra values for the scratch tests performed on the graphite test pieces. There are fewer test results at the larger wheel diameters in comparison to the rest of the results presented in Chapter 4. The first 7 results from the graphite test work were left out of the analysis due to the tests being performed at different scratch depths. This was due to variation in the graphite

test piece geometry between samples. To rectify this, a datuming pass was performed before every scratch test to ensure a constant scratch depth. The roughness of the graphite surfaces produced from the test is significantly larger than those for the metallic test pieces in Figure 4.3.1. This is due to the static nature of the test. In a grinding process multiple abrasive grains overlap during the cutting process forming a much smoother surface. With this test, the wheel remains stationary so the graphite surface formed provides an imprint of the static topography of the grinding wheel resulting in a rougher surface finish. Figure 4.3.2 shows a clear increase in the graphite surface roughness with decreasing wheel radius with values ranging from 4.5 up to 10.0 Ra. The trends are similar for all the chip thickness models which indicate that the application of the various chip thickness models does not have a significant impact on this output. The reason for the increase in Ra is due to changes either in the dressing or scratch conditions at the different grinding wheel diameters. The reason for this change is explored later in this section.

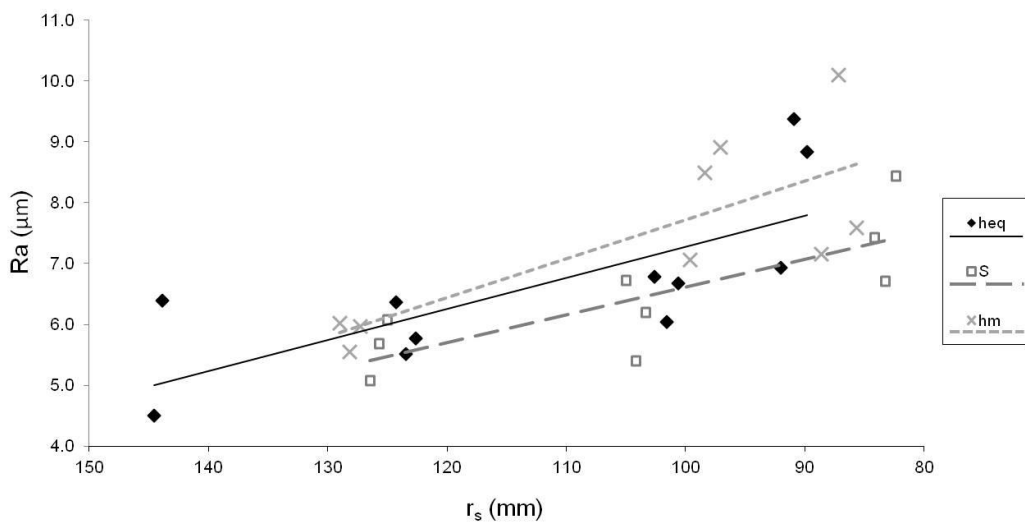


Figure 4.3.2 Measured surface roughness Ra versus wheel radius for cut surfaces on graphite test pieces.

In addition to the surface roughness measurement, force data was recorded for the graphite scratch test. Similar to the results presented in Figure 4.3.2, the first 7 results have been left out due to a change in the experimental procedure. Figure 4.3.3 details the force measured for each of the scratch tests performed. The

vertical force shows a small decrease in value with grinding wheel radius. This corresponds with an increase in surface roughness. The trend is less visible for the horizontal force. The S model appears to show an increase in horizontal graphite scratch force F_{hG} with wheel radius, but this is largely affected by the outlier data point at around 200N. This appears to be the only point with such high variation.

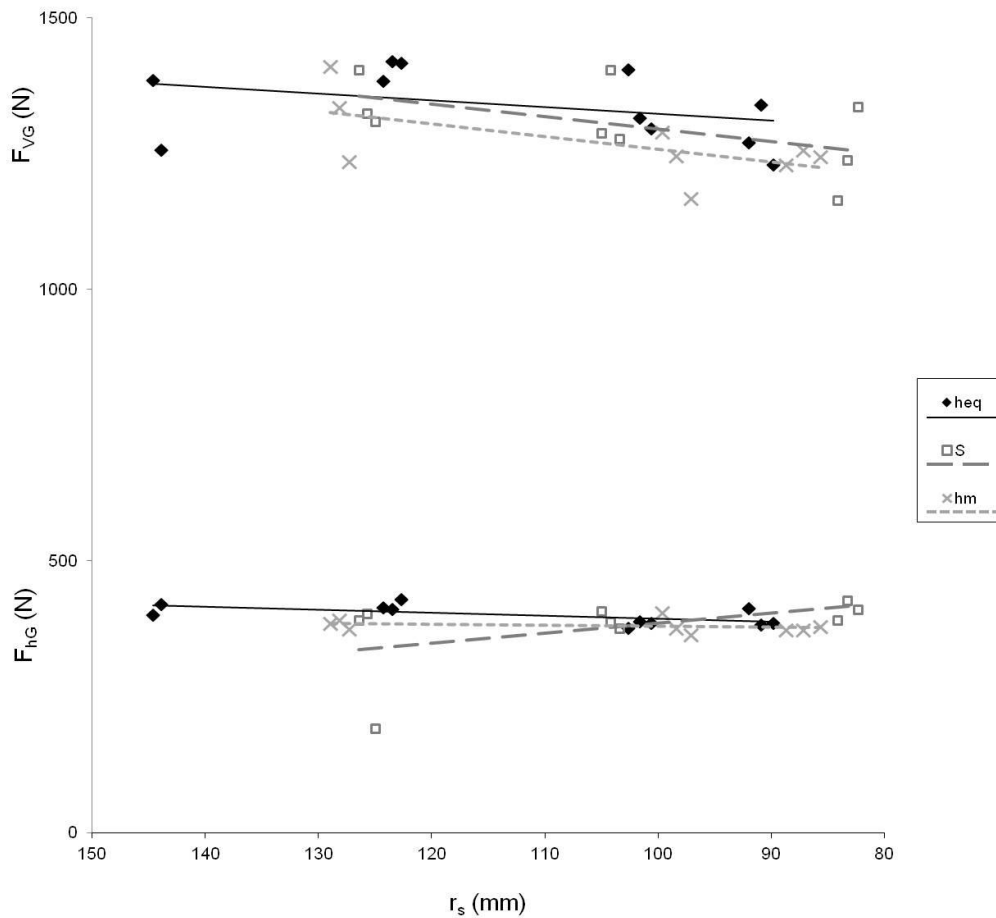


Figure 4.3.3 Vertical and Horizontal Force versus grinding wheel radius for static graphite scratch tests.

A useful parameter to evaluate is the friction coefficient between the wheel and workpiece for the graphite scratch test which is calculated by dividing F_{hG} by F_{VG} . The results for the graphite friction coefficient are detailed in Figure 4.3.4. It shows that the coefficient remains consistent over the course of the experiment.

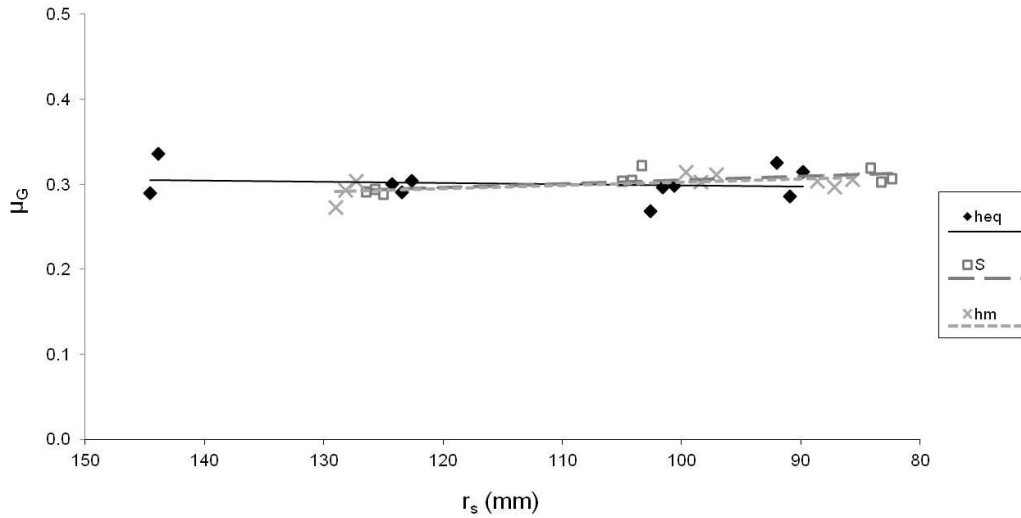


Figure 4.3.4 Calculated Friction Coefficient versus grinding wheel radius for static graphite scratch tests.

Explanations for the roughness and force trends for the graphite results focus on the topography of the grinding wheel. The wheel topography is influenced primarily by the CD process for this experiment. This includes the amount of material removed by the CD process after the wheel has left the Inconel workpiece. The clearance distance from the workpiece material for each cut before the dressing wheel was retracted is 35mm. As the dress rate was set to 1 μ m per revolution, the amount removed from the periphery of the wheel varied as a result of changes in the grinding wheel speed and diameter. Figure 4.3.5 details the amount of grinding wheel radius dressed away during the clearance move. The approximate grain diameter for the wheel specification is included for reference. This gives an indication of how many grain layers were theoretically removed during the clearance move. The figure shows that the amount removed increased as the wheel reduced in diameter. The S model data set shows the slowest rate additional wheel dressing over the progression of the experiment. Conversely, the h_m model shows the highest rate of additional dressing at the small grinding wheel diameters. The results show that more of the wheel is removed during the clearance move at the small wheel diameters for all the chip thickness models applied. This would have the effect of removing more grains that do not have sharp profiles as a result of the metal cutting process. This

would promote rougher wheel topography for the graphite test resulting in higher values of Ra and lower force outputs.

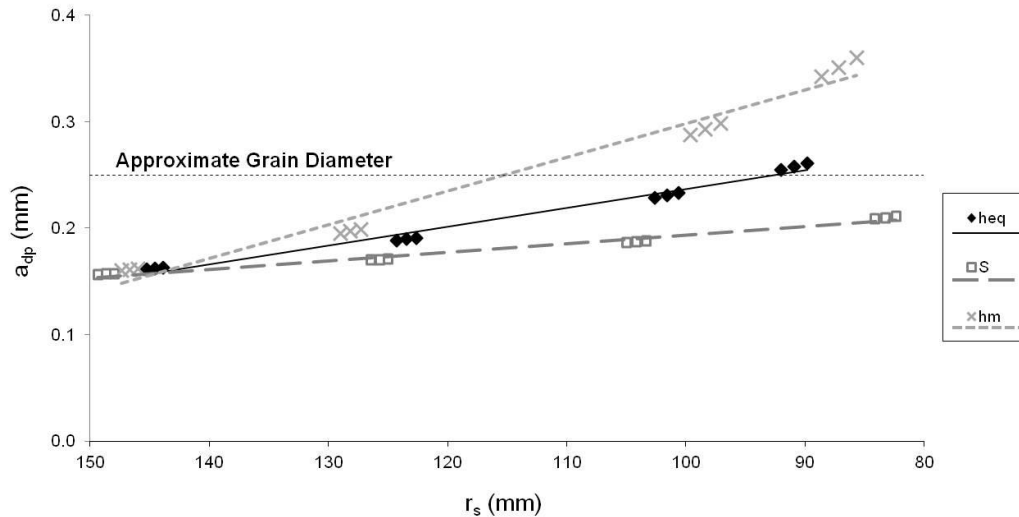


Figure 4.3.5 Amount of wheel dressed during clearance move from workpiece versus grinding wheel radius.

The issue associated with Figure 4.3.5 is that the individual chip thickness models show different rates of additional wheel dressing amount a_{dp} , whereas the results for roughness and force for the graphite trials appear to be independent of chip thickness model applied. An alternative explanation for the change in force and roughness values comes from looking at the number of grains in contact and the depth they penetrate into the graphite surface during the scratch test. This is explained in Figure 4.3.6 by the diagram detailing some theoretical grains on the periphery of a grinding wheel. The calculations have been performed utilising theoretical grain protrusions of 0.25mm. In addition a theoretical value for distance between grains L was calculated by Malkin [5] $L = \frac{1}{C \cdot b_c}$ using the number of cutting points per unit area C , and the effective cutting width b_c . The results show that the heights of a , b and c in Figure 4.3.6 all double from a grinding wheel diameter of 300mm to 150mm. In a practical application using a static wheel, this would have the effect of less overlap between the grain scratch profiles at lower diameters which would result in a rougher surface. This is more likely to account for the change in roughness results for the graphite test as the effect would be similar for all the various chip thickness models.

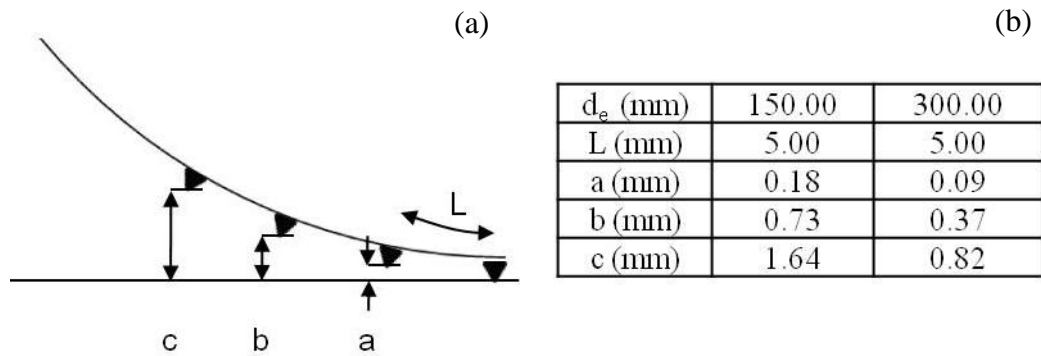


Figure 4.3.6 Explanation of grit placement for constant spacing at varying grinding wheel diameters; (a) diagram of grit placement and distance values, (b) Table of results for different diameters.

The results for the surface outputs are heavily influenced by the application of CD within the cutting process. The trends for all the surface testing do not significantly differentiate between the chip thickness models. This provides a good level of confidence that the variations in the mechanical and thermal outputs were due to changes in the contact zone effects and not changes in the wheel topography. In addition, the consistency of the results produced by the graphite testing is encouraging, as it could be utilised to good effect in an experiment where large differences in wheel topography are expected.

4.4 The Effect of Vibration on Results

Vibration can impact on the outputs of a machining process in a variety of ways and can lead to high mechanical outputs, high wear and sometimes damage to machine tools and components. In the context of this work, a measurement of vibration through the embedded accelerometer was included to identify:

- Areas of the experiment that were significantly affected by vibration.
- Changes in the process vibration as a result of applying the different chip thickness models.

The vibration amplitude data was collected using an embedded accelerometer as detailed in section 3.5. The raw time domain signal is shown in Figure 4.4.1 (a) which details the amplitude of measured vibration against time. The result shows that a large sampling frequency was utilised, 50kHz for this experiment, by the density of the signal displayed. The signal also shifts towards more negative amplitudes as the time increases. This was identified as low frequency drift caused by the large vibration experienced during the grinding process. For a more consistent analysis of the signal, a high pass filter was applied at 10kHz to produce the treated signal in Figure 4.4.1 (b). The same treatment was applied to the signal for each cut performed to allow further analysis.

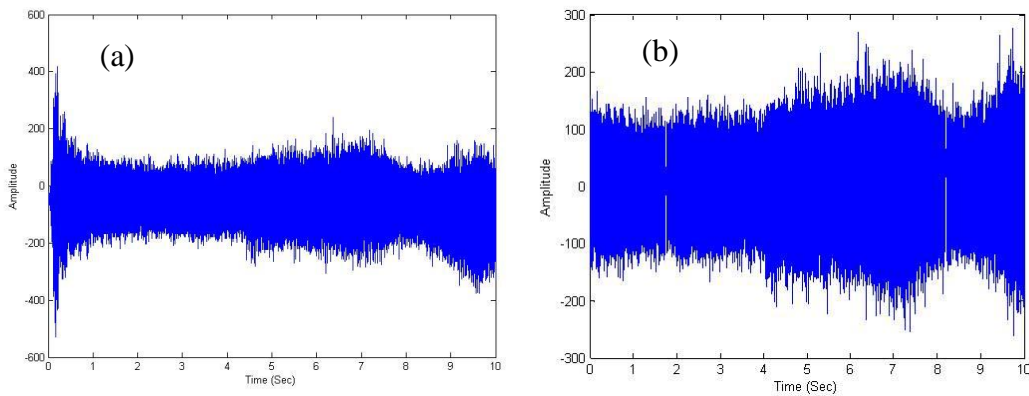


Figure 4.4.1 Time domain amplitude signal data from embedded accelerometer; (a) Raw untreated signal with low frequency drift, (b) Signal treated with High Pass filter.

In order to identify changes in the vibration signal, process monitoring techniques were applied. This included the use of the summary statistics applied to the time domain data as shown by Worden et al [82]. These give an efficient overview of the time domain under investigation and should highlight any significant changes in the vibration measurement. These include the use of centred moment statistics providing data for the mean, variance, skewness and kurtosis of the distributed data. The mean of the data sets are not included here in this analysis due to the symmetry of the treated signal resulting in a mean value of approximately zero for all the cuts measured.

The Variance in statistics, defined as the second central moment, provides a representation of how far the numbers in a distribution are spread out from each

other. In this particular setup, this will provide a reasonable approximation of the magnitude of the vibration due to the mean residing at approximately zero. Figure 4.4.2 details the individual values of variance for each individual cut setup. Linear trend lines have been applied to the individual chip thickness model data sets. Although different gradients are witnessed, the overall spread of the data shows that no significant trend is witnessed over the course of the experiment.

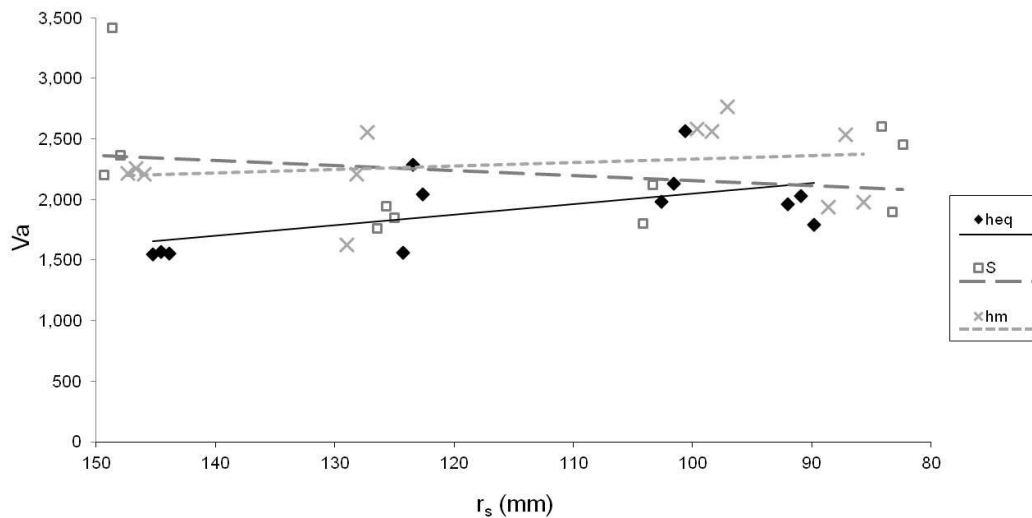


Figure 4.4.2 Variance value of treated amplitude data signal versus grinding wheel radius.

The third central moment of the data is defined as skewness. This is a measure of the asymmetry of the data distribution and can provide detail on whether a signal contains more high or low values. In this case, as the mean is near zero, a negative value of skewness indicates a negative skew effect; this means that fewer positive values are present within the data set. The opposite is true for a positive value of skewness. Figure 4.4.3 details the results for skewness. All the chip thickness models show small reduction in skewness with the grinding wheel radius. The change is small but similar for all chip thickness models indicating a reason associated with the changing wheel diameter. This could be due to the change in coolant interaction with the workpiece at the reduced wheel diameters. However, the data appears to show that the skewness is not significantly affected by the changing conditions in the experiment.

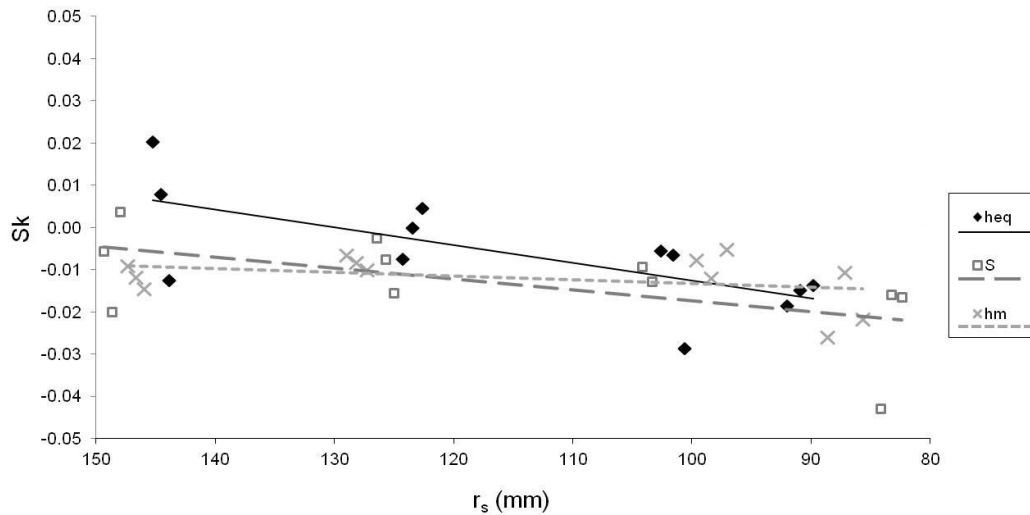


Figure 4.4.3 Skewness value of treated amplitude data signal versus grinding wheel radius.

Kurtosis is defined as the fourth central moment and provides a measure of the peakedness of the distribution. A higher value of kurtosis indicates that the variance witnessed is due to larger infrequent deviations from the mean rather than a more frequent amount of moderate deviations. Figure 4.4.4 shows the kurtosis against the wheel radius for the chip thickness models applied. The data set behaviour again appears constant over the course of the experiment with no significant difference between the chip thickness models applied. All the cuts performed are kurtotic as they all have results above a value of 3, the value of a normal distribution. This means the grinding signal variance comes more from infrequent larger deviations indicating some periodic large amplitude vibration. This is useful knowledge for future investigation in grinding dynamics.

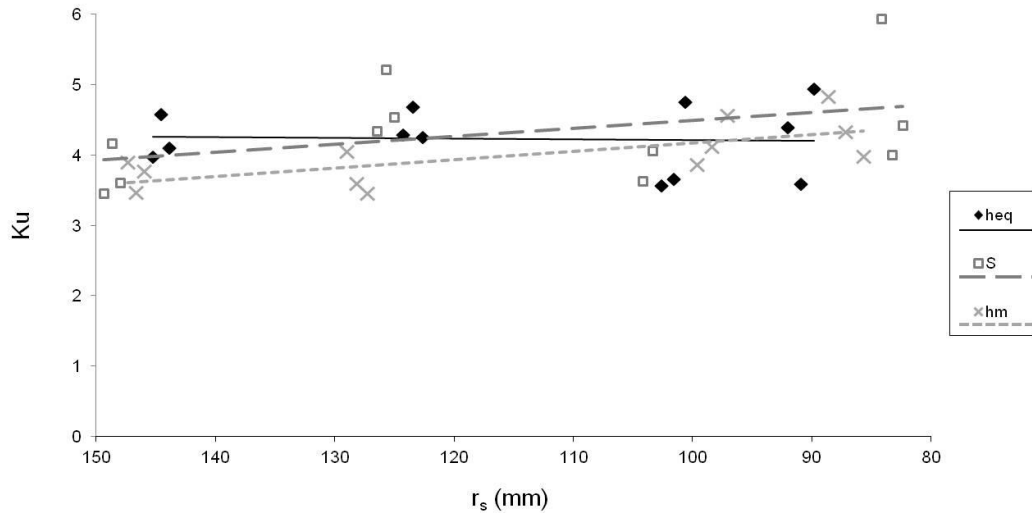


Figure 4.4.4 Kurtosis value of treated amplitude data signal versus grinding wheel radius.

Overall, the effect of vibration for this experiment does not appear to change significantly with changing wheel diameter or the application of different chip thickness models. In a similar manner to the results for the surface analysis, these results provide confidence that the changing behaviour in the mechanical and thermal outputs can be attributed to changes in the contact zone and not significant changes in the vibration of the grinding system.

4.5 Statistical Analysis of Results and Critique of Testing Methodology

Due to the random nature of the grinding process, as a result of undefined cutting edges, there is variation present in the majority of the results presented. This section utilises statistical techniques to identify whether output trends change due to a difference in the mean between experimental blocks or whether inherent scatter in the data accounts for the variations seen in the graphs presented in this chapter. This section includes the use of correlation and ANOVA techniques outlined in Chapter 3.

The results presented in this section use the same colour coding system presented in section 3.3 of this thesis. All the results for both the correlation and ANOVA analysis have been utilised with an alpha value/power of 0.05. A correct rejection

of the null hypothesis is labelled in green, borderline results in yellow and results highlighted in red indicate situations where you cannot reject the null hypothesis.

The results for the correlation between grinding wheel radius and the relevant process output are detailed in Table 4.5.1. The results associated with the mechanical outputs of the process (P_{Net} , F_v and F_h) all show a strong correlation with wheel radius highlighting that definite changes occur as a result of the changing wheel radius. Correlating against the wheel radius provides a useful measure of how well outputs change over the course of the experiment indicating the effect on the outputs of maintaining chip thickness. The output for T_c only shows good correlation for the h_m model which coincides with the results shown in section 4.2. Temperature measurement in grinding processes is difficult and a large amount of variability is experienced. It is still valid to identify some trends but the results are not statistically significant due to large amounts of scatter in the relevant data sets. The surface effects include the outputs from R_a to μ_G in Table 4.5.1. The results are mixed. Some of the outputs show good correlation for certain chip thickness models but not for others. These results reinforce the data presented in section 4.3 where no significant behaviour trends were associated with chip thickness models as the CD process seemed to dominate. However, variation in the data set was present, in some outputs more than others, indicating that the process does have inherent scatter in the outputs produced. Although the results imply that scatter was predominant, the range of the scatter as a proportion of the overall test results was quite low. This indicates that the surface measurement outputs remained consistent, producing no significant variation over the progression of the experiment. The same effect is noticed for the vibration outputs V_a , S_k and K_u .

	h_{eq}	S	h_m
P_{Net}	$r = 0.964$ $p = 0.000$	0.543 0.068	0.906 0.000
F_v	0.958 0.000	-0.971 0.000	0.993 0.000
F_h	0.981 0.000	-0.882 0.000	0.992 0.000
T_c	0.007 0.982	-0.427 0.166	0.741 0.006
Ra (Metal Test Pieces)	-0.462 0.130	-0.731 0.007	-0.565 0.055
Ra (Graphite Test Pieces)	-0.785 0.002	-0.344 0.273	-0.834 0.001
F_{vG}	0.306 0.333	-0.355 0.258	-0.563 0.057
F_{hG}	0.515 0.086	-0.356 0.256	-0.652 0.002
μ_G	0.117 0.716	0.333 0.290	0.439 0.153
V	-0.579 0.048	0.225 0.506	-0.215 0.503
Sk	0.695 0.012	0.568 0.068	0.359 0.251
Ku	0.049 0.880	-0.406 0.216	-0.693 0.012

Table 4.5.1 Table of results showing values for Pearson correlation coefficient between wheel radius and relevant process output and p-values for different chip thickness maintenance conditions.

An ANOVA analysis was also performed on the relevant data sets to assess if there was significant change in the mean output between the experimental blocks. The results are detailed in Table 4.5.2. The results are similar to above in terms of highlighting the outputs which experienced the most significant

variation during the experiment. The mechanical outputs show a definite change in the mean values between the experimental blocks. This provides real confidence that the experiment is capable of distinguishing between different chip thickness setups for constant productivity and highlights that changes are occurring in the contact zone. The measured surface temperature again showed that the variance was more due to the effects of scatter rather than significant changes between the experimental blocks. As a result only qualitative conclusions can be drawn. However, it is maintained that certain trends do exist on the outputs for T_c but it is understood that due to the inherent variation in the output that more samples would be required for future testing. The surface measurement and vibration outputs again show mixed results with some displaying variation from a change in the mean value and other from inherent process variation. This information combined with the graphical outputs confirms the assertion that the surface outputs are maintained to a consistent level during the experiment.

	h_{eq}	S	h_m
P_{Net}	$F_{Stat} = 40.19$ $p = 0.000$	7.48 0.010	32.35 0.000
F_v	46.47 0.000	39.27 0.000	500.76 0.000
F_h	92.41 0.000	24.65 0.000	198.83 0.000
T_c	1.26 0.352	0.57 0.650	3.78 0.059
Ra Metal	4.70 0.036	3.57 0.067	1.95 0.200
Ra Graphite	7.31 0.011	2.36 0.148	6.83 0.013
F_{vG}	3.02 0.094	1.50 0.287	8.84 0.006
F_{hG}	4.56 0.038	0.95 0.460	12.24 0.002
μ_G	0.87 0.496	2.96 0.098	2.45 0.139
V	3.76 0.060	2.22 0.174	1.96 0.199
Sk	2.48 0.136	1.65 0.262	3.90 0.055
Ku	0.36 0.781	2.05 0.195	3.17 0.087

Table 4.5.2 Table of results showing values for ANOVA F-statistic and p-values for process outputs under different chip thickness maintenance conditions.

The important conclusions from the statistical work show that the experiment has produced variation in the mechanical process outputs between experimental blocks for different chip thickness models at constant productivity. This allows for analysis of this change in grinding behaviour to be performed with data that is statistically significant. The results for temperature show that variation in the outputs is more due to scatter but it is maintained that certain trends can be seen

in the outputs displayed in section 4.2. Increased data samples would be required in future testing to confirm the trends identified for the temperature output.

The experiment has been effective in providing changes in chip thickness for constant productivity that can be identified in the experimental outputs. The application of CD largely contributed to providing consistent vibration and surface outputs. The experiment could be improved by performing increased amounts of testing to account for scatter in the temperature results. In addition, the application of alternative temperature measurement techniques such as PVD coatings may provide improved results. The experiment has shown adequate resolution to assess the impact of using chip thickness to provide improved control of the force and specific grinding energy.

4.6 Summary

The variation in chip thickness models applied to the grinding process had an impact on the mechanical outputs. The net power and the subsequent specific grinding energy calculated from this, reduced for all the chip thickness models applied at smaller wheel diameters. The amount of reduction witnessed was determined by the chip thickness model applied with the S model providing the least and the h_m model providing the largest decrease in SGE. In addition to the net power, the force was also influenced by the type of chip thickness model applied. The S model showed a force increase at small diameters, h_{eq} displayed a small decrease and the h_m model showed the largest decrease in force measured. This coincided with a reduction in the contact area between wheel and work piece. The force per unit area was calculated with the h_m model providing consistent results at all wheel diameters.

Thermal outputs from the process were also evaluated. The analytic heat flux displayed an increase for all chip thickness models at reduced wheel diameters; the S model showing the largest increase and the h_m model the least. This did not correspond directly with the measured surface temperature, though the order between the chip thickness models remained the same. The surface temperature increased for the S model, stayed constant for h_{eq} and reduced for h_m with a

decrease in wheel diameter. A significant amount of scatter was present in the temperature results. The reasons for the discrepancy between heat flux and measured temperature are investigated in Chapter 6. Post-process surface integrity analysis did not have sufficient variation in workpiece temperature to identify significant differences between chip thickness models. However, variation in the force results between the different chip thickness models were identified when looking at surface layer deformation.

Surface roughness data showed only small amounts of variation for the finished metallic workpiece surfaces. Results presented for graphite scratch tests showed slight increases in roughness and reduction in forces with a reduction in the grinding wheel radius. The graphite test appeared more influenced by the CD process and change in the wheel diameter as opposed to the application of different chip thickness models. The similarity in the output trends for the different chip thickness models for the surface outputs indicate that changes in the mechanical and thermal outputs can be attributed to effects in the contact zone. The results from the vibration measurement further reinforce this.

Results from the statistical analysis of the outputs highlights that the changes in the mechanical outputs are due to changes in the grinding conditions and not just inherent variation in the process. The statistics show more variation due to scatter in the temperature results but the trends from the graphical data are still visible. The mechanical and temperature data both appear to be effected by maintaining different chip thickness models over the operational life of the grinding wheel. The experiment is successful in providing a large enough range of chip thickness values at constant productivity to distinguish changes in the key mechanical outputs. An increased data set or improved temperature measurement technique would be required to provide statistical significance to the surface temperature results.

Chapter 5 - Effect of Wheel Speed and Contact Area on the Grinding Process

This chapter details the results of the experiments defined in section 3.5. The results assess the change in grinding behaviour at varying wheel speeds and contact areas. The aim of this modified pin on disc experiment is to determine the effect of these parameters on the grinding process outputs under flat contact conditions without the kinematics associated with peripheral grinding. These 2 variables change during the experiment presented in Chapter 4, even when a theoretical value of chip thickness is maintained. This provides further information on the why certain trend behaviour is witnessed in some of the output results presented in the previous chapter.

5.1 Effect of Wheel Speed

The wheel speed is often noted as having a significant impact on peripheral grinding processes, where an increase usually results in a reduction in cutting forces and energy requirements. The primary reason for this effect comes from a reduction in chip thickness associated with an increase in wheel speed for constant productivity conditions. For the work performed in Chapter 4, the wheel speed was altered to maintain the chip thickness at the different grinding wheel diameters for constant productivity. This section investigates the effect on the grinding process outputs by changing the wheel speed in isolation of changing wheel diameter.

The wear of each test pin was recorded to assess if this changed at different grinding wheel speeds. This was calculated by measuring the weight of the pin before and after a test cut in order to establish the volume lost during cutting. All the pins utilised for the wheel speed experiment are the same diameter. The rate of wear is plotted against grinding wheel speed in Figure 5.1.1. The terms wear rate and productivity are utilised to describe the rate of material removal from an

individual nickel pin in this experiment and are used interchangeably in this chapter. An exponential trend line provided the best fit to the data results indicating that the wear rate significantly increased at the higher values of grinding wheel speed within the range presented. The increase in wear rate can be attributed to a number of factors. Firstly, the increase in wheel speed will result in the abrasive grains performing more cuts in a set time period therefore removing material at a faster rate. However, this would create a linear increase in productivity. Another explanation considers that higher grinding wheel speeds result in higher temperatures in the contact zone as shown by Tawakoli [43]. This has the effect of making the material easier to machine which will result in increased productivity for constant force application. This explanation also coincides with increased burning witnessed on the pin surface at higher grinding wheel speeds.

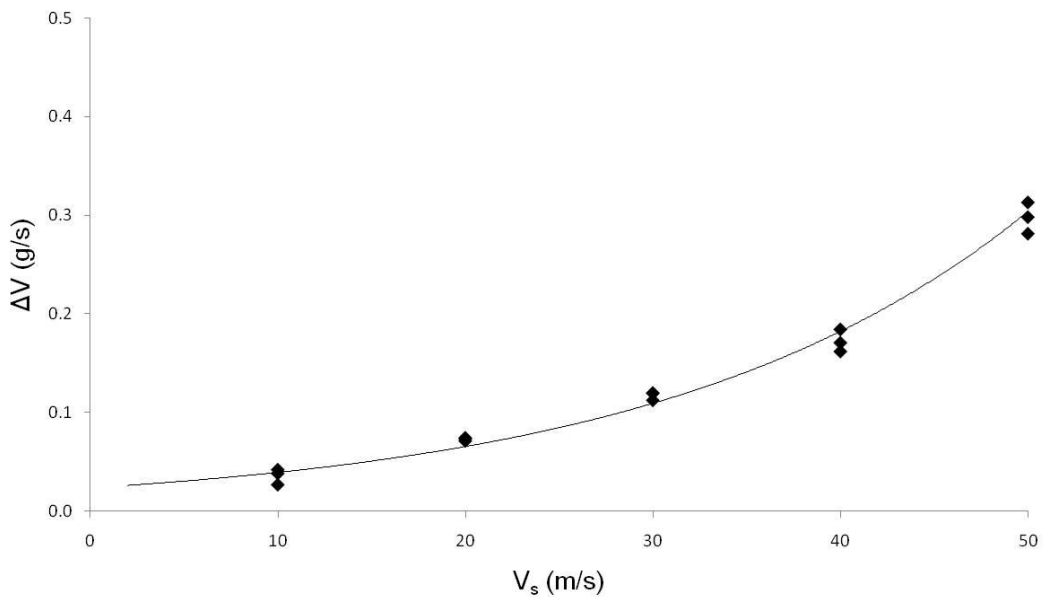


Figure 5.1.1 Graph detailing wear rate of Nickel Pin versus the grinding wheel speed for modified pin on disc trials.

Changes in productivity can influence the chip thickness of a grinding process. Malkin [5] provides a face grinding chip thickness model representing a process where stock material is being fed into the face of a rotating grinding wheel. This model best represents the grinding process performed in this experiment. The chip thickness calculation detailed in equation (5.1.1) contains a linear in-feed

rate of the material v_f . Using the wear data detailed in Figure 5.1.1 and the known geometry of the pins, the effective material in-feed rate v_f was calculated for all the experiments. These values were utilised in the calculation of chip thickness h_F for all the cut tests performed.

$$h_F = \frac{2}{Cr} \frac{v_f}{V_s}^{\frac{1}{2}} \quad (5.1.1)$$

Where $C = 0.93$, the amount of cutting grains per unit area of wheel, see section 3.2 ($1/\text{mm}^2$)

$r = 1$, the ratio of chip width to chip thickness, see section 3.2

Figure 5.1.2 shows the calculated chip thickness for the varying grinding wheel speeds. The results show similar values of h_F until the maximum wheel speed of 50m/s is applied. There is an approximate 20% increase in the value of chip thickness at 50m/s, although the value of h_F appears to start increasing at 40m/s. According to equation (5.1.1), this indicates that v_f increases at a faster rate than V_s at the higher wheel speeds. This reinforces the theory of increased temperature in the cut zone making the material easier to machine. This increase in productivity results in larger chip thickness for a constant force application. A trend line was not applied to this data as the step change in h_F only occurs at 50m/s and no fit appeared suitable. The test was originally designed to try and maintain chip thickness conditions by using constant normal force applied to a flat contact. However, it appears that both the chip thickness and productivity change at the different grinding wheel speeds.

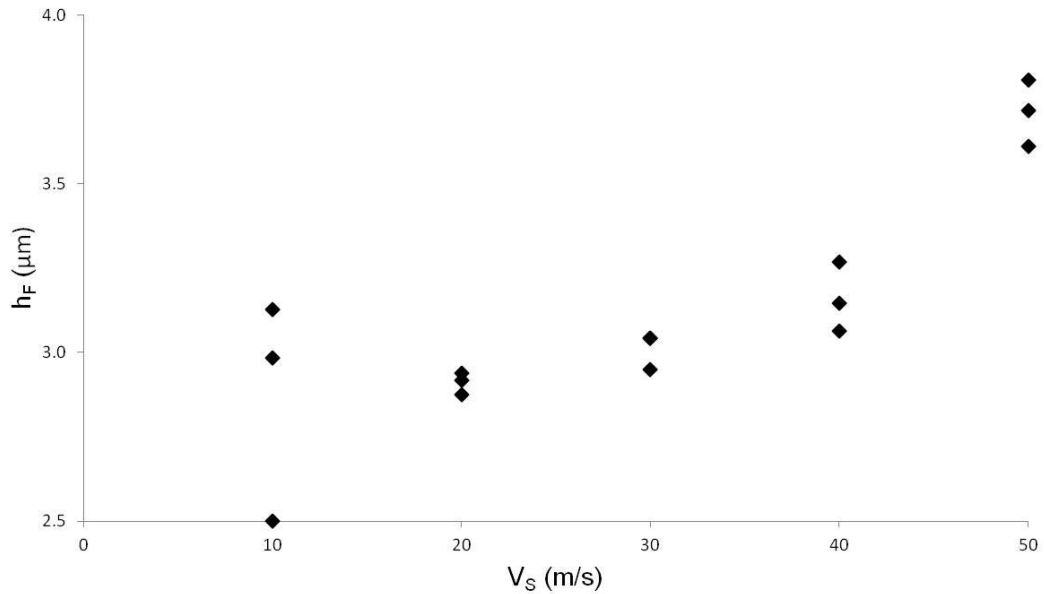


Figure 5.1.2 Graph of face grinding chip thickness h_F [5] versus the grinding wheel speed for modified pin on disc trials.

The primary function of the test rig detailed in section 3.5 is the measurement of friction forces in standard pin on disc tribological applications. For grinding, this is referred to as the force ratio μ [4]. It is calculated in the same way as friction, by dividing the horizontal force by the vertical force. But as the grinding process includes rubbing, ploughing and cutting, the term force ratio is utilised instead. It is a representation of how efficient the grinding process is and changed significantly with wheel speed in this application. A high value of force ratio indicates that more chip formation occurs with less deformation resulting in a high efficiency grinding process.

Figure 5.1.3 shows the force ratio reduces from 0.6 at 10m/s down to around 0.3 at 50m/s representing an approximate 50% reduction. A power law trend line was applied to the data providing a good approximation of the relationship. The power law would indicate that the force ratio would tend to a constant value with increasing wheel speed. The lowering of the force ratio with an increase in wheel speed indicates a transition in the grinding behaviour. Helletsberger [4] states that a decrease in force ratio indicates increased deformation at the contact zone causing high heat effects. In addition, Tawakoli [43] states that higher wheel speed results in increased temperature within the contact zone. Increased burning

was witnessed on the pin surface at the higher wheel speeds. As stated above, the increased heat in the contact zone causes softening of the material promoting increased material removal for constant applied force which was witnessed in Figures 5.1.1 and 5.1.2. This may also have the effect of reducing the horizontal force measured and subsequently reducing the value of μ .

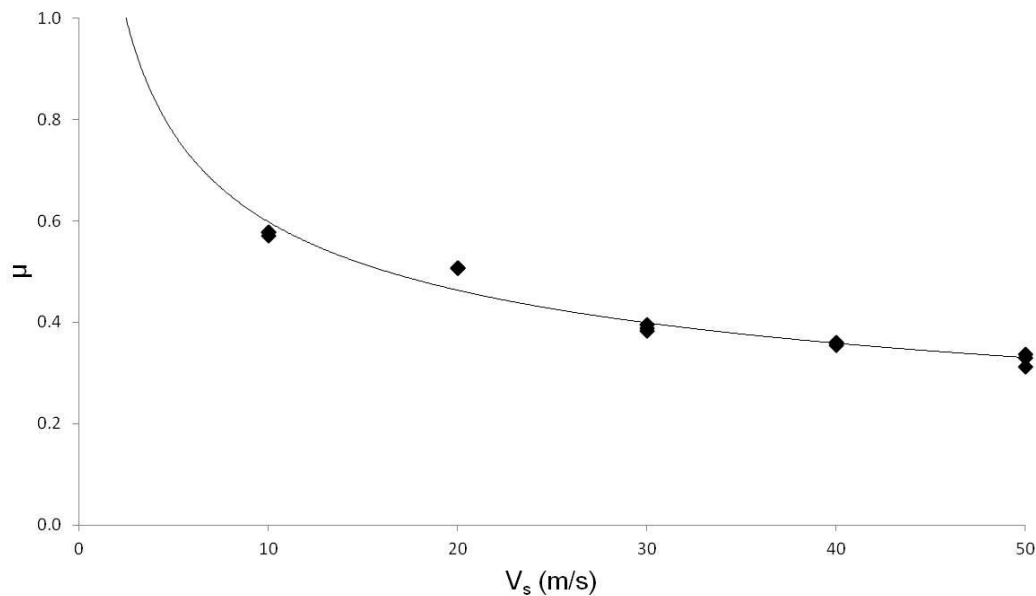


Figure 5.1.3 Graph of grinding force ratio versus the grinding wheel speed for modified pin on disc trials.

The measured power from the spindle is a useful output to identify the impact of changing wheel speed on the grinding process. Figure 5.1.4 indicates the Net Power increase coinciding with an increase in grinding wheel speed. The increase in net power measured coincides with the increase in productivity and chip thickness for this experiment. This suggests that net power is dependent upon the productivity and/or the chip thickness of the grinding process.

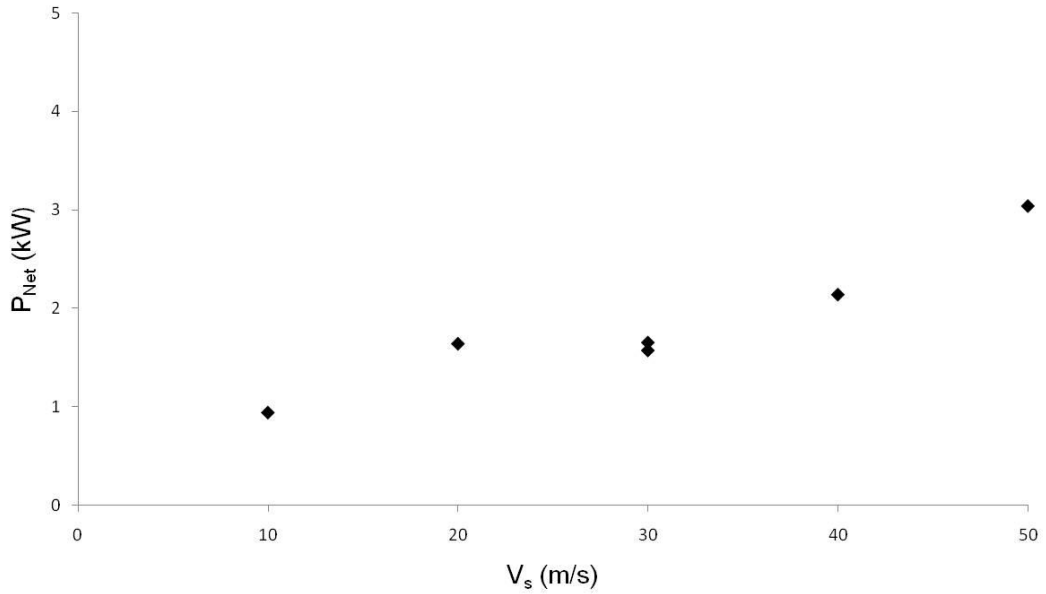


Figure 5.1.4 Graph of net power versus the grinding wheel speed for modified pin on disc trials.

The specific grinding energy (SGE) provides an additional measure of the efficiency of a grinding process. Although the testing represents a pin on disc tribology test and not a traditional peripheral grinding application, evaluating the specific grinding energy for each of the wheel speeds tested provides a useful assessment of the changing conditions at the contact. The specific grinding energy e_c for this test setup is calculated using equation (5.1.2):

$$e_c = \frac{P_{Net}}{Q_W} = \frac{P_{Net}}{v_f \cdot \frac{\pi \cdot d_{pin}^2}{4}} \quad (5.1.2)$$

Where v_f = face grinding material in-feed rate (mm/min)

d_{pin} = diameter of Nickel pin at grinding wheel interface (mm)

Figure 5.1.5 shows a specific grinding energy curve following a power law trend when plotted against the grinding wheel speed for this experiment. A decrease in specific grinding energy with increasing chip thickness and productivity is a common relationship presented in the grinding literature. For this experiment, the horizontal axis of Figure 5.1.5 effectively represents productivity or chip thickness, due to the increase witnessed at the higher values of V_s . The specific

grinding energy of the process decreases at higher wheel speeds which correspond with increased chip thickness and productivity.

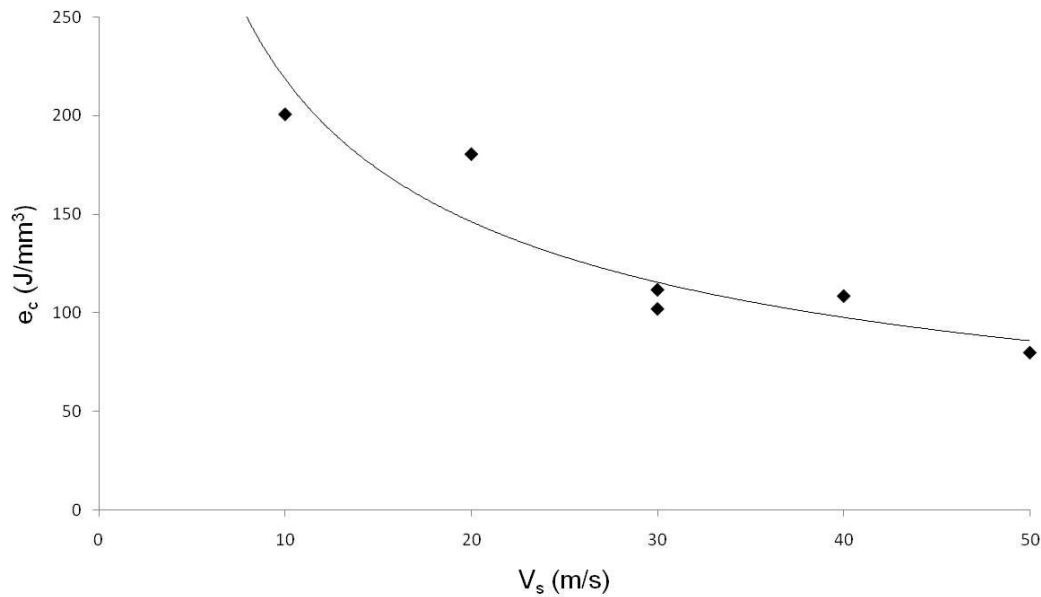


Figure 5.1.5 Graph of specific grinding energy versus the grinding wheel speed for modified pin on disc trials.

The surface roughness of the pin surface was measured after each test cut was performed to assess the impact of grinding wheel speed. The pin surface showed significant striation as seen in Figure 5.1.6 (a). This resulted in high values of R_a measured in comparison to the ground metallic surfaces detailed in Chapter 4. The lines on the pin surface are visible and follow the direction of the abrasive grain cutting paths. The reason for the highly identifiable surface marking, as opposed to a cut performed in peripheral grinding, is due to the pin surface being exposed to the entire grain arc of contact. In a traditional cutting mechanism, only a very small amount of a grain's cutting arc remains on a finished cut surface therefore significantly reducing the surface roughness. The effect is shown in Figure 5.1.6 (b). This is not the case for this modified pin on disc test setup where the entire contact of the grain arc is witnessed on the pin surface.

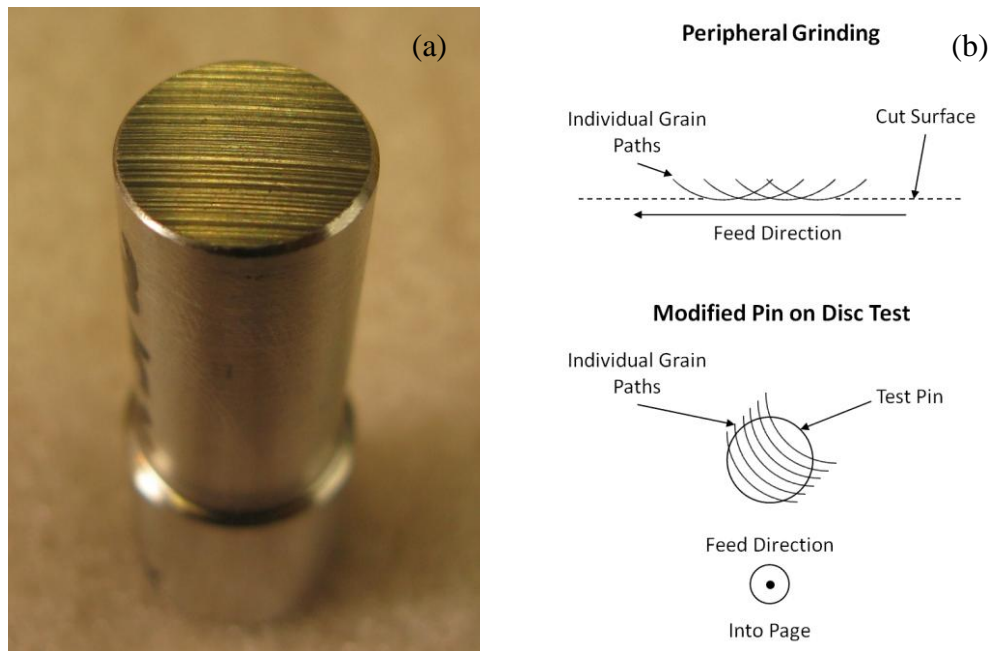


Figure 5.1.6 Surface topography of pin after testing; (a) Image of tested pin surface, and (b) Diagram detailing grain paths for different grinding setups.

Figure 5.1.7 details the measured Ra value of the pin surface against the grinding wheel speed. The results show an increase in surface roughness at the higher values of wheel speed. However, the increase is not linear and there are 2 sections of similar roughness values in the graph. A trend line showing a step increase at 30m/s is shown. The roughness associated with wheel speeds of 10 and 20m/s appear constant. The same is evident for wheel speeds of 40 and 50m/s. The mid-point of 30m/s has a spread of results similar to both the high and low wheel speed regions. This indicates a change in the contact zone conditions at a wheel speed of 30m/s, providing a change in Ra of approximately $1\mu\text{m}$. The change in mechanism corresponds with the increase in chip thickness identified at the higher grinding wheel speeds. Snoeys and Peters [67] showed that the measured Ra value of a ground surface is higher with an increase in grinding chip thickness. This is consistent with the results from this experiment.

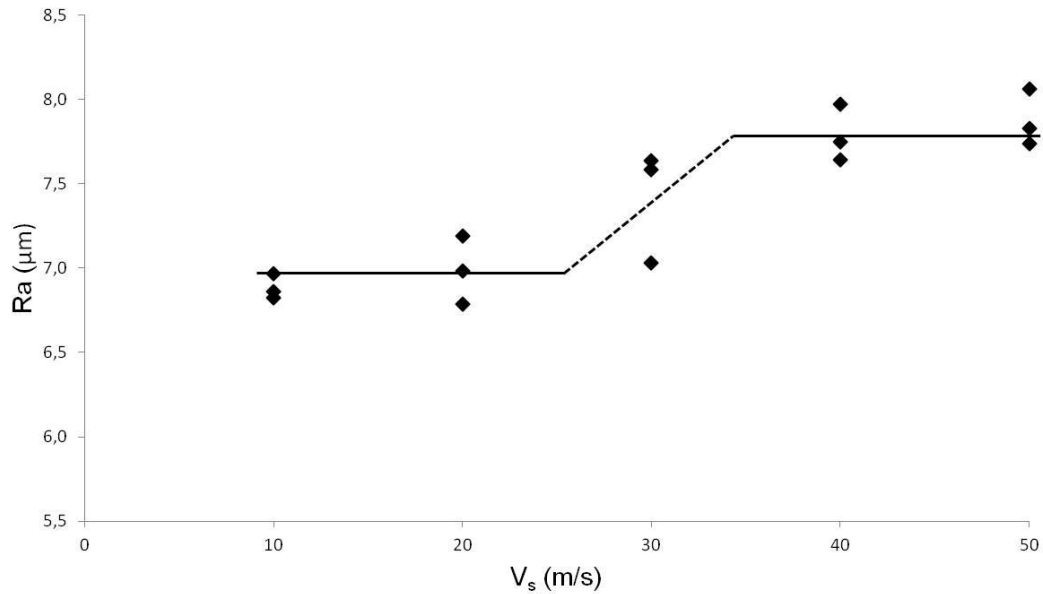


Figure 5.1.7 Surface roughness of pin surface versus grinding wheel speed.

Varying the wheel speed has a clear impact on the contact behaviour between the grinding wheel and the nickel pin. This is highlighted by the changes witnessed in the process outputs at the different grinding wheel speeds. It is proposed that the higher values of wheel speed appear to increase the temperature in the cutting zone leading to a softening of the material. This increases the productivity and subsequent chip thickness of the process resulting in increased material removal. This corresponds with reduced values of horizontal force and specific grinding energy. The change in wheel speed is significant in relation to the results of the machining trials where chip thickness is maintained. Although the productivity is constant for the machining trials, the change in wheel speed will have an impact on the contact zone conditions. This is explored further in Chapter 6 of this thesis.

5.2 Effect of Contact Area

For the peripheral grinding process utilised in Chapter 4, the contact area between the wheel and workpiece changes with wheel diameter for a constant depth of cut. This influences the number of abrasive grains in contact with the workpiece affecting the overall force experienced during the process. In addition, a change in contact area alters the length of time an abrasive grain is in contact

with the workpiece, which can affect the thermal outputs of the grinding process. This section investigates the effect of changing contact area on the outputs of the grinding process for flat contact conditions.

The testing included 5 different pin diameters that represent a range of contact areas as defined in section 3.5. The results using the 4mm and 8mm diameter pins, representing the smaller contact areas, have not been included in the graphs presented in this section due to problems encountered during testing. Figure 5.2.1 shows an example of the grinding wheel and the 4mm diameter pin after a test cut was performed. The small contact area resulted in the pin gouging into the grinding wheel surface as shown in Figure 5.2.1(a). This caused rounding of the pin surface as detailed in Figure 5.2.1(b). In addition, the dressing stick was not engaged at the gouged surface resulting in non continuous dressing (CD) conditions. This produced high values of horizontal force due to the pin gouging the wheel. This was not representative of the flat contact CD conditions required for comparison of the contact areas. As a result, a decision was made to exclude the 4mm diameter pin results.

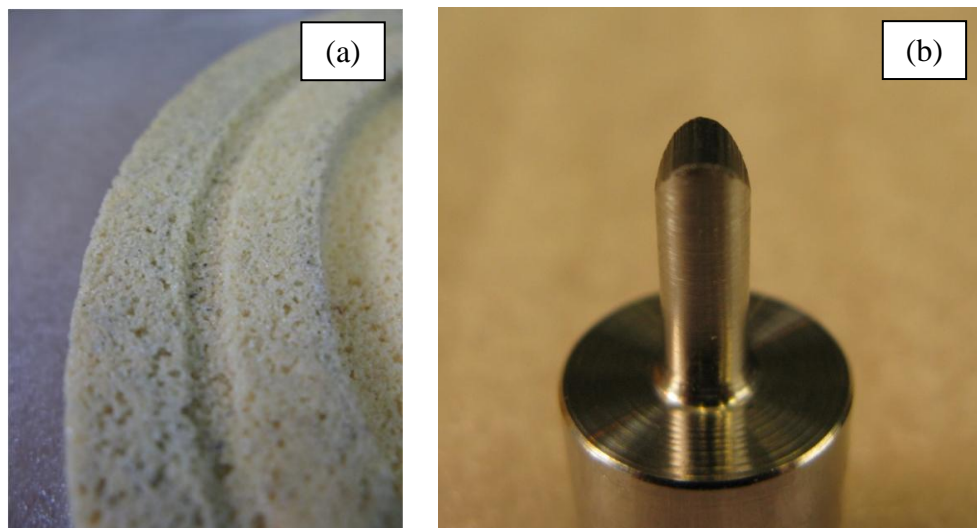


Figure 5.2.1 Experimental tooling after testing of 4mm diameter pin setup; (a) Grinding wheel with groove on surface and (b) Nickel pin with rounded end.

The reason for the gouging is perceived to be a result of a testing effect when using a small pin diameter. When using a smaller size pin there are less abrasive grains in contact during the cutting process. In addition, the stiffness of the pin is

reduced with the smaller 4mm diameter pin geometry. Observations during testing indicated that the contact conditions were less stable than for the larger pin diameters. Instability would lead to deflection and potential bending which would cause an edge of the pin to dig into the wheel surface. This stress concentration could be sufficient to cause grit fracture and instigate the noted effects of wheel gouging.

The 8mm diameter pin results were also not suitable for inclusion in the graphs presented in this section. As the contact pressure was maintained for all pin sizes, varying vertical force conditions were required depending on the contact surface area. The air pressure applied to the pneumatic cylinder on the test rig was directly responsible for the value of the vertical force application. At the smaller pin diameters of 4mm and 8mm, the air pressure required in the cylinder was low and difficult to regulate. As a result, the movement of the actuator arm to push the pin into the rotating grinding wheel was very slow. This resulted in the applied vertical force taking a long time to reach a steady value in the grinding contact. Figure 5.2.2(a) shows a typical force output for an 8mm diameter pin with the horizontal force not reaching a steady value during the experiment. The 12mm, 16mm and 20mm pin diameters all produced periods of steady force output during the experiment as shown in Figure 5.2.2(b), which are presented in the results. The effect shown in Figure 5.2.2(a) occurred using both the 4mm and 8mm diameter pin sizes. For this reason, the 8mm pin diameter results are also excluded from analysis in this section. It is important that the test effects were identified and understood as it provides confidence in the other results presented.

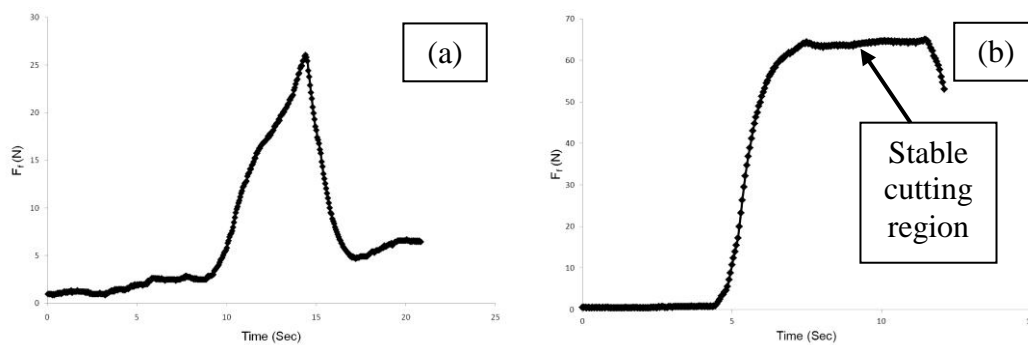


Figure 5.2.2 Graph of horizontal force versus time measured during testing; (a) For an 8mm diameter pin & (b) 12mm diameter pin showing stable cutting region.

All the results in this section were performed at constant wheel speed of 30m/s and the relevant outputs are presented in the same order as in section 5.1. The pin diameter is plotted on the abscissa for all the results presented as opposed to contact area. This is due to the pins being manufactured to defined diameter sizes representing different contact areas. The results in Figure 5.2.3 show the wear rate of the pin plotted against the pin diameter. Again productivity and wear rate are used interchangeably in this section. The results show a non linear increase in wear rate with increasing pin diameter. The higher values of wear rate/productivity are expected with a larger pin area as more material is in contact with the grinding wheel for the same force and wheel speed application. The calculated values for the material in-feed rate v_f are similar for all the pin diameters tested. As a result, the wear rate should be proportional to the contact area and subsequently the pin diameter. The relationship between contact area A_{Pin} and pin diameter d_{Pin} is defined in equation (5.2.1):

$$A_{Pin} = \frac{\pi \cdot d_{Pin}^2}{4} \quad (5.2.1)$$

Figure 5.2.3 shows the wear rate of the pin increases with the square of the diameter. This indicates that the wear rate increase was primarily due to the increased contact area at the larger diameters. In addition to the increased size of contact, the larger pin diameters have an increased arc of contact which may result in a temperature increase in the contact zone. This could have the effect, as described in section 5.1, of softening the material resulting in higher productivity for constant pressure conditions.

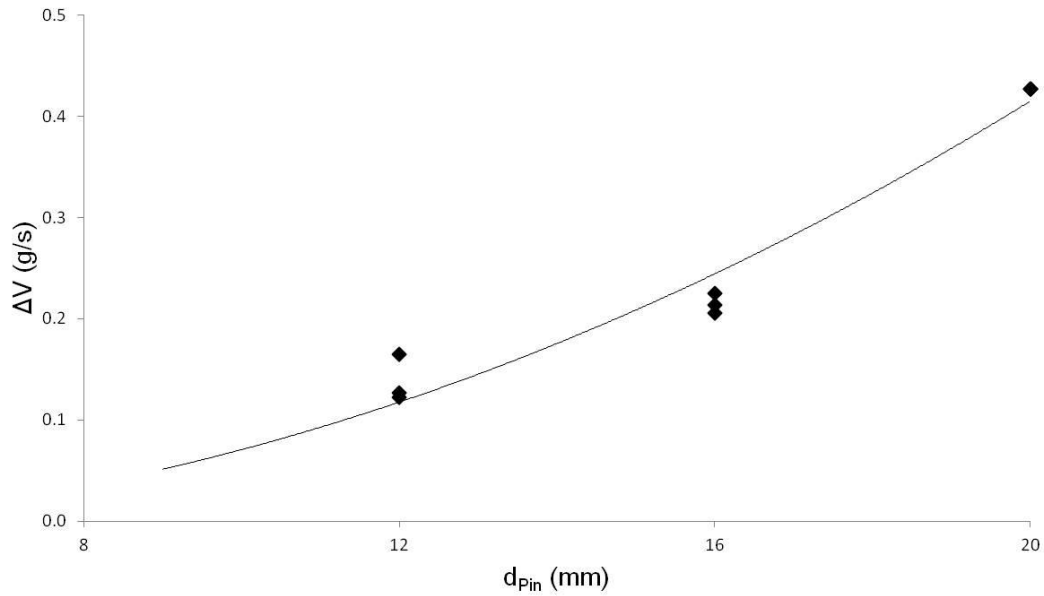


Figure 5.2.3 Graph of wear rate versus pin diameter for modified pin on disc trials.

The values for the estimated face grinding chip thickness are plotted against pin diameter in Figure 5.2.4. The values of h_F are similar for the 12 and 16mm diameters with the value increasing slightly for the 20mm diameter pins. An outlier point can be identified for the 12mm pin diameter. The effect of increased contact area is normalised in the calculation of material in-feed rate v_F . As a result, the increased value of h_F for the 20mm pin diameter requires an alternative explanation. It may be attributed to a small increase in productivity due to increased heat effects at this pin diameter although there is no measured data to quantify this. In addition, it can be seen that there is very little scatter in the data for the 20mm diameter pins indicating that the test is more repeatable at the larger pin diameters.

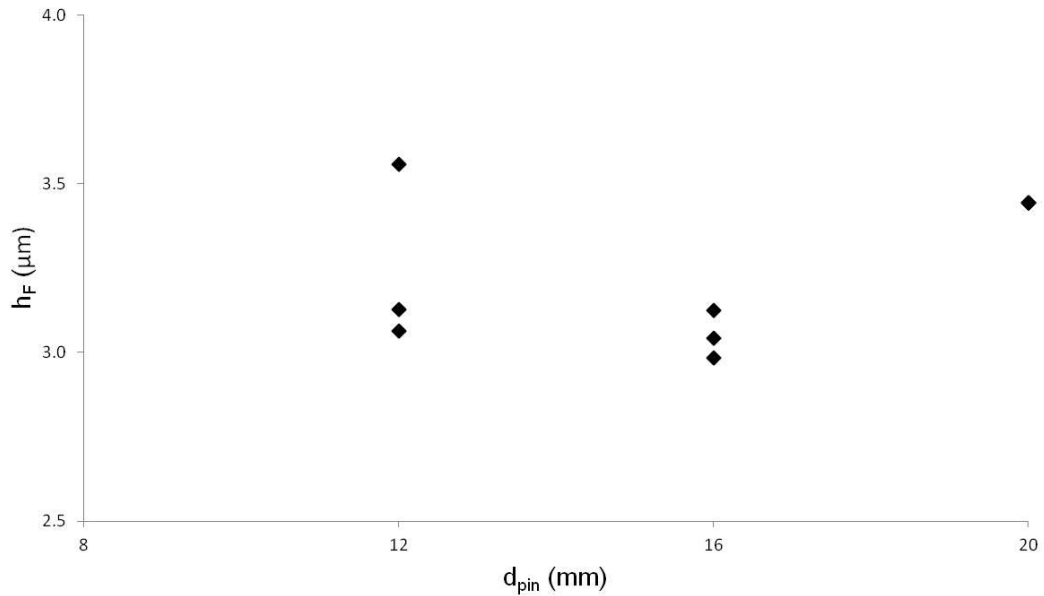


Figure 5.2.4 Graph of face grinding chip thickness h_F versus pin diameter for modified pin on disc trials.

The effect of contact area on the force ratio is detailed in Figure 5.2.5. The results show that the force ratio remains consistent for all pin diameters. There is a slight decrease in the value for the 20mm diameter pin but this appears within the error witnessed at the other diameters. Any decrease for the 20mm diameter pin would coincide with the higher value of chip thickness and potentially increased heat in the contact zone. This is similar to the effects witnessed for the increased grinding wheel speed. The value of approximately 0.4 presented in Figure 5.2.5 matches with the data performed at 30 m/s in Figure 5.1.3 showing good consistency between experiments. The value of 0.4 also correlates well with current grinding theory in relation to force ratio. The results presented in Figure 4.1.2 provide a value for the force ratio at the large wheel diameter of approximately 0.4. It is expected that the force ratio be independent of area for constant pressure application unless the increased heat in the contact zone impacts the grinding mechanism.

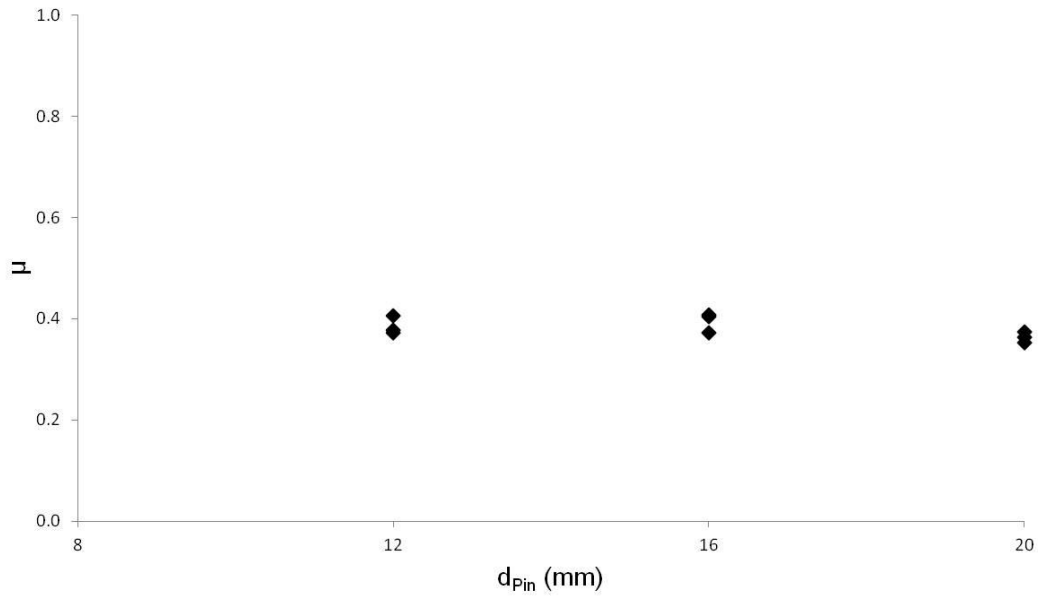


Figure 5.2.5 Graph of force ratio versus pin diameter for modified pin on disc trials.

Although the force ratio and chip thickness remain constant with only small changes witnessed at the 20mm pin diameter, a net power increase is shown in Figure 5.2.6. The net power increases with the square of the pin diameter. With an increase in pin diameter and subsequent contact area, more grains will be engaged in the cut zone providing increased mechanical requirements on the spindle. This indicates that the value of net power has a direct relationship to the amount of material removed for this test setup. This is also valid for standard peripheral grinding applications.

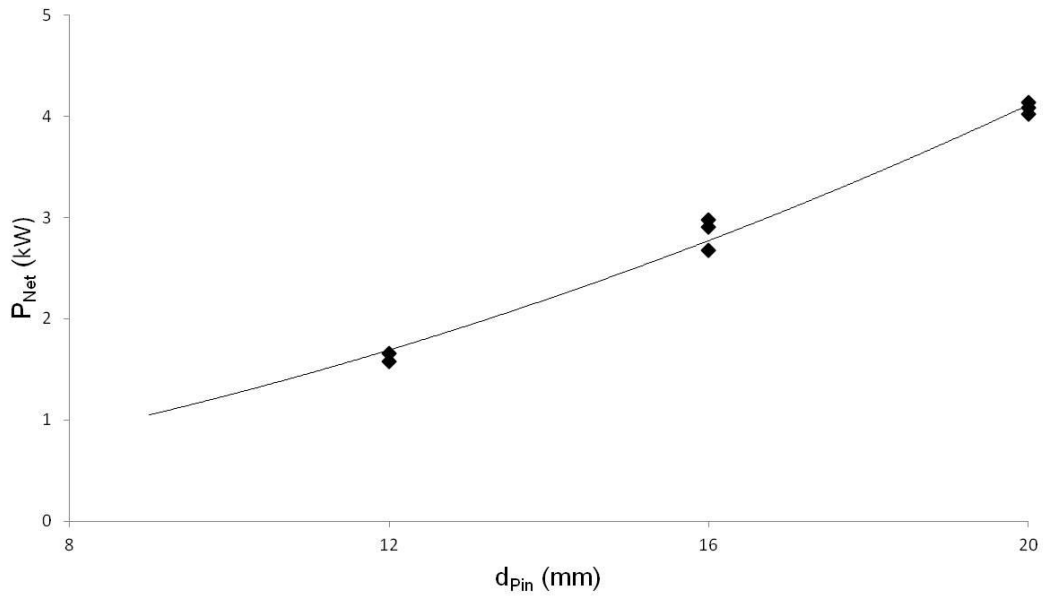


Figure 5.2.6 Graph of Net Power versus pin diameter for modified pin on disc trials.

The specific grinding energy is plotted against pin diameter in Figure 5.2.7. The values are near to $100\text{J}/\text{mm}^3$ similar to the results shown in Figure 5.1.5 at 30m/s. The results appear much more consistent in comparison to the effect seen with changing grinding wheel speed. The values remain constant at the 12 and 16mm diameters with a reduction witnessed for the 20mm pin diameters. The reduction in e_c at the 20mm diameter corresponds with the increase in chip thickness detailed in Figure 5.2.4. In traditional grinding theory [6], an increase in chip thickness or productivity leads to a reduction in specific grinding energy. This coincides with the idea of increased heat in the contact zone resulting in the material being easier to machine. This is the hypothesis for the reduced SGE at the larger pin diameter. A trend line has not been applied as the reduction in SGE only occurs at the 20mm diameter. The usual power law relationship relates specific grinding energy to chip thickness or productivity which does not vary significantly for this particular setup.

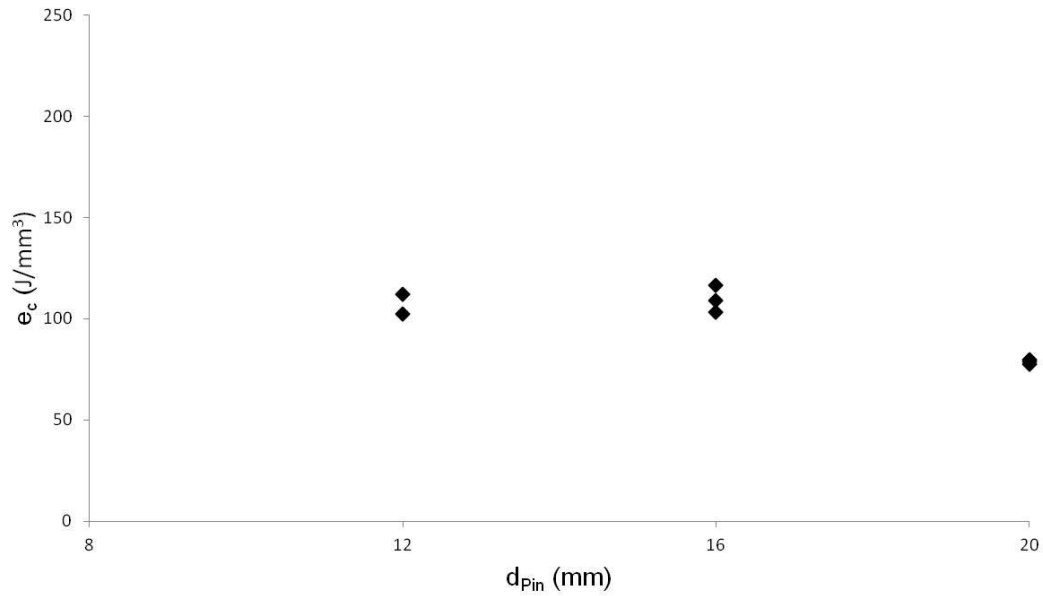


Figure 5.2.7 Graph of specific grinding energy versus pin diameter for modified pin on disc trials.

The surface roughness was measured after each grinding test providing similar values of Ra to those presented in section 5.1. These are plotted against pin diameter in Figure 5.2.8. The value of Ra reduces as the pin diameter increases. The change is quite small, measuring approximately $1\mu\text{m}$ but there does appear to be a clear negative trend. According to the results in section 5.1, an increase in h_F is associated with a higher value of Ra but this is not the case for the change in pin diameter. The slight reduction in Ra can be explained by the increased arc of contact with the larger pin diameters. If the abrasive grains are in contact for an increased distance, wear flats will have more time to develop during the cut. Increased wear flat area results in smoother surface profiles as more material overlaps the individual grain striations. This may also correspond with increased heat effects for larger pin diameters.

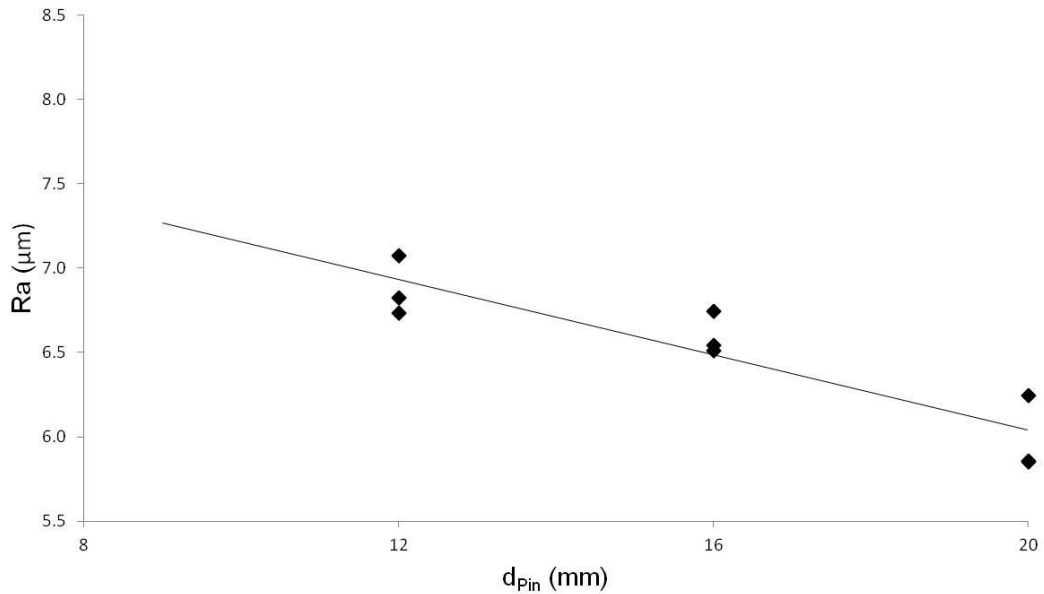


Figure 5.2.8 Graph of Ra versus pin diameter for modified pin on disc trials.

The contact area has some effect on the cutting process largely due to the change in arc of contact. The larger arc of contact exhibits the same impact on the grinding process outputs as seen with higher grinding wheel speed. However, the effect is much smaller in comparison. The change in contact area appears to have a much smaller effect on the outputs of the grinding process in comparison to the grinding wheel speed. The change in contact area between the 12mm and 20mm diameter pins is approximately 200mm^2 . The largest change in the contact area for the machining trials detailed in Chapter 4 is approximately 90mm^2 . The effect on the mechanics of the grinding process would be minimal with changing contact area. Although it is understood that the contact area has a significant impact on the overall force output due to the amount of grains in contact with the workpiece material.

5.3 Validity of Test

The relationship between specific grinding energy and productivity is a useful indicator of how representative the modified pin on disc testing setup is of the creep feed grinding process. Using the results from this chapter to reinforce trends witnessed in Chapter 4 requires that the modified pin on disc test setup is representative of a standard grinding process. The majority of grinding processes

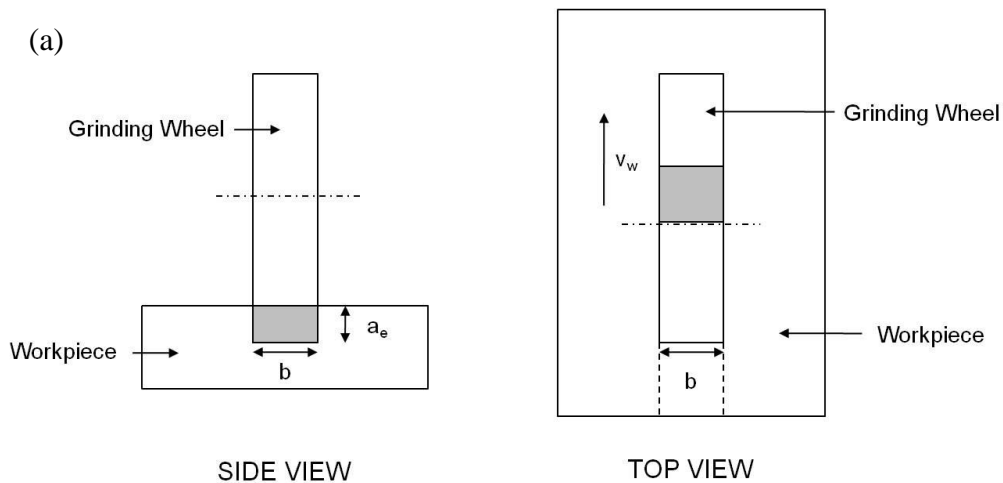
exhibit a power law relationship between the specific grinding energy and productivity [49]. The relationship is defined in equation (5.3.1):

$$e_c = A. Q'^{-t} \quad (5.3.1)$$

Where Q' = specific material removal rate ($\text{mm}^3/\text{s}/\text{mm}$)

A and t = constants dependent on workpiece material and abrasive grain type

The specific removal rate Q' is generally described as the material removal rate per unit width of cut b . This is due to the normally square contact of a grinding wheel contact with a workpiece material. The power requirement for a grinding process is proportional to the width of cut. The value of Q' is simple to calculate for a peripheral grinding process but the width of cut for the modified pin on disc setup is more difficult to quantify. Figure 5.3.1 shows the swept areas of material removal for different grinding setups. For Figure 5.3.1(a) the swept area is square so the specific removal rate can be calculated by dividing the productivity of the process by the wheel width b . In Figure 5.3.1(b) the setup is more complex as the swept area at the centre of the circle is larger than at the extremities.



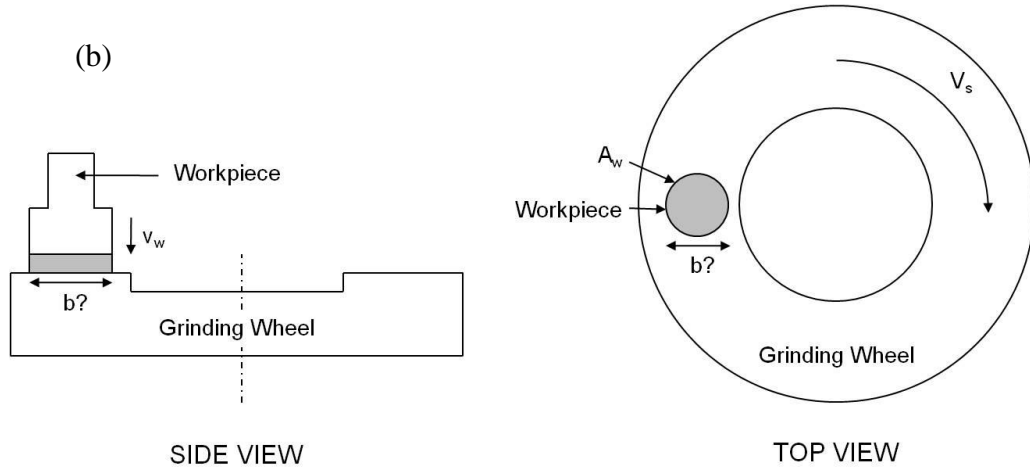


Figure 5.3.1 Diagram showing contact area shapes between grinding wheel and workpiece; (a) Peripheral Creep Feed Grinding and (b) Modified Pin on Disc Test Setup.

With respect to the circular contact presented, 2 varying methods of specific removal rates were calculated. One uses the pin diameter and the other uses the effective square radius of the pin contact area. They are detailed in (5.3.2) and (5.3.3) respectively:

$$Q'_d = \frac{A_w \cdot v_w}{d_{pin}} \quad (5.3.2)$$

$$Q'_{er} = \frac{A_w \cdot v_w}{A_w} = \frac{A_w \cdot v_w}{r_{esr}} \quad (5.3.3)$$

Where Q'_d = Specific material removal rate calculated using pin diameter
($\text{mm}^3/\text{s}/\text{mm}$)

Q'_{er} = Specific material removal rate calculated using effective square radius
($\text{mm}^3/\text{s}/\text{mm}$)

A_w = Contact area of the Nickel Pin Test Piece (mm^2)

r_{esr} = Effective square radius of the pin contact area (mm)

Using equation (5.3.2) provides a simplified method of calculating specific material removal rate. Figure 5.3.2 plots the SGE against this parameter. The results form a power law trend with the equation $e_c = 133.25Q'_d^{-0.504}$. This highlights that the grinding conditions appear to replicate the same behaviour as

witnessed in peripheral grinding applications. An increase in productivity largely witnessed at the higher grinding wheel speeds results in a lower value of specific grinding energy. Furthermore, the equation detailed above appears to closely replicate work by Stephenson and Jin [49]. This shows values for the constant A between 140 and 150, and t approximately 0.45 for grinding setups using Aluminium Oxide wheels on Steel and Inconel material. The modified pin on disc test appears to be representative test of the grinding process.

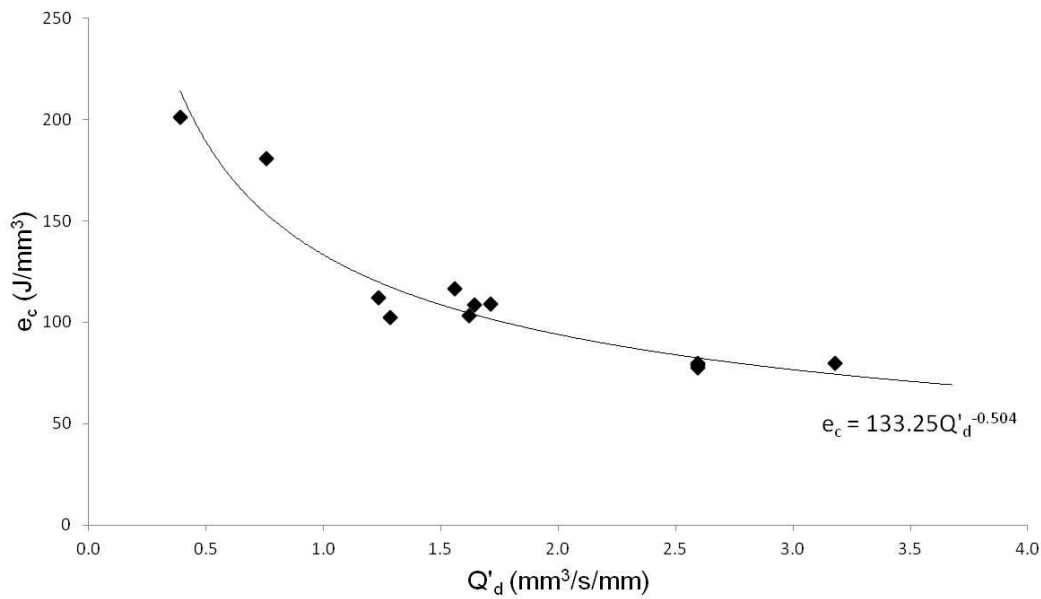


Figure 5.3.2 Graph of specific grinding energy versus diameter dependent specific removal rate for modified pin on disc trials.

As a further check of the results, the same relationship was plotted using the specific material removal rate detailed in equation (5.3.3). Here the overall material removal rate is divided by an equivalent square radius of the contact area. This takes into account some of the circularity of the contact and should provide a more representative specific removal rate. The results are plotted in Figure 5.3.3 with the trend approximated as $y = 141.62x^{-0.504}$.

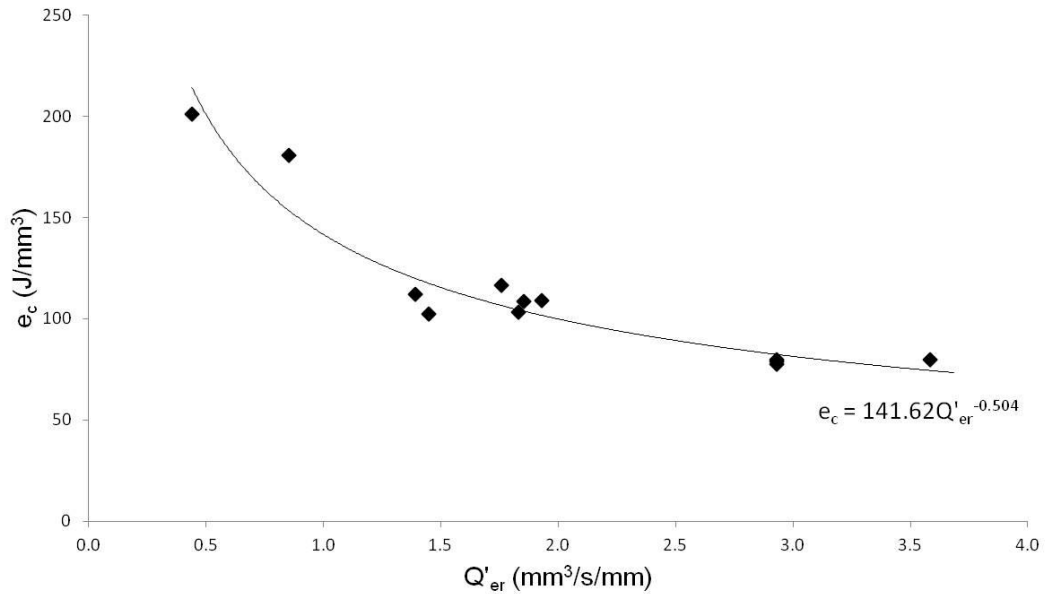


Figure 5.3.3 Graph of specific grinding energy versus effective radius dependent specific removal rate for modified pin on disc trials.

The results for both the relationships plotted in Figures 5.3.2 and 5.3.3 display power law trends comparable to peripheral applications in the literature. It is believed that the results produced in sections 5.1 and 5.2 provide useful context for explaining the behaviour associated with the maintenance of chip thickness models in the machining trials presented in Chapter 4.

5.4 Summary

The investigation into the effect of changing grinding wheel speed has shown that it has a significant impact on the outputs of the grinding process under the modified pin on disc test conditions. An increase in wheel speed for the same contact area and applied pressure results in a non-linear increase in the productivity of the process. This is likely to be an increase in contact zone temperature at the higher wheel speeds resulting in the material becoming easier to machine. This has the effect of higher wear rate/productivity which results in larger values of grinding chip thickness. As a result, a reduction in the force ratio of 50% was witnessed from a wheel speed of 10m/s to 50m/s. This indicates increased rubbing which coincides with the larger heat content at the higher wheel speed resulting in lower horizontal force requirements. The net power measured increased with an increase in wheel speed due to the higher

productivity. However, this resulted in a reduction in the specific grinding energy, a common trend witnessed in the grinding process with higher productivity cuts.

Changes in the contact area were also investigated through the testing of pins with varying diameters. The effect of changing wheel speed was more significant in comparison to contact area although some trends were identified. The wear rate/productivity of the pin material removal was dependent primarily on the amount of material in contact with the grinding wheel as opposed to changes in the cutting conditions. This resulted in similar values of chip thickness and force ratio for the different pin diameters. The 20mm pin diameter showed slightly higher chip thickness values combined with a small reduction in force ratio likely due to some increased heat effects. This resembled the same effect witnessed with the application of the high grinding wheel speeds. However, the impact on the process outputs was minimal in comparison to the grinding wheel speed. The net power measurement increased with pin diameter due to the increased material removal. The surface roughness reduced with an increase in wheel diameter. This is attributed to increased wear flat development with a larger arc of contact. The change in contact area has a small effect on the process outputs due to a change in the arc of contact but the impact is minimal in comparison to the change in grinding wheel speed.

Finally, specific grinding energy was plotted against specific removal rate to assess how well the modified pin on disc test represented traditional peripheral grinding applications. The results utilised data from both the wheel speed and contact area experiments within the data set. The plotted power law trends match well to previously documented work performed with Aluminium Oxide grinding wheels on Inconel 718 material. The test appears to be a good representation of the grinding process and the results provide useful information with respect to the work presented in Chapter 4.

Chapter 6 - Discussion

The discussion provides further analysis of the results detailed in Chapters 4 and 5. In addition, it combines data from the 2 experiments in Chapters 4 and 5 to explain the effect of varying chip thickness on the grinding process outputs. The analysis looks at developing the following key areas identified from the results:

1. Relationships between the different chip thickness models and process outputs
2. The effect of chip thickness and productivity on specific grinding energy
3. The effect of the different chip thickness models on the temperature output measured from the grinding process

In addition, the utilisation of chip thickness in grinding is discussed with examples of where the different models are most appropriate in providing improved control of the process outputs.

6.1 Relationship between Chip Thickness Models and Process Outputs

The individual chip thickness models utilised in Chapter 4 all concentrate on maintaining varying dimensions of theoretical chip geometry. The different chip thickness models are detailed in section 2.6 of this thesis but are presented again in Figure 6.1.1 for reference in this section. The S model represents a feed per cutting edge of a single grain contact, h_m relates to the maximum thickness of a comma shaped chip and h_{eq} provides a thickness in relation to the volume of material removed as a single chip. Each model, when maintained during the experiments detailed in Chapter 4, provided improved control of different outputs measured from the grinding process. This section links the relevant chip thickness model to process output and investigates why consistency in the measured values is maintained.

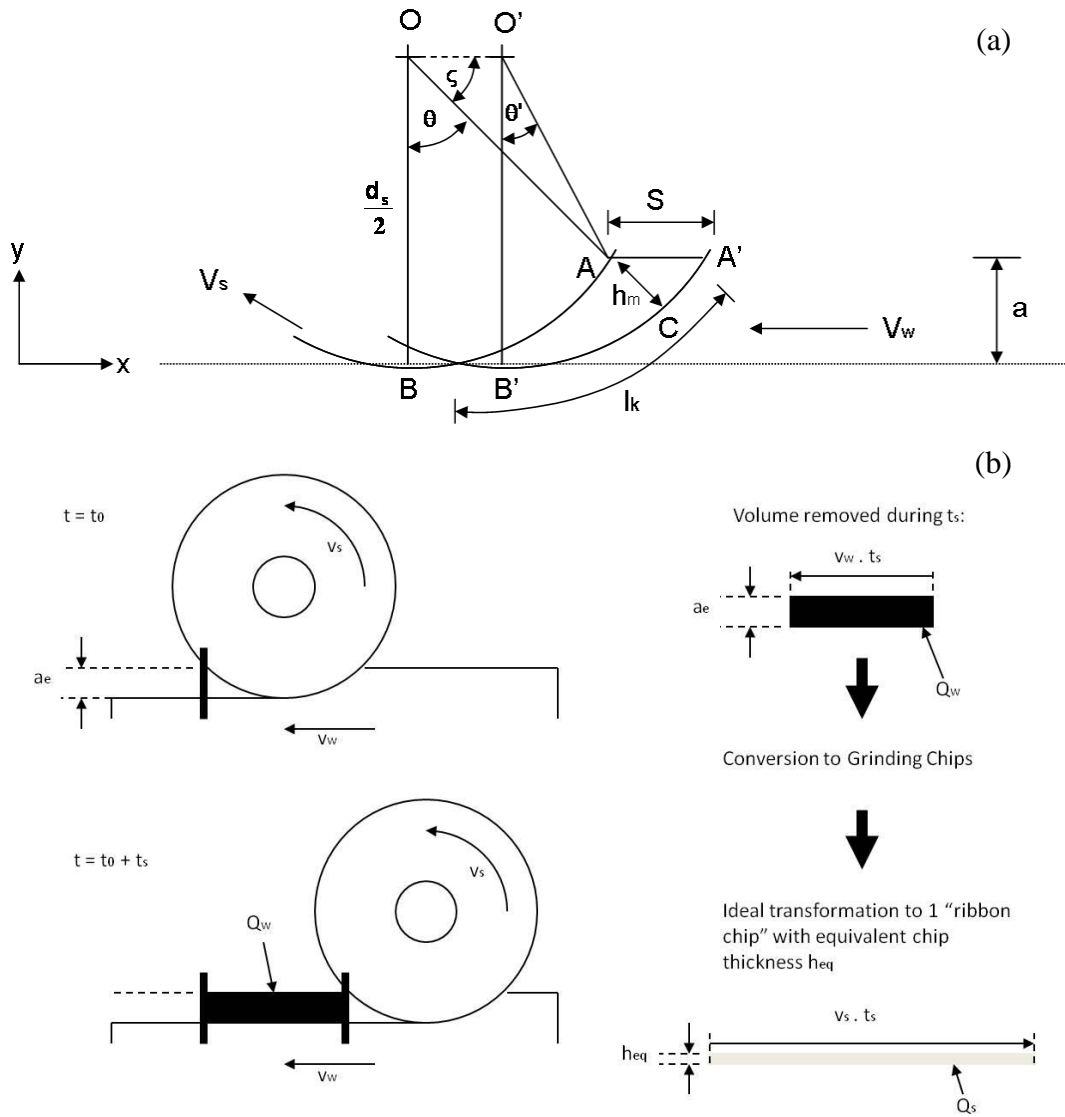


Figure 6.1.1 Diagram detailing geometric representation of chip thickness parameters; (a) S and h_m parameters, and (b) h_{eq} parameter.

To assess the impact of S , h_{eq} and h_m individually on the process outputs, each chip thickness parameter was plotted versus the wheel radius for each of the chip thickness models maintained. Figure 6.1.2 presents an example using theoretical chip thickness parameters A, B and C, of how the results are plotted.

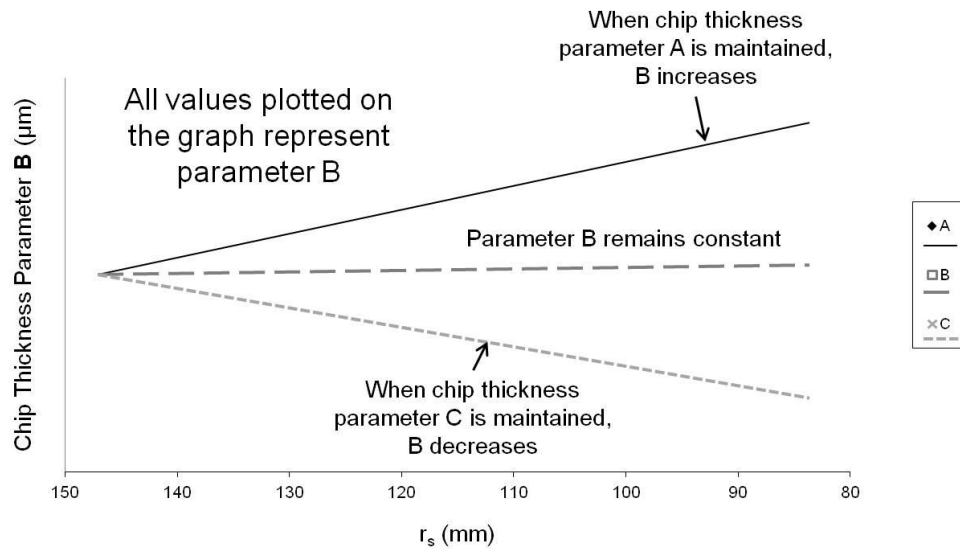


Figure 6.1.2 Example graph detailing how the chip thickness parameters are plotted versus the wheel radius and the trends associated with maintaining the varying chip thickness models.

Figure 6.1.2 shows the theoretical chip thickness parameter B versus the grinding wheel radius. The results for B are plotted for the 3 different data sets where parameters A, B and C are maintained respectively. This highlights the trends in parameter B under the different maintenance conditions as the wheel reduces in diameter. The outputs for the chip thickness parameters used in the experiments of Chapter 4 can be seen in Figures 6.1.3(a), 6.1.6(a) and 6.1.8(a) for S , h_{eq} and h_m respectively. The line styles and colours for each chip thickness maintenance data set are identical to the results presented in Chapter 4. The rationale for presenting the results in this way is to look for trends between each chip thickness parameter and associated grinding outputs.

The S Parameter and Net Power

The first process output to be considered is the net power due to its direct link with specific grinding energy. Maintenance of net power for constant productivity is important as higher power would cause an increase in specific grinding energy, which could lead to potential workpiece burn that can affect the surface integrity of a component. The output trends for net power P_{Net} are identical to the specific grinding energy e_c for the results presented as productivity was kept constant. The chip model trend that best matched the behaviour of P_{Net} was the S parameter. The trends for S, calculated for all the

chip thickness data sets, and P_{Net} are detailed in Figures 6.1.3(a) and (b) respectively. It can be seen that the value of S , for all the chip thickness data sets, appear to follow the same trend as the net power calculated from the spindle output.

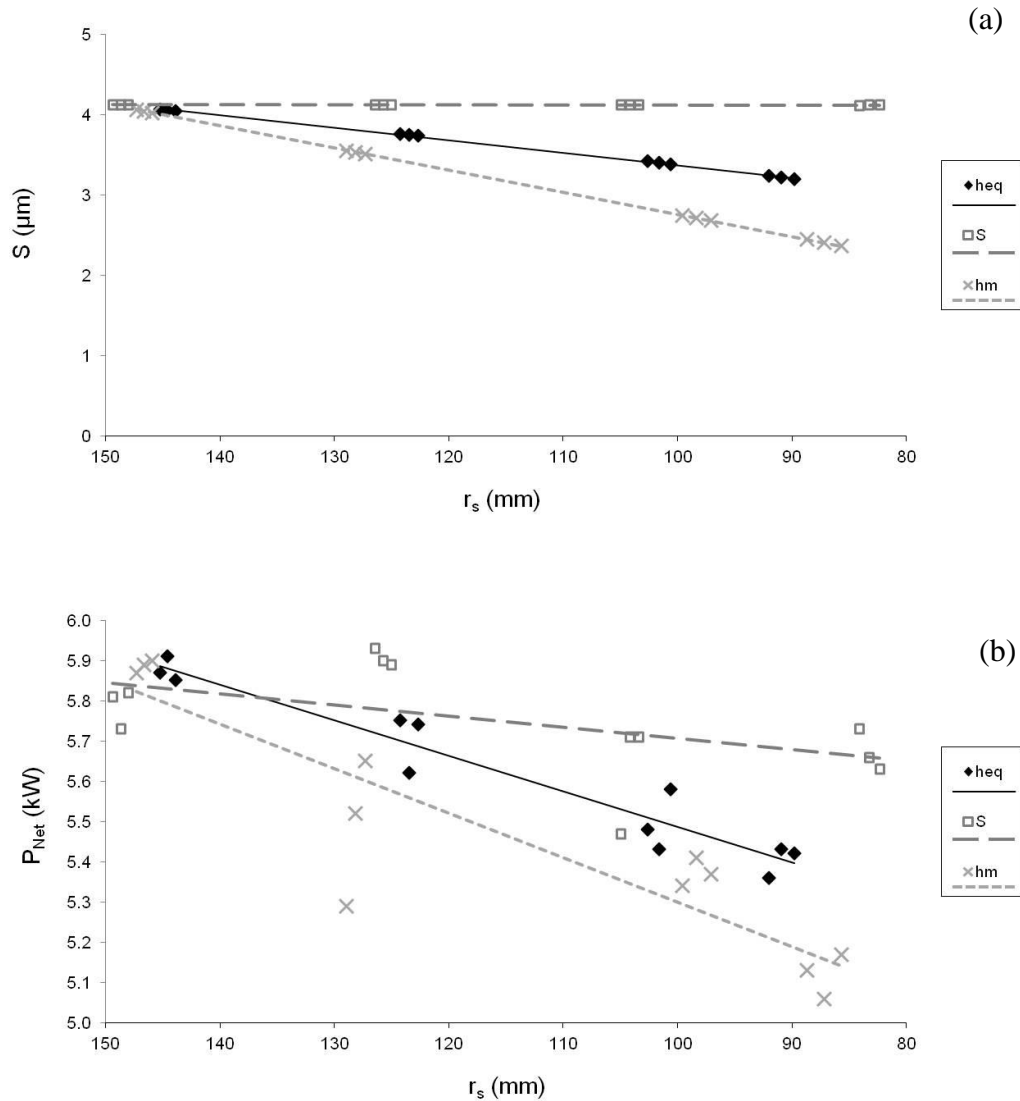


Figure 6.1.3 Comparative trends for chip thickness parameter and grinding process output; (a) S chip thickness parameter, and (b) Net Power output.

The value of S can be considered as the rate at which the wheel moves into the workpiece material. It is calculated from the time a theoretical grain is engaged in the arc of contact multiplied by the linear workpiece feed rate. Power is defined as the rate at which work is performed or energy is converted. When a grain interacts with the workpiece material, work is done through the metal

removal process. The amount of work performed can be related to the volume of material removed. Although productivity is constant for these experiments, the rate at which material is removed from the cut zone varies due to changes in geometry and grinding wheel speed. These changes are investigated through Contact Layer Theory.

The contact layer is described by Tawakoli [43] as the topmost layer below the area of contact between the wheel and the workpiece as detailed in Figure 6.1.4(a). It is the part of the workpiece that is interacting with the grinding wheel grits and is considered to have varying thickness and heat content depending on the process parameters and chip thickness. The contact layer theory also relies on the concept of equilibrium temperature for a cutting edge engaged in the workpiece material. An individual cutting edges temperature will only rise to a certain level then remains constant during the remainder of the cutting profile. Tawakoli states that as the wheel speed increased so too will the contact layer temperature and the surface temperature of the material as shown in Figure 6.1.4(b). The increase in the surface temperature of the material is due to the increased number of grit interactions within the contact layer at higher grinding wheel speeds. With an increased amount of grit interactions there is more friction in the contact layer resulting in an overall increase in temperature. This is similar to the effect witnessed in section 5.1 for the modified pin on disc trials. The increased wheel speed can lead to material softening making the contact layer easier to remove. The increase in contact layer temperature does not always correlate to an increase in measured surface temperature within a grinding process. This is dependent on the amount of heat flowing into a workpiece which is affected by the temperature of the contact layer and its thickness which directly affects the time taken to remove it.

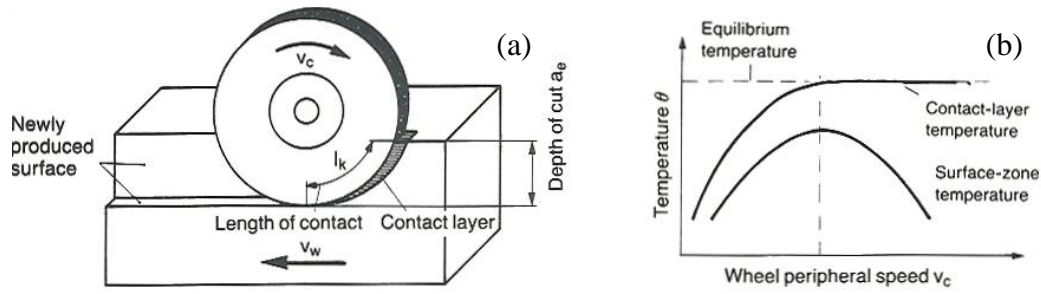


Figure 6.1.4 Contact Layer Theory; (a) Image highlighting contact layer zone & (b) Graph detailing the link between wheel speed and temperatures associated with the contact layer and ground surface by Tawakoli [43].

The time to remove the contact layer can have a significant impact on the surface temperature of the ground material and the outputs of the grinding process. Tawakoli [43] provides calculations for the time taken to remove the contact layer based on process parameters and the subsequent chip thickness as detailed in equations (6.1.1 – 6.1.2).

The volume of the contact layer per unit width of wheel is calculated as:

$$V'_{sch} = l_k \cdot h_{eq} \quad (6.1.1)$$

Where V'_{sch} = volume of contact layer per mm of wheel width (mm^3/mm)

l_k = length of contact arc engagement (mm)

The relationship between the specific removal rate and the contact layer volume gives the time to remove the contact layer:

$$t_{sch} = \frac{V'_{sch} \left(\frac{\text{mm}^3}{\text{mm}} \right)}{Q'_w \left(\frac{\text{mm}^3}{\text{mm.s}} \right)} \quad (6.1.2)$$

Where t_{sch} = time taken to remove the contact layer (s)

The time to remove the contact layer for all the cuts performed in Chapter 4 is detailed in Figure 6.1.5. The values show that the time to remove contact layer is constant when the S parameter is maintained and reduces for both the h_{eq} and h_m

models with a reduction in wheel radius. The h_m model provides the largest decrease. Any variation in contact layer time witnessed is due to a change in the contact layer volume as the specific removal rate is constant. The S parameter is the only value that when maintained results in constant rate of contact layer removal.

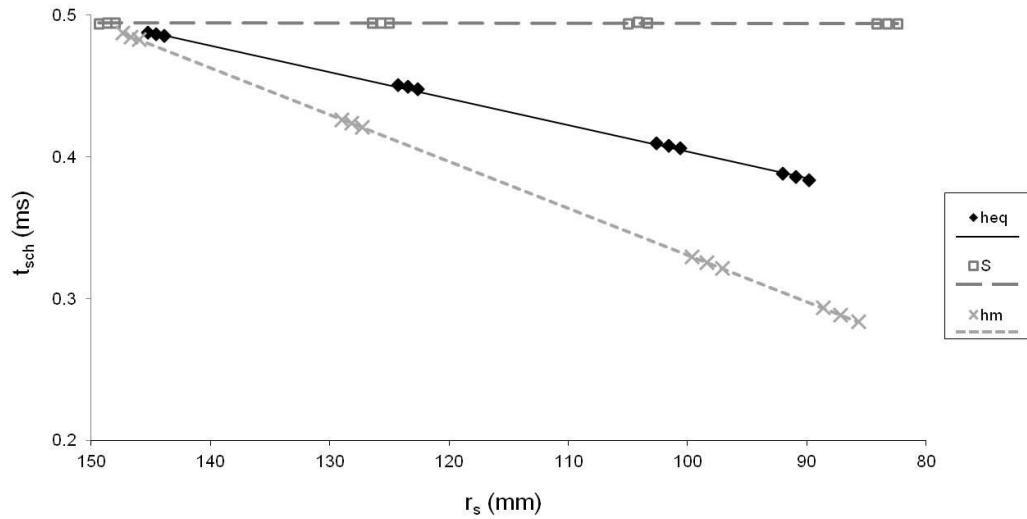


Figure 6.1.5 Graph of time to remove Contact Layer versus grinding wheel radius.

The trend of the contact layer removal time appears to match the output trends for the S parameter and the Net Power. The time taken to remove the contact layer is consistent at all wheel diameters when the S parameter is maintained. As a result, the rate of work required to remove the contact layer would be consistent when maintaining the S parameter. This results in similar power requirements at the different wheel diameters. Figure 6.1.5 also shows that the time for contact layer removal reduces when h_{eq} and h_m are maintained. This provides an explanation for the reduction in net power and specific grinding energy at the reduced wheel diameters when these chip thickness parameters are maintained in the machining trails. There are still subtle differences between the graphs presented in Figure 6.1.3 but in general the S parameter appears to provide a reasonable control of the net power grinding output due to its maintenance in the rate of removal of the contact layer.

The h_{eq} Parameter and Force

The force produced in a manufacturing process is an important output for consideration as large values can cause spindle deflection and potential damage to the component, the fixturing assembly and machine tool components. The change in chip thickness parameter h_{eq} over the diameter range of the wheel was representative of the trend witnessed for the force outputs results. Both trends are detailed in Figure 6.1.6. As the radius of the grinding wheel reduces, the value of h_{eq} increases when S is maintained and decreases when h_m is maintained. A similar trend is witnessed for the force output from the grinding process.

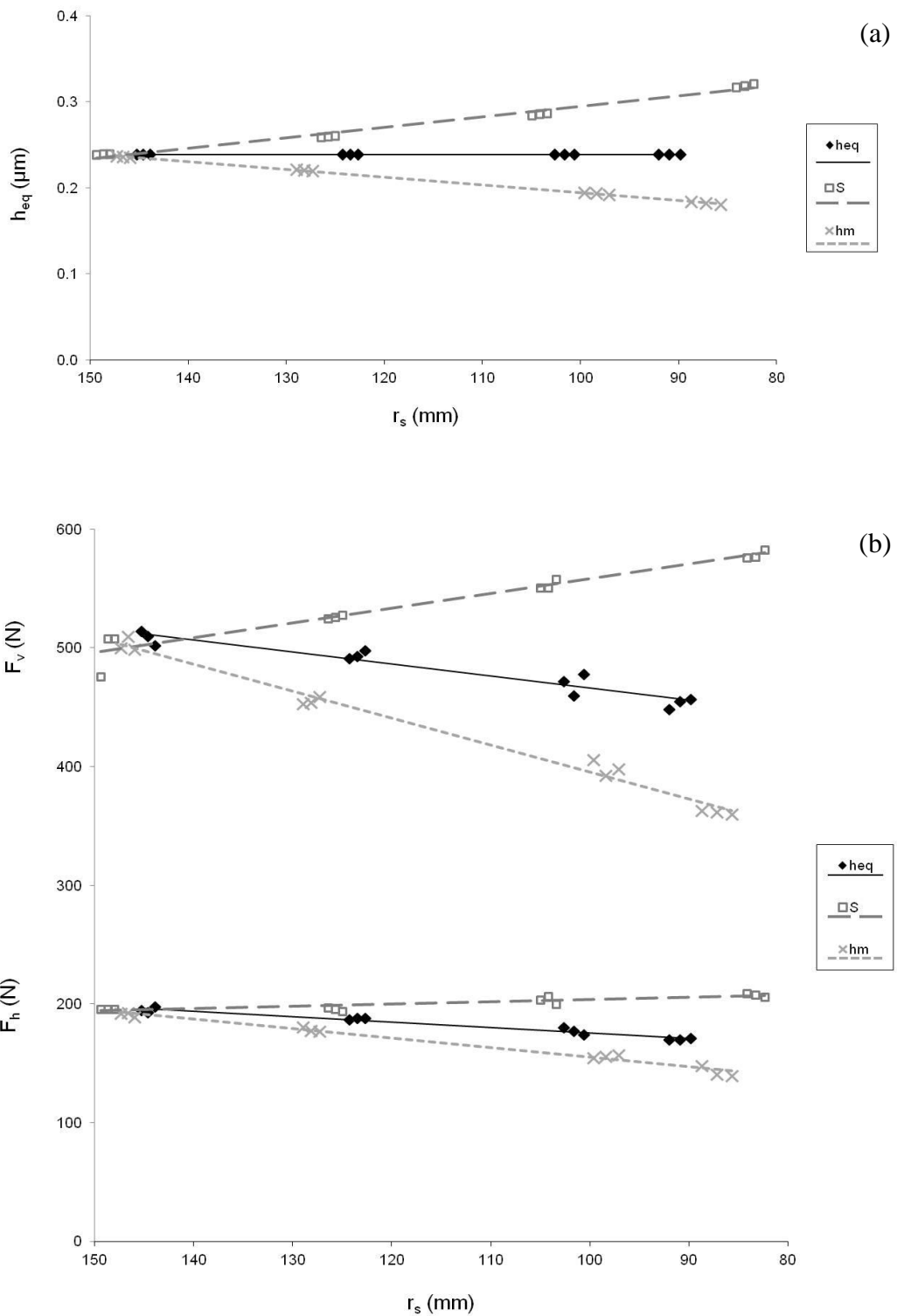


Figure 6.1.6 Comparative trends for chip thickness parameter and grinding process output; (a) h_{eq} chip thickness parameter, and (b) Force output.

Research previously performed by Snoeys et al [67] shows a strong linear relationship between Force and the value of h_{eq} . The empirical data detailed in

this work is presented in the form of grinding charts which was discussed in Chapter 2 of this thesis. An example of the relationship between specific force (N/mm of wheel width) and h_{eq} is shown in Figure 6.1.7. The results are plotted on a log-log scale graph and display a linear relationship between the 2 parameters.

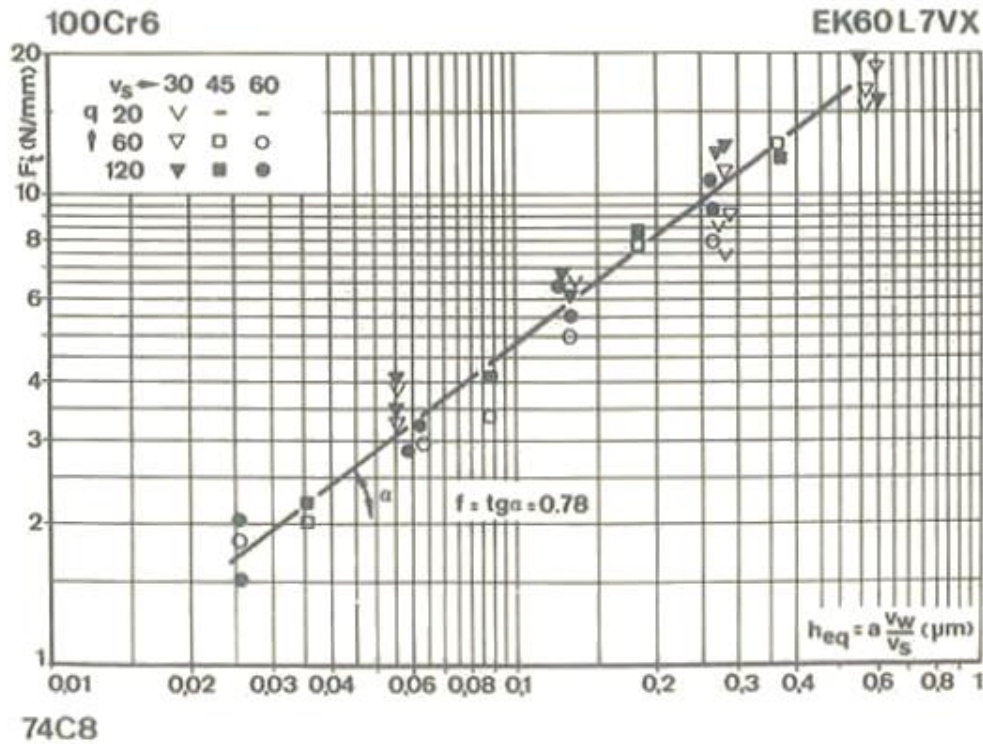


Figure 6.1.7 Empirical grinding results showing relationship between Force and h_{eq} by Snoeys and Peters [67].

To explain the relationship between h_{eq} and the overall force output, the force required to remove the contact layer is considered. The contact layer, as described above, is the topmost area beneath the contact area of the wheel and workpiece. The volume of this is dependent upon the arc of contact and the thickness which is determined by the h_{eq} parameter. There is an amount of energy and therefore force required to remove this volume of material. This can be related to h_{eq} by considering the force required to remove the contact layer volume. Mechanical work is utilised to relate force to energy and is shown in equation (6.1.3).

$$W = e = F \cdot d \quad \text{then} \quad F = \frac{e}{d} \quad (6.1.3)$$

Where W = mechanical work (J)

e = energy (J)

d = distance over which the force is exerted (mm)

The specific grinding energy can be utilised to estimate the energy required to remove the contact layer volume. Using the relationship presented in equation (6.1.3), the force applied over the contact layer length can be estimated as shown in equation (6.1.4).

$$F_{sch} = \frac{e}{d} = \frac{e_c \cdot V_{sch}}{l_c} = \frac{P_{Net}}{a_e \cdot v_w \cdot b} \cdot \frac{h_{eq} \cdot l_c \cdot b}{l_c} = \frac{P_{Net}}{Q'} \cdot h_{eq} \quad (6.1.4)$$

Where F_{sch} = Force required to remove contact layer volume (N)

Equation (6.1.4) shows that the force required to remove the contact layer has a direct relationship to the net power, productivity of the process and the value of h_{eq} . The value of F_{sch} based upon equation (6.1.4) and the results for P_{Net} presented in Chapter 4 is plotted in Figure 6.1.8. The trend of the graph follows the force trend measured by the dynamometer. The values are smaller in comparison to the horizontal force values in Figure 6.1.6. This could be due to the variation in the values of spark out force measurement, which are discussed in section 4.1, and could have affected the force measured from the dynamometer.

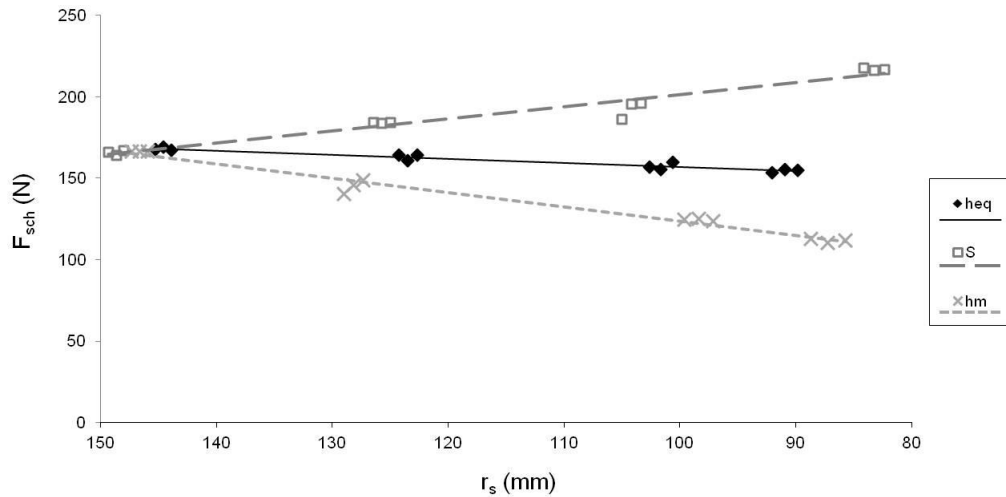


Figure 6.1.8 Force required to remove the contact layer volume versus grinding wheel radius.

The values presented in Figure 6.1.8 are similar in value to the horizontal force outputs shown in Figure 6.1.6 as these directly relate to the grinding power. The overall force outputs are linked to the equivalent chip thickness h_{eq} because of the size of the contact layer. The volume of the contact layer is dependent on h_{eq} because the equivalent chip thickness provides a good ratio of how far the abrasive grains are plunging into the contact area for every wheel rotation. The contact layer theory also explains why a small reduction in force is witnessed even when h_{eq} is maintained. This is due to the reduction in contact arc at the smaller wheel diameters leading to a reduced size of contact layer volume.

Variation in the h_{eq} parameter appears to best correlate with any changes presented in the overall force measured. This is because of its relationship to the size of the contact layer. An increase in the size of the contact layer means that an increased amount of energy and therefore force is required to remove the material. This also reinforces the use of h_{eq} to represent the thickness of the contact layer volume as it provides good correlation with certain grinding process outputs. The h_{eq} parameter appears to provide a good estimation of the contact layer volume as the results for the net power and force outputs of the process correlate well to the change in its calculated size and the time required to remove it.

The h_m Parameter and Force per Unit Area

Figure 6.1.9 shows the comparison in trend behaviour for h_m and the force per unit area results from Chapter 4. Whereas the overall force is important with respect to component and machine tool integrity, the force per unit area provides a useful comparison between processes by normalising for contact area. In addition, it can also provide a useful indication of the wear behaviour for non CD processes. Higher values would lead to increased grain or bond fracture of the grinding grits thereby increasing the radial wear of the grinding wheel [6]. Figures 6.1.9(a) and 6.1.9(b) show the trends of h_m and F'' are similar with the h_m model data set showing consistent specific force outputs especially for the horizontal force direction. The specific vertical force displays a small reduction in value at the small wheel diameters when h_m is maintained. The trends for h_m when maintaining the h_{eq} and S parameters show an increase in Figure 6.1.9(a) as the wheel reduces in diameter. This corresponds with the specific force outputs detailed in Figure 6.1.9(b).

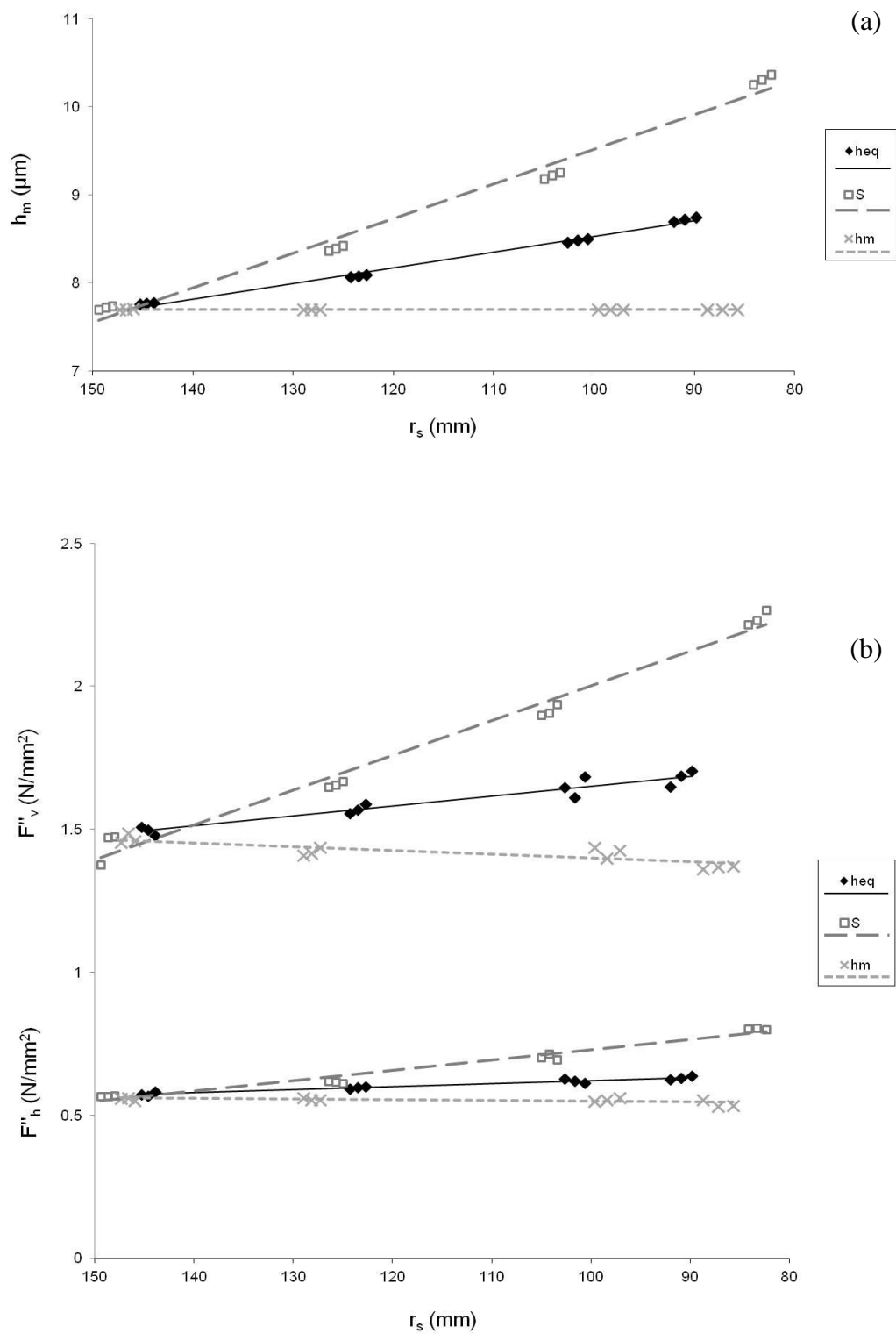


Figure 6.1.9 Comparative trends for chip thickness parameter and grinding process output; (a) h_m chip thickness parameter, and (b) Force per Unit Area output.

Werner [11] presented a model for force output when investigating the technical fundamentals of creep feed grinding. The model was developed from

experimental data to describe the force output with changing depth of cut for constant material removal rate surface grinding process. The model is detailed in equation (6.1.5) and includes process constants to be determined:

$$F = K_1 \cdot \frac{Z'}{V_s}^{2\epsilon-1} \cdot a_e^{1-\epsilon} \cdot d_s^{1-\epsilon} \quad \text{for values of } 1.0 > \epsilon > 0.5 \quad (6.1.5)$$

$$F \propto \frac{Z'}{V_s}^{2\epsilon-1} \cdot a_e^{1-\epsilon} \cdot d_s^{1-\epsilon} \quad (6.1.6)$$

Where $Z' = Q' =$ specific material removal rate ($\text{mm}^3/\text{s}/\text{mm}$)

To understand the Force per Unit Area F'' , the force is divided through by the contact area:

$$F'' \propto \frac{\frac{Z'}{V_s}^{2\epsilon-1} \cdot a_e^{1-\epsilon} \cdot d_s^{1-\epsilon}}{l_k \cdot b} \quad (6.1.7)$$

Where $b =$ cut width (mm)

$l_k =$ contact arc length (mm)

Considering b as a constant and expanding for Z' :

$$F'' \propto \frac{\frac{a_e \cdot v_w}{V_s}^{2\epsilon-1} \cdot a_e^{1-\epsilon} \cdot d_s^{1-\epsilon}}{a_e \cdot d_s^{1/2}}$$

$$F'' \propto \frac{v_w^{2\epsilon-1}}{V_s} \cdot a_e^{2\epsilon-1+1-\epsilon-1/2} \cdot d_s^{1-\epsilon-1/2}$$

$$F'' \propto \frac{v_w^{2\epsilon-1}}{V_s} \cdot a_e^{\epsilon-\frac{1}{2}} \cdot d_s^{\frac{1}{2}-\epsilon}$$

$$F'' \propto \frac{v_w}{V_s} \cdot \frac{a_e}{d_s} \propto \frac{v_w}{V_s} \cdot \frac{a_e}{d_s} \cdot 2^{\epsilon - \frac{1}{2}} \quad (6.1.8)$$

The equation presented in (6.1.8) can be compared to the formula for h_m :

$$h_m = \frac{4}{Cr} \frac{v_w}{V_s} \cdot \frac{a_e}{d_e} \cdot \frac{1}{2} \quad (6.1.9)$$

Showing a strong link between force per unit area and the value of h_m :

$$h_m \propto F'' \propto a \cdot \frac{v_w}{V_s} \cdot \frac{a_e}{d_e} \cdot \frac{1}{2} \quad (6.1.10)$$

As shown in equation (6.1.10), there appears a strong analytical link between the maintenance of F'' and the chip thickness parameter h_m for the model presented. As shown in section 3.2, the calculated number of grits per unit area C for the grinding wheel utilised in this experiment was 0.93 per mm^2 . As this value is so close to 1, the force per unit area is a close representation of the force per abrasive grain for this setup. As the h_m parameter is calculated based on the maximum chip thickness experienced by a single theoretical abrasive grain, maintaining this value should provide similar force results for an individual grain of constant placement and geometry. Obviously, the stochastic nature of the grinding process means that the force applied to each grain won't be constant as they are randomly placed in the grinding wheel structure. However, the results detailed above show that the h_m parameter provides the best method of predicting and maintaining constant force per unit area of wheel workpiece contact.

6.2 Effect of Chip Thickness and Productivity on Specific Grinding Energy

The analysis presented in section 6.1 considers the influence of maintaining different values of chip thickness for changing wheel diameter on the outputs of the grinding process. Figure 6.1.3 showed a link between the chip thickness parameter S and the net power output from the grinding process. The trend in net power is the same as specific grinding energy for the results presented in Chapter 4 as the productivity of the test cuts remains constant. Although changes in the specific grinding energy were witnessed in the experiment, the maximum variation in the output was 10% when h_m was maintained over the diameter range tested. Grinding literature [6] states that even small variations in the grinding chip thickness can result in significant changes in the specific grinding energy as described by the power law relationship detailed in equation (4.1.1). However as discussed in Chapter 2, the majority of the changes in chip thickness tested to assert this theory also include a change in the productivity of the grinding process. This section investigates whether it is changing chip thickness or productivity that has the most influence on the specific grinding energy of a process.

The results produced in Chapter 5 considered a constant force process on the modified pin on disc test rig. Due to changes in the contact zone conditions at the different grinding wheel speeds, the process experienced variation in both chip thickness and productivity. This corresponded with a change in specific grinding energy but it is unknown whether this is due to variation in chip thickness or productivity. Figure 6.2.1 plots the specific grinding energy versus the chip thickness for each of the data sets produced in Chapters 4 and 5. The specific grinding energy from Chapter 4 is plotted for h_m and CTR, with the results from Chapter 5 plotted for h_F . A general term for a normalised chip thickness h is plotted on the abscissa which represents values of h_m , CTR and h_F and how they change compared to the initial value over the course of the experiment. The comparison of the data sets is useful as the results from Chapter 4 show the effect of changing chip thickness for constant productivity whereas the testing presented in Chapter 5 experienced changes in the material removal rate. The

graph clearly shows that the change in e_c with h is far greater for the results in Chapter 5 where there was also a change in productivity. The figure shows that specific grinding energy appears to be more dependent on productivity as opposed to chip thickness.

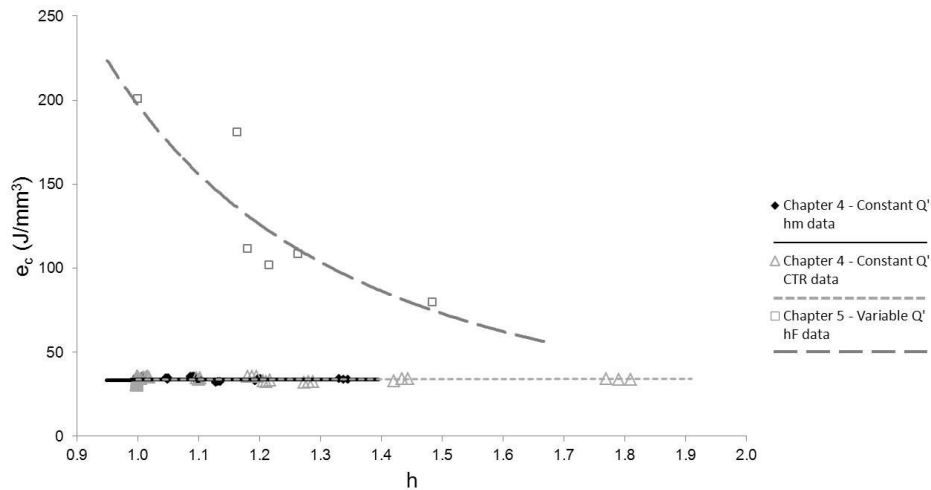


Figure 6.2.1 Graph of e_c versus h for thesis data from both cutting trials and modified pin on disc experiment.

To validate the impact of productivity on the grinding process, a power law relationship was applied to the specific grinding energy data plotted in Figure 6.2.2. This figure plots specific grinding energy versus the productivity of the process using the data from both experimental chapters. The power law provides a good fit but there is a change in the power law scaling exponent from approximately -0.5, detailed in section 5.3, to approximately -0.7 for this curve. The Chapter 4 results provide useful data at a higher value of productivity which changes the power law exponent. The power law trend represents the typical relationship between specific grinding energy and productivity. Figure 6.2.2 highlights the power law relationship between e_c and Q' further reinforcing the assertion that productivity has a larger impact on the specific grinding energy of a process in comparison to undeformed chip thickness.

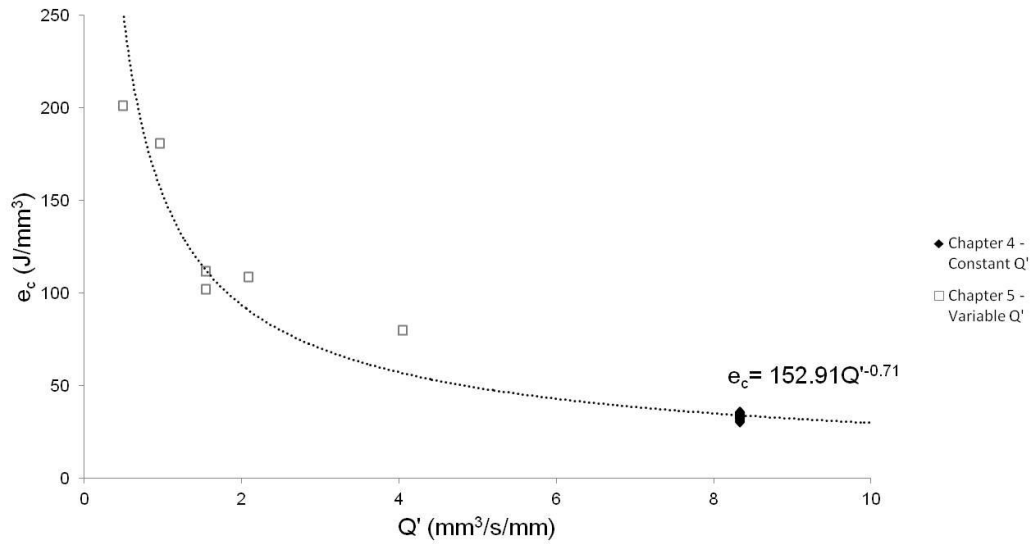


Figure 6.2.2 Graph of e_c versus Q' for thesis data from both cutting trials and modified pin on disc experiment.

The original relationship according to Shaw [6] shows the link between specific grinding energy and chip thickness as shown in equation (6.2.1).

$$u \sim \frac{1}{t^n} \quad (6.2.1)$$

Where $u = e_c =$ specific grinding energy (J/mm³)

$t =$ undeformed chip thickness (mm)

$n =$ constant

However it is shown that the relationship for specific grinding energy is more dependent on the productivity of a process. A more suitable relationship as described by Stephenson and Jin [49] is shown in equation (6.2.2).

$$e_c = A \cdot Q'^{-t} \quad (6.2.2)$$

Where A and $t =$ constants

$Q' =$ specific productivity (mm³/s/mm)

Although a strong link exists between e_c and Q' , it can be seen from Chapter 4 that changing chip thickness does have some impact on the process outputs. It is proposed that the specific grinding energy is always dependent on rate of material removal. This also matches well with the engineering mechanics

definition of energy. Changes in chip thickness at constant productivity result in microscale changes in the rate of material removal from the contact zone. This is different to changes in Q' which indicates much larger scale changes in the material removal rate related to the overall process productivity. Interestingly, the productivity appears to have significant influence over the specific grinding energy but the chip thickness has a very significant impact on overall force. This is explained by contact layer theory in section 6.1.

This section highlights a significant piece of information in relation to specific grinding energy and the influence of chip thickness on its value. Early theory proposed that specific grinding energy is dependent upon chip thickness however it is suggested that the main effect is due to the simultaneous change in productivity. Productivity has a larger impact on the specific grinding energy of a process in comparison to the undeformed chip thickness. The relationship presented in equation (6.2.2) is a better representation of the grinding process behaviour. However, chip thickness still has significant impact on the forces experienced during the grinding process.

6.3 Relationship between Chip Thickness and Temperature

The maintenance of the different chip thickness models also had an impact on the surface temperature output from the grinding process. The results presented in Section 4.2 of this thesis show data for the estimated surface temperature and the trends associated with maintaining the various chip thickness models. Figure 6.3.1 details again the surface temperature results for reference in this section. The results show that the temperature can range by up to 35°C at the small grinding wheel diameters depending on the chip thickness model applied. In addition, it was shown that the heat flux at the cut zone increased for all the chip thickness models at the reduced diameters due to a decrease in contact area. This section investigates why the measured surface temperature follows the trends detailed in the figure below.

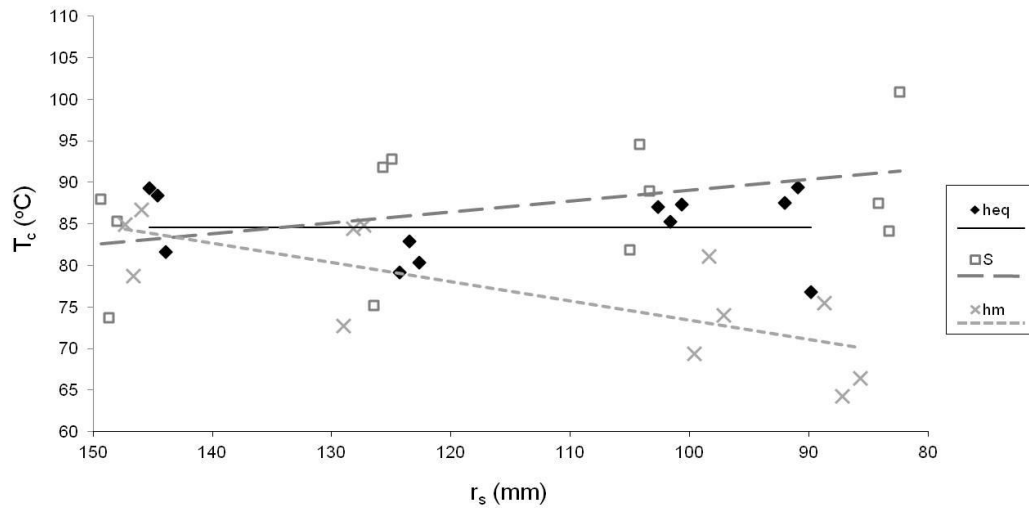


Figure 6.3.1 Graph of surface temperature versus wheel radius for the different chip thickness models maintained in Chapter 4.

The temperature variation in the ground surface is affected by the amount of heat generated in the contact zone and the distribution of that heat energy. The time taken to remove the hot contact layer zone is influenced by the workpiece feed rate as detailed in Figure 6.3.2. It is shown here that if the workpiece speed v_w exceeds the spreading speed of the heat front v_T , then the majority of the heat is dissipated through the grinding chips. Whereas if v_w is significantly less than v_T , then a significant amount of heat can be distributed into the workpiece surface. The results obtained in Chapter 4 utilised constant productivity with a constant value of v_w . As a result, the effect detailed in Figure 6.3.2 is assumed to have minimal impact on the temperature variation witnessed. The trends seen in Figure 6.3.1 must therefore be attributed to either changes in the amount of heat created in the contact zone or a change in the removal mechanism of this heat from the contact zone. These are dependent on other changing variables in the experiment.

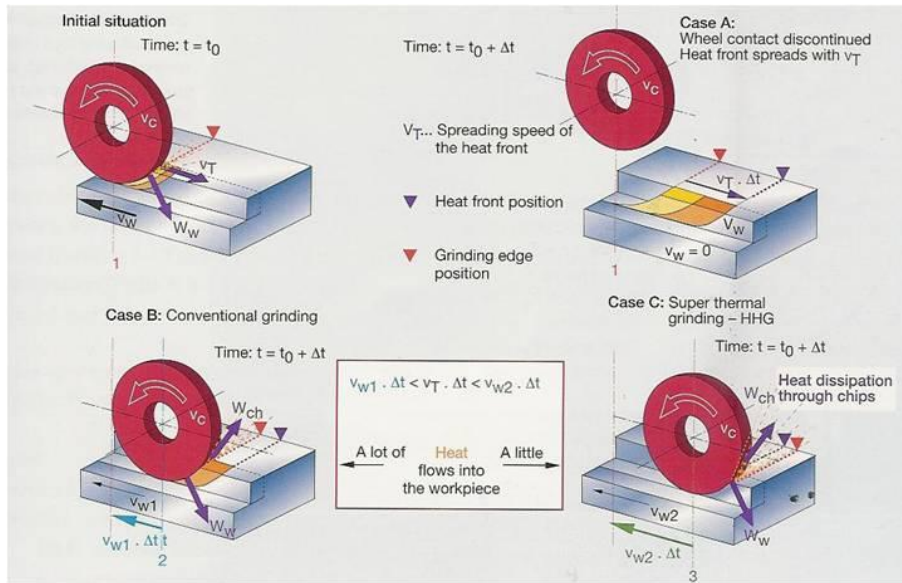


Figure 6.3.2 Variation in heat dissipation as a result of different workpiece feed rates by Helletsberger [4].

The variables that changed during the machining trials experiment were the contact area and wheel speed that were investigated in Chapter 5. Figure 6.3.3 shows the surface temperature outputs from Chapter 4 versus the contact arc length, which for a constant width of cut represents contact area. There appears no significant impact on estimated surface temperature with changing contact area. There is significant spread in the results but this is consistent over the range of contact lengths applied indicating that the variation in estimated surface temperature is not dependent on the size of the contact area.

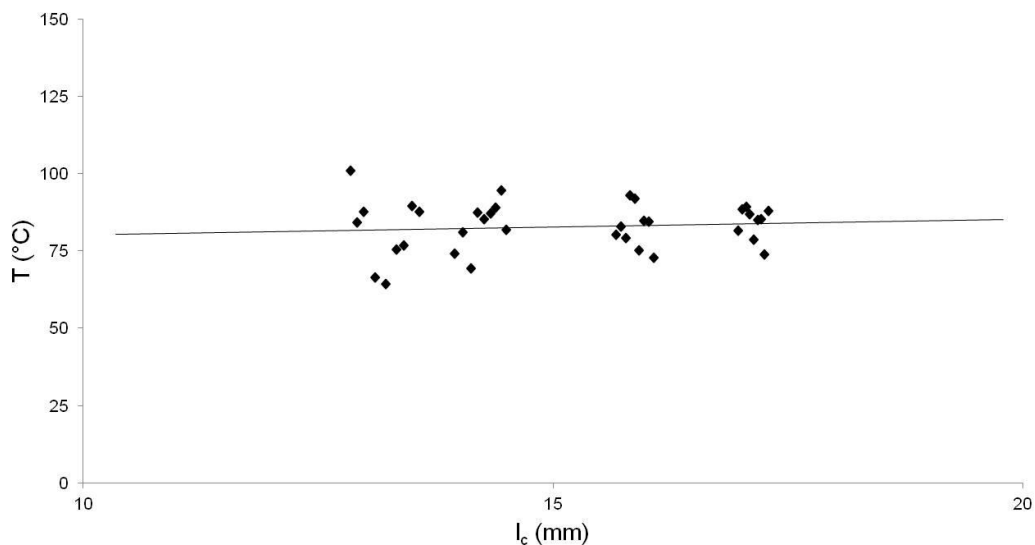


Figure 6.3.3 Surface temperature versus wheel workpiece contact length.

The surface temperature is plotted against the grinding wheel speed in Figure 6.3.4. This provides a clearer trend showing a reduction in surface temperature with increasing wheel speed. The graph does not differentiate between the different chip thickness model data sets but does clearly display the obvious impact of wheel speed on temperature that requires investigation.

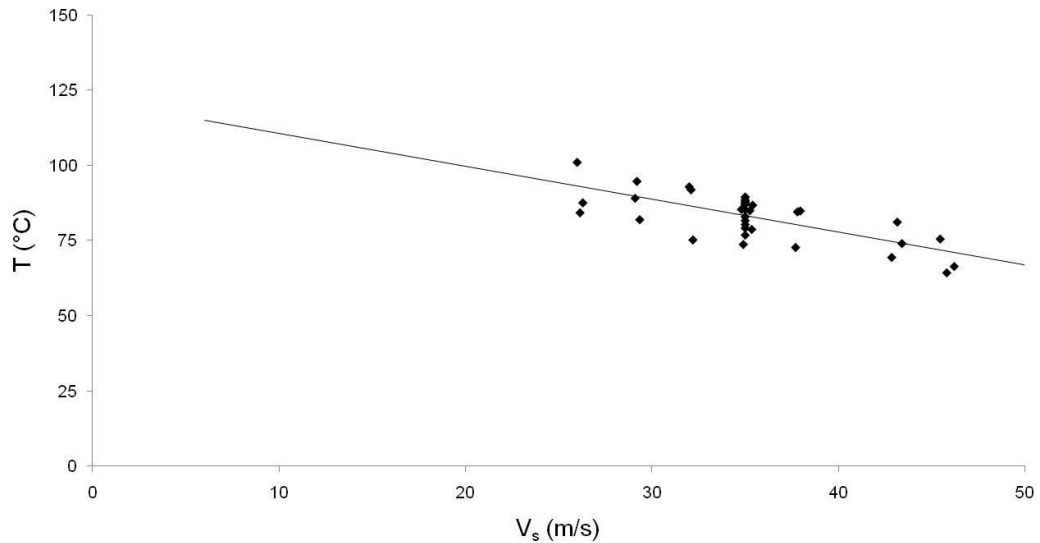


Figure 6.3.4 Measured surface temperature versus grinding wheel speed.

The workpiece temperature of a grinding process can be affected by a number of factors in the contact zone. An area of theory that has seen much research is that of Heat Partitioning and Convection Coefficients which are introduced in section 2.5 of this thesis. According to Rowe [83], heat is assumed to be conducted to the workpiece, wheel, chips and fluid within a grinding system. The majority of energy consumed within a grinding process is converted to heat. The total value of this in grinding is represented by the heat flux as shown in equation (6.3.1) with each partition defined in (6.3.2):

$$q_t = q_w + q_s + q_{ch} + q_f \quad (6.3.1)$$

where $q_t = \frac{P_{Net}}{l_{k.b}} = \text{total heat flux (W/mm}^2\text{)}$

$q_w = \text{heat flux to workpiece material (W/mm}^2\text{)}$

$q_s = \text{heat flux to grinding wheel (W/mm}^2\text{)}$

$q_{ch} = \text{heat flux to grinding chips (W/mm}^2\text{)}$

q_f = heat flux to cutting fluid (W/mm²)

$$\begin{aligned}
 q_w &= h_w \cdot T_{max} \\
 q_s &= h_s \cdot T_{max} \\
 q_f &= h_f \cdot T_{max} \quad T_{max} \leq T_b \\
 q_{ch} &= h_{ch} \cdot T_{ch}
 \end{aligned}
 \tag{6.3.2}$$

Where h = convection/conduction factor (W/m²K)

A significant amount of the heat flux generated within a creep feed grinding operation is dissipated to the cutting fluid. This can be up to 95% of the total heat flux according to Malkin [52]. Interestingly within the context of this analysis, the convection coefficient for the cutting fluid h_f is the only coefficient detailed in equation (6.3.2) influenced by the grinding wheel speed. This is because the wheel speed has a direct impact on how much fluid is dragged through the cut zone. The calculation for h_f is detailed in (6.3.3).

$$h_f = 0.94 \cdot \beta_f \cdot \frac{\overline{v_s}}{l_c} \tag{6.3.3}$$

where $\beta_f = \overline{k \cdot \rho \cdot c}$ = thermal property of the cutting fluid (J/m²sK)

k = thermal conductivity (W/mK)

ρ = cutting fluid density (kg/m³)

c = specific heat capacity (J/K)

The value of h_f is dependent on the 2 variables V_s and l_c which both change over the course of the experiments in Chapter 4. The constant β_f is determined from fluid properties. Figure 6.3.5 details the value of h_f for pure water when applied to the chip thickness model data sets from Chapter 4, to assess how the coefficient changes over the course of the experiment. It is shown that the coefficient remains constant for the S parameter and increases for both h_{eq} and h_m . An increase in h_f indicates that an increased amount of cutting fluid is dragged through the cut zone and would result in an improved capability to remove heat generated during the process. This should lead to a reduction in the surface temperature.

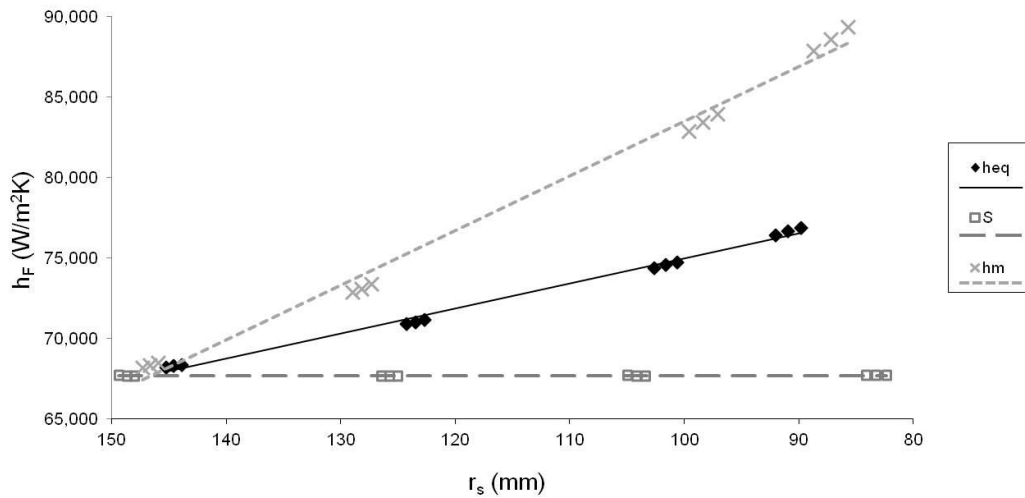


Figure 6.3.5 Cutting fluid convection coefficient for pure water versus wheel radius.

The exact value for h_f is unknown for the current setup but can be calculated by using the results from experimentation applied to equation (6.3.2). An assumption is made that T_{\max} is defined by the estimated surface temperatures from section 4.2. The calculation for h_f using the experimental results is presented in equation (6.3.4). The average heat flux and surface temperature from Block 1 in the machining trials was utilised to calculate an initial value of the fluid convection coefficient h_{fi} . This was then used to establish an initial constant value for β_{fi} .

$$h_{fi} = \frac{15.37e^6 (W/m^2)}{84.1+273 (K)} = 43031 (W/m^2K) \quad (6.3.4)$$

leading to a value of $\beta_{fi} = 1009 (J^2/m^2 K^2 s)$

This initial value of β_{fi} was utilised to calculate the values of h_f for all the cuts performed in the machining trials over the entire wheel diameter range. The value of T_{\max} for each of these cuts was calculated using the heat flux output and the associated convection coefficient. The predicted surface temperature T_{\max} is plotted in Figure 6.3.6. The trends for the different data sets presented in the graph resemble the behaviour from the measured surface temperature detailed in section 4.2. It appears that the effect of wheel speed is significant with respect to

altering the fluid convection coefficients which impacts on the measured surface temperature output of the grinding process.

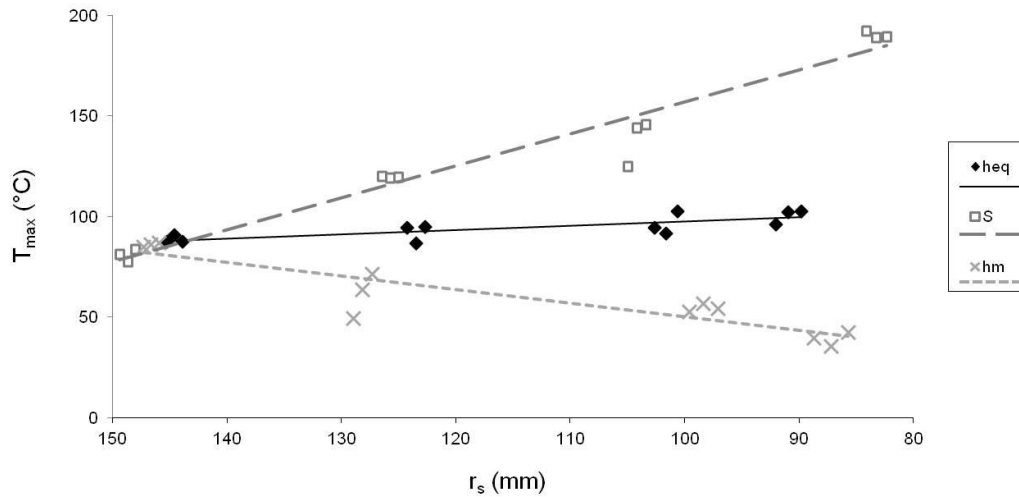


Figure 6.3.6 Predicted surface temperature versus wheel radius.

The variation in predicted surface temperature presented in Figure 6.3.6 is much larger in comparison to the measured results from section 4.2. The difference between the predicted and measured surface temperatures can only be related to incorrect values of β_f or q_f used in the calculation of T_{max} for the different grinding wheel diameters. It is difficult to understand how the fluid constant β_f would alter with a change in wheel diameter or grinding wheel speed. More likely is that the amount of heat flux passing to the fluid alters depending on the position of the fluid nozzle in relation to the grinding wheel. At the smaller grinding wheel diameters, the nozzle orifice is at a greater distance from the cut zone which would impact the amount of fluid entering the cut zone. Further investigation would be required in order to establish the reasoning for the discrepancy between the predicted and measured surface temperatures in the experiment. However, it does appear that the use of cutting fluid convection coefficients explains the behaviour witnessed from the temperature measurements especially when the heat flux increased with reducing wheel radius for all the chip thickness models applied. The application of different chip thickness models has a twofold impact on the measured temperature output of the process with changing wheel diameter. Firstly, the overall heat flux experienced

by the workpiece changes depending on the chip thickness model applied due to changes in the specific grinding energy. Secondly, the effectiveness of the cutting fluid in removing heat from the contact zone is affected by the grinding wheel speed as explained by the cutting fluid convection coefficients. Although the variation in temperature witnessed in the machining trials is not large, the concept of using wheel speed to maintain the amount of heat flux transferred to the cutting fluid should be a consideration in the use of chip thickness models. This is especially relevant in the application of creep feed grinding.

6.4 Utilisation of Chip Thickness in Grinding

The aim of the research was to provide a greater understanding of the relationship between chip thickness and the outputs of a grinding process. An objective was to provide examples of where chip thickness can be used to provide greater control of the process outputs. To achieve this, the testing performed in the thesis focussed on maintaining values of chip thickness in order to maintain the outputs of the process. Consistency in the process outputs is of value to production engineers allowing them to ensure product quality. This section discusses the optimum chip thickness model to apply to provide consistency in the process outputs for changing grinding wheel diameter in a constant productivity CD process.

Net power from the spindle is directly related to the specific grinding energy (SGE) of the process. Optimum grinding processes exhibit as low a value for SGE as possible as most of the energy required by the process is converted to heat. A large amount of heat can have negative consequences on the surface integrity of components. Considering the experiments performed in Chapter 4, all the chip thickness models showed a reduction in specific grinding energy as the wheel reduced in diameter. From the point of view of maintaining e_c , the S parameter provided the most consistency as it maintained a constant removal rate of the contact layer between the grinding wheel and workpiece. However, the application of the h_{eq} and h_m models reduced the SGE at lower wheel diameters. As a result, all chip thickness models are seen as appropriate to use as none of them provide an increased value of SGE at the reduced wheel diameters. The

largest influence on the value of specific grinding energy is the productivity of the process as shown in section 6.2.

The overall force experienced by the workpiece was significantly affected by the application of different chip thickness models. This is important in production as high force values can cause spindle deflection, leading to inaccurate cut dimensions, and deflection in workpiece fixture assemblies. The overall force output can be maintained by applying a constant value of h_{eq} . This is due to the contact layer volume being closely related to h_{eq} . The size of the contact layer governs how much force and energy are required to remove it. Maintaining h_{eq} or h_m ensures that the overall force output from the process does not increase as the wheel reduces in diameter.

The maintenance of the h_m model provided a constant force per unit area as the wheel reduced in diameter. The other chip thickness models caused an increase in the specific force output value. The specific force output is more beneficial as a comparator between processes and to provide an estimation of the force applied to individual abrasive grains. As a result, the application of h_m would be more beneficial under non CD conditions as maintaining a consistent force per unit area could be utilised to control wheel wear for changing grinding wheel diameter. Further investigation under non CD conditions is required to understand the use of h_m to gain increased control of the wear experienced during the grinding process.

The workpiece temperature is of high importance in production, especially in grinding processes where burn of the component can impact the operational performance of a component. The application of the different chip thickness models has an influence on the workpiece temperature by altering the heat flux generated in the contact zone and changing the convection capability of the cutting fluid which is dependent on wheel speed. Section 6.3 highlights that the wheel speed should either remain constant or increase as the wheel reduces in diameter. When the h_{eq} and h_m models are applied, the workpiece temperature either remains consistent or reduces as the increase in heat flux with reducing diameter is offset by an increase in the ability of the cutting fluid to remove heat

from the contact zone. Essentially more fluid is passed through the cut zone with a higher wheel speed and smaller contact arc length, which helps reduce the heat in the contact zone. This is especially relevant for creep feed grinding where the majority of the heat flux is transferred to the cutting fluid during the process. For a production operation, the wheel speed should at least remain constant or increase as the grinding wheel diameter reduces.

The results detailed in Chapter 4 show that not all the process outputs can be maintained as the wheel reduces in diameter regardless of the type of chip thickness model maintained. However, certain chip thickness models can be utilised to maintain specific critical outputs. The various models used in this thesis all maintain different process outputs under CD conditions. But the maintenance of certain outputs can lead to changes in others. For example, use of the S parameter aids in the maintenance of net power output over the course of the experiment but resulted in higher surface temperatures and force at the smaller grinding wheel diameters. The choice of chip thickness parameter should be made on the analysis of what is most cost effective and least detrimental to the component quality.

In consideration of the above for use in production, the overall recommendation is the application of the h_{eq} model. This is based upon there being no increase in the value of specific grinding energy, force or temperature as the wheel reduces in diameter. In addition, the same argument can be made for utilising the h_m model but this model incorporates an increase in wheel speed which will result in an increased amount of wheel dressing during the CD process. This would unnecessarily increase the cost of the process.

In addition to providing consistent outputs from the grinding process, the equivalent chip thickness h_{eq} also appears to provide the best estimation of force and energy requirements for the process. It is a simple formula that is a ratio of material removed against the grinding wheel speeds which represents how far the abrasive grains penetrate into the workpiece material at the contact zone. This is shown in the contact layer theory which utilises the h_{eq} parameter and shows good correlation with the outputs of the grinding process. Attempting to identify

and use individual chip sizes to predict outputs in grinding is complicated. The use of macro scale parameters such as productivity and h_{eq} , related to specific grinding energy, force and temperature, appear to be the best method of relating inputs to outputs when implementing grinding processes.

The above recommendation of using h_{eq} to maintain process outputs is made based upon the conditions set within a CD process. This may not however be as beneficial for a non CD process where the effect of changing wear behaviour at different grinding wheel diameters will be significant. Preliminary work detailed in Chapter 3 showed potential benefits of being able to maintain the amount of radial wear through increased wheel speed at smaller wheel diameters. Due to the different challenges presented with non CD applications, and the effect of wear which would have an impact on the mechanical and thermal outputs, it is suggested that this would form the basis of future work. It is apparent that the implementation of different chip thickness models can have significant impact in the control of certain outputs of the grinding process which could be of value to production engineers under similar constant material removal conditions.

The relationships discussed in this section are valid for the specific experiment conditions for this particular setup. This includes the application of continuous dressing and the use of a constant material removal rate for the creep feed grinding of Inconel 718 using a Makino A99 machine tool. Although the use of different grinding setups with alternative materials may produce variation with respect to the magnitude of the process outputs, it is proposed that the trend behaviour between the chip thickness models and the process outputs would remain the same. This is due to relationships drawn between the changes in the contact layer and the effect on the process outputs which should translate well to other materials and types of grinding processes. Other non-controlled influences e.g. machine tool stiffness, are proposed to have the same effect.

6.5 Summary

The results in section 6.1 show that the maintenance of different chip thickness models provides consistency in certain outputs of the process. The S parameter

and net power follow a similar trend over the course of the experiment as it governs the removal rate of the contact layer. The trend in h_{eq} corresponds with the overall force output. This is due to the force requirement being determined by the size of the contact layer to be removed which is dependent on the value of h_{eq} . The value of h_m closely resembles the trend seen in the force per grit/unit area output as it is derived by considering the maximum chip thickness experienced by an individual abrasive grain. The work shows that different outputs of the grinding process can be maintained through the application of different chip thickness models.

The comparison between the 2 experiments performed in Chapters 4 and 5 provided a unique insight into the significance of changing productivity and chip thickness on the specific grinding energy. Section 6.2 showed that the specific grinding energy output is influenced significantly more by productivity as opposed to chip thickness. This highlights an important shift in some theory where chip thickness is used to govern the magnitude of specific grinding energy. It is thought that SGE is purely related to rate of material removal. For constant productivity processes any changes in chip thickness only change the amount of material removal on a small scale. However, changes in chip thickness do have a significant influence on the overall force experienced by the workpiece as this impacts the size of the contact layer.

The application of different chip thickness models affects the workpiece temperature by altering the amount of heat flux generated in the contact zone and altering the ability of the cutting fluid to remove heat from the contact zone at different grinding wheel speeds. An increase in grinding wheel speed allows more cutting fluid to be drawn through the contact zone allowing an increased amount of heat to be transferred to the fluid. This is very important in creep feed applications where the majority of heat flux generated at the contact zone is transferred to the cutting fluid. The application of h_{eq} and h_m were considered suitable for application as neither resulted in a temperature increase at the small grinding wheel diameters.

Application of chip thickness models can aid in the maintenance of certain outputs of a grinding process. This is useful in grinding processes where changes in critical outputs such as workpiece temperature can result in component damage. However, no current chip thickness model provides control over the entire process and it appears beneficial to consider the interaction at the contact zone from a macro perspective in terms of contact layer as opposed to individual chip thickness geometry. For the experimental setup detailed in Chapter 4, the use of h_{eq} parameter is suggested to be the optimum method of maintaining the process outputs in production. This is due to there being no detrimental effects on the machine or component integrity with changing wheel diameter. Maintenance of the h_m parameter also provides these conditions but the increase in grinding wheel speed would increase the amount of grinding wheel consumed for the CD process which is undesirable. The h_m parameter would be more useful for non-CD applications as it could be utilised to help maintain consistent wear on the grinding wheel at varying wheel diameters. In addition, this could also provide the ability to increase the productivity of the process whilst maintaining the value of critical outputs. However, further work would be required to develop this.

Chapter 7 - Conclusions and Further Work

The study of the relationship between chip thickness and the outputs of the grinding process has shown that they are closely linked. Application of different chip thickness models can be used to maintain certain key outputs of the process at different grinding wheel diameters for a constant productivity process. However, it has been shown that both the productivity and chip thickness in grinding have a significant impact on the process each affecting the outputs in different ways. In addition, although chip thickness has a relationship with the grinding process outputs, it is best considered as a macro parameter as opposed to considering the size of individual chips for an abrasive grain. The following details the main conclusions from the work performed:

- Maintenance of the S chip thickness parameter is the optimum method for maintaining Net Power and Specific Grinding Energy for a constant productivity process. This is due to the S parameter providing a constant rate of contact layer volume removal. The time to remove the contact layer represents the rate at which the wheel plunges into the workpiece material. It is shown that this is closely related to the rate of mechanical work performed which governs the power requirements during grinding.
- The h_{eq} chip thickness parameter presents the best method for controlling the overall force experienced by the workpiece from a grinding process. The force is governed by the size of contact layer to be removed which is estimated using contact arc and h_{eq} . Variation in equivalent chip thickness h_{eq} results in a change in contact layer volume which changes the force requirement for the grinding process.
- Maintenance of the h_m chip thickness parameter provides a method of maintaining the force per unit area for the grinding conditions presented in this thesis. This is due to the h_m parameter representing the maximum

thickness of a comma shaped chip from an individual abrasive grain. It is analogous to the h_{ex} parameter in milling. The force per unit area is useful as a comparator between processes to understand if a change in parameters presents increased loading conditions on an individual grain. This would be very useful when considering non CD processes where individual grain load can have a significant impact on the wear mechanism experienced.

- Contact layer theory is useful in providing explanations for the change in process output behaviour for different chip thickness conditions. Development of the theory indicates that the size of the estimated contact layer is closely linked with the overall force output as shown in (6.1.4). The rate of removal of the contact layer volume shows good correlation with the net power of the grinding system. It appears that contact layer theory provides a good estimation of the mechanical outputs from the system and should be incorporated into chip thickness theory for grinding processes. The contact layer estimation is dependent upon the equivalent chip thickness h_{eq} , which appears to provide a good estimation of the contact layer volume. The h_{eq} parameter is a useful chip thickness parameter as it estimates the grinding process from a macro perspective as opposed to individual chips produced from the grinding grains. It is asserted that this is a more suitable approach in grinding when cutting edges are not well defined.
- It is proposed that the value of Specific Grinding Energy (SGE) is more dependent on the productivity of a grinding process Q' as opposed to the applied value of chip thickness. This provides an alternative view with respect to some of the grinding literature. Work by Shaw [6] details the value of specific grinding energy changing significantly with chip thickness. The variation in specific grinding energy against chip thickness was plotted for both constant and varying productivity conditions. The results showed that the value of SGE changes by a small amount with varying chip thickness at constant productivity. The change is much

larger when the change in chip thickness corresponds with a change in productivity. It is proposed that the specific grinding energy is always dependent on rate of material removal which also matches with the physical definition of energy. Changes in material removal rate for different chip thicknesses at constant values of Q' are related to the change in the contact layer removal volume. This is small in relation to large changes in productivity as a result of applying different material removal rates.

- The application of different chip thickness models has an impact on the measured workpiece temperature in the creep feed grinding process. This is due to changes in the heat flux at the contact zone. In addition, changes in grinding wheel speed affect the value of the cutting fluid convection coefficient which impacts the amount of heat removal from the contact zone. Maintenance of the h_{eq} parameter provides a consistent workpiece temperature output. Application of the h_m model shows a decrease in workpiece temperature at smaller grinding wheel diameters. Increased wheel speed or a reduction in the arc of contact provides improvement in the cooling effectiveness of the cutting fluid as it allows more cutting fluid to pass through the cut zone. This is of significance in the creep feed process where the majority of heat generated at the cut zone flows to the cutting fluid. The use of chip thickness models should be combined with the calculation of cutting fluid convection coefficients to maintain the temperature of the workpiece for creep feed conditions.
- Increased grinding wheel speed and arc of contact appear to result in additional heating in the contact zone making the material easier to machine. It is proposed that increased heat in the contact zone has the effect of increasing the productivity of the process under constant normal force conditions. This was witnessed during the modified pin on disc testing. The wheel speed has a much larger impact on this effect as opposed to arc of contact. This can have the effect of reducing the

specific grinding energy under constant productivity peripheral grinding conditions at higher wheels speeds.

- Face grinding using the modified pin on disc setup can be used to investigate peripheral grinding conditions and is useful to assess the effect of parameters in isolation of complex grain kinematics. The SGE results for both the peripheral and face grinding applications show a power law relationship between SGE and Q' . The equations representing the power law relationship for the modified pin on disc test match well to the grinding literature for Inconel 718 grinding with aluminium oxide [49]. This highlights the benefit of using tribological testing techniques to provide additional information to machining trial results.

These conclusions lead to a number of recommendations for the utilisation of chip thickness in creep feed grinding processes, these include:

- Utilisation of the h_{eq} grinding chip thickness parameter for CD processes to maintain constant process parameters over the operational life of the grinding wheel. Maintaining the value of h_{eq} results in constant force and temperature outputs as the wheel reduces in diameter. The h_{eq} parameter maintains wheel speed for constant productivity and is preferable to other chip thickness models as it provides good control of the process outputs and has reduced wheel consumption through dressing in comparison to application of the h_m chip thickness model.
- For process control in non CD applications, the use of the h_m parameter would be beneficial from the perspective of controlling radial wheel wear. The h_m parameter corresponds with the force experienced by an individual grinding grain which could be used to provide consistent radial wear in non CD applications.

The conclusions and recommendations illuminate areas of future research within this subject area. These focus on the application of chip thickness models under

different process conditions including different grinding setups and material types. In addition, it considers the integration of contact layer theory and cutting fluid convection coefficients to provide improved models for control of the outputs for a grinding process. The recommendations for future work include:

- Application of similar experiments under non CD conditions utilising improved output measurements. The main objective would be the development of a chip thickness model in order to control radial wheel wear in a creep feed process.
- Investigation into predicting specific grinding energy and force requirements for a grinding process using material properties and contact layer theory. This could be further developed to predict and validate the change in force and energy requirements for varying productivity grinding processes with different material types.
- Refinement of the modified pin on disc testing to include temperature measurement of the contact zone. This would aim to measure the extent of surface temperature increase as a result of changing arc of contact and grinding wheel speed in isolation of chip thickness.
- Improved modelling and understanding of the temperature behaviour associated with the wheel speed and cutting fluid convection coefficients. Ability to predict the temperature changes associated with changing wheel geometry and wheel speeds for a creep feed grinding process. Increased temperature data and alternative measurement techniques could be utilised for this research.

Chapter 8 - References

1. J.M. Bond. A method for process control and mapping of Viper / Creep Feed grinding. Report, Rolls-Royce PLC, 13-06-2000.
2. H.Z. Li, K. Liu and X.P. Li, A new method for determining the undeformed chip thickness in milling., *Journal of Materials Processing Technology*, 113 (2001) 378-384.
3. X. Chen, W.B. Rowe, B. Mills, et al, Analysis and simulation of the grinding process. Part IV: Effects of wheel wear., *International Journal of Machine Tools and Manufacture*, 38(1-2) (1998) 41-49.
4. H. Helletsberger, *Grinding Processes - Cutting with undefined edges.*, ed., Tyrolit, Austria., 2004.
5. S. Malkin, *Grinding Technology: Theory and applications of machining with abrasives.*, First Edition ed., Ellis Horwood Limited, Chichester., 1989.
6. M.C. Shaw, *Principles of Abrasive Processing*, ed., Oxford University Press, Walton Street, Oxford., 1996.
7. I. Marinescu, W.B. Rowe, B. Dimitrov, et al, *Tribology of abrasive machining processes*, ed., William Andrew, 2004.
8. C. Andrew, T.D. Howes and T.R.A. Pearce, *Creep Feed Grinding*, ed., Holt, Rinehart and Winston, 1985.
9. C. Guo and S. Malkin, Analytical and experimental investigation of burnout in creep-feed grinding, *Annals of the CIRP*, 43(1) (1994) 283-286.
10. J.G. Wager and D.Y. Gu, Influence of up-grinding and down-grinding on the contact zone, *Annals of the CIRP*, 40(1) (1991) 323-326.
11. G. Werner, Application and technical fundamentals of deep and creep-feed grinding, *SME Technical Paper*, (1979) MR 79-319.
12. C. Guo and S. Malkin, Energy partition and cooling during grinding, *Journal of Manufacturing Processes*, 2(3) (2000) 151-157.
13. C.P.R. Hill, J.R. Watkins and C. Ray, *Method and apparatus for grinding*, U.S.P.a.T. Office, Editor. 1998, Rolls-Royce: United States.
14. D.J. Stephenson, T. Jin and J. Corbett, High efficiency deep grinding of a low alloy steel with plated CBN wheels, *CIRP Annals - Manufacturing Technology*, 51(1) (2002) 241-244.
15. J. Badger, Factors affecting wheel collapse in grinding, *CIRP Annals - Manufacturing Technology*, 58 (2009) 307-310.
16. N.E. Ye and T.R.A. Pearce, Some observations on profile wear in creep-feed grinding, *Wear*, 92 (1983) 51-66.
17. S. LaChance, A. Warkentin and R. Bauer, Development of an automated system for measuring grinding wheel wear flats, *Journal of Manufacturing Systems*, 22(2) (2003) 130-135.
18. T.R.A. Pearce, T.D. Howes and T.V. Stuart, The application of continuous dressing in creep feed grinding., *Proceedings 20th International MTDR Conference, Birmingham*, (1979) 383-390.
19. S. Sekine, I. Inasaki and S. Kobayashi, Creep Feed Grinding of Inconel 718 with Continuous Dressing, *Transactions of the Japan Society of Mechanical Engineers, Part C* 52 (1986) 2558-2562.

20. I. Inasaki, Creep-feed grinding with continuous dressing, *Annals of the CIRP*, 36(1) (1987) 227-230.
21. W. Osterle and P.X. Li, Mechanical and thermal response of a nickel-base superalloy upon grinding with high removal rates, *Materials Science and Engineering*, A238 (1997) 357-366.
22. H.K. Tonshoff, H.G. Wobker and B. G, CBN Grinding with Small Wheels, *Annals of the CIRP*, 44(1) (1995) 311-316.
23. M. Wakuda, M. Ota, H. Ueda, et al, Development of Ultrahigh Speed and High Power Cam Grinding Machine (1st Report) - Characteristics of Ultrahigh Speed Grinding of Chilled Casting, *Journal of the Japan Society for Precision Engineering* 64(4) (1998) 593-597.
24. X. Chen and W.B. Rowe, Analysis and simulation of the grinding process. Part II: Mechanics of grinding., *International Journal of Machine Tools and Manufacture*, 36(8) (1996) 883-896.
25. R. Komanduri, Some aspects of machining with negative rake tools simulating grinding, *International Journal of Machine Tool Design and Research*, 11 (1971) 223-233.
26. T. Matsuo, S. Toyoura, E. Oshima, et al, Effect of grain shape on cutting force in superabrasive single-grit tests, *Annals of the CIRP*, 38(1) (1989) 323-326.
27. R.L. Hecker, I.M. Ramoneda and S.Y. Liang, Analysis of wheel topography and grit force for grinding process modeling., *Journal of Manufacturing Processes*, 5(1) (2003) 13-23.
28. D.L. Butler, L.A. Blunt, B.K. See, et al, The characterisation of grinding wheels using 3D surface measurement techniques., *Journal of Materials Processing Technology*, 127 (2002) 234-237.
29. U.S.P. Durgumahanti, V. Singh and P.V. Rao, A new model for grinding force prediction and analysis, *International Journal of Machine Tools and Manufacture*, 50 (2010) 231-240.
30. M.F. Ashby and D.R.H. Jones, *Engineering Materials 1: An introduction to their properties and applications.*, Second Edition ed., Butterworth-Heinemann, Oxford., 1996.
31. H. Chang and J.J. Wang, A stochastic grinding force model considering random grit distribution, *International Journal of Machine Tools and Manufacture*, 48 (2008) 1335-1344.
32. M.C. Shaw, Energy conversion in cutting and grinding., *Annals of the CIRP*, 45(1) (1996) 101-104.
33. T. Jin and D.J. Stephenson, Heat flux distributions and convective heat transfer in deep grinding., *International Journal of Machine Tools and Manufacture*, 46 (2006) 1862-1868.
34. K. Hokkirigawa and K. Kato, An experimental and theoretical investigation of ploughing, cutting and wedge formation during abrasive wear, *Tribology International*, 21 (1988) 51-57.
35. M. Barge, G. Kermouche, P. Gilles, et al, Experimental and numerical study of the ploughing part of abrasive wear, *Wear*, 255 (2003) 30-37.
36. H. Wang and G. Subhash, An approximate upper bound approach for the single-grit rotating scratch with a conical tool on pure metal, *Wear*, 252 (2002) 911-933.
37. K. Kato, Micro-mechanisms of wear - wear modes, *Wear*, 153 (1992) 277-295.

38. O. Vingsbo and S. Hogmark, Single-pass pendulum grooving - A technique for abrasive testing, *Wear*, 100 (1984) 489-502.
39. M. Barge, J. Rech, H. Hamdi, et al, Experimental study of abrasive process., *Wear*, 264 (2008) 382-388.
40. K. Steffens and W. Konig, Closed loop simulation of grinding., *Annals of the CIRP*, 32(1) (1983) 255-259.
41. T.A. Nguyen and D.L. Butler, Simulation of surface grinding process, part 2: interaction of the abrasive grain with the workpiece, *International Journal of Machine Tools and Manufacture*, 45 (2005) 1329-1336.
42. N. Fang, Tool-chip friction in machining with a large negative rake angle tool., *Wear*, 258 (2005) 890-897.
43. T. Tawakoli, *High Efficiency Deep Grinding*, ed., Mechanical Engineering Publications Limited, 1993.
44. G.Q. Cai, B.F. Feng, T. Jin, et al, Study on the friction coefficient in grinding, *Journal of Materials Processing Technology*, 129 (2002) 25-29.
45. M. Abbasi, S. Kheirandish, Y. Kharrazi, et al, On the comparison of the abrasive wear behavior of aluminium alloyed and standard Hadfield steels, *Wear*, 268 (2010) 202-207.
46. F. Klocke, R. Engelhorn, J. Mayer, et al, Micro-analysis of the contact zone of tribologically loaded second-phase reinforced sol-gel-abrasives, *CIRP Annals - Manufacturing Technology*, 51(1) (2002) 245-250.
47. D. Wenfeng, X. Jiuhua, C. Zhenzhen, et al, Grindability and surface integrity of cast nickel-based superalloy in creep feed grinding with brazed CBN abrasive wheels, *Chinese Journal of Aeronautics*, 23 (2010) 501-510.
48. A.J. Bell, *Temperatures in high efficiency deep grinding*, in *School of Applied Sciences*. 2008, University of Cranfield: Cranfield.
49. D.J. Stephenson and T. Jin, *Physical basics in grinding*, in *European Conference on Grinding*. 2003: WZL, Aachen.
50. T. Jin, D.J. Stephenson and J. Corbett, Burn threshold of high-carbon steel in high-efficiency deep grinding, *Journal of Engineering Manufacture*, 216 (2002) 357-364.
51. A.-M.O. Mohamed, A. Warkentin and R. Bauer, Use of surface roughness measurements to improve the estimation of heat partitioning in grinding, *Journal of Materials Processing Technology*, 211 (2011) 566-572.
52. S. Malkin and C. Guo, Thermal analysis of grinding, *Annals of the CIRP*, 56(2) (2007) 760-782.
53. X.F. Pu, H.J. Xu, X.F. Hu, et al, Workpiece burn and its prediction in creep feed grinding - Experimental research of the temperature variance process in contact zone, *Annals of the CIRP*, 37(1) (1988) 541-544.
54. J. Webster, E. Brinksmeier, C. Heinzl, et al, Assessment of grinding fluid effectiveness in continuous-dress creep feed grinding, *Annals of the CIRP*, 51(1) (2002) 235-240.
55. J.A. Webster, Improving surface integrity and economics of grinding by optimum coolant application, with consideration of abrasive tool and process regime., *Journal of Engineering Manufacture*, 221 (2007) 1665-1675.

56. X.P. Xu, Y.Q. Yu and H.J. Xu, Effect of grinding temperatures on the surface integrity of a nickel-based superalloy, *Journal of Materials Processing Technology*, 129 (2002) 359-363.
57. X. Chen, W.B. Rowe and D. McCormack, Analysis of the transitional temperature for tensile residual stress in grinding, *Journal of Materials Processing Technology*, 107 (2000) 216-221.
58. Q. Huang and J.X. Ren, Surface integrity and its effects on the fatigue life of the nickel-based superalloy GH33A, *International Journal of Fatigue*, 13(4) (1991) 322-326.
59. L.C. Zhang, T. Suto, H. Noguchi, et al, A study of creep-feed grinding of metallic and ceramic materials, *Journal of Materials Processing Technology*, 48 (1995) 267-274.
60. B.B. Fathallah, N.B. Fredj, H. Sidhom, et al, Effects of abrasive type cooling mode and peripheral grinding wheel speed on the AISI D2 steel ground surface integrity, *International Journal of Machine Tools and Manufacture*, 49 (2009) 261-272.
61. D.J. Stephenson, J. Corbett, E. Laine, et al, *Burn threshold studies for superabrasive grinding using electroplated CBN wheels*, in *4th International Machining and Grinding*. 2001, Society of Manufacturing Engineers: Troy, Michigan.
62. R. Komanduri and Z.B. Hou, A review of the experimental techniques for the measurement of heat and temperatures generated in some manufacturing processes and tribology, *Tribology International*, 34 (2001) 653-682.
63. M.A. Davies, T. Ueda, R. M'Saoubi, et al, On the measurement of temperature in material removal processes, *Annals of the CIRP*, 56(2) (2007) 581-604.
64. N.K. Kim, C. Guo and S. Malkin, Heat flux distribution and energy partition in creep-feed grinding, *Annals of the CIRP*, 46(1) (1997) 227-232.
65. T. Jin and D.J. Stephenson, A study of the convection heat transfer coefficients of grinding fluids, *CIRP Annals - Manufacturing Technology*, 57 (2008) 367-370.
66. T. Kato and H. Fujji, Temperature measurement of workpieces in conventional surface grinding, *Journal of Manufacturing Science and Engineering*, 122 (2000) 297-303.
67. R. Snoeys and J. Peters, The significance of chip thickness in grinding, *Annals of the CIRP*, 23(2) (1974) 227-237.
68. H.K. Tonshoff, J. Peters, I. Inasaki, et al, Modelling and simulation of grinding processes., *Annals of the CIRP*, 41(2) (1992) 677-688.
69. W. Konig, H. Schreitmuller, F. Sperling, et al, A survey of the present state of high speed grinding, *Annals of the CIRP*, 44 (1971) 275-283.
70. P.-L. Tso, An investigation of chip types in grinding., *Journal of Materials Processing Technology*, 53 (1995) 521-532.
71. S. Coromant, *Metal Cutting Guide*. 2007.
72. A.V. Gopal and P.V. Rao, A new chip-thickness model for performance assessment of silicon carbide grinding., *International Journal of Advanced Manufacturing Technology*, 24 (2004) 816-820.
73. E. Brinksmeier and A. Glwierzew, Chip formation mechanisms in grinding at low speeds, *Annals of the CIRP*, 52(1) (2003) 253-258.

74. J. Tang, J. Du and Y. Chen, Modeling and experimental study of grinding forces in surface grinding., *Journal of Materials Processing Technology*, 209 (2009) 2847-2854.
75. J.C. Aurich, P. Herzenstiel, H. Sudermann, et al, High-performance dry grinding using a grinding wheel with a defined grain pattern., *Annals of the CIRP*, 57 (2008) 357-362.
76. C. Heinzl and N. Bleil, The use of the size effect in grinding for work hardening, *Annals of the CIRP*, 56(1) (2007) 327-330.
77. H. Huang, Machining characteristics and surface integrity of yttria stabilized tetragonal zirconia in high speed deep grinding, *Materials Science and Engineering*, A345 (2003) 155-163.
78. Y. Maeda, M. Masuda, Y. Koizumi, et al, A study on creep-feed grinding of heat-resisting alloy - Influence of grinding wheel wear on grinding speed, *Journal of the Japan Society for Precision Engineering*, 59 (1993) 1301-1306.
79. Z. Shang, H. Huang, K. Tang, et al, Coolant effect on grinding performance in high-speed deep grinding of 40Cr Steel, *Metalfinishing*, (2008) 16-21.
80. H. Helletsberger, *Conditioning of Grinding Tools*, ed., Tyrolit, Austria., 2003.
81. M. Massam, *Thermal Characteristics of Grinding Fluids*, in *School of Applied Sciences*. 2008, Cranfield University.
82. K. Worden, W.J. Staszewski and J.J. Hensman, Natural computing for mechanical systems research: A tutorial overview, *Mechanical Systems and Signal Processing*, 25 (2011) 4-111.
83. W.B. Rowe, Thermal analysis of high efficiency deep grinding, *International Journal of Machine Tools and Manufacture*, 41 (2001) 1-19.

Appendix A

Rhenus R-Flex

Products	Mineral oil content [%]	Polar/EP additives	Working concentration as of %	Material	Notes on use
The special lubricants					
r.rhenus R-SEVEN ¹⁾	39	Polar	5	Aluminium, steel	Universal coolant, optimum use on machining centres and transfer lines, e.g. for complex aluminium operations incl. thread-cutting and Mapal reaming.
r.rhenus R-COOL-S micron ¹⁾	41		4	Cast iron, steel and alu-alloys	Grinding and light machining. WGK 1
r.rhenus R-FLEX	0	Polar/EP	2/2	Difficult to machine steel, aluminium and special alloys. G, X, N, Z	The two-component coolant: r.rhenus R-Flex lub – the ester coolant r.rhenus R-Flex em – the emulsifier package Flexibly adjustable cutting performance, minimal foam development.]
r.rhenus FU 60 T ¹⁾	0	Polar	5	Difficult to machine steel, aluminium and special alloys.	Ester coolant for intricate machining and forming. WGK 1
r.rhenus XF 80 MG	36	Polar	5	Magnesium	Special coolant for magnesium operations, minimises the hydrogen generation.
r.rhenus FS 71 ¹⁾	66		6	Steel, aluminium, NE-metals S, N	White emulsifying universal coolant with high mineral-oil content.
r.rhenus XY 120 HM	0		3	Hard metal	Grinding product for production of hard metal tools.

Hocut 768

Hocut 768

High performance synthetic coolant

DESCRIPTION

Hocut 768 is a specially formulated blend of synthetic polymers designed to give maximum performance without the use of mineral oil. Biostable additives and corrosion inhibitors have been incorporated to give long sump life and excellent corrosion protection.

APPLICATION

The high lubricity offered by emulsions of Hocut 768 ensures excellent surface finish and extended tool life on a wide range of steel, titanium and nickel alloys.

Hocut 768 is a versatile high lubricity product and applications range from high speed form grinding of high nickel alloys to broaching of automotive conrods.

The synthetic formula is designed for very low foam in the highest pressure machines and to give maximum filterability in fine filtration systems.

RECOMMENDATION FOR USE

General machining	4% - 6%
Heavy duty machining	6% - 10%
Creep feed grinding	6% - 10%

TYPICAL PHYSICAL PROPERTIES

TEST	TYPICAL VALUE	TEST METHOD
<i>Neat concentrate</i>		
Appearance	Clear pale yellow oil	HI
Specific gravity @ 15.5°C	1.08	ASTM D1298
Refractometer factor	2.08	HI
<i>Emulsion at 5%</i>		
Appearance	Transparent colourless	HI
pH in use	8.7-9.2	HI

ADVANTAGES

- Mineral oil free
- Excellent corrosion protection
- Long sump life
- Prolongs tool life
- Stable in hard water
- No sticky residues
- Chlorine free
- Efficient rejection of tramp oil
- Very low foam for highest pressure systems
- Maximum filterability
- Rolls Royce CSS approved

STORAGE

Metal working coolants should be stored indoors in clean, dry conditions. Protect from frost. Recommended storage temperature is between 5°C and 35°C. Tops should be replaced on all containers when not in use. Use stock in delivery rotation. As with all metal working coolants, a shelf life of six months can be anticipated.

HEALTH AND SAFETY

Health and Safety Data Sheets are supplied to customers to comply with Section 6 of the Health and Safety at Work Act 1974, and should be closely studied prior to handling or use of the product. Copies are available from your Technical Health and Safety Officer. Various other advisory publications are available from the Health and Safety Executive and Her Majesty's Stationery Office.

14768
04/07

All data given in this Product Data Sheet are typical of this material. It does not however constitute a specification. We reserve the right to modify products without prior notice. All products, services and information supplied are provided upon the terms of our standard Conditions of Sale from time to time in force.

Houghton plc
Beacon Road, Trafford Park, Manchester M17 1AF
Tel +44(0) 161 874 5000
Fax +44(0) 161 874 5001
E-mail uk.enquiries@houghtoneurope.com



Appendix B

Run Order	Block	Dressing Type	Cut Direction	Q' (mm ³ /s/mm)	r _s (mm)	v _w (mm/min)	a _e (mm)	V _s (m/s)	h _m (μm)	P _{Net} (kW)	F _v (N)	Ra (μm)
RO1	1	Non-CD	Up	35	243.230	1050	2	36	11.58	20.6	1886	1.93
RO2		Non-CD	Up	60	239.200	1200	3	36	13.76	24.7	2397	2.48
RO3		CD	Up	35	238.200	1050	2	36	11.64	19.1	1516	1.30
RO4		CD	Up	35	237.700	1050	2	36	11.65	19.3	1505	1.25
RO5		Non-CD	Down	35	235.447	1050	2	36	11.67	17.8	1389	2.08
RO6		Non-CD	Down	35	235.409	1050	2	36	11.70	18.0	1436	2.20
RO7		Non-CD	Up	35	226.159	1050	2	37	11.63	19.9	1876	2.09
RO8		Non-CD	Up	60	225.659	1200	3	37	13.77	25.2	2331	2.16
RO9	2	CD	Up	35	219.000	1050	2	37	11.72	19.8	1432	1.93
RO10		Non-CD	Up	35	216.454	1050	2	38	11.60	19.7	1801	2.25
RO11		Non-CD	Up	35	215.954	1050	2	38	11.61	19.9	1674	2.03
RO12		Non-CD	Down	35	213.483	1050	2	38	11.64	18.1	1357	2.29
RO13		Non-CD	Up	60	212.483	1200	3	38	13.79	23.5	2265	2.34
RO14		Non-CD	Down	35	209.479	1050	2	38	11.70	18.1	1351	2.40
RO15		Non-CD	Up	60	206.700	1200	3	39	13.71	25.0	2192	2.41
RO16		CD	Up	35	206.200	1050	2	39	11.59	20.2	1297	1.37
RO17	3	Non-CD	Up	60	195.000	1200	3	40	13.73	25.4	2222	2.61
RO18		Non-CD	Up	60	192.701	1200	3	40	13.77	25.0	2179	2.54
RO19		Non-CD	Up	35	190.901	1050	2	40	11.67	20.2	1725	2.11
RO20		CD	Up	35	187.005	1050	2	41	11.59	20.3	1229	1.16
RO21		Non-CD	Down	35	186.137	1050	2	41	11.60	18.1	1235	2.16
RO22		CD	Up	35	183.802	1050	2	41	11.64	20.0	1230	1.21
RO23		Non-CD	Down	35	182.929	1050	2	41	11.65	18.4	1297	2.39
RO24		Non-CD	Up	35	181.929	1050	2	41	11.67	20.4	1597	1.97

Table B.1 Table of cuts performed for preliminary experiments including process parameters, chip thickness and outputs.

Appendix C

Run Order	Block	Chip Thickness Maintained	v_w (mm/min)	a_e (mm)	V_s (m/s)	r_s (mm)	S (μm)	h_{eq} (μm)	h_m (μm)	P_{Net} (kW)	F_v (N)	F_h (N)	T_c ($^{\circ}\text{C}$)	Ra (μm)
RO1	1	S	500	1	35.00	149.350	4.12	0.238	7.70	5.8	476	196	88	1.18
RO2			500	1	34.90	148.678	4.12	0.239	7.72	5.7	508	196	74	1.37
RO3			500	1	34.80	148.005	4.12	0.239	7.74	5.8	508	196	85	1.47
RO4		h_m	500	1	35.25	147.331	4.06	0.236	7.70	5.9	500	192	85	1.36
RO5			500	1	35.35	146.645	4.04	0.236	7.70	5.9	510	193	79	1.38
RO6			500	1	35.40	145.954	4.02	0.235	7.70	5.9	499	189	87	1.37
RO7		h_{eq}	500	1	35.00	145.259	4.06	0.238	7.75	5.9	514	195	89	1.42
RO8			500	1	35.00	144.568	4.05	0.238	7.76	5.9	510	193	88	1.43
RO9			500	1	35.00	143.874	4.04	0.238	7.77	5.9	502	198	82	1.41
RO10	2	h_m	500	1	37.70	129.000	3.55	0.221	7.70	5.3	453	181	73	1.43
RO11			500	1	37.80	128.162	3.53	0.220	7.70	5.5	454	178	85	1.44
RO12			500	1	37.95	127.317	3.51	0.220	7.70	5.7	459	177	85	1.44
RO13		S	500	1	32.20	126.463	4.12	0.259	8.37	5.9	525	197	75	1.46
RO14			500	1	32.10	125.733	4.12	0.260	8.39	5.9	526	196	92	1.48
RO15			500	1	32.00	125.001	4.12	0.260	8.42	5.9	528	194	93	1.42
RO16		h_{eq}	500	1	35.00	124.267	3.76	0.238	8.06	5.8	491	187	79	1.43
RO17			500	1	35.00	123.460	3.74	0.238	8.07	5.6	493	188	83	1.35
RO18			500	1	35.00	122.648	3.73	0.238	8.09	5.7	498	188	80	1.41
RO19	3	S	500	1	29.35	105.000	4.12	0.284	9.18	5.5	551	204	82	1.46
RO20			500	1	29.20	104.199	4.12	0.285	9.22	5.7	551	207	95	1.48
RO21			500	1	29.10	103.396	4.12	0.286	9.25	5.7	558	200	89	1.46
RO22		h_{eq}	500	1	35.00	102.589	3.41	0.238	8.46	5.5	472	180	87	1.41
RO23			500	1	35.00	101.611	3.40	0.238	8.48	5.4	460	177	85	1.45
RO24			500	1	35.00	100.624	3.38	0.238	8.50	5.6	478	174	87	1.37
RO25		h_m	500	1	42.85	99.627	2.75	0.194	7.70	5.3	406	155	69	1.33
RO26			500	1	43.15	98.395	2.71	0.193	7.70	5.4	393	156	81	1.40
RO27			500	1	43.40	97.138	2.68	0.192	7.70	5.4	398	157	74	1.54
RO28	4	h_{eq}	500	1	35.00	92.000	3.23	0.238	8.69	5.4	448	170	88	1.46
RO29			500	1	35.00	90.910	3.21	0.238	8.71	5.4	455	170	89	1.49
RO30			500	1	35.00	89.807	3.19	0.238	8.74	5.4	457	171	77	1.51
RO31		h_m	500	1	45.45	88.690	2.44	0.183	7.70	5.1	363	148	76	1.43
RO32			500	1	45.80	87.222	2.41	0.182	7.70	5.1	362	141	64	1.49
RO33			500	1	46.20	85.717	2.36	0.180	7.70	5.2	360	140	66	1.59
RO34		S	500	1	26.30	84.173	4.12	0.317	10.25	5.7	576	209	88	1.55
RO35			500	1	26.15	83.278	4.12	0.319	10.31	5.7	577	208	84	1.60
RO36			500	1	26.00	82.378	4.12	0.321	10.36	5.6	583	206	101	1.50

Table C.1 Table of cuts performed for Chapter 4 machining trials including process parameters, chip thickness and outputs.